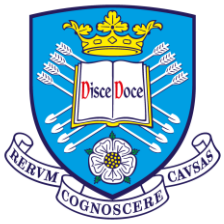

The University Of Sheffield.

Biomass Chemical Looping Gasification for Power Generation

Usama Mohamed

Submitted for the degree of Doctorate of Philosophy

The University of Sheffield

Faculty of Engineering

Department of Mechanical Engineering

March 2021

This page intentionally left blank

ABSTRACT

Chemical looping gasification (CLG) technology has proven to present itself as a promising alternative to conventional thermal power generation processes, offering potentially higher efficiencies and lower costs. To determine its feasibility on a large scale, a biomass chemical looping gasification combined cycle (BCLGCC) model using Aspen Plus software was developed, validated using experimental data and scaled up to 650 MW. A techno-economic and sustainability analysis was then conducted and compared to 4 other power generation technologies with and w/o CCS. BCLGCC presents promising economic and environmental results, showing that the efficiencies of the CCS and Non-CCS plants equal to 36% and 41%, respectively, with COE (including government subsidies) for both CCS and Non-CCS equal to 15.9 ¢/kWh and 12.8 ¢/kWh, both of which are lower than the average COE in the UK.

A life cycle energy use, CO_2 emissions and cost input evaluation of a 650 MW BCLGCC and a BIGCC/CIGCC power generation plants with and w/o CCS are analysed then compared to coal/biomass combustion technologies. The life cycle evaluation covers the whole power generation process including biomass/coal supply chain, electricity generation and the CCS process. Gasification power plants showed lower energy input and CO_2 emissions, yet higher costs compared to combustion power plants. Coal power plants illustrated lower energy and cost input; however higher CO_2 emissions compared to biomass power plants. Coal CCS plants can reduce CO_2 emissions to near zero, while BCLGCC and BIGCC plants with CCS resulted in negative 680 and 769 kg-CO_2/MWh, respectively. Regarding the total life cycle costs input, BCLGCC with and w/o CCS equal to 149.3and 199.6 £/MWh, and the total life cycle energy input for both with and without CCS is equal to 2162 and 1765 MJ/MWh, respectively.

Finally, a set of BCLG experiments were conducted in a fixed bed reactor using fresh hematite and pine sawdust. The experiments consisted of testing the effect of temperature, biomass to oxygen carrier (OC) ratio and multiple cycles on the gas yield, LHV, cold gas efficiency, carbon conversion, XRD results, SEM imagine of the surface of the OC and EDX data. The results showed that the carbon conversion was low compared to when using other sources of biomass, and consequently LHV, gas yield, cold gas efficiency. Moreover, it was observed that as temperature, reaction time and B/OC ratio increased the surface of the oxygen carrier would undergo sintering and agglomeration, with the oxygen being consumed reducing the main component of the hematite (Fe_2O_3) into three phases including Fe_3O_4, FeO and Fe.

ACKNOWLEDGMENTS

Firstly, I want to start by thanking God (Allah) the most gracious most merciful for everything that I was able to achieve and accomplish throughout my time as a PhD student. I would also like to also thank my mum, dad, my brothers Hamza and Ahmed and the rest of my family for their interest in my research as well as their immense support throughout my ups and down during my PhD.

Secondly, I would like to express my sincere gratitude to my advisor Prof. William Nimmo for the continuous support of my PhD study and related research, for his patience, motivation, and immense knowledge. His guidance helped me in all the time of research and writing of this thesis. I could not have imagined having a better advisor and mentor for my PhD study.

Moreover, I would like to thank Prof. Qun Yi from Taiyuan University of Technology (TYUT) for his support and knowledge during my first year while he was a visiting professor at the University of Sheffield. I would also like to thank him for giving me the opportunity to complete a 3.5-month academic exchange program in China at TYUT and the Chinese Academy of Science. I would also like to thank Yingjie Zhao, Yi Huang, Huan Zhou and Guoqiang Wei for their very warm welcome and support during my time in China.

Last but not least, I want to thank my dear friends, more like brothers, Yousef Salem my partner in crime during my first year as well as Muhammed Saleh and Ben Mills for spending all those hours in the university library doing work while motivating and encouraging me to keep on persevering throughout this PhD.

DECLARATION

I, the author, declare that this Thesis is my own work. I am aware of the University's guidance on the Use of Unfair Means (www.sheffield.ac.uk/ssid/unfair-means). This work has not been previously presented for an award at this, or any other, university.

JOURNAL PUBLICATIONS

Chapter 4 contains the following publications:

- **Mohamed, U**., Zhao, Y., Huang, Y., Cui, Y., Shi, L., Li, C., Pourkashanian, M., Wei, G., Yi, Q. and Nimmo, W., 2020. Sustainability evaluation of biomass direct gasification using chemical looping technology for power generation with and w/o CO_2 capture. Energy, 205, p.117904.

The author of this thesis worked on developing the methodology alongside the support of Qun Yi (mentor during my academic exchange program in China), created the experimental plans, conducted the experimental work and is the first author of the manuscript.

Chapter 5 contains the following publications:

- **Mohamed, U**., Zhao, Y., Shi, L., Wei, G., Yi, Q. and Nimmo, W., 2021. Evaluation of Life Cycle Energy, Economy and CO_2 Emissions for Biomass Chemical Looping Gasification to Power Generation. Renewable Energy, xxxx, pp.xx-xx (*Under 2nd Stage Review*)

The author of this thesis worked on developing the methodology, created the experimental plans, conducted the experimental work and is the first author of the manuscript.

- Yi, Q., Zhao, Y., Huang, Y., Wei, G., Hao, Y., Feng, J., **Mohamed, U**., Pourkashanian, M., Nimmo, W. and Li, W., 2018. Life cycle energy-economic-CO_2 emissions evaluation of biomass/coal, with and without CO_2 capture and storage, in a pulverized fuel combustion power plant in the United Kingdom. Applied energy, 225, pp.258-272.

The author of this thesis helped in data collection, reviewing and editing the manuscript.

EXCHANGE PROGRAM

- Taiyuan University of Technology, Taiyuan, China **(2 months)**
- Chinese Academy of Science, Guangzhou Institute of Energy Conversion (CAS – GIEC), Guangzhou, China **(1.5 months)**

CONFERENCE PRESENTATIONS

- Yi, Q., Wei, G., Huang, Z., Chen, K., Li, W., Shen, L., Song, T., Nimmo, W. **Mohamed, U.**, 'Syngas-power Production from Biomass Direct Gasification Using Chemical Looping Technology', UK – PK Research Links Workshop on Fuels and Energy Systems, Cambridge, UK, 27th – 28th March 2018.
- **Mohamed, U.**, Yi, Q., Nimmo, W. (2018) 'A Thermodynamic Analysis Comparing Between Conventional Gasification and Chemical Looping Direct Biomass Gasification using Aspen Plus Software', Green Energy and Municipal Solid Waste Management Solutions Workshop, Astana, Kazakhstan, 12th September 2018.
- **Mohamed, U.**, Yi, Q., Nimmo, W. (2019) 'UK Energy Policies and Biomass Direct Gasification Using Chemical Looping Technology for Power Generation', Research Exchange Workshop, Dalian City, China, 27th – 28th July 2019.
- **Mohamed, U.**, Yi, Q., Nimmo, W. (2019) 'Modelling and Techno-Economic Performance Evaluation of Biomass Chemical Looping Gasification for Power Generation', The 4th International Conference on Alternative Fuels, Energy and Environment, Tiachung, Taiwan, 18th – 21st October 2019.

Contents

LIST OF FIGURES

LIST OF TABLES

NOMENCLATURE & ABBREVIATIONS

NET – Negative Emission Technology

BECCS – Bioenergy with CO_2 Capture & Storage

CHP – Combined Heat and Power

CLT – Chemical Looping Technology

BCLG – Biomass Chemical Looping Gasification

BCLGCC – Biomass Chemical Looping Gasification Combined Cycle

CLC – Chemical Looping Combustion

CLOU – Chemical Looping Oxygen Uncoupling

CLR – Chemical Looping Reforming

CLWS – Chemical Looping Water Splitting

DBC – Direct Biomass Combustion

PCC – Pulverized Coal Combustion

IGCC – Internal Gasification Combined Cycle

CIGCC – Coal Internal Gasification Combined Cycle

BIGCC – Biomass Internal Gasification Combined Cycle

FR – Fuel Reactor

AR – Air Reactor

FBR – Fluidized Bed Reactor

BFB – Bubbling Fluidized Bed

CFB – Circulating Fluidized Bed

WGS – Water Gas Shift

CCS – Carbon Capture & Storage

MEA – Monoethylene Amine

OC – Oxygen Carrier

GT – Gas Turbine

ST – Steam Turbine

ASU – Air Separation Unit

HRSG – Heat Recovery Steam Generation

FGD – Flue Gas Desulphurization

SCR – Selective Catalytic Reduction

SNCR – Selective Non-Catalytic Reduction

ESP – Electrostatic Precipitator

LCA – Life Cycle Analysis

LCI – Life Cycle Inventory

LCIA – Life Cycle Inventory/Impact Analysis

IECM – Integrated Environmental Control Model

DoE – Department of Energy

NETL – National Energy Technology Laboratory

TLCEI – Total life cycle energy input

TLCCI – Total life cycle cost input

TLCCE – Total life cycle CO_2 emission

ADP_{fossil} – Abiotic depletion potential

AP – Acidification potential

EP – Eutrophication potential

POCP – Photochemical ozone creation potential

ODP – Ozone depletion potential

XRD – X-Ray Diffraction

SEM – Scanning Electron Microscope

EDX – Energy Dispersed X-Ray Spectroscopy

CGE – Cold Gas Efficiency

CGY – Combustible Gas Yield

LHV – Lower Heating Value

HHV – Higher Heating Value

W_{Gross} – Gross Power of the power plant

W_{Syngas} – Power caused by fuel gas compression

W_{OC} – Power required for OC circulation

W_{CCS} – Power required for CO_2 capture and storage

Y_n – Gas yield of gaseous component

V_n – Volume of gaseous component

$M_{Biomass}$ – Mass of biomass

X_C – Carbon conversion

M_C – Mass fraction of carbon

I_1 - equipment cost of reference equipment

Q_1 - production capacity of the reference equipment

n - scale exponent

BEC – Bare erected cost

TOC – Total overnight cost

TPEC – Total plant equipment cost

TPC – Total plant cost

TCI – Total Capital Investment

COE – Cost of Electricity

OC_{VAR} – Variable operational cost

OC_{FIX} – Fixed operational cost

CRF – Capital recovery factor

ACC – Annual capital cost

CF – Capacity factor

N – plant life

i – discount rate

$COST_{Annual}$ – Total annual cost for the OC

$COST_{OC}$ – Cost for the OC per unit mass

M_{OC} – Total solid inventory

LT_{OC} – OC lifetime

TOC_S/TOC_R – Total overnight cost of scaled/reference plant

VC_S/VC_R – Variable cost of a scaled/fixed plant

FC_S/FC_R – Fixed costs of a scaled/reference plant

MW_S/MW_R – Net power of scaled/reference plant

x_{ij} – indictor j for the process i

X_{ij} – Normalised indictor j for the process i

1 CHAPTER 1: INTRODUCTION

1.1 Energy Policy Overview

The fast growth of developing economies around the world and rapid increase in world population are intrinsically linked with the increase in energy demands. The U.S Energy Information Administration estimated that the total world energy consumption is to increase by 28% in 2040 relative to 2015 [1]. The energy sector in particular contributes towards 41% greenhouse gas emissions through the use of fossil fuel and is expected to have the fastest growth rate [2]. Approximately 86% of worldwide energy consumption is from fossil fuel due to them being abundant and geographically spread over the world, hence considered as a cheap and reliable source of energy [3]. However, due to fears concerning the imminent and long-term risks associated with their use, it is imperative to push towards sustainable sources of energy. As a result, the Paris Agreement in 2016 aimed to maintain temperature rise below 2°C by the end of this century relative to pre-industrial levels with efforts to further limit the increase by 1.5°C [4]. This has encouraged several nations to reduce their CO_2 emissions and move towards renewable energy. The United Kingdom's long-term target was to reduce their greenhouse gas emissions by at least 80% by the year 2050, relative to 1990 levels [5]. However, recently the UK House of Commons passed a net zero carbon emissions bill to be achieved by the year 2050 [6], which means that radical change in the entire UK's economy and power generation sector is required to achieve this target. In order to control CO_2 emissions, De Gouw et al., suggested two pathways: either phasing out as much fossil fuel and moving towards renewable energy or developing technologies with higher energy efficiency [7]. Moreover, it has been widely remarked that this target would be impossible to achieve without the employment of Bioenergy [8]. The push towards reducing greenhouse gasses into the atmosphere can be done by either improving power generation efficiencies, employing carbon capture & storage, or moving towards renewable energy. Drax power plant, one of the largest in the UK will be ending its commercial coal power usage by March 2021, four years ahead of its 2025 deadline [9], with many other coal power plants having already closed or getting closer to their closure date [10]. This comes alongside the ban of selling petrol and diesel cars in the UK after the year 2035 [11]. Coal production and import into the UK has also dropped by 27% and 56% in 2020's first quarter relative to 2019's first

quarter, respectively, due to the decrease in demand from power generators [12]. Moreover, in April 2020, 11 industry and energy leading companies in the UK signed an agreement to transform the Humber region into the world's first 'zero-carbon cluster' by 2040 [13]. Furthermore, recently the UK went for a record period of 68 days coal-free [14]**.** Even though the UK are working towards eliminating coal from its power industry, the steel industry still heavily relies on coal, however current research is directed to test the feasibility of replacing coal with biomass [15]. With increased research and development of post- and pre-combustion capture technologies [16], CO_2 capture and storage (CCS) is seen as a promising technology in mitigating CO_2 emissions with its potential to help reduce global emissions by 20% by 2050 [17]. However, I believe that deployment of CCS technology would not be possible without negative emissions incentive from the government due to the costs associated with deploying the technology. In 2019 the UK generated 19.8% of its energy demand from low carbon sources with bioenergy accounting for the highest contribution of 37%. Since the year 2000, bioenergy experienced the fastest increase in capacity with an increase from 0.9% to 7.3%, as shown in Table 1.1 [18], showing the potential and effectiveness of bioenergy as a renewable and alternative growing source of energy for the UK.

Table 1.1. Renewable energy sources trend for the past 20 years [18]

	2000	**2010**	**2016**	**2017**	**2018**	**2019**
Nuclear	8.4%	6.3%	8.0%	7.9%	7.3%	7.0%
Wind	0.0%	0.4%	1.6%	2.2%	2.5%	2.9%
Solar	0.0%	0.0%	0.5%	0.5%	0.6%	0.6%
Hydro	0.2%	0.1%	0.2%	0.3%	0.2%	0.3%
Bioenergy	0.9%	2.7%	5.8%	6.2	6.8%	7.3%
Transport fuels	0.0%	0.6%	0.5%	0.5%	0.7%	0.9%
Other	0.0%	0.0%	0.7%	0.7%	0.7%	0.8%
Total	**9.4%**	**10.2%**	**17.4%**	**18.3%**	**18.9%**	**19.8%**

However, reaching the aforementioned targets and reducing GHG emissions into the atmosphere using traditional measures (renewable energy and improving efficiencies) might not be sufficient to reduce CO_2 emissions to the desired levels. As a result, new technologies capable of removing CO_2 from the atmosphere, known as negative emission technologies (NETs) will be essential to reach those targets. The increased interest in this field has led to

the first International Conference on Negative CO_2 Emissions at Chalmers University of Technology in Sweden in 2018 [19]. Out of the various NETs, the majority of low-carbon technologies rely on coupling CCS technologies with renewable fuels such as biofuels, known as bioenergy with CO_2 capture and storage (BECCS) [20–23]. Figure 1.1 from McCulloch et al., [23] briefly illustrates the concept of BECCS.

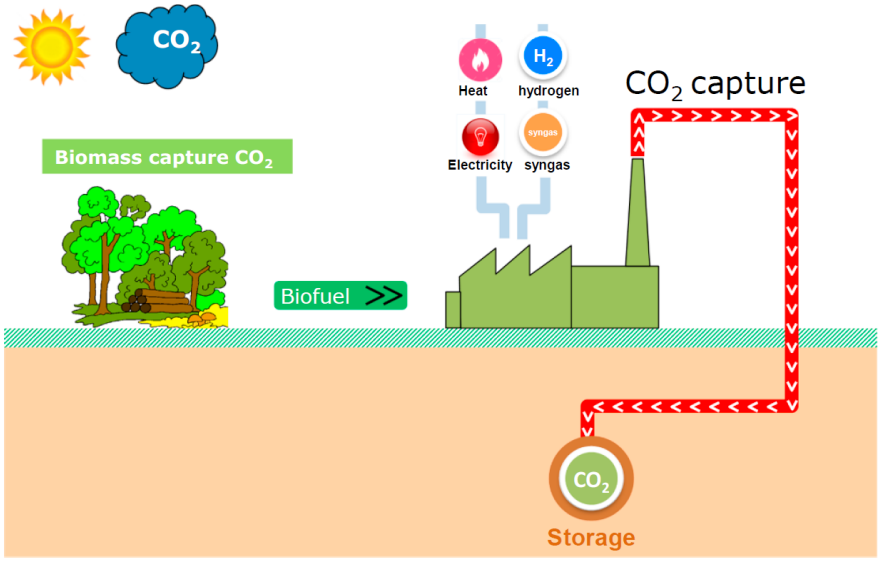

Figure 1.1. A general concept of BECCS [23]

In a comprehensive review on the views in the research and regulation of deploying bioenergy technology, Creutzig et al. [24] identified the strengths of BECCS as the following:

1) BECCS can be applied on a wide range of technology applications (power plants, industry, biomass refineries or gasification plants).
2) Will help in reaching the CO_2 emission reductions target in time.
3) BECCS negative emissions can compensate for residual emissions in other sectors that would be difficult to cut down emissions, for example industrial (pulp and paper, cement, iron and steel) or transport.

On the other hand, some negatives that should be considered about BECCS is the need for large amount of land. This can have an effect on the extent of negative emissions when taking into consideration the emissions in the biomass supply chain. Additionally, it can also have an effect on food production, biodiversity and land usage for other purposes [25].

1.2 Biofuels

Bioenergy can be classified into three different forms according to their physical state, namely gaseous biofuels, liquid biofuels, and solid biofuels. Gaseous biofuel is mainly biogas generated from anaerobic digestion, pyrolysis gas from biomass torrefaction or syngas from waste gasification. Liquid fuels are mainly biodiesel, ethanol and pyrolysis oil, whereas solid biofuels are mainly biomass. This thesis will focus on solid biofuel (biomass). Lignocellulosic biomass sources provide an inexpensive, abundant and renewable alternative source of energy [26]. Even though biomass has a lower energy density than coal due to its carbohydrate structure resulting in relatively higher H/C and O/C ratio (1.2-1.8 and 0.4-0.9, respectively), as shown in Figure 1.2. In addition, its high moisture content increases the overall cost of the process (transport, drying, chipping, etc.). However, biomass contains higher volatile content (75 – 85%) and less fixed carbon content [27] which makes it more desirable for gasification processes, due to better reactivity, hence higher conversion rate of the solid fuel [28]. Moreover, biomass generally has lower pollutants (sulphur and heavy metals) and ash content compared to coal, making ash treatment process less energy intensive. That being said, biomass ash has a high alkaline metal content, which helps in capturing sulphur but also causes corrosion and reduces ash melting point [29]. The issue with low ash melting point is that it causes the bed material to coalesce and form large agglomerates within the bed, hence resulting in partial or complete bed de-fluidization and unscheduled plant shutdown.

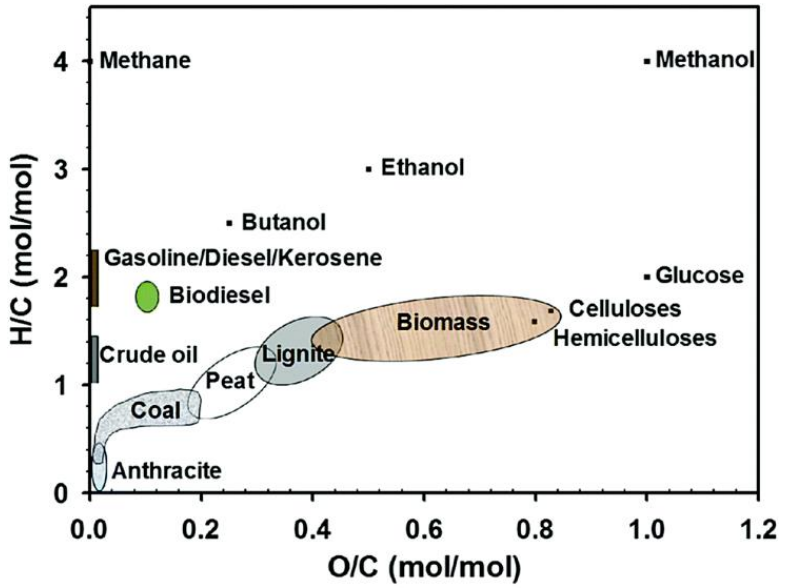

Figure 1.2. van Krevelin diagram comparing between H, C and O content of different solid fuels [30]

1.3 Biomass Classification

Biomass is a biological material derived from living or recently living organisms. This can apply to either animal or plant derived materials. However, in this report the term 'biomass' will refer to plant-based materials. Biomass can be classified through two main approaches; using either its origin or based on its properties [31, 32].

- **Origin of the biomass**
  1. Primary residues: By-products of forest products and food crops. (Straw, maize, cereal, etc.)
  2. Secondary residues: By-products of biomass processes in the production of products or food. (food and beverage industry, saw and paper mills, etc.)
  3. Tertiary residues: By-products of used biomass materials (e.g. demolition and waste wood)
  4. Energy Crops.
- **Based on properties**
  1. Wood and woody fuel
  2. Herbaceous fuels
  3. Wastes
  4. Derivates
  5. Aquatic
  6. Energy crops

1.4 Biomass Composition

The basic components of plant-based biomass are cellulose, hemicellulose, proteins, lipids, starch, hydrocarbon, simple sugars, water, ash and other compounds. Biomass bulk composition for carbon, hydrogen and oxygen are 30 – 60%, 5 – 6% and 30 – 45%, respectively. These are the common values between all types of plant-based biomass. Moreover, biomass may consist of up to approximately 1% nitrogen, sulphur and chlorine as well as traces of heavy metals for example cadmium and lead (usually less than coal). However, compared to coal, biomass contains more silica, chlorine and potassium but less aluminium, iron, titanium and sulphur [33].

1.5 Fuel Analysis

Fuel testing is an important aspect in power generation as it gives us a general understanding of the fuel behaviour and expected power output. By testing the fuel composition this will give a better understanding on how the fuel should be handled and if pre-treatment is required as well as a general understanding to what emissions are expected for gas treatment. Fuel composition can be analysed using several approaches including:

- Proximate Analysis: Provides an approximation to the fixed carbon (char), volatile matter, ash and moisture content in the fuel.
- Ultimate Analysis: Provides a more accurate elemental percentage of C, H, O, N, S and Cl, which determines the syngas yield for gasification and the pollutant emissions such as HCN, NO_X, NH_3, H_2S and SO_X.
- Sulphur Analysis: Provides data on the amount and distribution of sulphur between pyrites, sulphates and organics in a compound.

1.6 Fuel Properties

Fuel attains its properties from its content, which can be categorized as the following;

1.6.1 Heating Value

Heating value also known as the calorific value (energy content). On a dry basis, it is referred to as the Higher Heating Values (HHV), whereas in the presence of moisture it is referred to as Lower Heating Value (LHV). The energy content is generally correlated with the amount of carbon, oxygen and hydrogen composition in biomass. An increase in oxygen content results in a decreased biomass heating value. The heating value is also effected by the amount of cellulose, hemicellulose and lignin in the plant. Hemicellulose and cellulose contain a higher percentage of oxygen compared to lignin (mainly carbon). Therefore, higher lignin presence increases the heating value of biomass due to its lower degree of oxidation [34].

1.6.2 Moisture Content

Typical moisture content in biomass is between 25 – 60wt%, depending of the type of biomass, season, weather, location, etc. Biomass high moisture content is associated with several adverse effects on the process, including: handling, storing, loss of dry matter due to decomposition, causing feed inlet blockages, delays in ignition, energy and time required for ignition, and delays in devolatilization. Moreover, a high moisture content reduces the heating value of the fuel. Additionally, high moisture content will result in larger volume of flue gas, consequently requiring larger equipment dimensions [35].

1.6.3 Volatile Matter

Typically, between 60 – 80wt% of biomass, therefore most of the weight is lost during the devolatilization stage. The release of volatiles is rapid, resulting in high biomass reactivity. Products of the devolatilization process include: carbon monoxide, carbon dioxide, light hydrocarbons, moisture, hydrogen and tars. The yield and rates of this process is dependent on temperature, fuel characteristics and heating rate [36].

1.6.4 Ash

Ash content in biomass varies depending on the source. An advantage for biomass over coal is the low ash content, however the quality of biomass causes an issue. Compared to coal, biomass contains more alkali metals and silica which lowers its melting temperature. Although a large amount of the alkalis escape as gas phase in the presence of chlorine, however some still remain in the ash. This coupled with silica lowers the ash melting point, resulting in agglomeration which could lead to shutting down of unit due to low fluidization quality. Hence, the use of certain types of biomass could be limited. Other metals present in the ash such as Mg and Ca increases the melting point of the ash. Ash composition differs from one biofuel to another which effects ash sintering and softening which could be detrimental to the process. Therefore, controlling the melting temperatures is essential according to the type of biomass to avoid sintering or slagging [32].

1.6.5 Chlorine

One of the major differences between coal and biomass is the presence of chlorine. It can be found between percentages ranging from less than 0.1% and up to 2wt% (dry fuel). As chlorine vaporizes it forms HCl, Cl_2 gas and alkali chlorides which causes corrosion at high temperature [37].

1.7 Biomass Pre-processing

Although biomass is considered a renewable source of energy. However, it comes along with a pre-treatment process to improve its quality, therefore improving the efficiency of the power generation process, hence using fossil fuel in its pre-treatment. This is due to the low energy density and high moisture content of biomass, which results in additional capital and operational costs to the entire thermochemical conversion process. These processes include

drying, grinding and densification [38]. Biomass has a low energy density, therefore will require larger quantities for a certain power generation compared to coal, hence would increase transportation cost. Therefore, it is pelletized to increase its energy density. Moreover, some biomass has high moisture content which is treated to reduce handling costs as well as increase its energy density for higher efficiencies at the power plant.

1.8 Biomass to Energy

Biomass can be converted into an energy source via two main processes which can be categorised as either thermochemical or biochemical processes. Biochemical processes include anaerobic digestion, fermentation and biophotolysis, whereas thermochemical processes include pyrolysis, gasification and combustion. Biochemical processes are better compared to thermochemical processes in their environmental friendliness (destroys waste and lower CO_2 emissions) and lower energy requirement. However, these advantages are outweighed by their very slow kinetics compared to thermochemical processes, stringent biomass constraints, low fuel conversion efficiency, high amount of water consumed by microorganisms and the inability of some cellulosic biomasses to convert via biochemical processes. On the other hand, thermochemical processes are generally faster, can handle various types of biomass, and they completely utilize the biomass which results in a higher conversion efficiency. Additionally, they can be retrofitted into already developed conventional coal powered plants. This thesis will only focus on energy generation using thermochemical process [39].

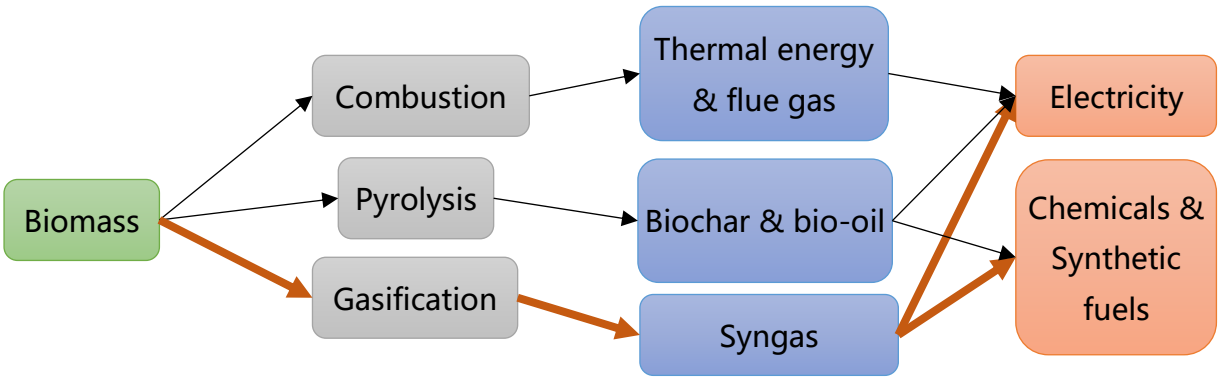

Figure 1.3. Thermochemical biomass conversion process route

Figure 1.3 categorizes the thermochemical processes of converting biomass into energy, the products and end use. Pyrolysis (R1) refers to the conversion of biomass into biochars and bio-oils in the absence of an oxygen source at approximately 400 – 600°C. Gasification (R2)

process is known as the partial oxidation of fuel to produce synthesis gas (CO and H_2), tar and char at approximately ≥800°C which can be used in electricity generation and producing valuable chemical products. Whereas combustion (R3) is the full oxidation of fuel to produce carbon dioxide, water and heat in the form of steam at approximately 1000 – 1400 °C [40].

$$Biomass \rightarrow char\ (mainly\ C) + CO + CO_2 + H_2 + CH_4 + H_2O + tar \quad \text{(R1)}$$

$$Biomass + \frac{1}{2}O_2 + steam \rightarrow CO + H_2 \quad \text{(R2)}$$

$$Biomass + O_2 \rightarrow CO_2 + H_2O \quad \text{(R3)}$$

Each is associated with its advantages and disadvantages. Pyrolysis has the capability of replacing fossil-fuel petroleum oil, which can be treated using conventional refineries; however, the process is energy intensive due to its endothermic nature [39]. Gasification allows for production of a variety of chemical products (methanol, fuels and other hydrocarbons) from syngas according to the market needs, however, tar formation is a disadvantage as it reduces gasification efficiency and could block downstream equipment [41]. Finally, combustion is a relatively simple process, nevertheless, it results in releasing harmful emissions (NO_X, SO_X, PAH, etc.) as well as ash fouling and slagging while having the lowest energy conversion efficiency [42].

Table 1.2 gives a comparison between the efficiencies of each process, showing that gasification gives the highest efficiency (55 – 65%) process.

Table 1.2. Comparison between the three thrmochemical converison of solid fuel [39]

Process	Products	Energy Conversion Efficiency (%)
Direct Combustion	Electricity	25
Rapid Pyrolysis	Pyrolytic oil, gas, char	37 – 45
Gasification	Synthesis Gas	50 – 60

Table 1.3 summarizes the currently operating biomass-based thermal power plants in the UK. Nearly all biomass power plants in the UK use combustion-based technology with a few operating biomass gasification power plants. Combustion is known as the complete burning of the fuel under enriched oxygen atmosphere to generate thermal energy while producing CO_2 and H_2O, whereas gasification is the partial combustion of the fuel under depleted oxygen conditions to produce CO and H_2 (syngas). Even though biomass combustion is a simple process to generate electricity, but its net efficiency (34 – 37%) is lower compared to gasification processes (36 – 40%) [43 – 48].

As a result, biomass gasification is explored in hope to find more effective processes that would improve biomass utilization in power generation. Biomass gasification dates back to the 18th century, were it was developed by a French engineer called Philippe Le Bon. The process was initially used to produce 'wood gas' for gas lighting. The gas used for lighting was known as town gas, which mostly comprised of coal gas. This was used until after World War 2 where it was replaced by natural gas. However, the interest in wood gas during the early 1920's was shifted to be used for transport fuel, but faced several technical issues [49]. During the late 1970's, as the oil crisis began, there was a huge shift in the UK's source of energy towards coal. During that period, several coal gasification technologies developed and became commercialized to produce synthetic fuels using the Fischer Tropsch process. However, a decrease in oil prices during the following years, resulted in the technology not finding its share in the market. Nevertheless, throughout the last decade research into this area was brought back to life, though directing it towards biomass fuel utilization instead of coal to tackling climate change [50]. Currently the largest waste wood gasification power plant in the UK, Cheshire generates 21.5 MW of electricity, which is expected to reduce GHG emissions by 65,000 tonnes of CO_2 equivalent per year [51], with several smaller plants in operation and in construction/commissioning stage [52].

Table 1.3. Summary of all biomass-based power plants in the UK [53, 54]

Name of Plant	Size (MWe)	Tonnes of biomass/year	Plant Type	Technology	Company
Blackburn Meadows	30	270,000	Electricity	Air Combustion	Eon
Brigg Renewable Energy Plant	40	328,840	CHP	Air Combustion	BWSC plc
Chilton Biomass Energy Centre	15.45	120,000	CHP	Air Combustion	Veolia
Craigellachie Wood, Moray	15	150,000	CHP	Air Combustion	Estover Energy
Cramlington Biomass CHP Plant	27.7	270,000	CHP	Air Combustion	Estover Energy
Discovery Park Biomass Plant	27	240,000	CHP	Air Combustion	Kent Renewable Energy Ltd
Drax Power Station	2000	13,200,000	Electricity	Air Combustion	Drax
Ely Power Station	38	312,398	Electricity	Air Combustion	MRE UK
Eye Power Station	16.53	134021	Electricity	Air Combustion	EPR (Eye) Ltd
Glanford Power Station	15	92,000	Electricity	Air Combustion	MRE UK
Goosey Lodge Biomass Plant	16	84,489	Electricity	Air Combustion	Wykes Engineering Co.(Rushden) Ltd.
Iggesund Paperboard Biomass Power Station	44	663,000	CHP	Air Combustion	Iggesund Paperboard (Workington) Ltd.
Ince Biomass Energy Plant	21.5	170,000	CHP	Advanced Thermal Treatment Oxygen Gasification	Ince Bio Power Ltd
Irine Paper Mill CHP Plant	26.04	371,000	CHP	Air Combustion	UPM Kymmene
Londonderry Biomass Plant	15.8	250,000	CHP	Air Combustion	Evermore Energy
Lynemouth Power Station	420	3,000,000	Electricity	Air Combustion	EPH
Margam Biomass Plant 1	15	196,000	Electricity	Air Combustion	Western Bioenergy Ltd
Margam Biomass Plant 2	40	355,000	Electricity	Air Combustion	Glenmont Partners
Markinch Biomass Plant	65	328,000	CHP	Air Combustion	RWE Npower Cogen
Ridham Biomass Plant	25	160,000	CHP	Air Combustion	MVV Energie
Sleaford Renewable Energy Plant	38.5	328,840	CHP	Air Combustion	Statkraft/Glenmont Partners
Snetterton Biomass Plant	44.2	328,840	Electricity	Air Combustion	BWSC plc
Steven's Croft	46	512,000	Electricity	Air Combustion	Eon
Tempelborough Biomass Plant	48.96	270,000	CHP	Air Combustion	Templeborough Biomass Power Plant Ltd
Thetford Power Station	41.5	457,000	Electricity	Air Combustion	MRE UK
Tilbury Green Power biomass plant	60	650,000	Electricity	Air Combustion	Tilbury Green Power
UPM Shotton Paper Burner	20	457,456	CHP	Air Combustion	UPM Kymmene
Wilton 10	33	261,000	Electricity	Air Combustion	Sembcorp International
Birmingham Bio Power	10.3	67,000	Electricity	Air Gasification	CoGen
Welland Bio Power	10.6	72,000	Electricity	Air Gasification	CoGen

1.9 Conventional Gasification Process

A typical biomass gasification mechanism undergoes four main steps including: drying, pyrolysis, combustion and reduction. These steps are summarized in Figure 1.4 with the reactions summarised in Table 1.4 [27, 55]. The order of the combustion and gasification stages in the mechanism could differ depending on the reactor configuration. However, for a fluidized bed reactor (the reactor that will we focused on in this thesis) follows the order of the stages shown in Figure 1.4.

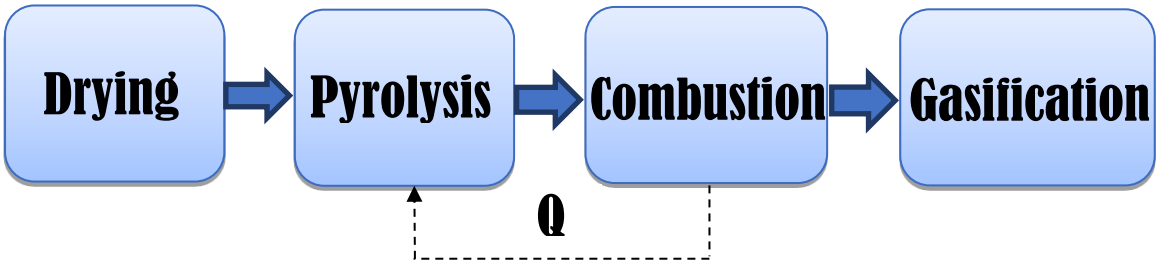

Figure 1.4. Four steps for gasification mechanism

Drying: Moisture escapes from the biomass at high temperatures around 110°C; however, it does not decompose during this step due to it not having sufficient energy for the endothermic chemical reactions to take place. (Reaction 1, Table 1.4)

Pyrolysis (Devolatilization): After the biomass is dried, it absorbs sufficient energy allowing the devolatilization reaction to take place at around 350°C. Biomass decomposes in the absence of oxygen into its heavy and light hydrocarbons as well as char as shown in reaction 2, Table 1.4. The energy required to allow this endothermic reaction to take place is supplied by the energy released during the combustion reactions.

Combustion: The products formed during the biomass pyrolysis reaction are oxidized using either air, pure O_2, CO_2 or steam, as a result producing CO, CO_2 and H_2O. These reactions are exothermic; hence they supply heat for the endothermic biomass pyrolysis reaction to take place. (Reactions 3 – 5, Table 1.4)

Gasification: This step can also be called reduction process as it happens in the absence of oxygen. Reactions that take place in this step result in the formation of CO, CO_2, H_2 and CH_4. (Reactions 6 – 11, Table 1.4)

Table 1.4. Conventional gasification mechanism reactions

	Conventional Gasification Reactions
	Biomass drying
1	$C_nH_{2m}O_x$ (Wet Biomass) $\rightarrow C_nH_{2m}O_x$(Dry Biomass) + *water vapour*
	Biomass pyrolysis
2	$C_nH_{2m}O_x \rightarrow$ char + tar + syngas $(CO, H_2, CO_2, CH_4, C_nH_{2m})$,
	Combustion
3	$2C + O_2 \rightarrow 2CO$ (Oxidation)
4	$2CO + O_2 \rightarrow 2CO_2$ (Oxidation)
5	$2H_2 + O_2 \rightarrow 2H_2O$ (Oxidation)
	Gasification
6	$C + H_2O \rightarrow CO + H_2$ (Primary water gas)
7	$C + 2H_2O \rightarrow CO_2 + H_2$ (Secondary water gas)
8	$CH_4 + H_2O \rightarrow CO + 3H_2$ (Methane reforming)
9	$C + CO_2 \rightarrow 2CO$ (Boudouard)
10	$C + 2H_2 \rightarrow CH_4$ (Methanation)
11	$CO + H_2O \rightarrow CO_2 + H_2$ (Water gas shift)
	Tar Reforming
12	$Tar + H_2O \rightarrow CO_2 + H_2 + CO + hydrocarbons + \cdots$
	Hydrocarbon reforming
13	$Hydrocarbon + H_2O \rightarrow CO_2 + H_2 + CO$

Recently several technologies have been developed for biomass gasification processes [56, 57, 58]. Conventional gasification processes generally takes place with sub-stoichiometric quantities of oxidant (using air or enriched O_2 air with steam as the gasifying agent) [59]. Steam is also used to increase the concentration of hydrogen in the syngas and provide oxygen partial combustion of char. The fluidized bed gasification process in a fluidized bed

gasifier starts by blowing air/pure oxygen and steam from the bottom of the furnace causing bed particles to fluidize. The bed temperature is typically in the range of 950 – 1020°C to achieve high carbon conversation (90 – 95%), decomposing tar, phenols, oils and other liquid by-products. The bed material could be silica, sand, ash, etc. Fuel and sorbent material (optional for sulphur capture, usually lime or dolomite) are simultaneously injected into the gasifier. The amount of air injected is usually controlled since excess air will lead to complete combustion and enhanced NO and N_2O formation, whereas little oxygen will reduce the syngas calorific value. The syngas produced then travels through the freeboard up the riser, exiting the furnace. The factors affecting sorbent efficiency to capture sulphur are the sulphur content in the fuel, sorbent reactivity, bed temperature, and the amount of recycled solids [60 – 62].

However, drawbacks associated with using air or pure oxygen reduces the effectiveness of the process. The use of air as the gasification medium results in a highly N_2 concentrated syngas, reducing its energy density from 9 – 15 MJ/m^3 (using pure O_2) to 3.5 – 7 MJ/m^3 [27]. Whereas, using pure oxygen increases the parasitic energy as well as capital and operational costs of the whole process due to the requirement of an additional energy intensive air separation unit (ASU). Moreover, the high amount of tar formed during conventional gasification reduces the gasification efficiency (due to lower carbon conversion) and can block downstream equipment. Tar formation can be controlled via five different methods including mechanism methods, self-modification, thermal cracking, catalytic cracking, and plasma method. This as a result reduces blockage of downstream equipment and improves biomass utilization, however it comes at an increase in energy penalty and costs [41]. Alternatively, a new emerging gasification technology known as chemical-looping gasification (CLG) offering potentially higher efficiencies and lower costs is presented and discussed in the following chapter [32, 63].

1.10 Research Objective

- The aim of this research is to investigate and evaluate the feasibility of an alternative biomass utilization technology that would support leading a path towards a carbon neutral 2050 in the UK.
- This thesis will focus more on the use of chemical looping technology in the field of gasification. An extensive literature review has been conducted (Chapter 2) to identify gaps that are restricting the commercialisation of the current technology.
- Fill the gap within literature in understanding and testing the feasibility of this power generation technology in a large scale from a technical, economic and sustainability perspective
- Explore the life cycle energy, cost, CO_2 emission and environmental impact of establishing a large-scale power plant
- Understand the role and effect of the oxygen carrier and its effect in different operational conditions is not well investigated.
- Compare BCLGCC power plant to conventional thermochemical power plants

1.11 Thesis Outline

The first chapter sets a foundation for the political and environmental motives behind this research and the need for a push towards renewable and sustainable sources of energy, specifically focusing on biomass and its application in power generation. The second chapter conducts a comprehensive literature review on the subject of Biomass Chemical Looping Gasification (BCLG) and points out the gaps within literature, which allows for a clear methodology (chapter 3) to be laid out for the following three chapters (chapters 4, 5 & 6) to fill the gap within literature. Chapter 4 conducts a techno-economic & sustainability analysis of a BCLGCC power plants. Chapter 5 conducts a life cycle assessment. Chapter 6 conducts a set of bench-scale BCLG tests followed by some material characterization. Finally summarizing and suggesting further work in chapter 7.

2 CHAPTER 2: CHEMICAL LOOPING TECHNOLOGY

2.1 Introduction

Chemical looping technology is essentially the oxidation of the fuel using lattice oxygen (Metal Oxide: Me_XO_Y) in the form of a metal oxide instead of molecular oxygen (from air or pure oxygen) in a cyclic process. Instead of one gasifier reactor, two reactors are used, namely; a Fuel Reactor (FR) and an Air Reactor (AR). The oxygen rich metal oxide is injected into the FR as a solid form where it is reduced to Me_xO_{y-1}, hence supplying the oxygen source to the biomass in a lattice form. The reduced oxygen carrier (Me_xO_{y-1}) is then circulated into the (AR) closing the loop where it is oxidized back to its initial state (Me_xO_y) using oxygen from air. What gives this process an advantage compared to conventional power generation technology is the mitigation of an air separation unit for oxygen production or the mitigation of a carbon capture process when using air. Coupling biofuels with chemical looping and CCS technology could be an option that could lead the way for bio-energy carbon capture and storage (BECCS). There are several types of chemical looping technologies which can be used for different processes (gasification, combustion, reforming, etc.), using solid, liquid and gaseous fuels which result in the production of syngas/H_2 or heat for power generation [64 – 66]. These technologies are listed below and elaborated further in the following section.

1) Chemical looping combustion (**CLC**)
2) Chemical looping with oxygen uncoupling (**CLOU**)
3) Chemical looping reforming (**CLR**)
4) Chemical looping gasification (**CLG**)
5) Chemical looping coupled with water splitting (**CLWS**)

2.1.1 Types of Chemical Looping Technology

2.1.1.1 Chemical Looping Combustion (CLC)/Chemical Looping Oxygen Uncoupling (CLOU)

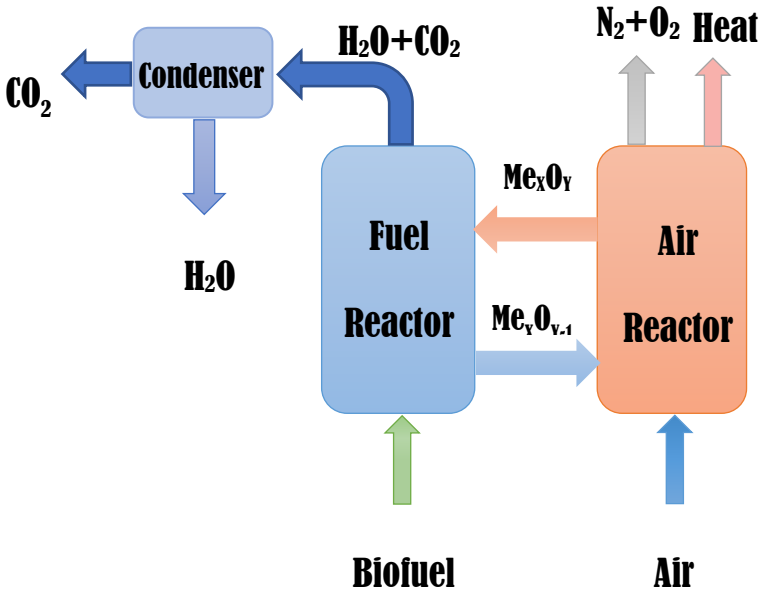

Figure 2.1. Configuration of a CLC/CLOU technology

As illustrated in Figure 2.1, in **CLC** the OC is reduced in the fuel reactor by reacting with the biofuel resulting in complete combustion (**R1**) to produce CO_2 and H_2O. The flue gas is then condensed to separate the H_2O and capture the CO_2 for storage or use. The reduced OC is then regenerated (oxidized) in the air reactor by reacting it with air (**R2**).

$$C_nH_{2m}O_P + (2n + m - p)Me_xO_y \rightarrow nCO_2 + mH_2O + (2n + m - p)Me_xO_{y-1} \quad \text{(R1)}$$

$$(2n + m - p)Me_xO_{y-1} + (n + 0.5m - 0.5p)O_2 \rightarrow (2n + m - p)Me_xO_y \quad \text{(R2)}$$

CLOU requires the use of specific oxygen carries that have the ability to react reversibly with gas phase oxygen at high temperature [67], hence able to release gaseous oxygen in the fuel reactor (**R3 – reversible reaction**) to react with the biofuel (**R4**) in a similar way to conventional combustion. The OC is regenerated by reversing **R3** in the air reactor.

$$2Me_xO_y \leftrightarrow 2Me_xO_{y-1} + O_2 \quad \text{(R3)}$$

$$C_nH_{2m}O_P + (n + 0.5m - 0.5p)O_2 \rightarrow nCO_2 + mH_2O \quad \text{(R4)}$$

CLC is usually focused on gaseous and liquid fuels, whereas **CLOU** is for solids. Solid fuels can also experience in-situ gasification integrated with **CLC (iG-CLC)**. This is done by drying and devolatilizing the solid fuel to produce char, volatile matter and water (**R5**), followed by gasfying the char with CO_2 and/or H_2O (**R6 – R7**), which are also the fluidizing medium. The OC then reacts with the volatile matter, H_2 and CO (**R8 - R10**). Finally, the final product of all the aforementioned processes is heat which is used to generate electricity.

$$Biomass \rightarrow Char(C) + Volatile\ matter + H_2O \quad \text{(R5)}$$

$$Char(C) + H_2O \rightarrow H_2 + CO + Ash \quad \text{(R6)}$$

$$Char(C) + CO_2 \rightarrow +2CO + Ash \quad \text{(R7)}$$

$$nMe_xO_y + Volatile\ matter \rightarrow nMe_xO_{y-1} + mCO_2 + pH_2O \quad \text{(R8)}$$

$$Me_xO_y + H_2 \rightarrow Me_xO_{y-1} + pH_2O \quad \text{(R9)}$$

$$Me_xO_y + CO \rightarrow Me_xO_{y-1} + CO_2 \quad \text{(R10)}$$

2.1.1.2 Chemical Looping Water Splitting (CLWS)

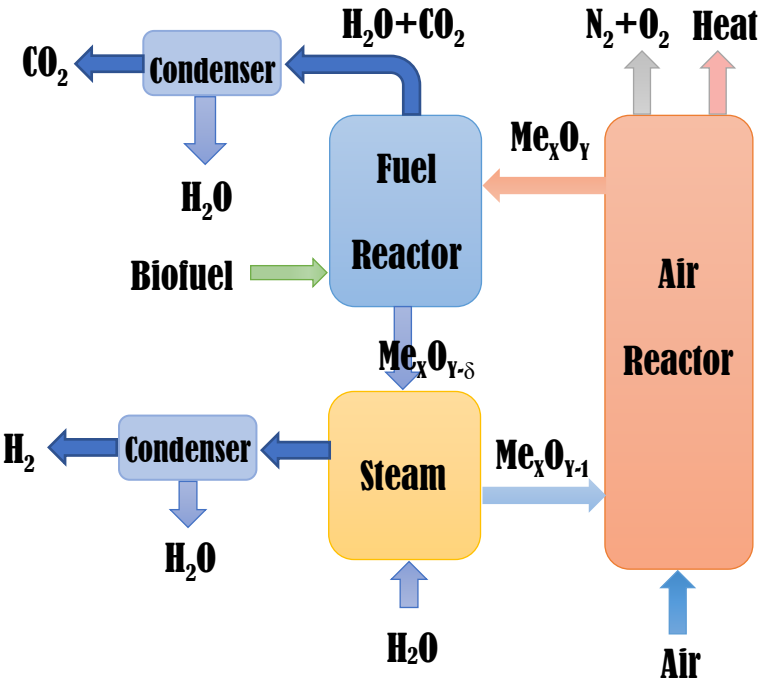

Figure 2.2. Configuration of a CLWS technology

CLWS (Figure 2.2) is similar to CLC in the sense that fuel is combusted using an OC in a fuel reactor (**R11**). However, the OC is then sent to a steam reactor where it reacts with water to produce H_2, while at the same time partially re-oxidizing the OC (**R12**). The oxygen carrier is then sent to an air reactor where it is completely regenerated by reacting it with air (**R2**). This process can be used for solid, liquid and gaseous fuels if coupled with the appropriate CLC process.

$$C_nH_{2m}O_P + (2n + m - p)Me_xO_y \rightarrow nCO_2 + mH_2O + (2n + m - p)Me_xO_{y-\delta} \quad \text{(R11)}$$

$$Me_xO_{y-\delta} + H_2O \rightarrow Me_xO_{y-1} + H_2 \quad \text{(R12)}$$

2.1.1.3 Chemical Looping Reforming (CLR)/Chemical Looping Gasification (CLG)

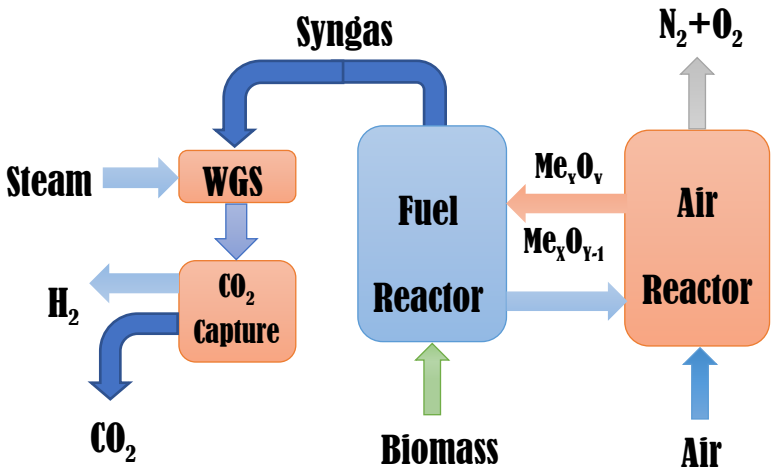

Figure 2.3. Configuration of a CLR/CLG technology

CLG and **CLR** (Figure 2.3) processes focus on the generation of syngas/H_2 instead of heat for electricity generation. The syngas can be sent to a Fischer-Tropsch reactor to produce chemical (NH_3, methanol, synthetic fuels, etc.). **CLR** is for gaseous and liquid fuels, whereas **CLG** is for solid fuels. The reactions that take place in the fuel reactor are the partial oxidation with the metal oxide (**R13**), steam reforming (**R14**) and the water-gas shift reaction (**R15**).

$$C_nH_{2m}O_P + (2n + m - p)Me_xO_y \rightarrow nCO + mH_2 + (2n + m - p)Me_xO_{y-1} \quad \text{(R13)}$$

$$C_nH_{2m}O_P + H_2O \rightarrow nCO + mH_2 \quad \text{(R14)}$$

$$CO + H_2O \leftrightarrow CO_2 + H_2 \quad \text{(R15)}$$

If the end product is to have H_2, the syngas is passed through a water-gas shift (WGS) unit where the syngas reacts with steam as shown in **R14** to produce more H_2 and CO_2. The CO_2 is then captured using pre-combustion capture processes to produce pure H_2. The H_2 can then be sent to a combined cycle where it is combusted to generate electricity or used as a transport fuel.

When it comes to choosing the metal oxide also known as the oxygen carriers and weighing their pros and cons, while comparing between different options and their categories several things should be taken into consideration which is discussed in section 2.1.5. Moreover, even though the system seems to be simple as previously explained in this section but like any new technology, they come with some drawback when it comes to deployment. These will be elaborated on in section 2.1.6.

2.1.2 Mechanism and Kinetics of Solid Biofuels

Since this thesis will only focous on solid biofuels, the following mechnisms of iG-CLC, CLOU and CLG will be elaborated on since they are specific for solid fuels. With all the three different processes, biomass is initially dried then pyrolysed to produce char, tar and pyrolysis gas (H_2, CO, CO_2, CH_4, C_XH_Y, etc.) in the fuel reactor. In iG-CLC, the pyrolyisis gas completely reacts with the oxygen carrier to produce CO_2 and H_2O, whereas the tar is catalytically cracked hence converted into a gas which reacts with the oxygen carrier. The char is gasificed by steam/CO_2 injected into the reacter which produces syngas which reacts with the oxygen carrier. CLG experiences the same mechanism as iG-CLC however with less oxidents (oxygen carrier/ H_2O/CO_2), hence the final product is syngas (CO and H_2). In CLOU, the oxygen carrier releases O_2 at high temparatures which reacts with the char, tar and pyrolysis gas resulting in complete combustion. The oxygen carrier also acts as a catalyts in cracking tar. Figure 2.4 gives a visual illustrates of the three mechanisms.

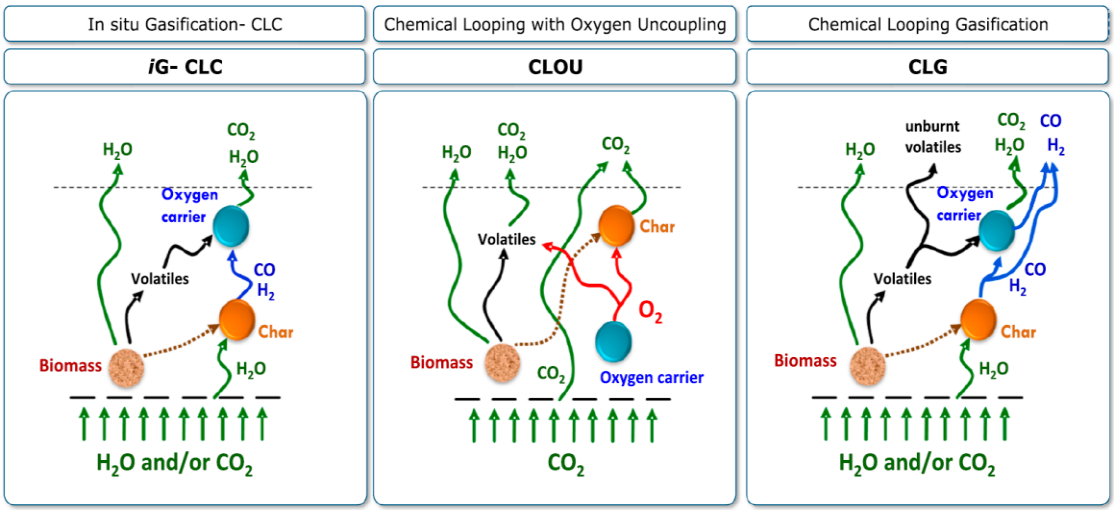

Figure 2.4. Mechanism for solid biofuels in chemical looping processes [64]

Referring to the reaction mechanism mentioned earlier, the biomass gasification process can be categorized into three sections: 1) biomass pyrolysis, 2) gas−solid reaction between the pyrolysis gas and the OC, and 3) solid−solid reaction between the biomass char and the OC.

To describe the kinetics of the first two sections (biomass pyrolysis and gas-solid reaction), the shrinking core model is commonly used [68, 66]. This model describes the solid particle as it gradually shrinks throughout the reaction (biomass devolatilization and lattice oxygen reaction with volatiles on the OC surface), hence starts with consumption from the surface of the particle inwards [69, 70]. However, there are plenty of drawbacks associated with the shrinking core model since it assumes particle sphericity and that it would remain spherical after the reaction.

Regarding the solid-solid reaction between biomass and the OC, two possible models are suggested namely, the random nucleation and subsequent growth model [71, 72] and the modified random pore model [73, 74]. The biomass char and OC react on the surface, gasifying the char into syngas while a layer of residue is deposited on the OC surface, confirming the first model. The latter model takes into consideration the competition between expansion and overlap in the pores. Solid-solid reactions tend to require higher residence time, hence tend to slow down reactions.

2.1.3 Advantages of Biomass CLG

This thesis will focus on solid biomass fuel to generate syngas/H_2, hence will be using CLG process. Biomass chemical looping gasification (BCLG) is associated with several potential advantages compared to conventional gasification: firstly, the oxygen carrier can provide a source of oxygen while avoiding the cost depleting process of adding an air separation unit. Secondly, the lattice oxygen has a higher chance of partially oxidizing the fuel compared to molecular oxygen (stronger oxidizing strength), resulting in an increase in a higher quality syngas (less CO_2). Moreover, tar cracking is enhanced due to the oxygen carrier's catalytic effect during biomass pyrolysis [75], as a result a downstream thermal cracking process can be eliminated, hence improving the overall gasification process. Furthermore, chemical looping processes result in a reduction in exergy loss due to it undergoing moderate flameless gasification compared to the conventional thermochemical processes which undergoes more intense flame gasification [76]. Finally, an appropriate oxygen carrier should be selected to ensure adequate properties to convert the pyrolysis gas and for catalytic tar cracking, while maintaining a low degree of combustion to prevent a decrease in the syngas heating value.

2.1.4 Biomass Feedstock

Several experiments have been conducted on different types of biomass in CLG, with most focusing on terrestrial and solid waste biomass and very little on aquatic biomass. The different types of biomass that have been used can be classified into 3 categories namely terrestrial, aquatic and solid waste. From the terrestrial biomass 7 different types of biomass have been tested including rice husk [77 - 79], rice straw [80 - 82] wheat straw [83], pine [84 - 86], corn stalk [87], peanut shell [87], eucalyptus wood [88] and vegetable oil [89], whereas for aquatic biomass only chlorella vulgaris [90, 91] was tested and for solid wastes, sewage sludge [92] and polyethylene [93] were tested.

There are several factors within biomass that affect the efficiency and kinetics of the CLG process. Hight percentage of fixed carbon according to the proximate analysis could lower the gasification rate and decrease efficiency, this is due to the slow solid-solid reaction between

the OC and the char. Moreover, biomass has a high concentration of alkali/alkaline earth metal which improves the performance in the short term [94, 95], but also causes the ash melting point to decrease hence result in sintering [96], therefore reducing the lifespan of the OC. Choosing a biomass with low ash contact can increase OC lifetime. According to biomass compositions, terrestrial biomass in general has the highest volatiles to fixed carbon ratio with a low ash content, therefore more research has been conducted on them with more focus on pine. Another option is chlorella vulgaris (aquatic) which has a high volatile to fixed carbon ratio, higher than the rest of the terrestrial biomass with higher ash and nitrogen (~10wt.%) content. From the solid waste, sewage sludge has nearly double the reactivity compared to terrestrial biomass due to the double in volatile to fixed carbon ratio value, it has a much higher ash composition (~50%). Finally, since biomass has lower sulphur, there is less chance of it poisoning the OC, however, it should be considered when using solid waste.

2.1.5 Oxygen Carrier (Metal Oxide)

Oxygen Carriers (OC's) play an important role in assessing the feasibility and efficiency of the CLPs. They go through multiple cycles, which can result in a decrease in their physical integrity and chemical strength. Such processes require OC's to possess certain qualities, ensuring process optimization. These qualities are numerous which include long-term stability, environmental friendliness, physical strength, redox reactivity, low production cost, high melting point, resistance to agglomeration and attrition [97]. Some examples of OC are iron, cobalt, manganese, nickel, and copper oxides. However, OC can come in many different forms which is discussed later in this chapter. Before analysing the different oxygen carriers based on the aforementioned characteristics, the redox potential of the oxygen carriers should be determined. The Ellingham diagram provides a complete study demonstrating the standard Gibbs free energies of several oxygen carriers as a function of temperature as shown in Figure 2.5. In simple terms the Ellingham diagram is used to predict the spontaneity and the shift of reaction equilibrium (extent of reaction) at a certain temperature between a metal, its oxide, and oxygen. However, Ellingham's diagram can be adjusted to assist in selecting the suitable

OC for the various CLPs in Figure 2.5B. This is done by splitting the diagram into three different zones based on three reactions;

Reaction 1: $2CO + O_2 \rightarrow 2CO_2$ ➔ Line 1

Reaction 2: $2H_2 + O_2 \rightarrow 2H_2O$ ➔ Line 2

Reaction 3: $2C + O_2 \rightarrow 2CO$ ➔ Line 3

These zones represent the oxidizing properties of the metal oxides.

Zone A: Above line 1 on Figure 2.5B. Generally strong oxidizing properties and can be used for CLC and CLG processes. Metal oxides in this zone include; NiO, CoO, CuO, Fe_2O_3 and Fe_3O_4.

Zone B: Between lines 2 and 3 on Figure 2.5B. Weaker oxidizing properties compared to metal oxides in zone A, hence can only be used for CLG processes. Metals in this zone include CeO_2 and FeO.

Zone C: Below line 3 on Figure 2.5B. Metal oxides cannot be used as an oxygen carrier, therefore considered inert for this application. Metals in this zone include Cr_2O_3, TiO_2, ZrO_2, Al_2O_3 and SiO_2.

Transition Zone: Between lines 1 and 2 on Figure 2.5B. Metal oxides have the ability to act as partial oxidizers, converting H_2 into H_2O while keeping CO unreacted, producing high H_2O content in the syngas. Metals in this zone include SnO_2. These are generally used to improve the mechanical properties and lifespan of the OCs.

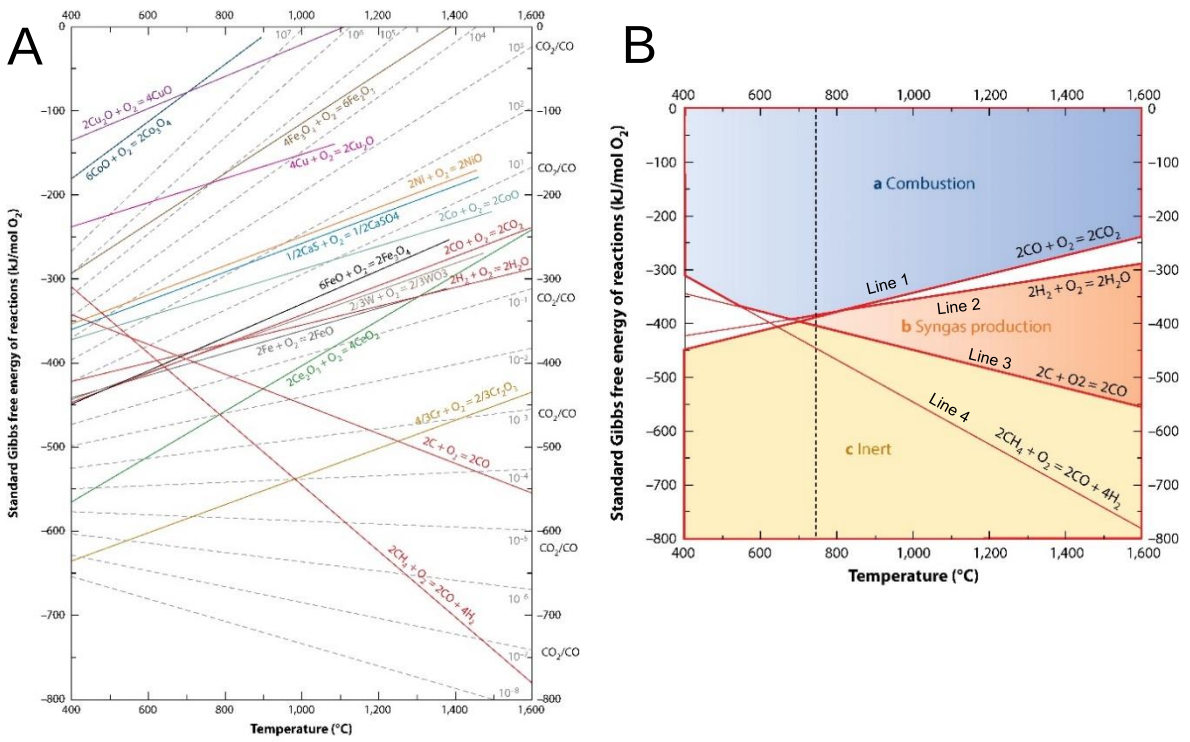

Figure 2.5. Ellingham diagram showing the standard Gibbs free energies of several oxygen carriers as a function of temperature [97]

Based on the aforementioned, CLG can be achieved via two approaches. The first approach is by using metal oxides from zone B to mainly produce syngas, which cannot further oxidize due to thermodynamic restrictions. Second approach is by using sub-stoichiometric amounts of metal oxides from zone A, hence preventing complete oxidation. However, the latter approach has been researched more and appears to be more promising. Ni, Co, Mn, Cu and Fe-based oxygen carriers are the most common ones being researched into. A comparison between the advantages and disadvantages of these metal oxides is shown in Table 2.1. Comparing between all these materials as oxygen carriers, Fe seems to be the most attractive option due to its low cost, ability to withstand conditions inside a combustor (good stability at high temperature), non-toxic in nature and has no negative environmental impact. Even though it has its down sides as a low oxygen transport carrier, it will be used in this process for CLG instead of CLC which gives it a slight advantage. Other oxygen carrier materials do have their strengths; however, this thesis will focus on iron-based oxygen carriers. Table 2.2 summarizes the reactions taking places in a chemical looping gasification process using an

iron-based oxygen carrier. OCs can also appear in several other forms and not just as metal oxides including oxide mixtures, polymetallic oxides, natural ores, and industrial materials.

Table 2.1. Comparing between the common types of metal oxide oxygen carriers [98, 65]

Metal Based Material	Advantages	Disadvantages
Nickel	• High catalytic reactivity • Can reduce NO_X emissions	• Increase in circulation results in a decrease in metallic Ni, hence reducing catalytic performance • Low porosity leads to suppressed reaction rate • Can be poisoned by sulphur • High cost • Toxic
Copper	• High reactivity • High oxygen transfer capacity • Relatively low toxicity • Sulphur in fuel do not affect performance	• Causes agglomeration due to low relatively melting point (1085°C) • Relatively high cost • Low resistance to attrition
Manganese	• Low toxicity • Inexpensive	• Reactivity can be suppressed in the presence of sulphur • Reacts with some typical supporting materials resulting in stable and unreactive materials
Cobalt	• High reactivity • High oxygen transport capacity	• High cost • Environmental concerns • Reacts with some typical supporting materials resulting in complete loss of reactivity • Negative health effects
Iron	• Low cost • High mechanical strength • High melting point • Environmentally benign • No tendency for carbon or sulphide/sulphate formation	• Relatively low oxygen transport capacity • Reactively low reactivity • Agglomeration issues

Oxide mixtures: A mixture of oxides are added to improve the reactivity within the reactor. Some oxides can be added either as catalysts, oxygen suppliers or have bifunctional capabilities. Alkali/Alkali earth metal oxides can be used as a catalyst to enhance reduction capability of Fe-based OCs, but cannot act as oxygen suppliers [99, 100]. Calcium oxide can be used to capture CO_2 produced during the reaction, hence increasing concentration of H_2 in the product stream [101, 102]. Other transition metals can be added in combination which

can serve as catalysts as well as oxygen suppliers [103 - 105]. However, the downside with oxide mixtures is that they cannot maintain their structures and hence their function and start forming new solid solutions after multiple cycles, therefore not maintaining their effectiveness throughout the process.

Polymetallic oxides: These are OCs made up of two or more metallic ions which result in a synergistic effect during the gasification reaction. In general, Fe^{3+} is coupled with other metallic ions to form polymetallic oxides since they have good characteristics yet low reactivity. Different metals can my used to tune the reactivity of the Fe-based OC such as Ni in $NiFe_2O_4$, enhancing its tar removal ability, yet reducing syngas quality due to higher oxidation ability [106, 107]. Another example is $BaFe_2O_4$ which has a high reactivity with char (solid-solid reaction), but weaker reactivity with the syngas hence having a good syngas quality [108]. $CaFe_2O_5$ and $CaFe_2O_4$ can also be used due to their high reactivity, with the former having the ability to maintain its surface structure compared to the latter, hence enduring multiple cycles [109]. Other polyoxide oxygen carriers have also been tested including $MnFe_2O_4$, $LaFeO_3$ and $CoFeO_4$ which showed better tar cracking capabilities compared to Fe_2O_3 [88, 110]. With multiple cycles, some metal ions might break from the main structure which could result in a decrease in the reactivity. When some metal ions interact with the ash, it could promote sintering.

Natural ore: Natural ores have an advantage compared to synthetic OCs due to their high abundance, low cost and relatively good mechanical strength. Since OCs generally wear out with time, the reactor should be continuously supplied with fresh OC, and natural ores are a suitable option compared to synthetic fuels. Different types of natural ores have been previously tested including hematite [78], manganese ore [77, 111], Ilmenite [112] and copper ore [113, 114] commonly used and reported in literature for CLG. However, due to their low reactivity some have modified them and with oxides to increase their reactivity and selectivity [103].

Industrial waste: Industrial waste containing metal oxides that undergo pre-treatment can sometime be used as OCs**.** They tend to have low reactivity and undergo calcination for activation before being used. Some examples are red mud [115] and copper slag [116] which are residual wastes from the aluminium industry. Red mud is also a waste from leaching bauxite. The amount of active metal oxides in industrial wastes varies from industry to industry as well as process conditions.

Table 2.2. Chemical looping gasification mechanism reactions [117]

Rxn No.	Reaction	$\Delta H_{1073\ K}$/ (kJ/mol)
	Biomass pyrolysis	
1	$Biomass \rightarrow char + tar + syngas\ (H_2, CO, CO_2, CH_4, C_xH_y \dots)$	ΔH > 0
2	$C + H_2O \rightarrow H_2 + CO$ (Water – Gas Reaction)	+100.58
3	$CH_4 + H_2O \rightarrow 3H_2 + CO$ (Methane Reforming)	+224.26
4	$C + CO_2 \rightarrow 2CO$ (Boudouard Reaction)	+170.86
5	$CO + H_2O \rightarrow H_2 + CO_2$ (Water – Gas Shift)	-35.14
	Intermediates oxidation into secondary products by Fe_2O_3	
6	$H_2 + 3Fe_2O_3 \rightarrow H_2O + 2Fe_3O_4$	-5.83
7	$H_2 + Fe_2O_3 \rightarrow H_2O + 2FeO$	+30.27
8	$CO + 3Fe_2O_3 \rightarrow CO_2 + 2Fe_3O_4$	-40.97
9	$CO + Fe_2O_3 \rightarrow CO_2 + 2FeO$	-4.87
10	$CH_4 + 12Fe_2O_3 \rightarrow 2H_2O + CO_2 + 8Fe_3O_4$	+165.90
11	$CH_4 + Fe_2O_3 \rightarrow 2H_2 + CO + 2FeO$	+218.53
	Simultaneously liquid tar is catalytically cracked using oxygen carrier particles	
12	$tar \rightarrow H_2 + CO + hydrocarbons$	ΔH > 0
	As for the char produced, solid-solid reactions can occur	
13	$Char + Fe_2O_3 \rightarrow CO_2 + Fe_3O_4$	ΔH > 0
14	$Char + Fe_2O_3 \rightarrow CO + Fe_3O_4$	ΔH > 0

2.1.6 Challenges

Although BCLP's propose a potential alternative to substitute conventional thermochemical gasification processes, there are still some challenges associated with finding a suitable oxygen carrier that should be overcome before commercialisation.

Deactivation of looping materials during biomass conversion [65, 118]

- **Agglomeration:** The formation of clusters of oxygen carriers due to the adhesion of solid particles as a result of low melting point, this can result in bed defluidization and oxygen carrier deactivation. Iron based oxygen carriers in particular can result in agglomeration when mangnetite (Fe_2O_3) is reduced to wustite (FeO). However, when doping with composite support it can also be observed that mechanical strength and reactivity increases, hence reduces agglomeration.
- **Attrition:** Due to the nature of the fluidization process. As the OC circulates between the fuel and air reactors, it experiences a great deal of physical stress which can result in a reduction in size and chemical strength. This is very crucial for its lifetime.
- **Carbon Deposit:** The deposition of carbon on the OC can reduce its reactivity and performance. The extent of carbon deposition depends on several factors including; inert support, metal oxide, oxygen availability and OC/steam ratio.
- **Sulphur:** H_2S and COS are produced from biomass gasification processes. Reaction between the OC and sulphur compounds is inevitable. This can cause deactivation of OC's and formation of low melting point compounds resulting in problems during the process. However, sulphur content in biomass is less than in coal, giving it an advantage.
- **Ash:** Depending on the composition of ash, it can demonstrate negative or positive results. High concentration of Ca and Mg increases the melting point of the ash, hence reducing any signs of agglomeration and sintering. Whereas, the presence of Na or K reduces the melting point and can encourage agglomeration and sintering. Additionally, SiO_2 rich bed can react with K producing potassium silicate, resulting in major particle

sintering. Moreover, potassium can form a bond with Fe, hence weakening the Fe – O bond, resulting in the escape of the lattice oxygen from the oxygen carrier.

2.2 Reactors

2.2.1 Basic Principle of Fluidization

Fluidized beds reactors (FBRs) were first industrialised during the early 1930's by the Winkler process for coal gasification [119]. The basic principle behind gas-solid fluidised bed reactors is to suspend particles in a column, resulting in enhanced heat and mass transfer during chemical reactions. A packed bed of particles (bed material, sorbents, ash and solid fuel) is placed over a grate-like air distributer at the bottom of a vessel. Air is blown through the bottom of the reactor, causing the particles to move freely, hence taking a hydrodynamic fluid property. At the point when the drag force caused by the injected gas equals the weight of the particles, they behave as a fluid (can also be referred to as the 'liquid state'), hence the name fluidised bed. This ensures even mixing between fuel and air, along with even heat distribution.

Advantages associated with fluidised bed reactors (FBR's) are summarized by Khan et al., [33] as the following:

1) Uniform temperature distribution
2) High solid-gas exchange area
3) Ability to burn low-grade fuels with low calorific value
4) Ability to burn high ash content fuels
5) Ability to burn high moisture content fuels
6) Emissions performance (enhanced sulphur capture)
7) Re-use of non-hazardous by-products (e.g. gypsum)
8) Operated at lower temperatures resulting in less NO_X formation

However, they are still associated with several disadvantages including:

1) Requirement of a highly efficient solid – liquid separation process due to the formation of high amount of dust
2) High solid velocities result in erosion
3) Agglomeration of solid particles
4) Reduction in efficiency due to high pressure drop along the riser

FBRs are categorized into several technologies depending on their fluidization velocity. Figure 2.6 presents the four different categories, namely, fixed bed, bubbling fluidized bed, circulating fluidized bed and pneumatic transport reactor. However, this thesis will focus on bubbling and circulating beds as they are used for power generation (combustion/gasification) applications [60]. Although both follow the same principle, they vary in design parameters, which is simply due to the difference in fluidization velocity, bubbling fluidized bed (BFB) (1.0 – 3.0 m/s) and circulating fluidized bed (CFB) (3.0 – 6.0 m/s). Fixed bed has negligible fluidization velocity, whereas pneumatic is higher than 6 m/s [27].

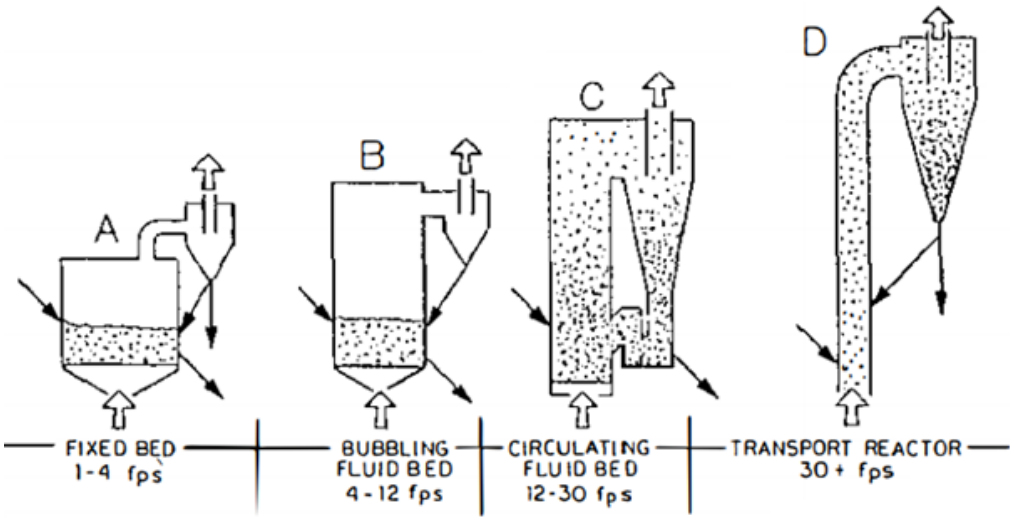

Figure 2.6. Fluidization Regimes, fps: feet per second [60]

2.2.2 Differences Between CFB and BFB

A BFB is generally divided into two section: the bed and the freeboard. The low fluidization velocity of bubbling fluidized gasifiers results in the bed material mainly fluidizing in the lower section of the furnace, causing a non-uniform and violent mixing (Figure 2.7A) which causes some particles to jump up to the splashing zone (section of the freeboard, just above the bed).

Depending on how small the particle size is, some could elutriate with the flue gas out of the boiler. However, the particle concentration density is high at the bottom of the boiler (bed) but lean up the freeboard. The bed acts as a heat buffer, hence controlling the heat transfer between particles in the bed. This coupled with the low fluidization velocity and high residence time in the boiler, makes it more suitable for fuel with varying moisture content, large particles and low calorific value fuels. Due to most of the combustion/gasification taking place in the bed, it is usually lined with a refractory layer, protecting it from high temperatures, corrosion, and erosion [120, 121].

The concentration of particles in a BFB can vary from high to low. When particle concentration is low, particles kinetics dominate solid viscosity and solid pressure is close to zero. Whereas at high solid concentrations, frictional stresses dominate solid viscosity and solid pressures increase. The drag between phases describes the momentum exchange and is expressed by the drag coefficient in the momentum equation. The Syamlal & O'Brien drag model is expressed as shown in Equation 2.1.

$$\Phi_{sg} = C_D \frac{3\varepsilon_s \varepsilon_g \rho_g |U_g - U_s|}{4 v_r^2 d_s} \quad [2.1]$$

The minimum fluidization velocity (Umf) is defined as the superficial gas velocity when the drag force of the upward moving gas is equal to the weight of the particle bed and is expressed as shown below in Equation 2.2 [122].

$$U_{mf} = \frac{\varepsilon_{mf}^2 (1-\varepsilon_{mf})(\rho_s - \rho_g) g}{\Phi_{sg}} \quad [2.2]$$

On the other hand, CFB, Figure 2.7B, require a higher fluidization velocity, which allows the particles to travel higher up the freeboard through the 'travelling zone'. This high fluidization velocity creates high turbulence, which improves solid mixing as well as heat and mass transfer. Most particles fall back down along the walls causing internal recirculation, whereas other particles escape with the syngas from the top of the furnace. Before the flue gas is sent to the convective pass, it is passed through a cyclone to recycle the particles (bed material and fuel) back into the bed, ensuring constant bed material – to – fuel ratio. This rigorous mixing of the particles results in a better distribution across (an increasing density gradients

down the furnace) the furnace, hence a homogenic temperature distribution [120]. Figure 2.7 shows a schematic comparison between BFB (A) and CFB (B).

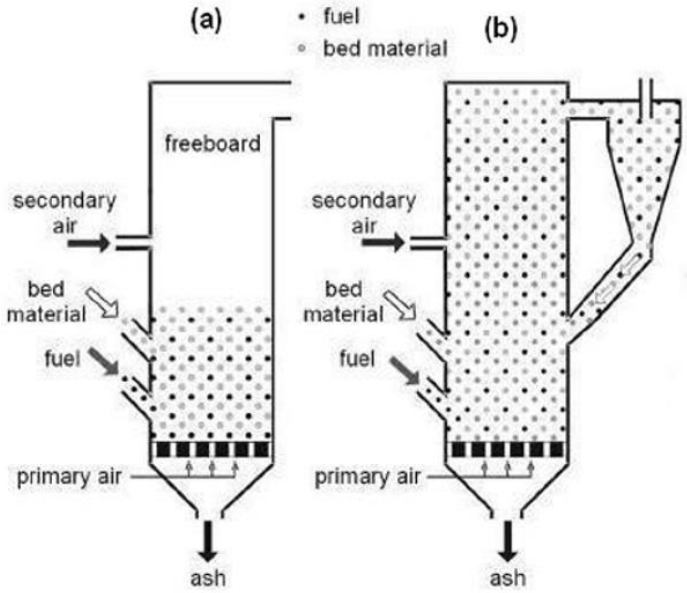

Figure 2.7. Schematic representations of a BFB (a) and a CFB (b) [27]

2.2.3 Chemical Looping Processes Reactor

Chemical looping processes displayed in Figure 2.1, Figure 2.2 and Figure 2.3 can be performed in various types of reactor configurations. Those configurations can be categorized as either interconnected fluidized beds (circulating or bubbling), moving bed connected to a fluidized bed riser or alternating fixed/packed beds.

In general, most chemical looping processes employ an interconnected fluidized bed configuration for the air and fuel reactors which specifically define the type of fluidized bed reactor used for both reactors. Several factors come into place to define the configuration to be used including the oxygen carrier reactivity, but most significantly the size of the unit. At low scale, the following configurations have been previously tested:

1) Bubbling fluidized beds for both reactors [123]
2) Annular shape reactor with double circulating fluidized bed (CFB) loops [124]
3) Spout-fluid bed instead of a bubbling bed for the fuel reactor [125]
4) Series of three interconnected bubbling beds (one fuel and two air reactors) [126]

5) Two bubbling beds in series to improve volatiles conversion [127]

However, the issues associated with bubbling fluidized bed (BFB) fuel reactors at larger scale, is that they are susceptible to the risk of significant unconverted fuel gas bypassing through the bubble phase, which is not tolerable in some CLPs. The gas slip can be reduced by decreasing the fluidization numbers in the reactor, while increasing the bed height. However, as a result the bed cross sectional area in the fuel reactor would increase, hence requiring more solid inventory. Therefore, Kolbitsch, et al., [128] suggested a turbulent or fast fluidization regime in the fuel reactor, allowing gas-solids contact over the whole height of the reactor and potentially allowing operation with lower solid inventories. This was used in the 120kW$_{th}$ unit for gaseous fuel at the Technical University of Vienna (TUV) with a circulating bed air reactor connected through a hydraulic link. Other pilot plants developed two interconnected circulating fluidized bed reactors for each, fuel and air reactor [129, 130, 131, 132].

Furthermore, Ohio State University (OSU) proposed a moving bed fuel reactor configuration in its design [133], where the oxygen carrier flows counter currently to the fuel in the fuel reactor. In this design, the volatile matter rises to the top of the reactor where it reacts with the oxygen, whereas the char reacts at the bottom of the reactor. All moving bed fuel reactors were designed for units operating at 25 kWth, however scaling up the moving beds can be a challenge due to the importance of ensuring a homogeneous solid and heat mixing within the reactor. Regarding the air reactor, it is generally a circulating fluidized bed connected to a riser. A key aspect for his configuration is ensuring an appropriate oxygen carrier particle size is used that would suit the air and fuel reactors. A moving bed reactor configuration has been used widely for CLWS process for the fuel and steam reactors [134].

Finally, packed beds have also been tested for CLT [135, 136]. It consists of two alternating fixed beds for alternating oxidation and reduction reactions to take place in two separate reactors. The time between alternating between both reactors is used to mildly fluidize the

beds after each cycle to level off concentration and temperature profiles. This configuration is generally used to test at higher pressures (1–3 MPa).

2.2.4 CLG Milestones and Pilot Scales

Chemical looping gasification of solid biomass has come a long way since it was first tested by Matsuoka et al. [137] in 2006. A lot of tests followed it using fixed and small-scale fluidized bed reactors, which focused on testing reaction conditions and mechanism. Recently in 2014, the first BCLG operation in a 10kW continuous circulating interconnected fluidized bed was established at the Guangzhou Institute of Energy Conversion [138]. The fuel reactor consists of a bubbling bed while the air reactor is made up of a bubbling fluidized bed at the bottom with a fast-fluidizing bed across the height of the reactor, with both reactors connected with a loopseal. The following year a 25kW dual fluidized bed reactor was established at Southeast University by Huijin et al. [81]. The design consisted of a fast-fluidizing fuel reactor, a bubbling fluidized steam reactor and a loopseal air reactor. Table 2.3 summarizes all the CLG currently established pilot scale continuous reactors.

Table 2.3. List of chemical looping gasification continuous units

Institute	Initials	Location	Configuration	Power (kW)	Reference
Southeast University	SU	Guangzhou (China)	BFB-CFB	0.6	93, 139
Guangzhou Institute of Energy Conversion	GIEC	Guangzhou (China)	BFB-CFB	10	138, 140, 141
Southeast University	SU	Guangzhou (China)	BFB-CFB	25	81, 79

2.3 Chemical Looping Gasification Research

Research into chemical looping gasification processes has been increasing in the past two decades. Experiments have been conducted on pilot scale, testing different types of oxygen carriers, biomass sources, conditions and set up which demonstrated higher efficiencies due to less energy penalties compared to conventional power generation processes [83-88].

However, this section will focus on discussing and analysing CLG experiments conducted on sawdust pine biomass using natural hematite as an oxygen carrier.

2.3.1 Experimental investigations and Process Variables

2.3.1.1 The Use of Hematite

Thermal gravimetric analysis shows that iron ore does not decompose during the heating process, suggesting that oxygen cannot escape as gaseous phase but remains as lattice oxygen [117]. In another paper, Huang et al., [142] demonstrates using a bubbling bed in a transport furnace that lattice oxygen in natural hematite can act as an oxidizing agent for gasification reactions. The author compared between using quartz and natural hematite as bed material and observed that gas product concentration remains relatively constant, low CO_2 and CO concentrations with time when using quartz. However, when natural hematite is used, the concentration of the syngas produced changed with time, initially high CO_2 concentration and low H_2, CH_4 and CO concentrations were observed followed by a decrease and an increase in the respective concentrations as the process carried on due to the depletion of oxygen in the oxygen carrier. The gasification efficiency when using hematite bed material (82.57%) is 19.21% higher than when using quartz (63.36%), which is due to the higher carbon conversion hence higher gas yield. However, as the oxygen carrier went through several cycles, its oxidation ability decreases. Moreover, BCLG demonstrated a lower concentration of CO and CO_2 compared to air/oxygen gasification, which is due to the stronger oxidizing effect of molecular oxygen. A similar experiment was set up by He et al., [143] where he compared between using silica sand and hematite particles as bed materials with parallel conclusions obtained.

Huang et al., [144] compares between biomass steam gasification (BSG), biomass pyrolysis (BP) and biomass chemical looping gasification (BCLG). The author concludes that BSG produces more CO_2 and H_2 compared to BP, because of steam decomposition, resulting in carbon being oxidized and H_2 being produces via the steam reforming reaction. Moreover, BCLG produces more CO_2 compared to BP as a result of hematite particles reduction

reactions, therefore showing that hematite can act as an oxidizing agent. However, it was noted that carbon conversion of BSG was higher than BCLG, suggesting that steam's reactivity is higher than the hematite oxygen lattice particles. Similar results were obtained by the same author in a different article [145] when comparing between BSG using silica sand bed and biomass gasification lattice oxygen (BGLO) which he defined as similar to BCLG but with the addition of steam. The author concluded that both steam and hematite can be used as an oxygen source and would consequently reduce the amount of steam required in BGLO for the same gas yield compared to BSG.

In addition, iron ore-based oxygen carrier has been proven from previous literature to have a double effect on gasification [146]. On one hand, it acts as an oxygen source through its lattice structure for biomass gasification. On the other hand, it provides a catalytic effect in tar cracking and reforming.

2.3.1.2 Effect of Temperature

CLG is a thermochemical process, which suggests that it is highly affected by variation in temperature. Previous literature, in general, have been in agreement regarding the effect of temperature. Huang et al., [117] set up a bubbling fluidized bed reactor placed in a transport furnace where he tested the effect of temperature on a BCLG reactor. The author observed that an increase in fuel reactor temperature favours an increase in H_2 and CO yields, yet a decrease in CO_2 and CH_4 yields. This can be explained according to the reactions taking place during the chemical looping gasification mechanism. The endothermic nature of the biomass pyrolysis reactions hence increases the carbon conversion (reactions 1 – 4, Table 2.2) favouring an increase in CO and H_2 concentrations, hence observed experimentally. Additionally, an increase in temperature shifts equilibrium of the endothermic CH_4 combustion reactions (reactions 10 and 11, Table 2.2) to the right, resulting in a decrease in CH_4 concentrations. However, this increase shifts the exothermic CO combustion reactions (equations 8 and 9, Table 2.2) towards the left to decrease CO concentration. The increase in temperature results in an increase in gas yield hence an increase in gasification efficiency.

This has been observed in several papers including [143, 145, 147, 148]. However, they experienced different percentage changes in concentration with temperature depending on the conditions (oxygen carrier, pilot plant set up, etc.).

Zeng et al, [149] set up a rig for a dual fluidized bed gasifier, which consisted of a fuel and a steam reactor for gasification and an air reactor to regenerate the oxygen carrier. The author tests the effect of increasing the temperature of the steam reactor which results in an increase in H_2 and a decrease in CO and CH_4 concentrations up to 910°C. Further increase has no effect on the gas concentration. Simultaneously, the cold gas efficiency and H_2 yield increases up to 910°C followed by a slight decrease as temperature further increases.

On the other hand, Ge et al., [79] used an interconnected fluidized bed and observed an overall decrease in H_2, CO and CH_4 concentrations, yet an increase in CO_2 as temperature increases, which contradicts other papers. It can be suggested that excess oxygen carrier was used in the reaction. This can be supported since the percentage of hematite in the bed allowed the temperature to remain stable without external energy input, suggesting that there could be enough OC to completely combust the biomass.

Wei et al., [141] Investigated the effect of increasing fuel reactor temperature on the air reactor flue gas. The author concluded that an increase in temperature reduced the amount of CO_2 produced in the air reactor, this is due to the increase in gasification/combustion of char particles in the fuel reactor, therefore decreasing the transfer of the char particles from the fuel reactor to the air reactor.

All the references mentioned above generally are in line with each other when looking at the effect of temperature on carbon conversion, combustible gas yield, lower heating value and cold gas efficiency. They observed that as temperature increased, all the aforementioned parameters increased in value. This effect can be attributed to the increased tar catalytic cracking, char conversion and increase in oxygen carrier reactivity with an increase in temperature.

2.3.1.3 Steam/Biomass (S/B) Ratio

Huang et al., [145] demonstrates that an increase in S/B ratio increases H_2 and CO_2 concentrations, but decreases CH_4 and CO concentrations. This is because steam provides molecular oxygen for char oxidation and hydrogen for hydrogen production. The water – gas shift and methane reforming reactions (reactions 2 and 3, Table 2.2) undergo an equilibrium shift towards the right-hand side, increasing H_2 and CO concentrations. However, CO concentration decreases due to it being consumed by the water gas shift reaction. Zeng et al., [149] observed a similar trend; however, CO_2 concentration experienced a slight decrease as S/B ratio increased more than 1. This could be due to excess steam being injected into the reactor (temperature is at 800°C) at approximately 120°C, therefore resulting in uneven reactor temperature distribution (reducing reactor overall temperature). This has also been observed by [79], [147] and [148].

Huang et al., [145] tested the effect of increasing S/B ratio and observed an increase in carbon conversion and gas yield up to a maximum of 0.85, according to steam's ability to increase tar cracking and reforming reaction. However, further increase resulted in a decrease in both values, which could be due to the uneven reactor temperature distribution when injecting excess steam. Similarly, Zeng et al., [116, 149] observed that the cold gas efficiency increases with an increase in S/B ratio up to 0.75 and 0.5, respectively, followed by a drop in value. However, Ge et al., [79] observed an increase in syngas yield with a constant increase in S/B ratio up to 1.4, which could be due to the excess in oxygen carrier resulting in maintaining higher temperatures.

Zeng et al., [150] suggests that using steam as a gasifying agent alongside the oxygen carriers consumes a lot of energy. Thus, the author suggested an alternative process called biomass self-moisturised chemical looping gasification (BSM-CLG) were biomass is dried then mixed with ionised water before being placed in the reactor. Therefore, a fixed bed reactor was set up to compare between BSM-CLG, dry biomass chemical looping gasification (DB-CLG) and biomass steam chemical looping gasification (BS-CLG). BSM-CLG demonstrated a higher gas

yield and LHV compared to the other two processes, however BS-CLG showed a higher H_2/CO ratio, which is due to the higher oxidation strength of steam, hence producing more CO_2.

2.3.1.4 Biomass/Oxygen Carrier (B/OC)

To obtain high-quality syngas, the biomass/oxygen carrier ratio is an important parameter in CLG. Huang et al., [145] has concluded that the percentage of oxygen carrier particles in the bed is crucial to achieve a required product. The amount of oxygen carrier should be chosen to keep the gasification temperature stable. High amount of oxygen carrier will result in complete combustion while little amount of oxygen carrier will result in insufficient amount of oxygen and gradual decrease in gasification temperature of the reactor.

Huang et al., [117] tested different B/OC ratios and concluded that increasing the B/OC ratio results in an increase in H_2, CH_4 and CO cumulative concentration and a decrease in CO_2 concentration. This is due to the increase in pyrolysis gas according to reaction 1 in Table 2.2, while keeping the amount of available lattice oxygen constant. This in return reduces the contact between pyrolysis intermediates and lattice oxygen, therefore CO_2 cumulative concentration decreases while increasing the rest. Additionally, this is also due to the effect of the Boudouard reaction (reaction 4), which reduces CO_2 into CO and the shift in reactions 6 – 11 (Table 2.2) equilibrium to the left due to the deficiency of Fe_2O_3. This has also been confirmed by Wei et al., [141]. However, in regard to the air reactor, CO_2 concentration increases while O_2 concentration decreases with an increase in feeding rate. This is due to the increased char entrainment from the fuel reactor to the air reactor, resulting in an increase in char combustion in the air reactor. Huang et al., [144] and Zeng et al., [150] tested the effect OC/B ratio rather than B/OC ratio and got similar however opposite trends.

Increase in biomass feeding rate (B/OC ratio) increases LHV due to more pyrolysis gas being produced, however, decreases the syngas yield and carbon conversion. However, the cold gas efficiency increases up to a maximum feeding rate then decreases. Cold gas efficiency is dependent on the gas yield and biomass composition, which means that the increase in LHV cannot compensate for the decrease in gas yield. This has been observed by [117], [141] and

[150]. Additionally, Huang et al., [144] suggests that an increase in biomass/oxygen ratio decreases the catalytic cracking of the tar, therefore decrease in carbon conversion.

2.3.1.5 Residence Time/Strength of Oxygen Carrier

He et al., [143] set up a CLG experiment in a single fluidized bed reactor placed in a transport furnace experiences a drop in CO_2 with an increase in CO and H_2 as time increases which can be associated with the Boudouard reaction (reaction 4, Table 2.2) and steam reformation (reaction 3, Table 2.2), respectively. This was followed by a decrease in all CO_2, CO and H_2 after 20 minutes due to the decrease in oxygen activity, hence just pyrolysis was taking place. A similar conclusion was observed by Huang et al., [144] and Huang et al., [145]. Similarly, Wei et al., [141] observed that the carbon conversion and cold gas efficiency decreases with time in an interconnected fluidized bed. This can be explained by the slight loss in oxygen carrier reactivity. Similarly, He et al., [143] tested the effect of 20 redox cycles using a fluidized bed reactor in a transport furnace. It was observed that after 5 cycles the oxygen carrier particles 5% of the hematite mass was lost, but from the 6^{th} to 20^{th} cycles the mass loss was less noticeable. This can be explained due to the rounding effect of the irregularities of the oxygen carrier that takes place during the first few cycles, resulting in fine particles breaking off and elutriating out of the reactor. In another paper, Huang et al., [142] experiences the same result and explains that the attrition rate of the OC decreases with time, which is associated with an increase in its mechanical strength. Moreover, Xue et al., [84] also tested the effect of reactive hematite with biomass char and observed a downward trend in gas yield and carbon conversion after 20 cycles, concluding that it was due to ash sintering on the oxygen carrier hence reducing contact with the active sites as well as reducing the specific surface area by covering the pores.

2.3.1.6 Oxygen Carrier Characterization

He et al., [143] conducted a SEM characterization on natural hematite oxygen carrier and two samples after undergoing a 20-cycle reaction and with pine sawdust in a fluidized bed reactor at 800°C and 850°C. The surface of the natural hematite was seen to be covered with granules

smaller than 5µm in addition to having a porous structure which is beneficial due to increased surface area, hence enhancing the reaction between the gas and the hematite. The results of the cycle tests showed a more uniform compact surface on the 850°C sample which was due sintering and agglomeration after the constant reduction and oxidation taking place in addition to the thermal stress. Whereas the 800°C sample exhibited larger pores and larger particle sizes. Huang et al., [151] reacted biomass char with natural hematite in a fixed bed reactor and conducted a SEM and XRD analysis on the oxygen carrier samples. An XRD test was conducted on fresh hematite, reduced hematite after reaction with biomass in inert atmosphere, reduced hematite in the presence of steam and a 20-cycle hematite sample. It was observed the Fe_2O_3 is the active phase in the fresh hematite with the Fe_2O_3 being reduced into FeO under inert atmosphere. However, in the presence of steam, some Fe_2O_3 is converted into Fe_3O_4. This is due steam being another source of oxygen and steam gasification of char being more thermodynamically favoured. This could help inhibit the agglomeration of the oxygen carrier. A SEM-EDX test was conducted followed by a BET test on the fresh hematite and 20 cycle hematite sample. It showed that the porous structure was maintained, however the porosity of the 20-cycle oxygen carrier was reduced due to sintering hence merging of small fragments to form large granules. Huang et al., [117] reacted pine sawdust and natural hematite in a fluidized bed reactor. This was followed by conducting a XRD and SEM tests on the oxygen carrier samples the reacted and regenerated at a range of 5 temperatures. It was observed that all Fe_2O_3, Fe_3O_4 and FeO phases were observed in the reduced oxygen carrier which could be due to the uneven reaction in the whole region of the oxygen carrier. Moreover, no new solid crystalline phase solutions were detected showing stability of the inert oxides. Regarding the SEM test, the porosity starts disappearing above 1113K due to thermal sintering. Huang et al., [142] conducted a cycle experiment, testing the effect on the XRD results when reacting hematite with pine sawdust in a fluidized bed reactor after 1, 5, 10, 15 and 20 cycles. It was observed that the reduced samples resulted in further reducing and formation of FeO as the number of cycles increased, which is explained due to

the uneven reduction in the fluidized bed reactor as number of cycles increase. This results in the regenerated oxygen carrier having Fe_3O_4 peak appearing.

Hu et al., [152] gasified Chlorella vulgaris algae using 99% purity Fe_2O_3 oxygen carrier in a fixed bed reactor, followed by conducting an XRD and SEM analysis on range of temperatures and OC to biomass ratios. Finally, Huang et al., [92] reacts sewage sludge with natural hematite at different biomass to oxygen carrier ratios and at different temperatures. This was followed by conducting a pore structure analysis on the fresh hematite and an XRD test on the range of samples from the different tests. Moreover, a 1 cycle and 12 cycle tests were conducted, and their oxygen carriers were tested XRD and SEM analysis.

2.3.1.1 Summary and Gap in Hematite Experimental Analysis Literature Review

From looking at all the previous literature there hasn't been any pervious experiments reacting pine sawdust with a hematite oxygen carrier in a fixed bed reactor. This coupled with the absence in understanding the effect of OC to biomass (OC/B) ratio, temperature, and residence time when gasifying pine sawdust using hematite oxygen carrier. Therefore, this thesis conducts a series of experiments at a range of temperatures, OC/B ratios and resident times in a fixed bed reactor. The reduced oxygen carriers are then analysed using XRD tests followed by conducting an SEM-EDX analysis on the OC/B and residence time samples. The temperature samples are regenerated back in the fixed bed using air and analysed again using XRD followed by a SEM-EDX analysis.

2.3.2 Techno Economics Literature Review

Research into scale-up of chemical looping technologies has progressed quite a bit in recent years, with several demonstration pilot plants being established all over the world. Table 2.4 puts together all the chemical looping pilot plants.

Table 2.4. Summary of all the chemical looping power plants

Organisation	Country	Plant Size	Oxygen Carrier	Reference
Technical University of Vienna (TUWIEN)	Austria	0.14 MW	Ni-Based/Ilmenite/Copper/ Manufactured combined oxide/ Iron-based	[153 – 155]
Darmstadt University of Technology	Germany	1 MW	Ilmenite / Cao-$CaCO_3$ looping/ Iron ore/Manufactured combined oxides	[156, 157]
Alstom Power, Inc	USA	3 MW	$CaSO_4$	[158]
Chalmers University of Technology	Sweden	12 MW	Ilmenite/Manganese Ore	[159]
Chalmers University of Technology	Sweden	10 kW	Ni-Based/Manufactured Iron-Based Oxides/Manufactured Combined Oxides/Ilmenite	[160]
Korean Institute of Energy Research	South Korea	0.2 MW	Nickel-Based	[161]
SINTEF	Norway	0.15 MW	Copper-Based/Ilmenite	[162]
Ohio State University (NCCC)	USA	0.25 MW	Manufactured Iron-based	[163]
Ohio State University	USA	25 kW	Manufactured Iron Based	[164]
Babcock and Wilcox	USA	0.25 MW	Manufactured Iron Based	[165]
Chalmers University of Technology	Sweden	0.1 MW	Ilmenite/Manufactured combined oxides/Iron ore	[166 – 168]
JCoal	Japan	0.1 MW	Ilmenite	[169]
Tsinghua University	China	1~3 MW	Fe_2O_3	Under construction
Southeast University	China	1~3 MW	Fe_2O_3	Under construction
Southeast University	China	3 kW	Fe_2O_3	[170]
Southeast University	China	10 kW	Nickle Based	[171]
Southeast University	China	25 kW	Natural Iron Ore/ Waste Iron Ore/Nickle Based	[81]
Southeast University	China	50 kW	Natural Iron Ore/ Waste Iron Ore	[172]
Huazhong University of Science and Technology	China	5 kW	Hematite	[173]
Huazhong University of Science and Technology	China	50 kW	Natural Iron Oxide/ Waste Iron Oxide	[174, 175]

IFPEN	France	10 kW	Manganese Ores/Manufactured Combined Oxide/Nickle Oxide/Copper Based	[126, 176 – 178]
Institute of Combustion and Power Plant Technology	Germany	10 kW	Iron Oxide/ Ilmenite	[179]
Western Kentucky University	USA	10 kW	Copper Based	[180]
Guangzhou Institute of Energy Conversion	China	10 kW	Manufactured Iron Based	[138]
Hamburg University of Technology	Germany	25 kW	Copper Based/Ilmenite	[127, 181]
Instituto de Carboquímica	Spain	50 kW	Natural Iron Oxide/ Waste Iron Oxide/Ilmenite	[182, 174]
VTT Research Centre	Finland	50 kW	Manganese Ore/ Ilmenite	[183]

However, several techno-economic evaluation of biomass chemical looping processes (BCLPs) have been conducted, with even less focused on biomass chemical looping gasification to power generation as reviewed by Zhao et al., [65]. Xu et al. only investigated chemical looping partial oxidation process for thermochemical conversion of biomass to syngas without considering the following power generation process [184]. Similarly, Kong et al, [185] develops an Aspen Plus model for chemical looping reforming to compare between conventional reforming processes and chemical looping reforming of biogas into H_2. Zeng et al., [186] used coal fuel to develop a chemical looping water splitting model to produce H_2. None of them considered coupling the process to a combined cycle and did not conduct an economic assessment. Yan et al., [187] compares between three chemical looping systems for hydrogen production via the aid of Aspen plus to design the models. These systems include biomass hydrogasification, methane reformation and calcium-looping based CO_2 absorption. Gopaul et al., [188] compared to two chemical looping gasification processes for unique hydrogen production: one scheme produces H_2 using a CaO sorbent for CO_2 capture and total sorbent recovery; another scheme produces H_2 using Fe-based oxygen carriers for near-total carrier recovery. Li et al., [189] established a novel process using Aspen Plus consisting of butanol production from sawdust biomass using CLG process. The author gives a detailed design followed by an economic assessment for the whole process. Moreover, although Cormos et al., [190] studied biomass direct chemical looping (BDCL) concept for hydrogen and

power co-production from the aspect of process configuration, simulation, thermal integration and techno-economic assessment, nevertheless, in his study chemical looping combustion of biomass (rather than biomass direct chemical looping gasification) coupled with three reactors (fuel reactor, air reactor and steam reactor) are proposed to produce hydrogen and power simultaneously. Similarly, Kuo et al., [191] developed a hydrogen and electricity co-production chemical looping power plant comparing between raw wood and torrefied wood. The author established a biomass steam gasification (BSG) process integrated with a chemical looping hydrogen production (CLHP) using iron-oxide and a combined heat and power (CHP) systems. The author uses Matlab and Aspen Plus to develop a detailed kinetics model of two counter current moving bed, which was used to obtain the maximum steam velocity in the moving bed. Moreover, a comparison between performance indications such as hydrogen thermal efficiency, overall system efficiency and hydrogen yield indicates that using terrified wood is preferable. Li et al., [192] developed a multistage model using Aspen Plus of a biomass direct chemical looping (DBCL) process, known as chemical looping water splitting (CLWS) for hydrogen production or power generation. A performance evaluation was conducted to obtain optimum conditions. It was then concluded that DBCL process is significantly more efficient than traditional biomass utilization processes. Zaini et al., [193] also developed an iG-CLC co-generation model using Aspen Plus with macroalgae feedstock to evaluate the relation between certain parameters and performance of the system. Sorgenfrei et al., [194] also conducted a similar test using iron-based oxygen however using coal as the feedstock. Yan et al., [195] developed an Aspen Plus model of a biomass/coal co-gasification iG-CLC to power plant coupled to a solid oxide fuel cell and CO_2 capture using mineral sequestration. Several key operational parameters were tested including biomass mass fraction, steam/carbon ratio, gasification temperature, and oxygen carrier/fuel ratio and its effect on both energy and exergy efficiencies as well as carbon capture rate. It was concluded that the energy and exergy efficiencies are equal to 39.9% and 37.6%, with 96.0% of the carbon within the coal and biomass can be captured. Zhou et al., [196] develops a chemical looping combustion model using Aspen Plus comparing between the use of different fuels (pine sawdust, almond shells and olivine stones) and two oxygen carriers (Fe_2O_3 and MnO_3).

Besides, Ge et al. [197] recently developed a 30 t/h biomass chemical looping gasification combined cycle (BCLGCC) model on aspen plus which was validated and used to conduct a thermodynamic analysis, testing the effects of temperature and steam/biomass ratio on the HHV, gas composition and power generation. However, the scale of the simulation plant is small (electricity output is about 30-32 MW), which is not suitable for gas-steam turbine combined cycle to produce power due to its bad economic feasibility, as a result no economic analysis or sustainability evaluation of the power plant was conducted in their study. Aghabararnejad et al. [198] compared between biomass conventional gasification using pure oxygen as the gasifying agent and a small scale 7 MW_{th} BCLG system using Co_3O_4 (8%)/Al_2O_3 by developing an Aspen Plus model of each. A basic economic analysis of the Total Capital Investment (TCI) and operational costs were investigated just for the gasification unit, but no techno-economic analysis was conducted for the whole power plant. The author also compared between BCLG and conventional air gasification and concluded that the LHV of the syngas is higher for the BCLG process, which is due to the high concentration of N_2 in the syngas when using air as the gasifying medium.

2.3.2.1 Summary and Gap in Techno-Economics Literature Review

Unlike the previous studies, this thesis will give a comprehensive techno-economic analysis followed by a sustainability evaluation of an industrial scale 650 MW (gross power) direct chemical looping gasification of biomass to power generation, especially, CCS included in the power plant are also considered and investigated. Allowing us to test the technical and economic feasibility of the process in large scale. An Aspen Plus simulation process of the whole biomass chemical looping gasification using hematite as oxygen carrier based on the experimental data from an interconnected fluidized bed reactor and the industrial or demonstration data was established and validated. A thermodynamic analysis using this model was conducted, discussing the effect of key parameters (oxygen carrier to biomass, gasification temperature, steam to biomass, pressure and WGS degree) that have a significant effect on syngas quality (net power output, syngas LHV and net efficiency) and quantity (gas yield) were investigated to obtain optimal conditions and maximum syngas output for the consecutive power generation process. This was followed by an economic feasibility analysis, of the entire biomass direct chemical looping gasification combined cycle power plant. A

sensitivity analysis of different key technical and economic parameters was then conducted to see which has the biggest impact on the COE. A sustainability evaluation for both the BCLGCC-CCS and non-CCS power plants at a scale of 650 MW (gross power) electricity output was also conducted, which was compared to other power generation technologies such as coal-fired power plants, biomass direct combustion, traditional coal gasification and traditional biomass gasification to power generation technologies with and w/o CCS, giving a comprehensive understanding of BCLGCC technology for further research and development.

2.3.3 Life Cycle Assessment Literature Review

The scope of many previous articles and research on gasification technology focused on conducting techno-economic-environmental analysis of gasification power plants using coal/biomass. This comprised of investigating the cost effectiveness, efficiencies, and internal factors of the plant with and without CCS technologies [44, 45, 199-204]. Others conducted studies on Life Cycle Assessment (LCA) on these power plants which looked at both internal and external factors, including analysing factors that affect economic, energy, and environmental performance through evaluating the feedstock supply chain, the power plant size and CO_2 capture, transport and storage [205-211]. In regard to chemical looping processes some LCA studies have been conducted, some using chemical looping for hydrogen production [212-216] and one for chemical looping technology coupled with a power-to-methane system [217]. However, in particular to chemical looping technology to power generation, only a few papers looked into conducting a life cycle assessment of the entire process.

Navajas et al. [218] conducted an environmental life cycle analysis of a natural gas based chemical looping combustion (CLC) to power generation process. The author investigated the effect on 14 environmental impact factors using Gabi 8.7 pro software on the CLC to power using five different oxygen carriers (2 nickel, 2 iron and 1 copper based) and compared them to a conventional natural gas combustion combined cycle plant with and without amine CO_2 capture. It was concluded that the CLC process did not add much environmental impact compared to the conventional process, since the impact associated with the oxygen carrier is

very insignificant in comparison to the rest of the feedstock. When CLC to power process is compared to conventional combustion with CO_2 capture, the CLC process resulted in lower environmental impact values which demonstrates the potential of CLC technology from a life cycle perspective in CO_2 capture. When comparing between the oxygen carriers, NiO-based OC's demonstrated the lowest global warming impact (GWI), however its downside is its toxicity, hence presenting Fe_2O_3 as the best alternative yet requiring some chemical and mechanical improvements. He et al. [219] conducted a life cycle greenhouse gas emission environmental assessment of a polygeneration process consisting of coal-based synthetic natural gas (SNG) production followed by a CLC process to power generation. The author calculated the GWI of each stage of the process and tested the effect of some key parameters on its value. The results of the novel process were then compared to a conventional SNG combustion system with air. Fan et al. [220] examined the GWI of a natural gas based CLC power plant and tested the relationship between GWI and four essential factors. These factors included the type of OC (Fe- and Ni-based), lifetime of the OC, GWP of the OC and the thermodynamic performances of the CLC power facility. The plant was developed, and factors were tested by establishing an Aspen Plus model. Results showed that Ni-based OC power plants favoured a higher plant efficiency compared to Fe-based OC power plant, hence resulting in a lower GWI value. However, Fe-based OC favoured a lifetime of the OC to be less than 2500hr whereas Ni-based OC favours higher longer operating hours. Petrescu et al. [221] compares between a conventional coal gasification power plant, a calcium looping CO2 capture power plant, and an indirect iron-based coal chemical looping (syngas production followed by chemical looping) power plant. The author developed a Gabi model for each of the processes and compared between 11 different environmental indicators. Chemical looping power generation showed the best values for reducing greenhouse gas emissions, whereas at the same time other factors effecting the environment showed an increase compared to conventional gasification. This was due to the use of additional up-stream processes for the OC and downstream CO_2 capture, transport, and storage. Fan et al. [222] also conducted a life cycle global warming impact analysis of a coal in-situ gasification

chemical looping gasification (iG-CLC) power plant using ilmenite and steam as gasification agents with CO_2 capture. A thermodynamic analysis to determine the optimum conditions for the best GWI was conducted, which included testing the effect of steam to carbon ratio, OC to fuel ratio, lifetime of the OC and type of OC. The iG-CLC process was compared to 7 other coal power generation technologies with CO_2 capture technology and resulted in being the 2nd lowest GWI after oxy-fuel combustion power generation plant. Finally, Tagliaferri et al. [223] conducted a LCA of a chemical looping air system (CLAS) for power generation using lignite coal, which uses a chemical looping process to produce oxygen for an oxyfuel combustion system. The LCA was conducted using Gabi software. The results of the CLAS for power generation process was then compared to conventional renewable and non-renewable power generation processes.

2.3.3.1 Summary and Gap in Life Cycle Analysis Literature Review

From looking at all the previous LCA literature for chemical looping power generation systems, there are no studies that refer to LCA of a biomass direct chemical looping gasification (BCLG) to power plant with and without CCS in the UK. Hence there is a need to provide more data for performance comparisons of life cycle energy-economy-environment evaluation between conventional power generation systems using coal/biomass and biomass chemical looping gasification combined cycle (BCLGCC) processes. Moreover, there has been no literature covering and quantifying the environmental impact of BCLGCC power plant life cycle. This is possibly due to the technology not having technological breakthrough yet and no suitable oxygen carrier is found, therefore the no motivations for research has gone into its life cycle analysis.

3 CHAPTER 3: METHODOLOGY

3.1 Techno-Economic & Sustainability Analysis: Methodology for Chapter 4

3.1.1 Aim

The aim of this chapter is to develop a methodology to test the techno-economic feasibility of a scaled up BCLGCC power plant, followed by conducted a sustainability evaluation of the system. In this section (section 3.1) a 10kW$_{th}$ interconnected fluidized bed biomass gasification chemical looping pilot plant reactor with hematite as an oxygen carrier was described. This was followed by demonstrating that the pilot plant BCLG reactor was under stable operation conditions and that the reactions between the biomass and the hematite were taking place, concluding that the results obtained from the reactor is reliable. Finally, a 650MW BCLGCC power plant model using Aspen Plus software was developed and validated using the results of the 10kW$_{th}$ BCLG pilot plant.

3.1.2 System Description & Materials

Figure 3.1 described a complete BCLGCC system for power generation. Biomass is gasified using a metal oxide to produce syngas which is then sent to a water gas shift (WGS) (which is needed for CCS scheme, Figure 3.1A) and carbon capture section where acid gas is separated from the syngas. The clean syngas is then sent to the combined cycle, consisting of a gas turbine, heat recovery steam generation unit and a steam turbine to generate electricity. The process for the Non-CCS plant is shown in Figure 3.1B. A BCLG subsystem model was established and validated based on a 10 kW$_{th}$ interconnected dual fluidized bed gasification reactors (Figure 3.2, a pilot plant that exists at the Chinese Academy of Science in Guangzhou). Images of the pilot plant can be found in the Appendix. The pilot plant consists of a bubbling bed FR, a cyclone to separate gas from particles escaping from the FR, a fast-fluidizing bed AR, another cyclone for the gas exiting the AR, an upper and a lower loop seal. The detail parameters of each part were described in a previous study [141].

Table 3.1. The properties of biomass sample and hematite oxygen carrier

Biomass									
Proximate analysis (wt.%,db)				Ultimate analysis (wt.%,db)					LHV (MJ/kg,db)
Moisture	Volatiles	Fixed carbon	Ash	C	H	O	N	S	18.71
8.39	84.31	6.88	0.42	46.44	6.21	47.29	0.05	0.01	
Hematite, wt.%									
O	Fe	Si	Al	Ca	Zn	P	Mg	K	Ti	Mn
30.1	64.61	2.83	1.4	0.09	0.53	0.10	0.08	0.02	0.03	0.05

Sawdust of pine collected from Guangdong province (China), was used as fuel in the tests. Natural hematite is selected as the oxygen carrier due to its low cost, ability to withstand conditions inside a combustor (good stability at high temperature; high melting point), non-toxic in nature and has no negative environmental impact. The properties of biomass and hematite are shown in Table 3.1. Fuel particle size ranging between 250 – 425 µm was used in the experiments. Hematite is the mineral form of iron oxide (Fe_2O_3), which crystallizes in the rhombohedral system. The hematite with particle sizes between 180-250µm used in these experiments was supplied by Guangdong Iron & Steel Group Co. Ltd.. According to the Fe^{3+} fraction, it is calculated that the Fe_2O_3 content is about 81.66% in the natural hematite. The detail description of each key units such as gasification (FR & AR), WGS and acid gas treatment and combined cycle are presented in the following section.

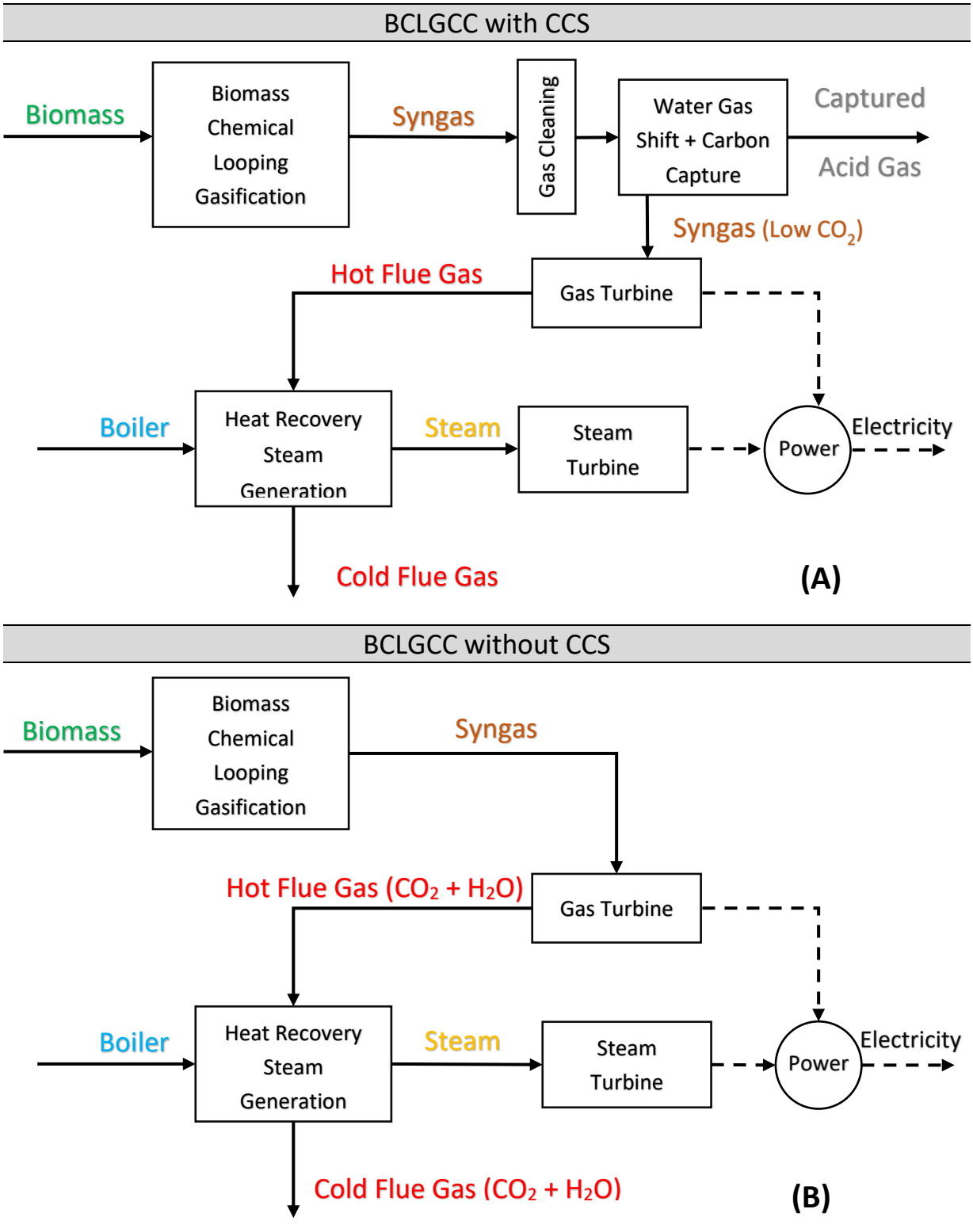

Figure 3.1. General block flowsheet of a BCLGCC to power generation with CCS (A) and without CCS (B)

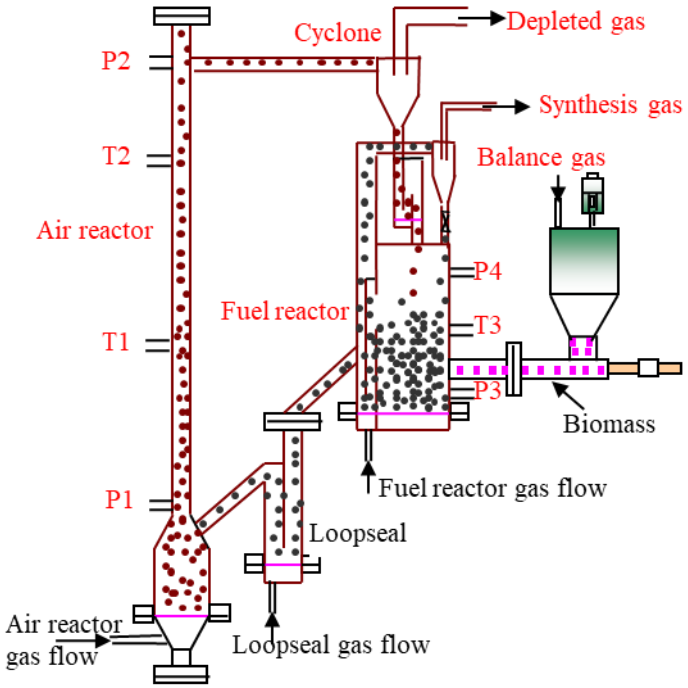

Figure 3.2. Schematic diagram of the interconnected circulating fluidized beds for BCLG

3.1.3 Description of the Key Units

3.1.3.1 Gasification (FR & AR)

Biomass is initially injected into the FR where it undergoes devolatilization, pyrolysis, combustion and gasification reactions in the presence of an iron-based oxygen carrier, providing lattice oxygen for the combustion/gasification reactions to take place. The depleted oxygen carrier passes through the lower loop seal into the AR where it is regenerated by reacting with molecular oxygen from air. The regenerated metal oxide is separated from the flue gas via a cyclone and sent back to the FR after passing through the upper loop seal. The two reactors are electrically heated in an oven which supplies heat for start-up and compensates heat loss during the operation. Thermocouples and differential pressure transducers were located at different points of the prototype to display the operating conditions and monitor the cycling stability of the fluidized bed in real time. The outlet gases from the air reactor and fuel reactor were induced with suction pump to an ice–water cooler where the steam was condensed and removed. The produced gases were collected using a gas bag and analysed by an offline gas chromatograph.

3.1.3.2 Water Gas Shift and Acid Gas Treatment

The syngas produced contains high amount of carbon and sulphur components. However, for this process to be carbon neutral and prevent sulphur emissions, they should be captured pre-combustion. Therefore, a Water Gas Shift (WGS) unit is added where syngas reacts with high temperature steam in a reactor, shifting the reaction towards producing more CO_2 and H_2. This is also a H_2S hydrolysis unit where the H_2S is converted into COS. Since the reaction taking places in the reactor is exothermic. The shifted syngas is cooled followed by a selexol acid gas treatment section, capturing 90% CO_2 and approximately 95 - 98% COS.

3.1.3.3 Combined Cycle

Gas turbines have been commonly used in power generation processes. A conventional natural gas fired gas turbine with a simple cycle generally has an efficiency of 35%. However, new power plants enhance the process with an additional heat recovery steam generator (HRSG) block followed by a steam turbine, which is known as a combined cycle. The reasoning behind that is for the heat in the exhaust gas to be captured via the HRSG process, converting feed water into steam which is sent to a steam turbine for power generation. A gas turbine (simple cycle) coupled with a HRSG and steam turbine. The heat recovered from the exhaust gas is used to generate high pressure steam which then passes through the steam turbine, dropping the pressure and temperature of steam, converting heat into shaft work to generate electricity. The steam turbine is divided into 3 stages: high-pressure steam, intermediate-pressure steam and low-pressure steam. This is due to the high pressure of steam which will result in large expansion if pressure is reduced all at once.

3.1.4 Modelling and Assumptions

A gasification model for a BCLG to power generation process has been developed based on restricted phase and chemical reaction equilibrium according to experimental study showing a stable and thermodynamic equilibrium results (Figure 3.3 and Figure 3.4). The results in sections 3.1.4.1, 3.1.4.2 and 3.1.4.3 were tests that were conducted by our collaborative partner (Chinese Academy of Science – Guangzhou Institute for Energy Conversion) to show us that the results produced from the rig in Figure 3.2 are reliable and can be used to validate our Aspen Plus Model.

3.1.4.1 Stability of Reaction System

From the Figure 3.2, P1 and P2 are the points where pressure was measured in the AR while points P3 and P4 are measured in the FR. The typical bed pressures throughout the reaction time are displayed on Figure 3.3. The pressures at points P1, P2, P3 and P4 remain relatively consistent and fluctuate around 0.56, 0.45, 1.05 and 0.18, respectively. This indicates that the system is in a stable operating condition and that the OC have been circulating from the AR to FR throughout the process.

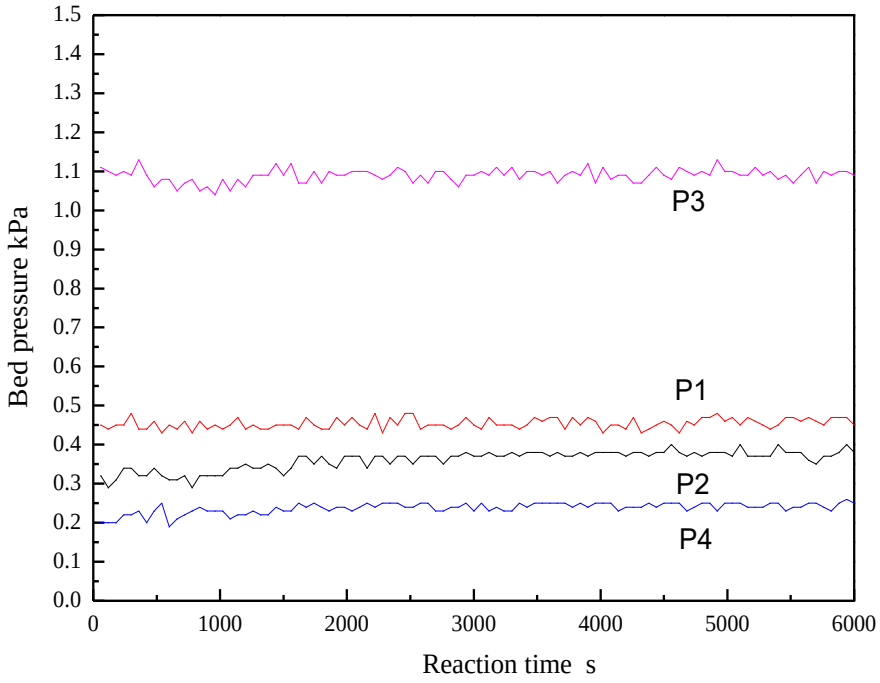

Figure 3.3. Bed pressure change with reaction time

3.1.4.2 XRD patterns of Oxygen Carriers

Experiments have been conducted on fresh, reduced and regenerated oxygen carrier samples, in which they were examined using X-ray diffraction to determine the crystalline phases formed on each sample. It was detected that the original crystal form of fresh oxygen carrier primarily constitutes of Fe_2O_3, SiO_2 and other metallic oxidizes (Al_2O_3, MgO, CaO etc.). Since the Fe_2O_3 plays a key role in the reaction process as lattice oxygen transfer medium and the SiO_2 in hematite oxygen carrier also has positive effects in preventing the aggregation or sintering for oxygen carrier particles. Therefore, in order to further highlight the evolution of

oxygen carrier crystal form in the reaction process, the diffraction peaks of iron oxides and SiO_2 are marked in the XRD spectra and the other impurities oxides in hematite are too little and can be ignored. The crystal form of fresh hematite oxygen carrier characterized by XRD is shown in Figure 3.4. Powder X-ray diffraction (XRD, X'Pert PRO MPD) using Cu Kα (40 kV, 40 mA), was used to analyse the crystal structure of fresh and reacted samples. The samples were scanned at a rate of 2° min^{-1} between 2θ = 10°–80° with a step of 0.0167°. The samples were degassed under vacuum at 493 K for 6h before measurement. The reduced samples and oxidized samples were collected from the fuel reactor and air reactor separately after 60 h of operation. There were three crystalline phases of Fe_2O_3, Fe_3O_4, and FeO in the reduced samples. Fe_3O_4 and FeO phase were not found in the fresh or regenerated samples of the fuel reactor, which manifested that Fe_2O_3 was mostly reduced to Fe_3O_4 and FeO. The results suggested that the oxygen carrier could return into its original form in the AR after it has been reduced in the FR. This result shows that the hematite (Fe_2O_3) is reduced and deoxidised during the BCLG process, meaning that it could lose and gain oxygen therefore most likely was a source of oxygen during the gasification reaction.

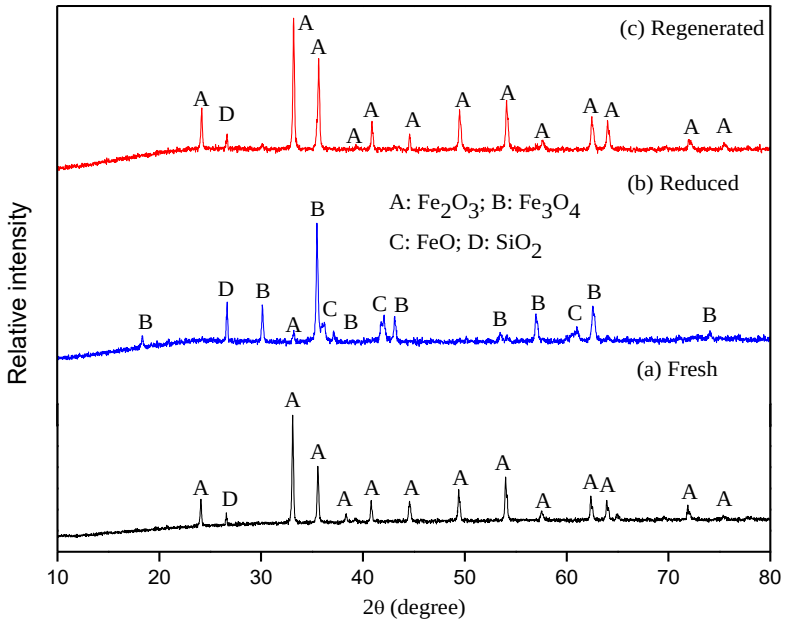

Figure 3.4. XRD patterns of fresh and used oxygen carrier

3.1.4.3 Equilibrium Composition of Gasified Gas

It is shown in Figure 3.5 that the equilibrium composition of gasified gas and carbon conversion rate changes over reaction time and number of cycles. It was clear that the reaction system (fuel reactor) reached thermodynamic equilibrium after 20 hrs, and the gas composition and carbon conversion rate maintained a stable status.

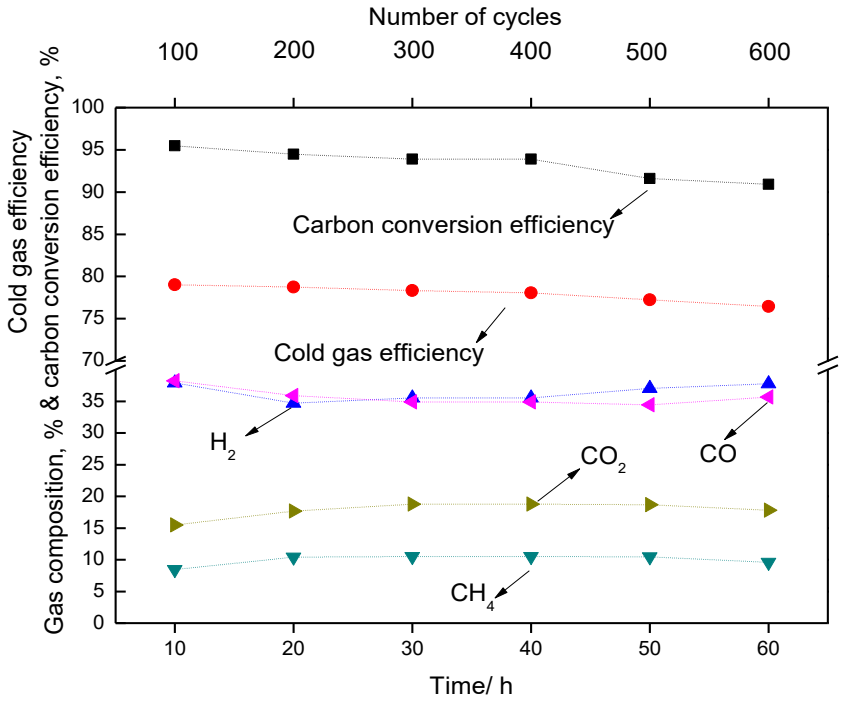

Figure 3.5. Gas composition, carbon conversion and cold gas efficiency as a function of reaction time and number of cycles

3.1.4.4 Creating the Model

Aspen Plus software (V10.0) package was used to simulate the reaction steps occurring in both processes. The property method chosen for the gas – solid modelling was PR-BM (Peng Robinson equation of state with Boston - Mathias modification) [224]. In the simulation, biomass, ash and slag were defined as nonconventional components. The HCOALGEN and DCOALIGT property models were used to determine their enthalpies and densities, respectively. All other components are considered as conventional components, with Fe_2O_3, Fe_3O_4, FeO and carbon being considered as solids. Different unit operation blocks were used to establish the process flowsheets. Table 3.2 explains the function of each unit block used in the gasification process flowsheet. Feedstock biomass is an unconventional component in the

Aspen Plus software, converting biomass to a conventional component is necessary before its gasification process. RYield reactor has a special function that can convert an unconventional component to a conventional component, which is widely used in coal or biomass pyrolysis and gasification [225, 226]. Therefore, in BCLG process, biomass (unconventional component) is initially injected into a RYield reactor where it is decomposed into its constituent components (conventional components). In general, this process is regarded as biomass pyrolysis which is only temporary placeholder. The actual yield distribution of the products out from RYield reactor is calculated using the FORTRAN statement calculation (see **Appendix**), a calculation method within Aspen Plus based on its given ultimate analysis, decomposing the biomass into its constituent components, including carbon, oxygen, hydrogen, sulphur, nitrogen and ash.

Table 3.2. Description of the operation blocks

Aspen plus block	Block ID	Description
RYield	DECOMP	Yield reactor – Based on mass balance this reactor converts the nonconventional biomass into conventional compounds, by decomposing biomass into constituent elements
RStoic	SLAGFORM	Stoichiometric Reactor - Reacts a percentage of unburnt carbon with the ash to form slag
RGibbs	FUEL-R	Gibbs free-energy reactor – Simulates the gasification reactions by using the direct minimization of Gibbs free energy to determine the equilibrium composition
Cyclone	B1	Cyclone – Separates ash from syngas by specifying split fraction
RStoic	AIRREAC	Stoichiometric Reactor - Air regenerates the oxygen depleted oxygen carrier. Moreover, air reacts with the unburnt carbon.
Cyclone	B2	Cyclone – Separates the oxygen carrier from the flue gas (Mainly N_2 and CO_2)

Since the ash is an unconventional component in Aspen Plus with an unknown composition, and the unreacted carbon mixing with the ash in biomass gasification, both the ash and the

unreacted carbon finally form slag. Therefore, the above process can be simulated by a stoichiometric reactor due to knowable quantities of the ash and the unreacted carbon. The stoichiometric reactor is used when the reaction kinetics are unknown or unimportant, but stoichiometry and extent of reaction are known. A stoichiometric reactor is generally used to react all the ash with the unreacted carbon to produce slag in biomass or coal gasification process [227]. The amount of ash would depend on the biomass ultimate analysis. The composition of slag changes depending on the gasification reaction conditions (depending on the amount of carbon conversion efficiency). On the basis of the above, those components out from the RYield reactor are then sent to a stoichiometric reactor where a percentage of carbon (the amount of unreacted carbon in gasification) reacts with the ash to form slag [55], and slag will not react in the FR.

The products from the stoichiometric reactor are sent to the RGibbs FR where they react with the oxygen carrier and steam. The main products from the reactions taking place in the RGibbs reactor are CO, H_2, CO_2, CH_4 and H_2O, as well as some trace components such as NH_3, H_2S and COS. The stream exiting the FR is sent to a cyclone where the syngas is separated from the solids (slag and reduced oxygen carrier) which are sent to the AR. In the AR, air is injected for oxygen to react with and regenerate the oxygen carrier for it to be recycled back into the FR. In general, a typical biomass gasification undergoes the following three main steps including: pyrolysis, gasification and combustion [228]. Biomass decomposes in the absence of oxygen into its heavy and light hydrocarbons as well as char. The energy required to allow this endothermic reaction to take place is supplied by the energy released during the combustion reactions. Since very little tar was collected in the experiments due to the catalytic effect of the oxygen carrier on tar cracking [229, 75], only char and pyrolysis gas products were considered in the biomass pyrolysis process in the simulation. All the reactions in BCLG process are presented in Table 3.3, especially, combustion reactions of biomass-derived gas with the iron ore in the FR proceeds through reactions (6-11) based on analysing the X-ray diffraction results of the OC (Figure 3.4). The simulation flowsheet for BCLG is presented in Figure 3.6.

Biomass gasification unit

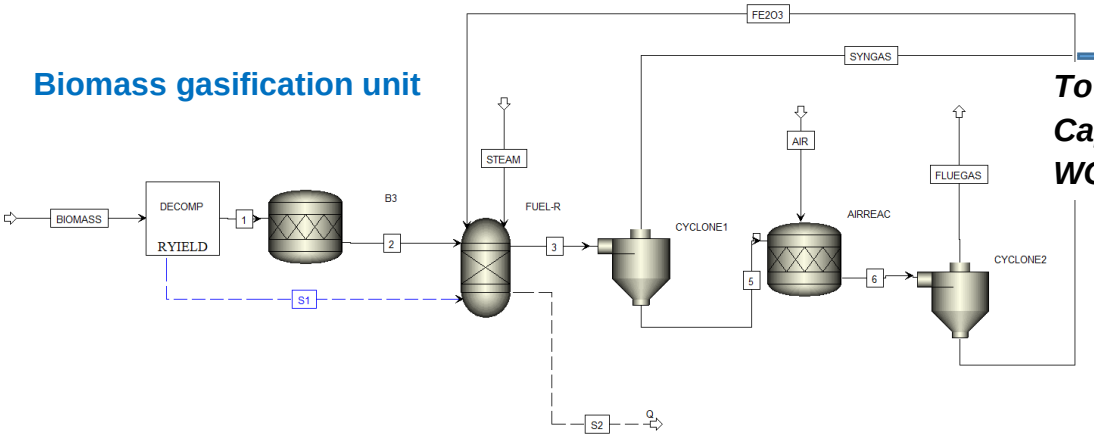

To Carbon Capture & WGS Unit

WGS & CO_2 separation Unit

Syngas

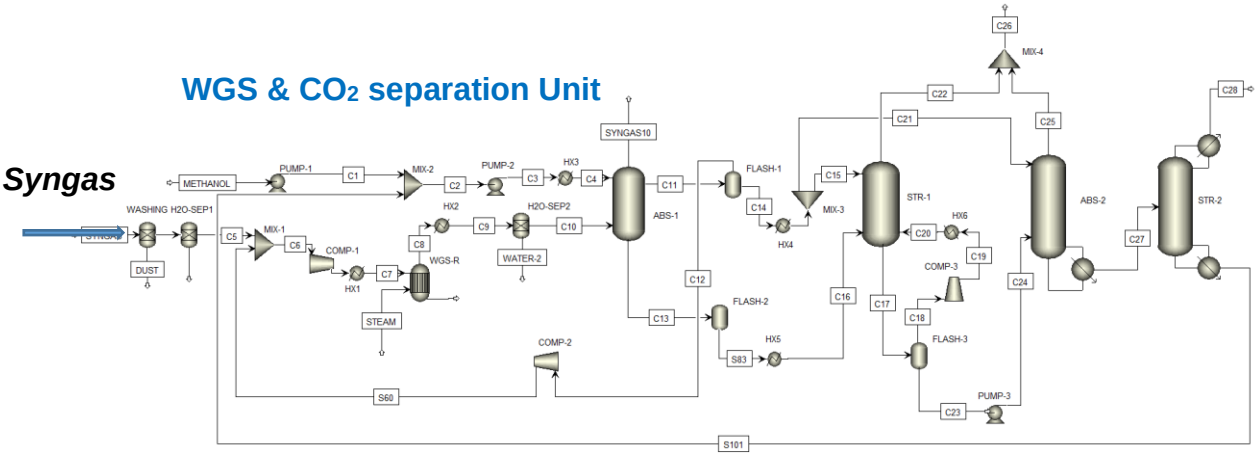

Gas turbine to power generation

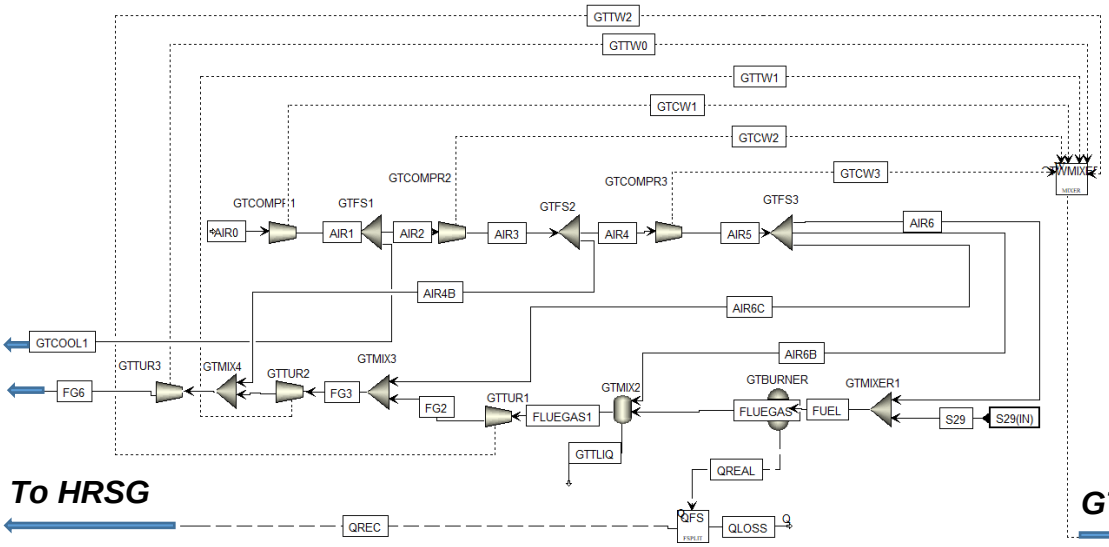

To HRSG

GT Power

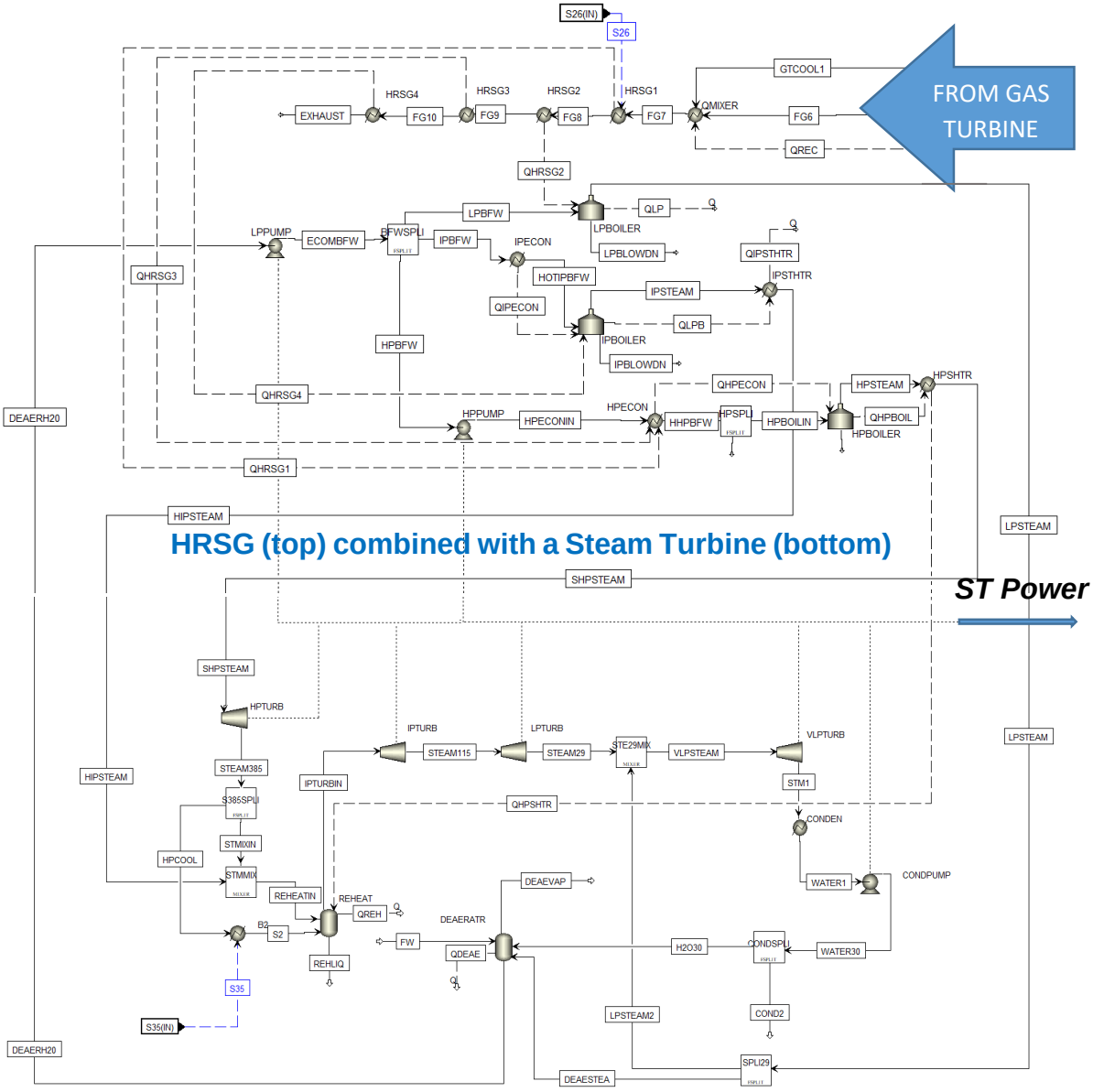

Figure 3.6. The simulation flowsheet of biomass chemical looping gasification to power generation

Table 3.3. Biomass Chemical Looping Gasification Reactions in the Fuel and Air Reactors

	Chemical looping gasification
Reaction Number	**Equations**
	Biomass pyrolysis
1	$C_nH_{2m}O_x \rightarrow \text{char} + \text{tar} + \text{syngas}\ (CO, H_2, CO_2, CH_4, C_nH_{2m})$, (Endo.)
	Biomass gasification
2	$C + H_2O \rightarrow CO + H_2$ (Endo.)
3	$CH_4 + H_2O \rightarrow CO + 3H_2$ (Endo.)
4	$C + CO_2 \rightarrow 2CO$ (Endo.)
5	$C + 2H_2 \rightarrow CH_4$ (Exo.)
	Combustion reactions
6	$CO + Fe_2O_3 \rightarrow 2FeO + CO_2$ (Exo.)
7	$CO + 3Fe_2O_3 \rightarrow 2Fe_3O_4 + CO_2$ (Exo.)
8	$H_2 + 3Fe_2O_3 \rightarrow 2FeO + H_2O$ (Endo.)
9	$H_2 + Fe_2O_3 \rightarrow 2Fe_3O_4 + H_2O$ (Exo.)
10	$CH_4 + 3Fe_2O_3 \rightarrow 2Fe_3O_4 + CO + 2H_2$ (Endo.)
11	$CH_4 + 4Fe_2O_3 \rightarrow 8FeO + CO_2 + 2H_2O$ (Endo)
	Water gas shift (WGS)
12	$CO + H_2O \leftrightarrow CO_2 + H_2$ (Exo.)
	Oxygen carrier regeneration (Air reactor)
13	$4Fe_3O_4 + O_2 \rightarrow 6Fe_2O_3$ (Exo.)
14	$4FeO + O_2 \rightarrow 2Fe_2O_3$ (Exo.)
15	$C + O_2 \rightarrow CO_2$ (Eno.)
	Contaminants
16	$N_2 + 3\ H_2 \rightarrow 2\ NH_3$
17	$S + H_2 \rightarrow H_2S$
18	$CO + S \rightarrow COS$

Several assumptions were taken when setting up the simulations including:

1. The process is taking place at steady state;
2. The gasification blocks FR and AR are isothermal;

3. Ash and slag are assumed to be inert therefore do not participate in chemical reactions;
4. Large molecular weight compounds (C_xH_y; were x>1 and y>4) are not considered in the gasification reaction;
5. Gas-solid separation was 99% efficient;
6. Acid gas treatment was assumed to be 90% CO_2 and 98% sulphur.

3.1.4.5 Model Validation of the Whole Plant

To ensure that the model is accurate and suitable to investigate thermodynamic characteristics of the gasification processes and the combined cycle, they should be validated with previous experimental results. Table 3.4 compares between experimental and simulation results for both the BCLG and combined cycle, respectively. It was noted that the difference between the simulation data and the literature or experimental data is within the rational range, implying that the established model is feasible for the simulation of the gasification and combined cycle processes. The other key models such as WGS, gas cleaning, CO_2 capture, heat recovery steam generation subsystem and gas-steam turbine combined cycle unit are modelled and validated using the following reference [230].

Table 3.4. Comparison of experimental and simulation results for BCLGCC

Variables	Conditions		Variables	Results	
	Literature	Simulation		Experimental results (vol. %)	Simulation results (vol. %)
Fuel reactor temperature, °C	800	800	H_2	34.36	39.22
Fuel reactor pressure, atm	1	1	CH_4	9.98	10.92
Steam/biomass ratio	0.85	0.85	CO	38.02	34.25
Oxygen carrier/biomass	5/3	5/3	CO_2	17.64	15.61
Carbon conversion efficiency, %	93	93	LHV (MJ/Nm^3, dry basis)	12.08	12.48
Flow rate of syngas, tonnes/hr	237.3 [230]	237.3	Gas Yield (Nm^3/kg, dry basis)	1.41	1.32
Flowrate of air, tonnes/hr	1605.3 [230]	1605.3			
Exhaust Temperature, °C	601.1 [230]	603.9			
Power Output, MW	319.6 [230]	310.1			

3.1.5 Data Evaluation

After developing the Aspen Plus BCLGCC model, this section will give a detailed explanation of the calculation method used to generate results in Chapter 4. Section 3.1.5.1 will give the calculation method for the technical analysis, section 3.1.5.2 will give the calculation for the economic analysis whereas section 3.1.5.3 will give the calculation method for the sustainability evaluation.

3.1.5.1 Technical Analysis (Method for Chapter 4, Section 4.1)

The technical indicators in this assessment are the Net Electric Efficiency (η_{Net}), Cold Gas Efficiency (CGE) and Lower Heating Value (LHV). To evaluate the performance of BCLG power

systems, the η_{Net} is calculated using Equation 3.1, which is in accordance to the first law of thermodynamics.

$$\eta_{Net} = \frac{(W_{Gross} - W_{Syngas} - W_{CCS} - W_{OC})}{LHV} \times 100 \quad [3.1]$$

where, W_{Gross} is the gross power of the power plant, W_{Syngas} is the power caused by fuel gas compression, W_{CCS} and W_{OC} are the power required for CO_2 capture and OC circulation, respectively.

The Cold Gas Efficiency (CGE) was calculated as the percentage of syngas heating value over the biomass heating value, as shown in Equation 3.2. CGE is useful in showing the amount of energy loss when converting the biomass into syngas.

$$\text{Cold gas efficiency}, \% = \frac{\text{Syngas LHV} \times Y_n}{Biomass\ LHV} \times 100 \quad [3.2]$$

where Y_n is the biomass gasified gas yield, which is calculated as the volume of a gaseous component (V_n) per mass of biomass ($M_{Biomass}$) used, as shown in Equation 3.3. The gas yield is useful in showing the amount of gas produced from 1kg of biomass.

$$\text{Gas yield } (Y_n) = \frac{V_n}{M_{Biomass}} \quad [3.3]$$

The LHV of the syngas mixture was determined by its gaseous composition and can be calculated using Equation 3.4.

$$\text{LHV} = 10110.71 \frac{\text{kJ}}{\text{kg}} (\%\text{wt. CO}) + 120850 \frac{\text{kJ}}{\text{kg}} (\%\text{wt. } H_2) + 50231.25 \frac{\text{kJ}}{\text{kg}} (\%\text{wt. } CH_4) \quad [3.4]$$

Since solid carbonaceous fuels negatively impact the environment, it is important that the amount of CO_2 generated during the process of power generation is measured and estimated. Even though biomass is used and is assumed to be carbon neutral, capturing the CO_2 after the power generation process can result in a negative emission, as a result aiding in tackling climate change. The reason for using gasification to generate electricity is due to it converting the carbonaceous fuel into syngas (H_2 + CO). This mixture of gas (syngas) then flows into a water-gas shift reactor, reacting with steam to increase H_2 concentration and convert the CO into CO_2. This allows us to capture the CO_2 pre-combustion, therefore reducing CO_2 emissions into the environment. Equation 3.5 was used to determine the degree of water gas shift achieved by varying the flowrate of steam, and Equation 3.6 was used to calculate the ratio of carbon captured from the syngas.

$$WGS\ Degree = \frac{CO\ in\ syngas - CO\ in\ shifted\ gas}{CO\ in\ syngas} \quad [3.5]$$

$$Carbon\ Capture\ Ratio = \frac{CO_2\ in\ shifted\ gas}{CO_2 + CO + CH_4\ in\ syngas} \quad [3.6]$$

3.1.5.2 Economic Analysis (Method for Chapter 4, Section 4.2)

The CLGCC power plant in this thesis is estimated using the method developed by NETL, which is described in [199]. It is a reliable tool when comparing between power plants. In this economic analysis, the Total Plant Cost (TPC) and the Cost of Electricity (COE) are calculated due to their wide application when comparing between power plants. To calculate these values, the cost of investment for an equipment is calculated based on market investigation to obtain reliable results. The market costs are used to estimate the cost of the equipment depending on the size using the Equation 3.7.

$$I_2 = I_1 \times \left(\frac{Q_2}{Q_1}\right)^n \quad [3.7]$$

where I_1 & Q_1 are the equipment cost and production capacity of the reference equipment, respectively, I_2 & Q_2 represent the equipment cost and production capacity of the estimated equipment, respectively. Symbol n represents the scale exponent. All cost values for each unit are given in Table 3.5, the detailed calculation of the Total Overnight Cost (TOC) is introduced in Figure 3.7. Figure 3.7 presents a flowchart summarizing the breakdown to calculate the TOC. The sum of all the units capital costs calculated using Equation 3.7 will give you the Total Plant Equipment Costs (TPEC). However, calculating the Bare Erected Cost (BEC) will need to take into consideration the direct and indirect costs which can be estimated by considering the assumptions in Table 3.6 [230], followed by adding the process and project contingencies (25% of BEC and 20% of BEC + Process Contingency, respectively) to calculate the Total Plant Cost (TPC). Finally, to calculate the Total Overnight Cost (TOC), the owner's cost is added to the TPC. Table 3.7 summarizes the values of all the parameters used to calculate costs.

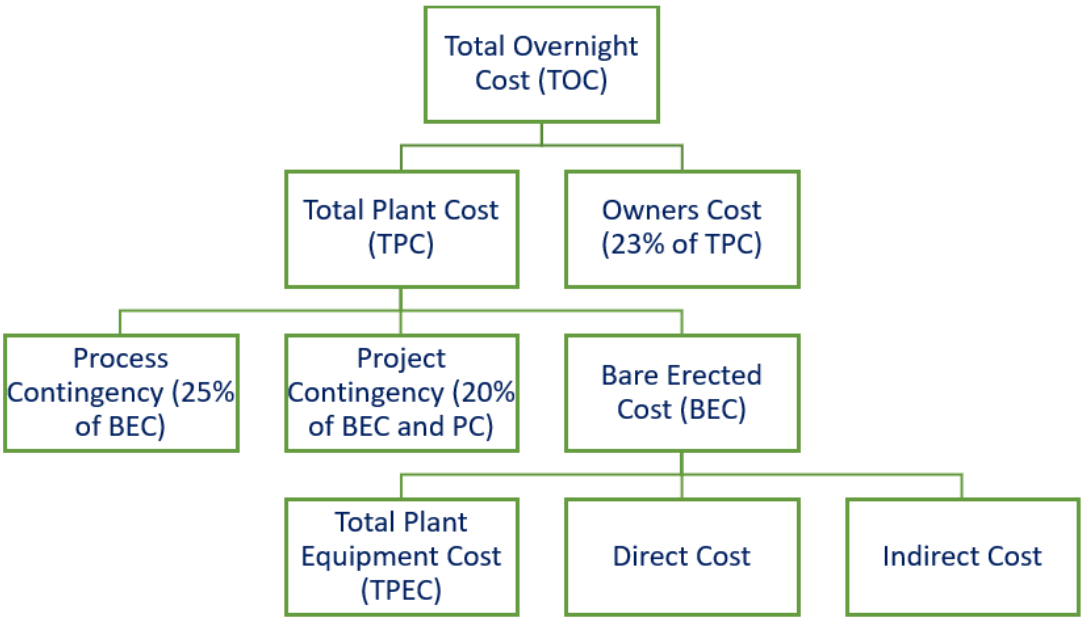

Figure 3.7. Flowsheet breakdown to calculate the TOC

Table 3.5. Parameters for scaling plant cost

Unit	Scaling Parameter	Reference cost (M$)	Reference scale	Scaling parameter	Reference
Gasification Units	Biomass flowrate, tonnes/hr	68.4	74.13	0.8*	[232]*/ [233]
WGS Reactor	H_2 + CO flowrate, kmol/s	21.33	2.45	0.65	[45]
CO_2 Absorption	Syngas flowrate, kmol/s	46.47	3.99	0.7	[45]
Gas Turbine	Power output, MW	28.57	266	0.75	[234]
HRSG	Heat Exchange, MW	23.13	355	1	[234]
Steam Turbine	ST gross power, MW	25.85	275	0.67	[234]
CO_2 Drying and Compression	CO_2 flowrate, kmol/s	55.39	4.18	1	[45]

Table 3.6. Direct and Indirect costs to calculate the BEC and estimate the owner's cost

Direct Cost	TEC	Owner's Cost	Estimate Basis
Purchased Equipment Installation	30%	Pre-production cost	6 months operating labour 1 month maintenance materials at full capacity 1 month non-fuel consumables at full capacity 1 month waste disposal 25% of one month's fuel cost 2% of TPC
Instrumentation and Control	20%	Inventory capital	0.5% of TPC 2 months supply of fuel at full capacity 2 months non-fuel consumables at full capacity
Piping	55%	Land	1.8% of TPC
Electric System	20%	Financing cost	2.7% of TPC
Buildings	12%	Other owner's costs	15% of TPC
Yard Improvements	15%	Total Owners Cost	23% of TPC
Services Facilities	40%		
Indirect Cost	**TEC**		
Engineering and Supervision	30%		
Legal Expenses	4%		

Table 3.7. Values of different parameters used when calculating costs

Parameters	Values	Reference
Capacity Factor	0.8	
Plant Life, years	25	
Discount Rate, %	10	
Capital Recovery Factor	0.11	
Energy for CO_2 capture, GJ/tCO_2	0.44	[235]
Total Fixed Operating Cost		
Labour Cost, $/hr	34.65	[200]
Working Hours Per Week, hr	40	
Operating Labour, 650 MW Plant	109	[236]
Operating Labour CCS plant	110% of Non-CCS	[237]
Operating Labour Burden	30% of base	[200]
Labour Overhead Charge Rate	25% of labour	[200]
Maintenance Labour	1.25% of labour	[200]
Property Tax & Insurance	2% TPC	[200]
Total Variable Operating Cost		
Price of OC, $/ton	95	[232]
OC Lifetime, hr	1315	[236]
Boiler Feed Water, $/ton	0.11	[184]
Cost of Biomass, $/GJ	12.4 (£10.0)	[43]

The COE of a power plant, which is the revenue received when generating electricity during the first year is calculated using Equation 3.8.

$$\text{COE} = \frac{\text{TOC}\times\text{CRF}+(OC_{VAR})(CF)+OC_{FIX}}{(\text{CF})(\text{kWh})} \quad [3.8]$$

where CRF is the Capital Recovery Factor, calculated using Equation 3.9, OC_{VAR} is the sum of all variable operational costs, OC_{FIX} represent the fixed operational cost CF is the Capacity Factor and kWh is the net kilowatt-hours of power generated at 100% capacity.

$$\text{CRF} = \frac{i}{1-(1+i)^{-N}} \quad [3.9]$$

where, i is discount rate and N is the plant life.

The total annual cost for the OC ($COST_{Annual}$) is calculated using Equation 3.10.

$$COST_{Annual} = COST_{OC} \times \frac{M_{OC}}{LT_{OC}} \quad [3.10]$$

where $COST_{OC}$ is the cost of the OC per mass, M_{OC} is the total solid inventory and LT_{OC} is the OC lifetime (1315 h) [235].

CCS technology can be used to reduce carbon emissions despite the fact that it reduces the efficiency and increasing the cost of the whole process, the Cost of CO_2 Capture can be another parameter to evaluate the economic feasibility of the process. It can be calculated using Equation 3.11;

$$Cost\ of\ CO_2\ Capture = \frac{(COE_{CCS}-COE_{Non\ CCS})\$/MWh}{(tCO_2/MWh)_{captured}} \quad [3.11]$$

To test the effect of plant size of the capital cost, variable cost, fixed cost and COE, Equations 3.12, 3.13, 3.14 and 3.15 are used, respectively.

$$TOC_S = TOC_R \times (\frac{MW_S}{MW_R})^{0.7} \quad [3.12]$$

$$VC_S = VC_R \times (\frac{MW_S}{MW_R}) \quad [3.13]$$

$$FC_S = FC_R \times (\frac{MW_S}{MW_R})^{0.7} \quad [3.14]$$

$$\text{COE} = \frac{\text{TOC}_S\times\text{CRF}+(VC_S)(CF)+FC_S}{(\text{CF})(\text{MW}_S)} \quad [3.15]$$

where, TOC_s and MW_s are the total overnight cost and net power of the scaled plant, whereas TOC_R and MW_R are the capital cost and net power of the reference plant, respectively. $VC_S\ and\ VC_R$ are the variable costs of the scaled and reference plant, respectively. $FC_S\ and\ FC_R$ are the fixed costs of the scaled and reference plants, respectively.

3.1.5.3 **Sustainable Assessment** (Method for Chapter 4, Section 4.3)

Sustainable indicators assist in assessing and providing a holistic and integrated evaluation of a process performance. This will allow us to understand the advantages and disadvantages of the analysed process. Four indicators are used to assess the sustainability of a process including, economic, environmental, social and technical sustainability.

- *Economic indicator* consists of the investment and production cost.

Investment cost: It is the capital investment cost of the power plant per unit capacity used to compare between different power plants.

Production cost (COE): The production cost of converting fuel (biomass or coal) into electricity, hence represented as the cost of electricity (¢/kWh).

The economic comparison was conducted between 10 different power generation processes (Table 4.3, chapter 4) based on previous literature and using Equations 3.12, 3.13, 3.14 and 3.15 to scale up plant size to 650 MW (gross power) in estimating the COE [75, 233, 45, 46 – 48, 239, 44, 204].

- *Environmental indicators.* Power generation processes requires the consumption of raw materials and energy, as well as releasing waste into the environment. This results in resource depletion and environmental degradation. The environmental indicators covered in this paper are the following: net energy efficiency (electricity efficiency), water consumption, renewability and pollution emissions.

Net energy efficiency: Power generation from coal/biomass is essentially converting them to a source of energy that can be easily utilized. A higher net energy efficiency of a power plant, indicates better fuel utilization, hence providing more power while lower pollutants emission into the atmosphere. The net energy efficiency can be calculated using Equation 1. The values for the net energy efficiency of other power plants (Table 4.3, chapter 4) are based on previous literature.

Renewability: A factor to measure sustainable development. It is a way to diminish the use of fossil fuels and promote renewable fuels. It is expressed as the mass ratio of the renewable feedstock to the total feedstock. Power generation processes that only use fossil fuel as energy source are given zero whereas ones that use biomass are given 100%.

Water Consumption: Due to environmental protection and water scarcity, one of the main goals for optimization of power plants is to reduce water consumption and its efficient use. The indicator for water consumption is calculated as tonnes of water per unit power output (tonnes/kWh).

Pollution Emission: Refers to SO_2, NO_X, CO_2 and dust emissions released from power plants which can cause detrimental effects to the environment. They are measured in grams per unit power output (g/kWh).

- *Social indicators* can be the fundamental elements in sustainability which includes community development and energy security.

Community Development: This indicator is qualitative which consists of more than one variable, however employment opportunities at the power plant is adopted as the main factor. It is calculated employee number per unit power output (employee number/MWe).

Energy Security: To ensure national security, having a reliable source of energy is essential. Biomass and coal can provide this security due to them being a reliable source. The energy security indicator is expressed as the ratio between the expected power capacity from the technology to the total electricity demand. It can also be affected depending on the government policies depending on the region. Currently in the UK there is no large-scale CCS power plants, hence all are given zero energy security. The rest are calculated based on the average percentage of energy contribution to the UK power supply.

- *Technical indicators.* Such indicator can be categorized into several variables including system reliability, system operability, technical maturity, etc. However, this study will only focus on technical maturity. Quantitatively technical maturity of each technology will be assessed using a categorical scaling method from 0 - 1, where 1 indicates a large scale industrial fully developed technology; 0.75 demonstrates pilot scale testing; 0.5 represents small test phase; 0.25 demonstrates laboratory test phase; and 0 indicates that basic research hasn't even started. Since coal fired power plant and biomass direct combustion have been tested widely in large scale before they both get 1, however with CCS (tested on pilot scale) it is given a 0.75. Similarly, coal IGCC was tested and developed in the UK during the 1970's, hence given a technical maturity value of 1 but 0.75 with CCS. Whereas with Biomass IGCC was not developed in large scale as much as coal, hence given 0.75 technical maturity and a

0.5 with CCS. BCLGCC has been tested in pilot scale and is still being developed hence was given technical maturity value of 0.5 with and without CCS.

To understand, evaluate and compare the overall sustainability of different power plants more clearly, the aforementioned indicators are normalised according to Equation 3.16 [238].

$$X_{ij} = \frac{x_{ij} - worst\{x_j\}}{best\{x_j\} - worst\{x_j\}} \quad [3.16]$$

where x_{ij} and X_{ij} represents the indicator and normalised indicator j for the process *i*, respectively; $\mathrm{worst}\{x_j\}$ and $\mathrm{best}\{x_j\}$ are assumed to be the worst and best cases of indicator j. The normalised indicator (X_{ij}) varies from 0 - 1. The higher the value the better its sustainability is.

3.2 Life Cycle Analysis: Methodology for Chapter 5

3.2.1 Aim

In the section the methodology for life cycle energy use, CO_2 emissions and cost input evaluation of a 650 MW BCLGCC and Biomass/Coal Integrated Gasification Combined Cycle (BIGCC/CIGCC) power generation plants with and without CCS is explained. These were then compared to coal/biomass combustion technologies. Therefore techno-economic results of all these power plants are required. The following sections develop models using Aspen Plus and IECM to extract BIGCC and CIGCC techno-economic data. In addition, a BCLGCC and BIGCC Gabi models were created to conduct an environmental impact assessment and compare between both processes. The process flow diagrams of the systems and units are then described. Finally, the calculation method is explained in details and plant and process inventory data are collected.

3.2.2 Life Cycle Analysis Strategy

The Life Cycle Assessment (LCA) strategy in this thesis is used to assess the Energy-Cost impact-CO_2 emissions associated with each process in the whole lifecycle. It can be used to understand the effect of CCS technology, fuels source and power generation technology on the energy – cost – CO_2 emissions distribution on power plants. In addition, an environmental impact assessment comparing between both CCS and non-CCS power plants was conducted.

A life cycle assessment was conducted in this thesis according to the ISO-14040 and ISO-14044 standards [240, 241] which included the following stages; defining the goal and scope of the study, creating a life cycle inventory (LCI), conducting a life cycle inventory assessment (LCIA) and interpretation.

As part of the first step in defining the goal and scope, we should define the research target, system boundaries, assumptions made, product function and functional unit. The following step is to create the LCI by collecting data from literature and listing the CO_2 emissions, energy required and cost input data for various processes in the plant. LCI allows you to calculate the LCIA which identifies and evaluates the amount and significance of the potential impact of a product system. This is done by identifying the impact categories of the product and evaluating the CO_2 emissions, energy and cost distribution for each system and its product.

3.2.3 Developing the Model

The Integrated Environmental Control Model (IECM, version 11.2), a software that presents a complete package to simulate the techno-economic performance of large-scale biomass/fossil fueled power plants [242] was used to evaluate data of a BIGCC power plant. The IECM was developed by Carnegie Mellon University with the help of the US Department of Energy's National Energy Technology Laboratory (DOE/NETL). It is commonly used as a computer modelling software that uses fundamental mass and energy balances, using both the user specific plant size and conditions alongside empirical relationships and sub models to calculate the performance, emissions and costs of a power plant for either CCS or Non-CCS [243].

The IECM computer model has a number of pre-defined fuel compositions which uses a look-up table to assign the syngas composition. In the BIGCC plant type model, when an arbitrary fuel composition is inputted, it cannot calculate the syngas composition, however the user can manually define a syngas composition for a respective fuel composition. An Aspen Plus model (Figure 3.8 and Table 3.8) was developed for a conventional oxygen-based biomass gasification plant, validated based on literature [243] (Table 3.9) and used to calculate the syngas composition of biomass, which was consequently inputted in the IECM software to give us the techno-economic results required for conducting a life cycle analysis for the BIGCC power plant. Technical values for the CIGCC were extracted from the IECM software using a pre-defined coal and syngas composition while economic values were taken from literature [200]. Moreover, values for the BCLGCC power plant were taken from our previous study, where a large scale 650MW power plant with and without CCS was simulated and validated followed by conducting a detailed techno-economic analysis [202]. Finally, values of the life cycle analysis of the coal and biomass combustion plants are taken from literature for performance comparison [245].

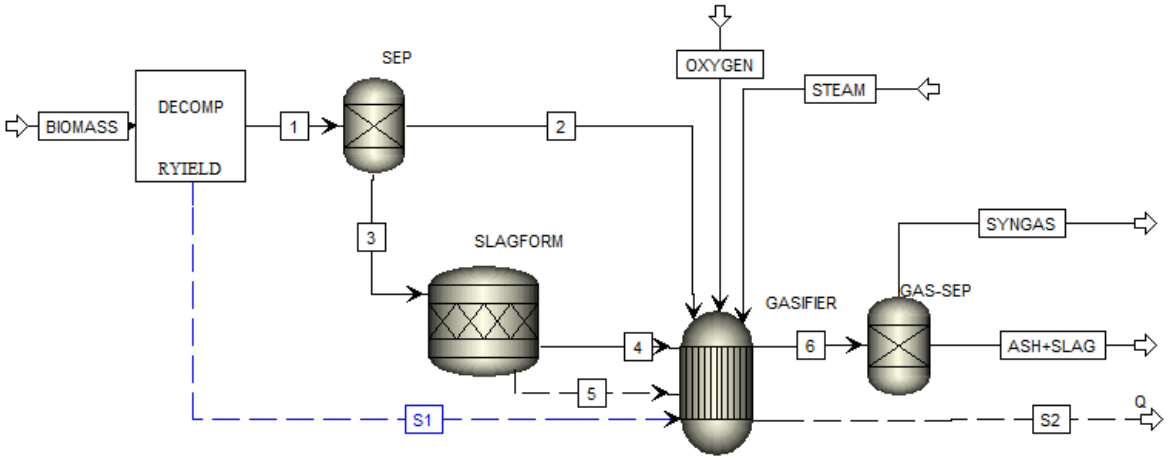

Figure 3.8. Aspen Plus model of a conventional gasification process

Table 3.8. Model block description

Aspen plus block	Block ID	Description	Conditions
Conventional gasification			
RYield	DECOMP	Yield reactor – Based on mass balance this reactor converts the nonconventional biomass into conventional compounds	Outlet Temp: 900°C
RStoic	SLAGFORM	Stoichiometric Reactor - Reacts a percentage of unburnt carbon with the ash to form slag	Outlet Temp: 900°C
RGibbs	GASIFIER	Gibbs free-energy reactor – Simulates the gasification reactions by using the direct minimization of Gibbs free energy to determine the equilibrium composition	Outlet Temp: 900°C
Cyclone	GAS-SEP	Cyclone – Separating ash from syngas by specifying split fraction	99% particle separation

Table 3.9. Conventional gasification model validation data

Gasification type	**Conventional Biomass Gasification**	
Fuel reactor temperature, °C	820	
Fuel reactor pressure, atm	1	
Steam/biomass ratio	0.352	
Oxygen/biomass	0.312	
Carbon conversion efficiency, %	86	
Gas	**Results**	
	Experimental results (%vol.) [244]	Simulation results (%vol.)
H_2	30 – 33	30.50
CH_4	9 – 11	9.55
CO	28 – 32	33.82
CO_2	22 – 27	26.12

3.2.4 Goal & Scope

Solid fuels with CCS technology have the potential to play a vital role in generating low carbon power in the UK. The goal of this research is to evaluate and compare the impact on life cycle energy – cost – CO_2 emissions distribution of 10 different gasification power generation technologies. This included evaluating and analyzing 1) BCLGCC with and 2) without CCS, 3) BIGCC with and 4) without CCS, 5) CIGCC with and 6) without CCS, followed by comparing those results with 7) Direct Biomass Combustion (DBC) with and 8) without CCS and 9) Pulverized Coal Combustion (PCC) with and 10) without CCS. Figure 3.9 shows simple flow diagrams of each of the power generation systems. A detailed description of each unit for the power generation systems can be found in the following section.

The technologies of the mentioned processes are selected from three different groups including, the feedstock (biomass or coal), thermal conversion technology (chemical looping

gasification, conventional gasification or combustion), and whether the plant is coupled with or without a CCS process (post combustion using MEA or pre-combustion using selexol).

Moreover, an environmental impact analysis on the BCLGCC and BIGCC with and w/o CCS life cycle is also conducted. The model flowsheet for both CCS and non-CCS processes (Figure 3.10) is established using GaBi software (commercial software created by Thinkstep) which contains a LCA database, featuring latest inventory data for life cycle based on industry. It can allow us to obtain appropriate data of the life cycle impact assessment (LCIA) for each stage of the process. The CML2001 impact assessment which limits uncertainties, developed by the Institute of Environmental Sciences at Leiden University is used in this assessment [246]. It categorizes the environmental impacts into the following categories:

1) Abiotic depletion potential (ADP_{fossil})
2) Acidification potential (AP)
3) Eutrophication potential (EP)
4) Photochemical ozone creation potential (POCP)
5) Ozone depletion potential (ODP)

3.2.5 Flowsheet and Unit Description

3.2.5.1 Flowsheet Description

Figure 3.9 (A&B) present a flowsheet of a BCLGCC without and with CCS, using milled biomass as feedstock which is gasified using an iron-based oxygen carrier at 875°C and 1 atm pressure. The depleted oxygen carrier is sent to the air reactor where it is oxidized and sent back to the fuel reactor. Syngas and ash are produced, where the syngas is cooled and passed through a gas cleaning process while ash is deposited. The syngas in the CCS process (Figure 3.9A) goes through an acid gas cleaning process using selexol to capture CO_2. The captured CO_2 is compressed, transported, and geologically stored. The syngas is compressed and sent to a combined cycle where it is combusted to generate electricity.

Figure 3.9 (C&D) shows a biomass/coal conventional oxygen based IGCC power plant with and without CCS processes. Oxygen is separated from the air in an air separation unit (ASU) and sent to a fluidized bed gasifier where it partially reacts with the biomass/coal at 850°C and 650 psia to produce syngas and ash. The ash is deposited while syngas is cooled down and cleaned. The CCS process (Figure 3.9D) demonstrates the carbon capture process using a water gas shift to produce more H_2 and CO_2, hence capturing the CO_2 to be compressed,

transported, and stored. The syngas is then sent to a combined cycle where it is combusted to generate electricity.

Figure 3.9 (E&F) demonstrates a biomass/coal air combustion power plant. Air completely combusts with the coal at 1700K – 1900K and biomass at 1600 – 1800K. The hot flue gas produced heats up water passing through the surface of the boiler to generate steam which passes through a steam turbine to generate electricity. The flue gas then passes through a gas cleaning unit before being emitted into the atmosphere. The CCS plants capture the CO_2 via a post combustion capture process using monoethylene amine (MEA), which is then compressed, transported and geologically stored.

A comprehensive energy, cost and CO_2 assessment will be achieved by conducting a detailed calculation of each process phase throughout the whole process for the BCLGCC, BIGCC and CIGCC with and without CCS power plants. Values for the CO_2 emissions, energy requirement and cost input distribution of the DBC and PCC plants with and without capture are taken from literature and compared with the other plants [245]. This is followed by conducting an environmental impact analysis on the BCLGCC and BIGCC power plants with and w/o CCS life cycle.

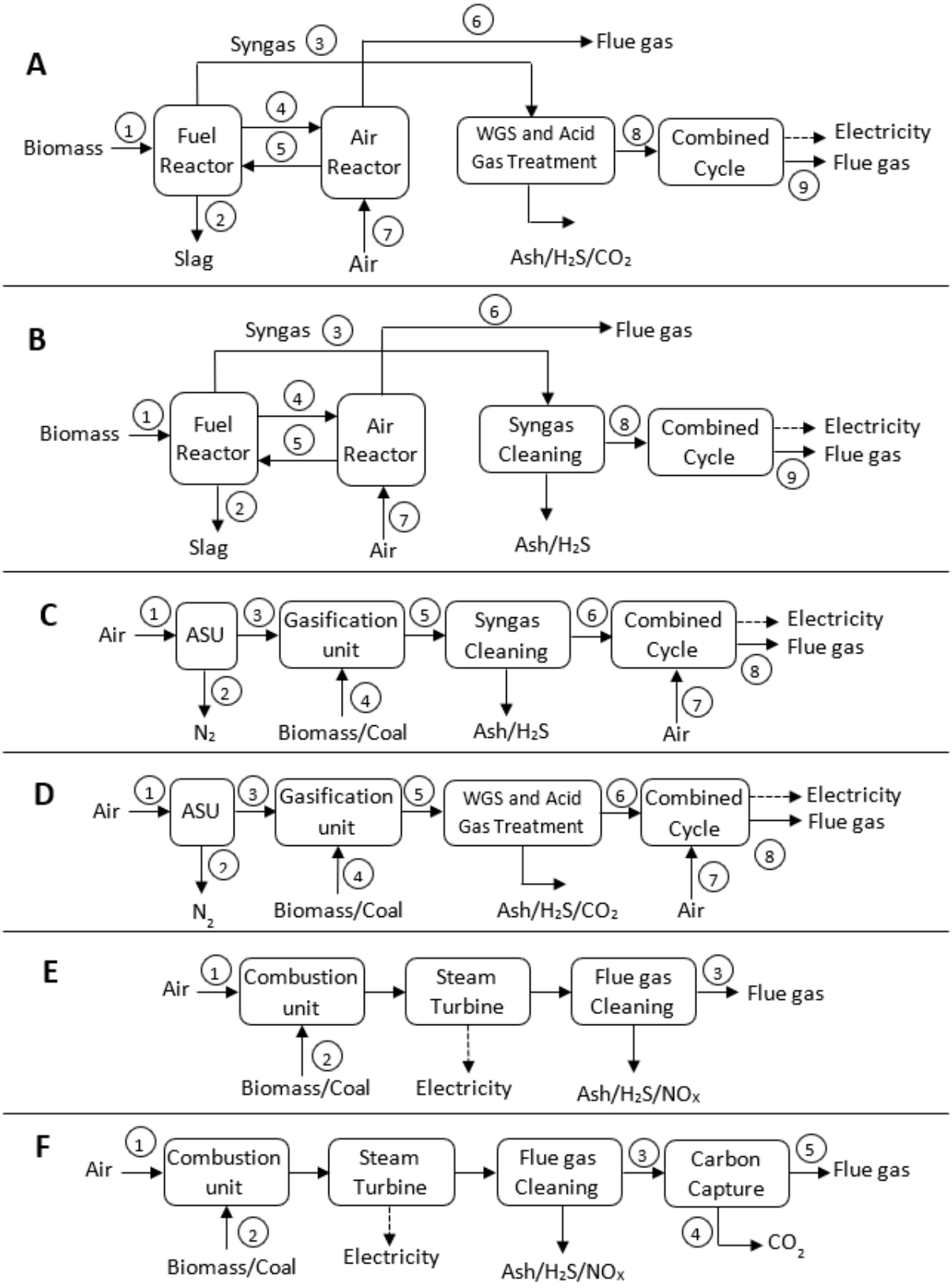

Figure 3.9. Simple flow diagram of the different power generation systems, where (A) BCLGCC with CCS, (B) BCLGCC w/o CCS, (C) biomass/coal IGCC w/o CCS, (D) biomass/coal IGCC with CCS, (E) biomass/coal combustion w/o CCS, (F) biomass/coal combustion with CCS

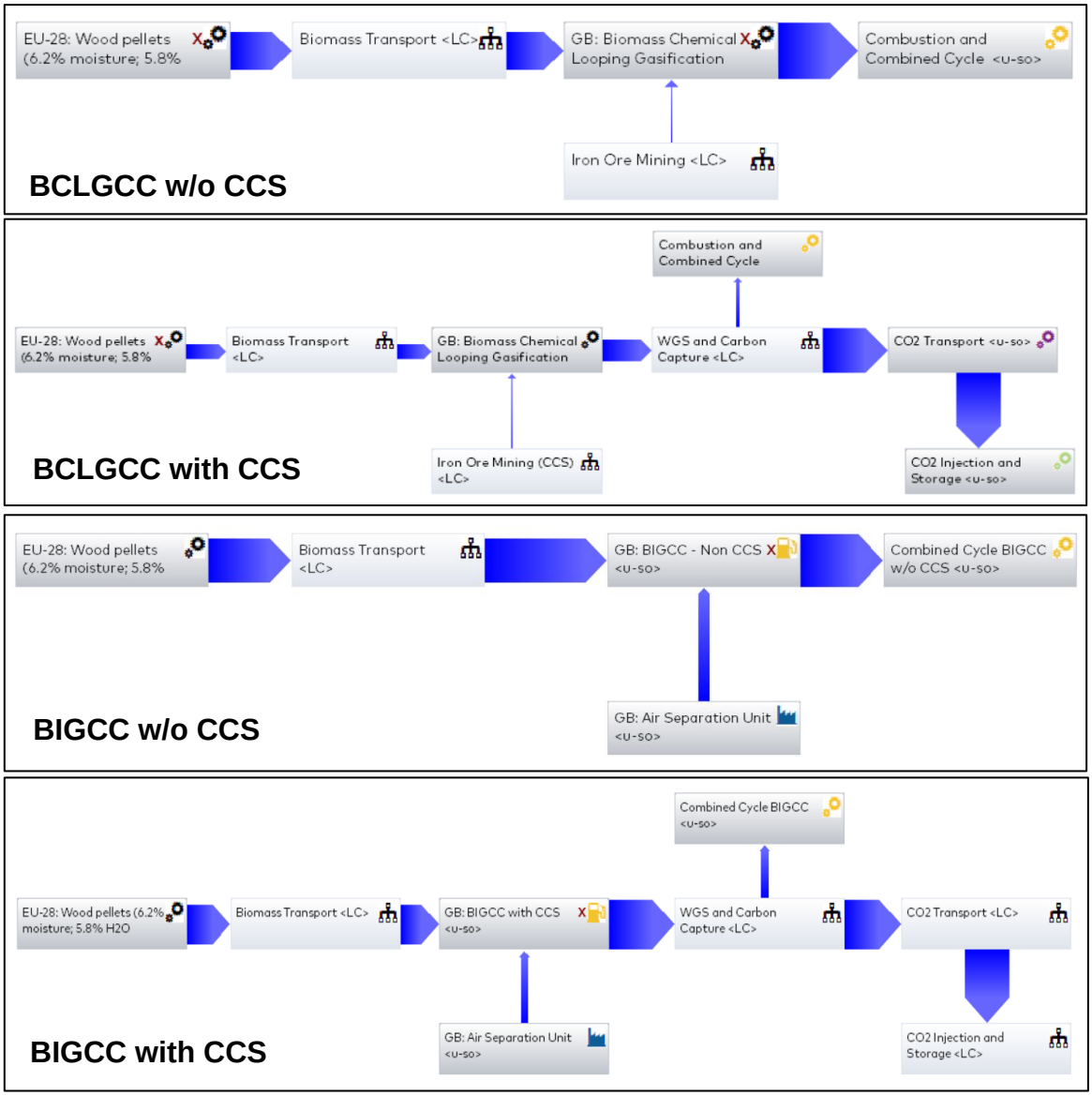

Figure 3.10. LCA BCLGCC and BIGCC with and w/o CCS model established using Gabi software.

3.2.5.2 Unit Description

This section will go into giving an introduction and brief explanation into each unit for biomass/coal combustion or gasification to power generation processes. Table 3.11 summaries the technologies and the operating conditions for all the processes in Figure 3.9. The components and composition of each stream is summarised in Tables A5 & A6 in the **Appendix**.

Combustion Unit

Combustion boilers can be classified into two systems, fixed bed combustors and fluidized bed combustors [247]. This paper uses a fluidized bed combustor for the coal/biomass combustion unit. The reactions taking place in the reactor are listed in Table 3.10. The

pulverised biomass/coal fuel and air mixture is injected into the combustion chamber via a series of burner nozzles from the side of the vessel. The burners are designed to allow additional secondary air to be simultaneously injected into the boiler hence controlling the fuel-air ratio inside the combustion chamber. Excess oxygen is injected into the chamber to ensure complete combustion of the fuel. Heat is transferred to the solid fuel particles by convection from the surrounding hot combustion gases as well as radiation from other combusting particles and the boiler heat transfer surfaces. In the combustion chamber, the solid particles heat up and vaporize resulting in mixing with primary air hence combusting as volatile flame. The char particles remaining in the bed continue to heat up but at a slower rate. Temperature and oxygen concentration are the two main factors that affect the combustion process at different zones in the boiler. The fuel – to – air ratio as well as the fuel type influences the volatile flame temperature. Coal can result in a volatile fuel temperature between 1700K – 1900K [248], while biomass since it has a lower calorific value can result in a volatile flame temperature of 1600K – 1800K [249, 250]. At optimal stochiometric air – to – fuel ratio mix, the flame temperature can reach its highest value. The air – to – fuel ratio can be adjusted in the primary combustion zone which as a result controls the flame temperature. Even though increasing the boiler's temperature can be advantageous to thermal efficiency and heat transfer, it can also increase nitrogen oxide emissions and intensify ash melting in the furnace, therefore controlling the combustion temperature is vital. At higher fuel – to – air ratio mixtures, the incompletely burnt product from the primary zone combusts with secondary air, while some cases requiring a tertiary air injection stage [251]. Moreover, another factor that can affect flame temperature is moisture content, which reduces the flame temperature by 100K for each 10% moisture by weight [252]. For higher level burn-out, it is ideal that the fuel particles should completely combust by the time they have reached the top of the boiler. This will allow for maximum thermal energy to be released to the combustion chamber. The thermal energy is then used to create steam to generate electricity. Heat is transferred to the steam generation section of the boiler via the combustion chamber wall which is surrounded by a water jacket. The generated steam goes through a steam drum and exits at the top of the boiler at high pressure over 150 bar or even supercritical pressures of more than 220 bar. The temperature of the steam can be further increased by passing it through super heaters, which are found within the combustion chamber. The steam turbines

are generally divided into 3 stages, high pressure steam, intermediate pressure steam and low-pressure steam. The operating conditions are stated in the steam turbine section.

Air Separation Unit

ASU configurations can vary from complete integration with the plant, where the compressed air from the turbine is sent to the ASU or a zero-integration stand-alone ASU with its own air compressor to increase the pressure of the air to the minimum pressure required for the cryogenic process. The latter process ensures operation stability and flexibility; hence the latter option is employed. In a cryogenic process air is cooled to a liquid state, then distilled to separate the oxygen from the nitrogen. The basic components of air separation is starting with filtering and compressing air, followed by removing contaminants, including water vapor and carbon dioxide (which would freeze in the process). The air is then cooled to very low temperatures through heat exchange and refrigeration process, and finally distilling the partially condensed air at about -185˚C to produce pure oxygen. The oxygen and waste streams are warmed by heat exchange with incoming air [253].

Gasification Unit

Biomass is initially injected into the gasification reactor where it undergoes devolatilization, pyrolysis, combustion and gasification reactions in the presence of an oxygen starved atmosphere providing limited oxygen for the combustion/gasification reactions to take place. The presence of limited amount of oxygen results in syngas (CO + H_2) being formed. Currently there are three main types of gasification reactors in use namely, entrained flow reactor, moving ben reactor and fluidized bed reactor [254]. However, for this study a fluidized bed reactor is used. Fluidized bed reactors have a bed of fluidizing particles which enhance the efficiency of mixing the fuel and heat within the reactor vessel. This allowed for a constant temperature to be contained within the vessel which is below ash fusion temperature. This avoiding bed defluidization and clinker formation, hence making it suitable for biomass fuel. Additionally, some char particles tend to escape with the syngas out of the vessel, however they are brought back into the reactor using a cyclone. The bed operates at a constant temperature of around 1800°F with fuel particle size ranging from 0.1 mm to 10 mm [255].

Table 3.10. Reactions taking place during the gasification/combustion process

Reaction No.	Equations
	Biomass pyrolysis
1	$C_nH_{2m}O_x \rightarrow char + tar + syngas\ (CO, H_2, CO_2, CH_4, C_nH_{2m})$, (Endo.)
	Biomass gasification
2	$C + H_2O \rightarrow CO + H_2$ (Endo.)
3	$CH_4 + H_2O \rightarrow CO + 3H_2$ (Endo.)
4	$C + CO_2 \rightarrow 2CO$ (Endo.)
5	$C + 2H_2 \rightarrow CH_4$ (Exo.)
	Combustion reactions
6	$2C + O_2 \rightarrow 2CO$ (Exo.)
7	$2CO + O_2 \rightarrow 2CO_2$(Exo.)
8	$2H_2 + O_2 \rightarrow 2H_2O$ (Exo.)
9	$2CH_4 + O_2 \rightarrow 2CO + 4H_2$ (Exo.)
10	$CH_4 + 2O_2 \rightarrow CO_2 + 2H_2O$(Exo.)
	Water gas shift (WGS)
11	$CO + H_2O \rightarrow CO_2 + H_2$ (Exo.)
	Contaminants
12	$N2 + 3\ H_2 \rightarrow 2\ H_3N$
13	$S + H_2 \rightarrow H_2S$
14	$CO + S \rightarrow COS$

Water Gas Shift and Acid Gas Treatment

The syngas produced contains high amount of carbon and sulphur components. However, for this process to be carbon neutral and to prevent sulphur emissions, they should be captured pre-combustion. Therefore, a Water Gas Shift (WGS) unit is added where syngas reacts with high temperature steam in a reactor, shifting the reaction towards producing more CO_2 and H_2. This is also a COS hydrolysis unit where the COS is converted into H_2S as shown in Reaction R16. The reaction takes place in the presence of a cobalt-molybdenum catalyst at around 500°F [256]. Since the reaction taking place in the reactor is exothermic, the shifted syngas is cooled followed by an acid gas treatment section, capturing approximately 99.5% H_2S and some CO_2. The syngas is also reacted in a water gas shift unit with steam as shown in Reaction R17, converting the CO into CO_2 and H_2O into H_2. Since high percentage of CO_2 is present in

the syngas (30 – 40%) it is preferred if a physical solvent is used to capture the CO_2. The physical solvents do not form chemical bonds with the CO_2 to capture it, however it physically adheres to the solvent. The CO_2 free syngas is sent to the downstream equipment, i.e combined cycle, while the solvent is sent to a stripper where the acid gas is stripped to regenerate the solvent for it to be recycled.

$$COS + H_2O \rightarrow H_2S + CO_2 \quad \text{(R16)}$$

$$CO + H_2O \rightarrow H_2 + CO_2 \quad \text{(R17)}$$

Carbon Capture and Flue Gas Cleaning

The flue gas produced after the combustion process between the solid fuel and air constitutes of a mixture of CO_2 and N_2 gases. The process by which CO_2 is capture is called post-combustion capture which uses absorption method instead of adsorption to capture the CO_2 molecules due to the lower concentration of CO_2 in the flue gas (approximately 15%). In this case a chemical absorbent monoethanolamine (MEA) is used to capture approximately 90% of the CO_2 in the flue gas [257]. Before the absorption process, the gas should be cleaned from any impurities such as SO_X, NO_X and particulate matter as they affect the performance of the system since they form heat stable salts with the solvent. SO_X concentration should be less than 10 ppm, which is achieved by adding a Flu Gas Desulphurization (FGD) unit. NO_X can be removed by implementing either of the 3 following technologies, 1) Selective Catalytic Reduction (SCR), 2) Selective Noncatalytic Reduction (SCNR) or 3) Low NOx burners. Particulate matter (i.e fly ash) can cause foaming in the absorber and stripping column, hence decreasing the performance. They can be captured using either an electrostatic precipitator (ESP), bag house filer, cyclone, or a venturi scrubber. Moreover, oxygen content in the flue gas can increase the chance of corrosion in the equipment as well as resulting in the degradation of the alkanolamine solvents. Hence oxygen level is recommended to remain below 1ppm when corrosion inhibitors are not used [258]. Flue gas is initially cooled down to approximately 45 – 50°C. This improves CO_2 absorption while minimizing solvent loss due to evaporation. The flue gas is then counter currently contacted with the lean solvent with a CO_2 loading of about 0.1 – 0.2 mol CO_2/mol MEA. After contacting with the CO_2 rich flue gas, it produces a rich solvent of about 0.4 – 0.5 mol CO_2/mol MEA loading [259]. The scrubbed gas is then washed with water to clean it from any traces of solvent and finally released into the atmosphere. The temperature in the absorption column is between 40° - 60°C. The rich

solvent is then heated in a stripper at temperatures between 100° - 120°C and around 1.5 – 2 atm pressure to be regenerated and pumped back to the absorber via a cross heat exchanger to bring its temperature back down to 40° - 60°C. This produces a high purity stream on 99% CO_2 [260].

Combined Cycle

- **Gas Turbine**

Gas turbines have the greatest impact on the efficiency and consequently the cost of combined cycle power plants relative to other units. The pressure ratio and firing temperature are the two basic parameters that the gas turbine efficiency depends on. As the firing temperature increases the turbine's size increases, resulting in an improved plant efficiency and reduction in plant costs. The most currently used gas turbines for IGCC plants are categorized as either F- or G- class with firing temperatures ranging between 1370 - 1430°C [261]. Recent developments in gas turbines are the H-class, J-class and the Japanese national turbine project, with firing temperatures of 1500°C, 1600°C and 1700°C, respectively. This increase in temperature with increases the efficiency requires cooling of the gas turbines to prevent components in the turbine such as blades from melting. To prevent the melting of gas turbine components, compressed air from the air compressor is sent to the turbine, hence providing adequate cooling. A combination of several cooling methods are implemented in modern gas turbines to allow for higher firing temperatures which consequently increases efficiency [262]. This paper used a 7F-class turbine.

- **Steam Turbine**

Gas turbines have been commonly used in power generation processes. A conventional natural gas fired gas turbine with a simple cycle generally has an efficiency of 35%. However, new power plants enhance the process with an additional heat recovery steam generator (HRSG) block followed by a steam turbine, which is known as a combined cycle. The reasoning behind that is for the heat in the exhaust gas to be captured via the HRSG process, converting feed water into steam which is sent to a steam turbine for power generation. A gas turbine (simple cycle) coupled with a HRSG and steam turbine. The heat recovered from the exhaust gas is used to generate high pressure steam which then passes through the steam turbine, dropping the pressure and temperature of steam, converting heat into shaft work to generate electricity. The steam turbine is divided into 3 stages: high-pressure steam turbine,

intermediate-pressure steam turbine and low-pressure steam turbine. This is due to the high pressure of steam which will result in large expansion if pressure is reduced all at once. The pressure of the high-pressure steam is equal to 1700 psia, while 600 psia for intermediate pressure and 65 psia for low pressure [263].

Table 3.11. Summary of the technologies and operation conditions

Unit	Operation Conditions
Fuel Reactor & Air Reactor	***Fuel Reactor*** **Reactor Type:** Fluidized Bed reactor **Temperature:** 875°C **Pressure:** 1 atm ***Air Reactor*** **Reactor Type:** Fluidized bed reactor **Temperature:** 975°C **Pressure:** 1 atm
Combustion	**Reactor Type:** Fluidized Bed Reactor **Temperature:** 1600 – 1900K
Gasification	**Reactor Type:** Fluidized Bed Reactor **Temperature:** 875°C **Pressure:** 62 bars
Air Separation Unit	**Technology:** Cryogenic Distillation **Temperature:** -185°C
WGS & Acid Gas Treatment	**Pre-combustion capture process:** Selexol process for CO_2 and H_2S capture. **Catalyst:** cobalt-molybdenum **Temperature:** 260°C
Flue gas/Syngas Cleaning	**NO_X removal:** Selective Non-Catalytic Reduction **SO_X removal:** Flue gas desulphurisation **Particulate matter:** Cyclone
Carbon Capture	**Post-combustion capture process:** MEA capture process **Absorber Temperature:** 40 – 60°C **Stripper Temperature:** 100 – 120°C
Combined Cycle	***Gas Turbine:*** **Temperature:** 1370 – 1430°C **Turbine class:** 7F class turbine

	Steam Turbine: **High Pressure Turbine:** 1700 psia **Intermediate Pressure Turbine:** 600 psia **Low Pressure Turbine:** 65 psia

3.2.6 Calculation Method and Plant Data

Table 3.12 presents the performance and cost summary of the 10 power plants. The BIGCC and CIGCC data presented in Table 3.12 are extracted from the reliable IECM software which was developed by Carnegie Mellon University with the support of the US Department of Energy's National Energy Technology Laboratory (DOE/NETL) as well as the "Cost and Performance Baseline for Fossil Energy Plants Volume 1: Bituminous Coal and Natural Gas to Electricity" [200] report by the US Department of Energy. Whereas the BCLGCC cost and performance data were extracted from my previously published work [202], where I developed and validated a 650MW Aspen Plus model, followed by conducting a techno-economic analysis. Finally, the PB and PCC power plants cost and performance data, as well as life cycle data was taken from our group's previously published work [245]. This is then followed by conducting a sensitivity analysis on the life cycle results to ensure the reliability of the results presented.

The system boundary is from cradle to grave, with the scope of the power plants include wood harvesting and transport, wood processing at the pellet plant, pellets transport (via rail, shipment and truck), wood pellets handling and storage, iron mining, iron transport to the power plant, coal mining and washing, coal transport to the power plant, power generation, CO_2 capture and compression, CO_2 pipeline transport, and CO_2 storage. This is summarized in Figure 3.11. All these process phases are investigated to achieve the proposed goal. The function of the process is to generate electricity and the functional unit (FU) is taken as one MWh for impartial comparison between different power generation technology with and without CCS. Since no other significant co-product is generated during the process, there is no multifunctionality, hence other products can be ignored.

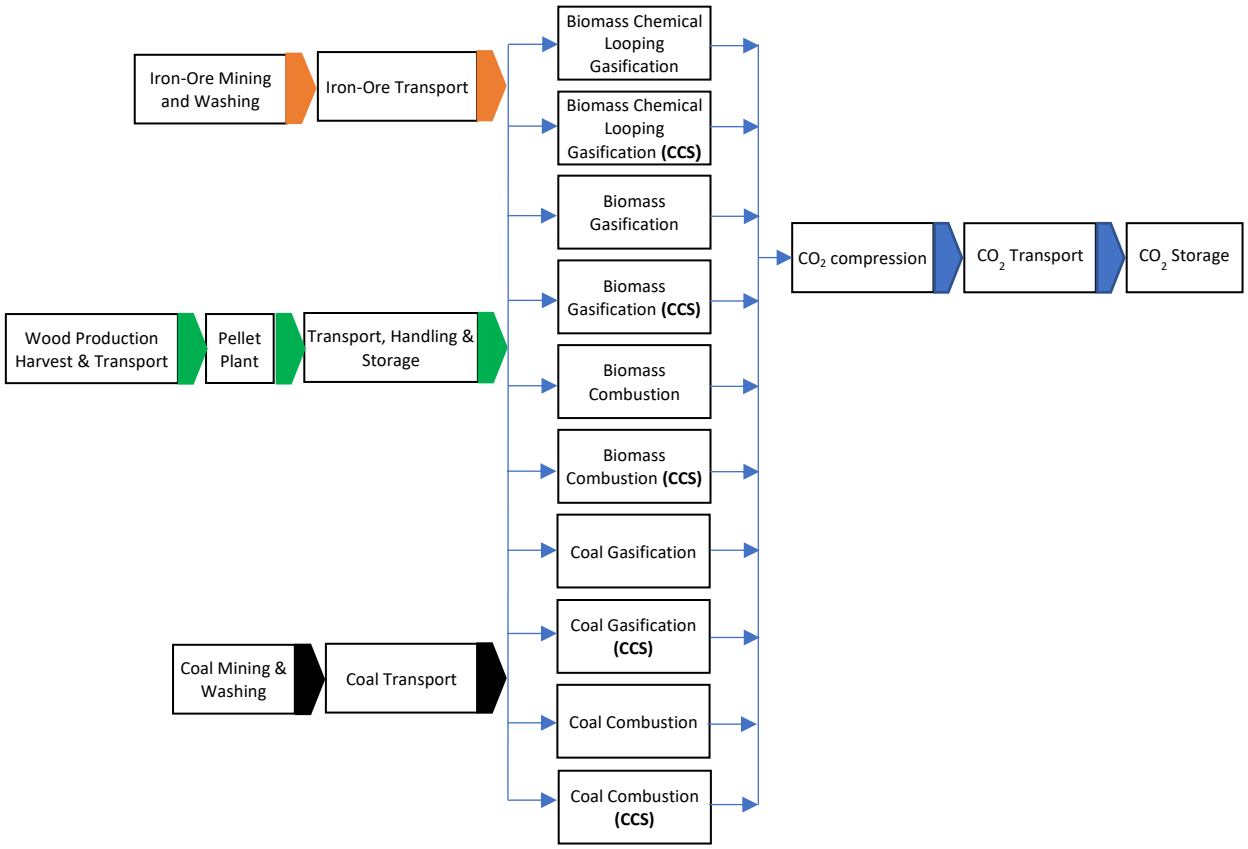

Figure 3.11. Complete life cycle scope of the biomass/coal gasification plants

Table 3.12. Cost and performance values for the life cycle analysis. [200, 202, 245]

Power Plant	BCLGCC		BIGCC		CIGCC		PB		PCC	
CCS/Non-CCS	Non-CCS	CCS	Non-CCS	CCS	Non-CCS	CCS	Non-CCS	CCS	Non-CCS	CCS
Fuel Type	Biomass		Biomass		Coal		Biomass		Coal	
Gross Power, MW	650	650	650	650	650	650	650	650	650	650
Net Power, MW	546	504	586	549	559	520	607	500	605	526
Net Efficiency, %	41	36	38.6	32.4	39.5	32.9	37.6	26.4	38.3	28.5
Feedstock Input, t/h	275	270	292	326	195	218	311	364	231	270
Capacity Factor, %	0.8	0.8	0.8	0.8	0.8	0.8	0.62	0.62	0.85	0.85
Plant Life, year	25	25	25	25	25	25	20	20	20	20
Discount ratio, %	10	10	10	10	10	10	10	10	10	10
CO_2 Capture Efficiency, %	0	90	0	90	0	90	0	90	0	90
Plant Capital Cost, £/kW	2101	2966	2268	3240	1970	2800	1212	2302	1184	2236

During the past decade, the UK has been moving away from coal power generation and has been increasing its biomass power generation sourced mainly from the United States which has been a reliable and steadily growing supplier in the past few years [264, 265]. The biomass pellets will be supplied from a pellet manufacturer in America, whereas bituminous coal is

domestically mined in the UK or imported from Russian, Colombia, Australia or the US [12], however in this thesis coal is assumed to be sourced from UK mines. The elemental composition (on a dry basis wt%, db) of the biomass pellets is 44.4% Carbon, 4.6% Hydrogen, 0.2% Nitrogen, 0.01% Sulphur, 43.5% Oxygen, 7.1% Moisture and 0.2% Ash, with the lower heating value (LHV) equal to 18.7 $MJ.kg^{-1}$. Whereas the elemental composition (on a dry basis wt%, db) of coal is 59.6% Carbon, 3.8% Hydrogen, 1.5% Nitrogen, 1.8% Sulphur, 5.5% Oxygen, 0.2% Chlorine, 12.0% Moisture and 15.6% Ash, with the lower heating value (LHV) equal to 24.61 $MJ.kg^{-1}$.

The equation to calculate the total life cycle energy input (TLCEI) per MWh electricity (MJ/MWh) of a power plant is expressed by Equation [3.17] shown below;

$$TLCEI = \frac{\sum_{i=1}^{n} E_i}{Total\ no.of\ hrs/yr \times Net\ Power\ Output\ (MW)} \quad [3.17]$$

where $\sum_{i=1}^{n} E_i$ is the energy consumption in the i_{th}sub process.

The equation to calculate the total life cycle CO_2 emissions (TLCCE) per MWh electricity ($kgCO_2$/MWh) of a power plant is expressed by Equation [3.18] shown below;

$$TLCCE = \frac{\sum_{i=1}^{n} CE_i + CE_{pp} + \sum_{j=1}^{n} CE_j}{Total\ no.of \frac{hrs}{yr} \times Net\ Power\ Output\ (MW)} \quad [3.18]$$

where CE_i and CE_j are the CO_2 emissions of the i_{th} sub process in feedstock supply chain and j_{th} sub process in CO_2 compression, transport and storage, respectively. CE_{PP} is the emissions at the power plant during electricity generation.

Similarly, the total life cycle cost input (TLCCI) per MWh electricity (£/MWh) of a power plant can be calculated using Equation [3.19];

$$TLCCI = \frac{\sum_{i=1}^{n} C_i + C_{pp} + V_{pp}}{Total\ no.of \frac{hrs}{yr} \times Net\ Power\ Output\ (MW)} \quad [3.19]$$

Where $\sum_{i=1}^{n} C_i$ is the total cost input (£/yr) of the i_{th} sub process from the feedstock supply chain as well as CO_2 transport and storage, C_{pp} is the total annual capital cost of the power plant (£/yr), and V_{pp} is the variable cost (£/yr).

The annual capital cost (ACC, £/yr) can be calculated using Equation [3.20];

$$\text{ACC} = \frac{Capital\ Cost \times i}{1-(1+i)^{-N}} \quad [3.20]$$

where i is the discount rate, 10% and the N is the plant lifetime in years (25 years) [43].

3.2.7 Life Cycle Inventory

Woody biomass is initially harvested and often chipped then transported to the pelleting plant via trucks or railways, most common methods for inland transport. Since the pellet plant is usually close to the harvesting ground the input cost, CO_2 emissions and energy input for the transport to pellet plant stage is assumed to be very negligible and taken part of the wood harvesting values. At the pellet plant, the untreated biomass chips are taken through the process of drying, size reduction and pelletization to make them suitable for transportation [266].

In this paper it is assumed that the power plants are located in the same region as the Keadby power station, United Kingdom. This is because it already has a large combined cycle gas turbine (CCGT) power stations in operation with current discussions regarding a Keadby 3 station which uses hydrogen energy is being proposed [267]. The region has a potential to play a vital role in supplying the UK's energy demands in the future as it is being transformed into the world's first 'zero-carbon cluster' by 2040. The first stage of biomass transportation is via rail for 149 km from Tifton, Georgia in the US to the port in Savannah [268]. The biomass feedstock is stored, handled, and loaded onto a Handymax ship (45,000-ton capacity [268]) and transshipped to the port of Hull, UK, covering 7,500 km [269]. From the port the biomass feedstock is transported via trucks to the power plant covering 63 km [270]. In regard to coal supply chain, all coal mines in the UK are opencast due to the closure of deep coal mines in recent years. The opencast mines are found to be distributed not far from the Keadby power plant at a range of 50 – 150 km. The coal supply chain to the power plant includes mining, washing and transport via rail (100km). According to the distribution of iron mines in the UK [271], they are approximately 200 km away from the location of the power plant. The supply chain process for iron ores is essentially iron mining and transport.

Finally, since the power plants are gasification based, hence produce syngas with a higher CO_2 concentration, a pre-combustion capture technology is used, i.e selexol process using polyethylene glycol dimethyl ether. The CO_2 is compressed to 11 MPa (sub-critical state) for

transportation using pipelines, due to them being the cheapest and most commonly used method for long distance CO_2 transport. Out of all the different geological CO_2 storage sites saline aquifers are used due to their large storage capacity. The CO_2 is then recompressed from 10.76 MPa to 15 MPa, the pressure used by most existing CCS projects before injection. Additionally, the CO_2 released during transportation and compression is also considered in the life cycle assessment according to the methodology developed by the IPCC report [272]. It was assumed that the storage site is 150 km [273] away from the power plant since storage sites are scattered around that distance.

All the data for each stage during the supply chain process for cost input, CO_2 emission and energy input is listed in Table 3.13. In addition, Tables (A1 – A4) in the **Appendix** summarize the life cycle inventory input and output data, respectively, for the environmental impact assessment using Gabi. These data have been extracted from the Aspen Plus model developed in section 1.3.4. Moreover, the iron-ore mining process life cycle inventory data, air separation unit energy consumption and the amount of selexol required for CO_2 capture are summarized in Table 3.14.

The data used for the life cycle calculation of each section was taken from published data in journals, government bodies, the IPCC reports, and the International Energy Agency (IEA) as shown in the references. Those are all reliable and accurate sources with peer reviewed work (almost all the data are from official authoritative data) showing that the data (Table 3.12 Table 3.13, Table 3.14) used in this thesis is reliable and acceptable.

Table 3.13. Life cycle inventory data for the life cycle analysis.

Energy Consumption	Value	Unit	References
Coal mining and washing	1.8	MJ/kg	[274, 275]
Coal Transport (100 km)	0.281	MJ/t km	[275]
Wood Harvesting & Transport	9.9	$MJ/MWh_{(biomass)}$	[268]
Wood Processing	573.3	$MJ/MWh_{(biomass)}$	[268]
Pellet Handling & Storage	3.8	$MJ/MWh_{(biomass)}$	[268]
Transport to port (by rail) - 145 km	11.1	$MJ/MWh_{(biomass)}$	[268]
Ocean Transport - 7500 km	0.03	MJ/t km	[268]
Transport to power plant (by truck) - 50 km	2.3	MJ/t km	[268]
Iron mining	124.4	MJ/t	[276]
Iron Transport (200 - 300km)	20.9	MJ/t km	[276]
CO_2 Capture		Calculated	
CO_2 storage (Injection compression)	7	kWh/t CO_2	[277]
CO_2 transport	2.4	kWh/t CO_2	[278]
CO_2 Emissions			
Coal mining and washing	49.74	kg/t	[245]
Coal transport (by rail)	0.0830	kg/t km	[275]
Wood production harvest and transport	1.6	$kgCO_2/t$	[268]
Wood processing in pellet plant	12.2	$kgCO_2/MWh_{(biomass)}$	[268]
Handling and storage	0.28	$kgCO_2/MWh_{(biomass)}$	[268]
Wood pellets transport to port (by rail)	0.01	$kgCO_2/t$ km	[268]
Wood pellets ocean transport	0.004	$kgCO_2/t$ km	[268]
Wood pellets transport to power plant (by truck)	0.12	$kgCO_2/t$ km	[268]
CO_2 compression (fugitive CO_2 emission compressor)	23.2	$tCO_2/MW/yr$	[277]
CO_2 transport (fugitive CO_2 emissions pipeline)	2.32	$tCO_2/km/yr$	[277]
Fugitive CO_2 emission from CO_2 storage	7.01	$kgCO_2/tCO_2$	[279]
Iron mining	9.8	$kgCO_2/t$ ore	[276]
Iron Transport (200 - 300km)	1.3	$kgCO_2/t$ ore	[276]
Cost			
Coal mining and washing	52	£/t	[245]
Coal transport (by rail)	5.93	£/t	[280]
Wood production harvest and transport	10.97	$£/MWh_{(biomass)}$	[268]
Wood processing in pellet plant	8.47	$£/MWh_{(biomass)}$	[268]
Loading port handling and storage	4.5	£/t	[266]
Wood pellets transport to port (by rail)	2.19	$£/MWh_{(biomass)}$	[268]
Wood pellets ocean transport	0.00036	£/MWh km	[268]
Wood pellets transport to power plant (by truck)	2.9	$£/MWh_{(biomass)}$	[268]
Receiving port handling and storage	4.5	£/t CO_2	[266]
Iron mining	75	£/t CO_2	[13]
Iron Transport (200 - 300km)	10	£/t CO_2	[281]
CO_2 transport & storage	25.275	$£/tCO_2$	[43]

Table 3.14. LCI data for used in the environmental analysis.

Stage	Inventory		
	Item	**Value**	**Units**
	Iron Ore Mining [276]		
Drilling	Diesel	0.03	kg/t ore
Blasting	Explosives	0.5	kg/t ore
Loading and Hauling	Diesel	2.2	kg/t ore
Crushing and Screening	Electricity	2.5	kWh/t ore
Stacking and Reclaiming	Electricity	0.5	kWh/t ore
Overall	Water	0.21	kg/t ore
	Waste rock	1.3	t/t ore
	Carbon Capture [282]		
Carbon Capture	Selexol	0.007	t/t-CO_2
	Air Separation Unit [283]		
Oxygen Production	Energy	0.2	kW/kg-O_2

3.3 Bench-Scale BCLG Experiments: Methodology for Chapter 6

3.3.1 Aim

The aim of this section is to summarize the methodology for conducting a bench-scale BCLG tests, followed by mentioning the material characterization tests performed on the oxygen carrier. Finally, the calculation method is laid out in details.

3.3.2 Materials

Sawdust of pine was used as the fuel and natural hematite was used as the oxygen carrier used in the following tests. The composition and description of both is summarized in section 3.2.1 and Table 3.1. The natural hematite was heated up in a furnace for 3 hours at 250°C to ensure it has reached its highest oxidation state as Fe_2O_3.

3.3.3 Experimental Setup

A fixed bed reactor was used to investigate the effect of using hematite oxygen carrier in biomass chemical looping gasification. The schematic diagram of the reaction equipment is shown in Figure 3.12. The experimental set up consisted of an electric heating furnace (including a temperature control system), a quartz tube reactor, a gas distribution system and a gas testing system. The fixed bed reactor was used for both fuel and air reactors.

During the experiment, a quartz wool sample (~0.2g) is placed on top of a porous plate in the middle of an 800mm long quartz tube reactor with an inner diameter of 15mm. Hematite

sample is then placed on the quartz wool in the reactor. Both top and bottom ends of the reactor are sealed by a stainless-steel joint. The tube is then purged with nitrogen for 25 minutes to create an inert atmosphere followed by heating the reactor including the carrier gas (nitrogen) to a desired reaction temperature. The reaction temperature was measured using a K-type thermocouple near the perforated plate inside the reactor. The volumetric flow of air and carrier gas (high purity N_2) were controlled by a mass flow controller. After the experimental temperature reached the desired reaction temperature, biomass fuel was dropped into the reactor using a ball valve that is used to seal the top of the reactor. The stopwatch is then started to record the reaction time. The carrier gas (N_2) is allowed to keep flowing from the top of the reactor during the reaction. The generated gas product escapes from the bottom of the reactor along with the carrier gas which is then bubbled through an isopropanol solution (placed in a Mengshi washing bottle) to remove any tar escaping with the gas product. This was followed by passing the gas through a Mengshi washing bottle filled with colour-changing silica gel for the drying process. The gas product is then collected in a sampling bag for it to be tested using gas chromatography (Agilent Refinery Gas Chromatograph, 7890A) analysis. After the reaction is complete, the heating element is switched off and the reactor temperature is allowed to cool back down to room temperature. The N_2 flowrate is then stopped. The hematite sample is taken for an XRD analysis. An X-ray diffractometer (XRD, X'Pert Pro MPD) with Cu Kα radiation (λ = 0.1542m) operating at 40 kV and 40 mA was used to analyse the crystal structure of the reacted OC sample. The sample was scanned at a scanning rate of 2°/min from 2θ = 5° to 80° at a step of 0.02°. This was followed by conducting a scanning electron microscope (SEM) and Energy Dispersive X-ray Spectrometer (EDX) tests using a Hitachi SU-70 instruments which was used for the morphology characteristics and elemental analysis of the OC. The reduced hematite samples (tested under different temperatures) were then placed back into the reactor on a quartz wool sample and heated up to 950°C. The N_2 gas was switched to air (100 ml/min) for the oxidation of some reduced oxygen carrier samples. After the experiment, the oxygen carrier was cooled to room temperature under N_2 atmosphere then collected for XRD and SEM-EDX analysis.

The following set of experiments were conducted: -

Blank Tests

- A blank experiment was conducted where silica beads are added in the reactor with the biomass instead of hematite and results were recorded at different temperatures

Temperature

- A set of chemical looping gasification reactions were conducted to measure the effect of temperature in the presence of hematite in a fuel reactor
- The reduced hematite is then regenerated in an Air reactor by reacting it with air
- The gas compositions were measured to calculate the gas yield, LHV and gasification efficiency
- The regenerated hematite is then characterized using an XRD and SEM-EDX

Oxygen Carrier/Biomass

- Similar procedure as temperature was used but testing different OC/Biomass ratios

Reaction Time

- Similar procedure as temperature was used but testing different reaction times

Table 3.15 summarizes the experimental conditions of the reactions taking place.

Table 3.15. Experimental Conditions

Species	Operation Parameters
Oxygen Carrier	Natural Hematite
Reaction Temperature	840°C (750°C, 800°C, 850°C, 850°C, 900°C)
Oxidation Temperature	950°C
Oxygen Carrier (OC) Mass	1.7g (Does not change with change in B/OC ratio)
Fuel	Pine Sawdust
Biomass Mass	1g (Changes with change in B/OC ratio)
Biomass/OC	0.61, 0.67, 0.73, 0.78, 0.89
Carrier Gas	N_2
Carrier Gas Flowrate	100 ml/min
Oxidizing Agent	Air
Oxidizing Agent Flowrate	100 ml/min
Reduction Time	45 min (10min, 20 min, 30min, 40 min, 50min)
Purge Time	25min
Oxidation Time	1 hour
Number of Cycles	9 Cycles
GC calibration frequency	Every 2 months

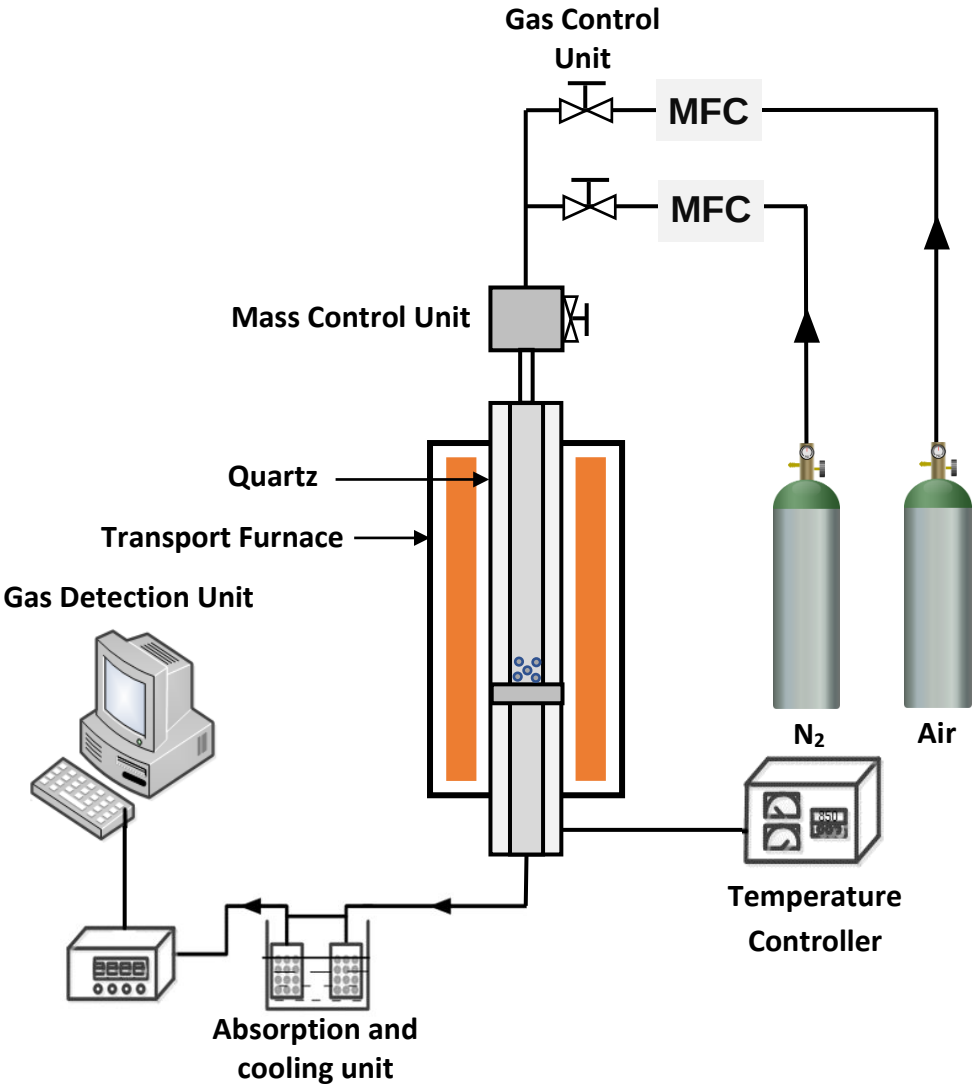

Figure 3.12. Experimental set-up of the BCLG tests

3.3.4 Data Evaluation

The gas products of the sawdust pine are mainly H_2, CO, CO_2, CH_4 and C_2H_4. In order to study the gasification reactions between hematite and sawdust pine, the following equations are used for analysis in this paper. Equation 3.21 is used to calculate the percentage of carbon conversion (X_C).

$$X_C = \frac{12\times273\times(V_{CO}+V_{CO_2}+V_{CH_4}+nV_{C_nH_m})}{22.4\times303\times m_0\times M_C}\times 100\% \quad [3.21]$$

Where, M_C represents the mass fraction of carbonaceous materials in biomass (%), V_{CO}, V_{CO2}, V_{CH4} and V_{CnHm} represent the volume of each component in the gas product at room temperature (L), m_0 represents the mass of biomass added in the experiment (g).

The lower heating values of syngas (LHV_{syngas}, MJ/Nm^3) is calculated using Equation 3.22.

$$LHV_{syngas} = 12.6 \times C_{co} + 10.8 \times C_{H_2} + 35.9 \times C_{CH_4} \quad [3.22]$$

Where C_{CO}, CH_2, C_{CH4} and C_{CnHm} represent the volume fraction of each component in the gas product (%).

The Cold Gas Efficiency (CGE) was calculated as the percentage of syngas heating value over the biomass heating value, as shown in Equation 3.23.

$$\text{Cold gas efficiency}, \% = \frac{\text{Syngas LHV} \times \text{Y}_\text{n}}{Biomass\ LHV} \times 100 \quad [3.23]$$

where Y_n is the biomass gasified gas yield, which is calculated as the volume of a gaseous component (V_n) per mass of biomass ($M_{Biomass}$) used, as shown in Equation 3.24.

$$\text{Gas yield } (\text{Y}_\text{n}) = \frac{\text{V}_\text{n}}{\text{M}_\text{Biomass}} \quad [3.24]$$

4 CHAPTER 4: TECHNO-ECONOMIC & SUSTAINABILITY ANALYSIS

4.1 Introduction

In this chapter a BCLGCC model was developed and validated using Aspen Plus software. The model was used to develop a scaled up 650MW power plant followed by conducting a technical, economic and sustainability assessment of the entire power plant and testing its feasibility in large scale. The results were then compared to four other power generation technology. The results in this chapter were presented in graphs and tabular form. The work in this chapter was conducted according to the methodology outlined in chapter 3 section 3.1.

4.2 Technical Assessment

Performance results of the CCS and Non-CCS power plants are listed in Table 4.1. Both CCS and Non-CCS power plants were set to have the same gross power output of 650 MW, with an inlet biomass flowrate of 6480 and 6600 tonnes/day, respectively. CCS power plant has a 90% CO_2 capture and resulted in a 5% decrease in efficiency (36%) compared to Non-CCS (41%). The BCLG reactions cannot occur at temperatures below 650°C, and the sintering of oxygen carrier is prone to occur when the temperature exceeded 1000°C [141]. A thermodynamic analysis was conducted to measure the effect of temperature of the FR (750 - 950°C) on gas composition, LHV, net power, cold gas and net efficiencies, while keeping the AR temperature 100°C higher than the FR. Similar tests were also conducted measuring the effect of pressure ranging from 1 to 13atm for both FR and AR, OC/B ratio ranging from 0 - 10, and S/B ratio from 0.2 - 1.8. The efficiency results showed in Table 4.1 that the difference between the CCS and Non-CCS process is around 5%, which is a low number compared to the difference between conventional power plants. The reason for that is the high biomass utilization efficiency within BCLGCC process, hence requiring less biomass therefore releasing less CO_2 which has to be captured. This results in less energy penalty for the CCS process.

Table 4.1. Performance results of both CCS and Non-CCS plants

Parameter	Non-CCS Plant	CCS Plant
Feed Rate, tonne/day	6600	6480
Gas Turbine Output, MW	417	377
Steam Turbine Output, MW	233	273
Gross Plant Size, MW	650	650
Syngas Compression, MW	95	92.2
OC Circulation, MW	8.8	8.8
CO_2 Capture Power	-	45.5
Net Power, MW	546	504
CO_2 Captured, %	-	90%
Amount of CO_2 captured, kmol/s	-	2.37
WGS Steam Flowrate, kmol/s	-	2.25
Biomass LHV, MW	1429	1403
Efficiency, %	41	36

4.2.1 Effect of Temperature

Temperature has a significant effect on the syngas composition. As shown in Figure 4.1A, as temperature increased from 750 °C, H_2 and CO experienced an increase in yield, whereas CH_4 and CO_2 yields decreased. The change in compositions reached a plateau at around 875°C, therefore, was taken as the optimum temperature, ensuing a balance between further increase in temperature and the percentage increase in efficiency. These effects can be explained by the thermodynamics of reactions (1 -12) in the Table 3.3 (Methodology chapter). The LHV of the syngas sent to the combined cycle, increased from 11.2 MJ/Nm^3 at 750°C to 12.3 MJ/Nm^3 at 800°C, which is due pyrolysis gas (having high LHV due to more CH_4 formation). However, as temperature further increases, the LHV decreases and plateaus at around 875°C. This decrease in LHV is compensated by an increase in gas yield due to increased carbon conversion, as a result increasing the CGE of the gasification process. This increase in CGE resulted in an increase in net power and consequently the net efficiency of the power plant. This can be observed in Figure 4.1B. Comparing BCLGCC w/o CO_2 capture with BCLGCC with CO_2 capture, as temperature increased from 750 °C H_2 yield increased

rapidly while CO_2 slightly increased. On the other hand, CH_4 composition decreased while CO remained negligible. The reason for that is due to the presence of a WGS unit, converting all the CO into CO_2, where 90% is captured. Since the ratio between C and H is 1 to 4 in CH_4, more H_2 is produced as it reacts with the OC as temperature increases. From Figure 4.1C and Figure 4.1D, an increase in temperature resulted in an increase in CGE due to increase gas yield, net power and net efficiency. The net efficiency of the capture power plant was approximately 6% lower than the non-capture power plant.

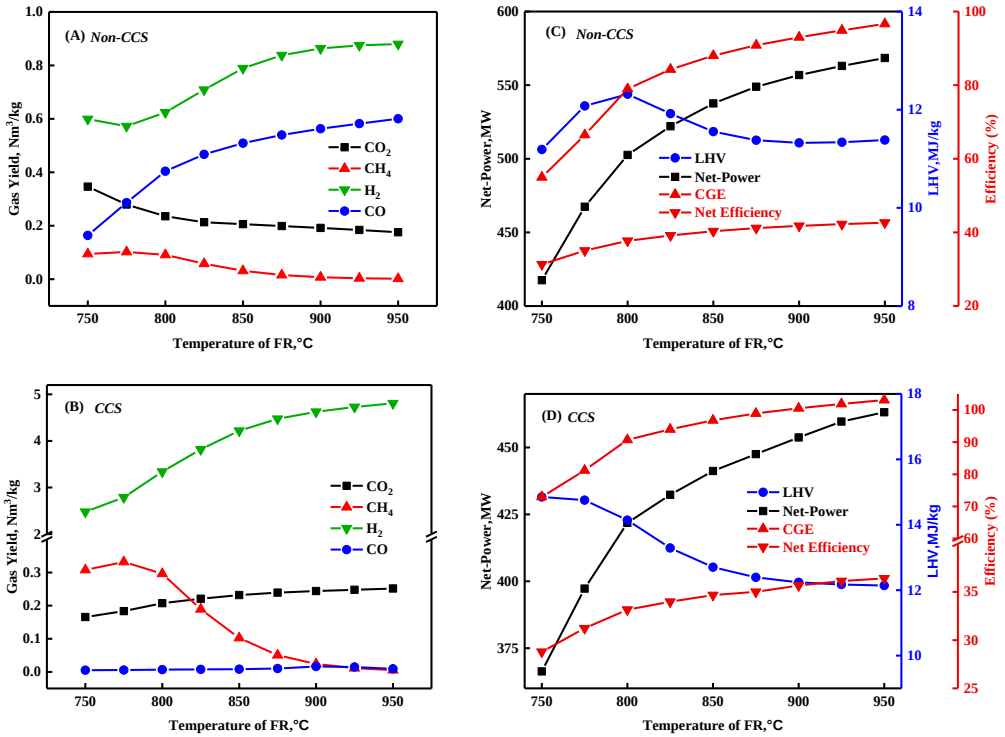

Figure 4.1. Effect of temperature on both CCS and Non-CCS power plants

4.2.2 Effect of OC/B Ratio

The OC/biomass (OC/B) ratio is an important parameter in BCLG to obtain high-quality syngas. High amount of oxygen carrier will result in complete combustion while little amount of oxygen carrier will result in insufficient amount of oxygen and gradual decrease in gasification temperature of the reactor. Figure 4.2A demonstrated that as the OC/B ratio increased from 0.30 to 2 H_2 yield increased, and similarly CO, CO_2 and CH_4 yield increased. This is because as we increase the OC/B ratio, the amount of lattice oxygen increases hence converting more carbon into CO/CO_2. Additionally, more OC results in an increased catalytic cracking of the tar, therefore resulting in higher amount of carbon being converted into syngas. Further increase in OC/B ratio beyond 2, stagnates CO yield while gradually increasing CO_2, while CH_4

and H_2 yields experience a gradual decrease, due to the increased oxidation, resulting in CO, CH_4 and H_2 being converted into CO_2 and H_2O. Compared to BCLGCC with capture, the trends in Figure 4.2B are similar, however, the CO and CH_4 yields can be assumed to be negligible while H_2 flowrate is approximately double, mainly due to the WGS and carbon capture processes. The slight increase in CO and H_2 compositions between 0.3 and 2 OC/B ratio resulted in an insignificant effect on the LHV compared to the effect it had on the gas yield which resulted in an increase in CGE. The increase in OC/B ratio from 0.3 to 2 OC/B also resulted in a 50 MW net power increase for the non-capture plant, but approximately 36 MW increase for the capture plant. As a result, increasing the net efficiency for both capture and non-capture plants by 2.6% and 4%, respectively. However, as OC/B increases more than 2, all factors gradually decrease due to complete combustion taking place, as demonstrated in Figure 4.2C &D.

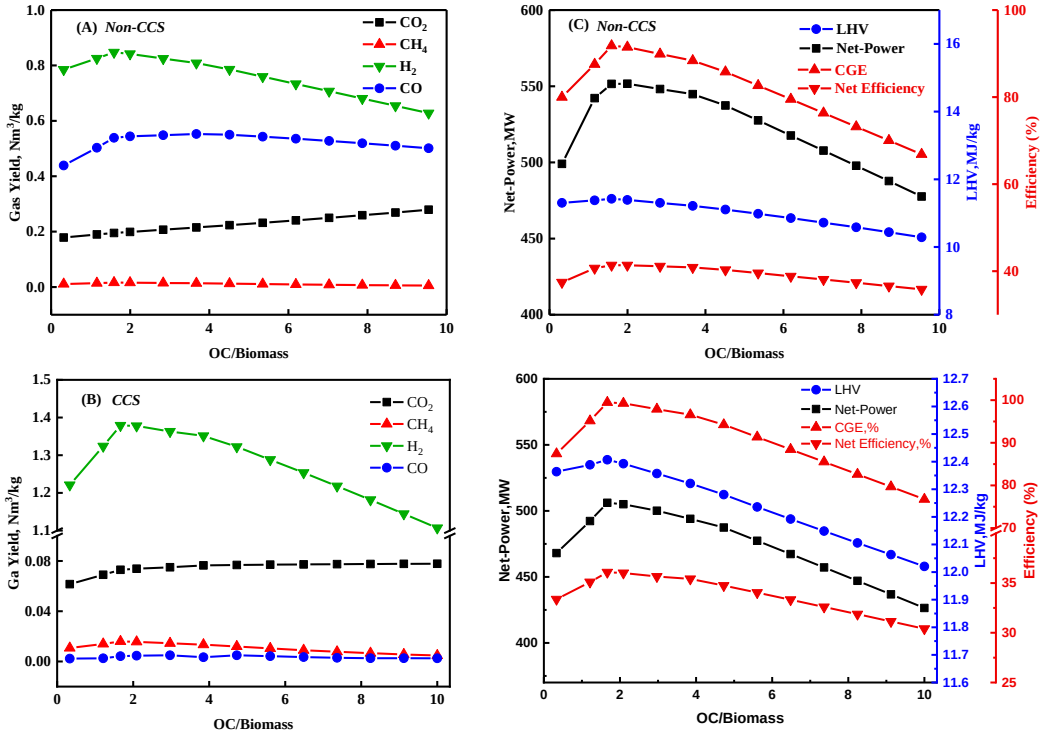

Figure 4.2. Effect of OC/Biomass ratio on both CCS and Non-CCS power plants

4.2.3 Effect of Pressure

As illustrated in Figure 4.3A, it can be seen that an increase in fuel reactor pressure shifts equilibrium towards the side with less gaseous moles. For the non capture plant, H_2 and CO flowrates decreased while CO_2 and CH_4 increased with an increase in pressure. The main

reason is that the gasification reactions (reactions 2, 3 and 4) in Table 3.3 (Methodology chapter) are restrained under high pressure, thus resulting in a decrease in H_2 and CO decrease as pressrue increases. However, a high pressure is conducive to generating CH_4 according to reaction 5 while suppressing CH_4 conversion (reaction 10). This consequently increased LHV from 11.4 MJ/Nm^3 to approximately 14 MJ/Nm^3, but reduced the gas yield therefore reducing CGE, net power and consequently net efficincy (from 41.2% to 35.6%), as demonstarted in Figure 4.3C. The capture plant, as shown if Figure 4.3B & D showed similar trends, however, experiencing a higher H_2 flowrate and a relatively constant CO and CO_2 flowrate. The net efficiency of non capture plant decreases by approximately 6% compared to capture plant which decreases by 4% as pressure increases from 1 to 13 atm.

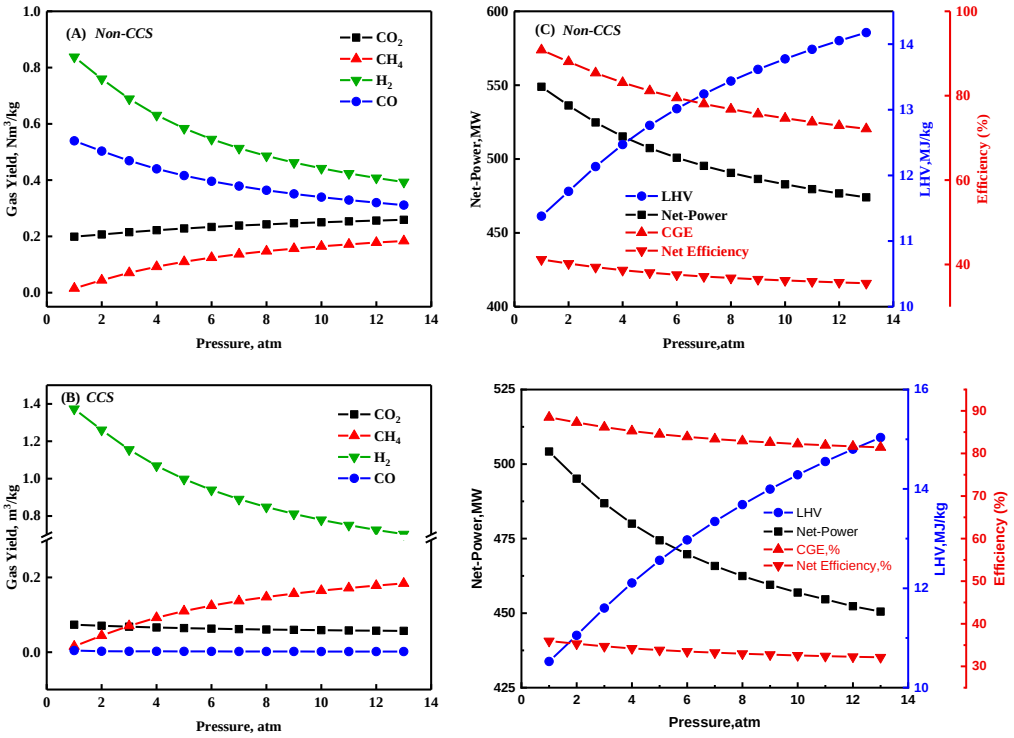

Figure 4.3. Effect of pressure on both CCS and Non-CCS power plants

4.2.4 Effect of Steam

An increase in S/B ratio resulted in an increase in H_2 and CO_2 but a decrease in CO and CH_4 yields as shown in Figure 4.4A. This can be explained according to the equilibrium shift of reactions 1, 2 and 12 in Table 3.3 (Methodology chapter) shifting towards the right-hand side, therefore increasing the CO_2 and H_2 concentrations. As shown in Figure 4.4B, the LHV decreases, since methane (has a high LHV) is consumed, to produce CO and H_2 which have a low LHV. This decrease in LHV results in the CGE also decreasing. However, increasing S/B ratio increases the combustible gas yield which increases the net-power generated,

consequently increasing the net efficiency. The optimum S/B ratio was taken as 1.5 since net efficiency started to plateau. This has only been tested for the Non-CCS power plant; however, the following section discusses the effect of WGS on the CCS power plant.

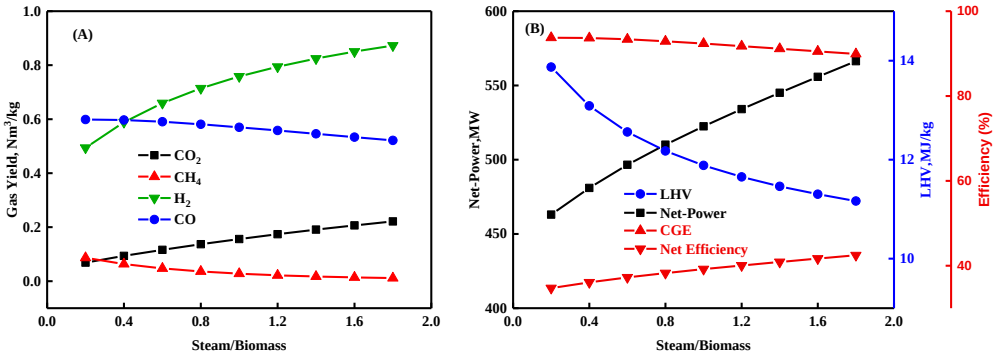

Figure 4.4. Effect of steam/biomass on both CCS and Non-CCS power plants

4.2.5 Effect of Multiple Parameters

In order to investigate the effects of multiple parameters on the system performance, we divided the factors into two categories, operation parameters (gasification temperature and pressure) and technological conditions (OC/B and S/B). The effects of them on energy efficiency of plants are presented in Figure 4.5. Temperature seems to have a higher impact on energy efficiency compared to pressure within the range that has been tested. Temperature results in a steeper increase in energy efficiency up to 875°C, whereas pressure has a gradual decrease in energy efficiency. Therefore, changing temperature would be more effective than changing pressure, high temperature and low pressure are beneficial to improving plant energy efficiency. Steam inputted into FR can obtain more H_2 and CO, increasing the effective composition of fuel gas thus enhancing system energy efficiency, however, OC provides enough heat for promoting steam reacting with other reactants, but exceeded OC will consume H_2 and CO via combustion reactions. Change in OC/B ratio resulted in a steep increase then a sharp decrease after reaching a peak at an OC/B ratio equal to 2. SO as to achieve the maximum energy efficiency of the plant, the OC/B ratio should firstly satisfy the reactor self-heating requirements, followed by a suitable ratio of OC/B to S/B to obtain the maximum energy efficiency of the plant.

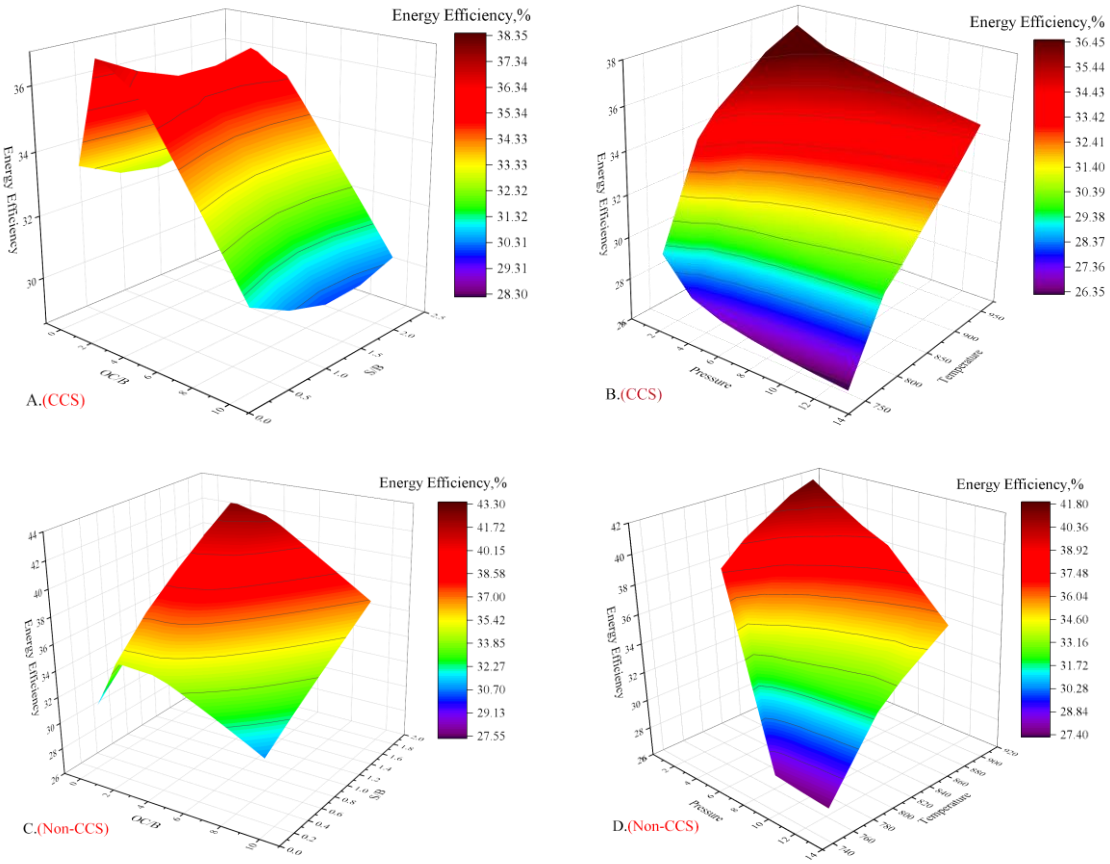

Figure 4.5. Interaction of operation parameters and technological conditions on energy efficiency of the plant

4.2.6 Carbon Capture

The results for testing the effect of water gas shift are outlined in Figure 4.6A and B. This is done by injecting steam in a Water Gas Shift reactor, where it reacts with the syngas, converting CO into CO_2 and H_2O into H_2. This allows for the CO_2 to be captured before the syngas combustion process. As steam flowrate increases, the degree of water gas shift increases (more CO converting into CO_2), increasing amount of carbon captured, consequently increasing the power consumption during the carbon capture process. As a result, the net efficiency of the power plant decreases from 37% to approximately 36%. This can be observed when steam flowrate is equal to 2.25 kmol/s steam flowrate (WGS Degree = 0.993 and Carbon Capture Ratio = 0.974). Further increase in steam does not have any effect on the WGS degree or carbon capture, hence was taken as the value for CCS tests. Even though an increase in carbon capture would reduce efficiency of the power plant it will support negative emissions technology especially with biomass being the source of fuel.

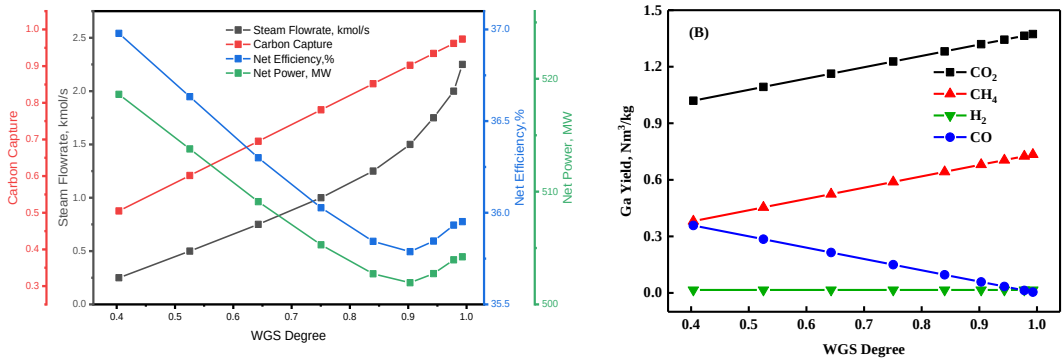

Figure 4.6. Effect of WGS degree on the CCS power plant

4.3 Economic Assessment

4.3.1 Cost Distribution

Based on the techno-economic analysis, FR temperate = 875°C, FR pressure = 1 atm, OC to Biomass ratio = 2, steam to biomass ratio = 1.5 and 0.993 WGS degree were taken as the optimum conditions to be used when conducting the economic analysis. It is noted that the above optimized conditions obtained in this paper are based on the thermodynamics analysis, hence, if we just consider the thermodynamics performance of the plant, these values can be used as general conditions and are suitable for all BCLGCC (w/o CCS) plant with different sizes. However, the economic impact values may change for a different plant size. The change in operation parameters and conditions will lead to variation in heat flow, mass flow and gas composition, thus affecting the device size as well as its investment. Since the economic performance are significantly influenced by the plant scale, those values are taken as optimum for a 650 MW (gross power) power plant (biomass input = 6600 tonnes/day (non-ccs) and 6480 tonnes/day (ccs)) in this study and not for all sizes. The economic analysis was based on the assumption that biomass price is equal to 12.4 $/GJ (£10), negative emissions incentive is equal to zero and the power plant is available 80% of the time. The amount of OC required in the process was increased by 10% to account for OC escaping the reactors with the syngas/flue gas. The breakdown cost in calculating the TOC, variable and fixed costs is presented in Table 3.7. Based on the data, the power plant with capture increased the capital cost by 30%, fixed cost by 20% and variable cost 1% compared to non-capture. The cost break-down is shown in Table 4.2.

Table 4.2. Summary of TOC, variable and fixed cost breakdown

	Non-CCS (M$)	CCS (M$)
Gasification Units	173	170
Gas Turbine	40	37
HRSG	56	55
Steam Turbine	23	26
WGS Reactor	-	32
CO_2 Absorption	-	33
CO_2 Drying and Compression	-	29
Total Equipment Cost (TEC)	292	382
Direct Cost	561	734
Indirect Cost	100	130
Bare Erected Cost (BEC)	953	1246
Process Contingency	238	312
Project Contingency	238	312
Total Plant Cost (TPC)	1429	1870
Owners Cost	329	430
Total Overnight Cost (TOC)	1759	2300
Annual Operating Labour (OL)	9.5	10.5
Maintenance Labour Cost	11.9	13.1
Administrative and Support Labour	5.4	5.9
Property Taxes and Insurance	28.6	37.4
Total Fixed O&M Cost	55.4	67.0
Biomass	558.8	548.1
Oxygen Carrier	7.35	7.20
Boiler Feed Water	0.8	0.7
Total Variable O&M Cost	567	556

4.3.2 Effect of Plant Size

The effect of COE including the breakdown contribution of capital, variable and fixed costs for both CCS and Non-CCS plants are shown in Figure 4.7A and B, respectively. The COE of the 650MW power plant was calculated using Aspen Plus data and Equation 3.8, however the costs for the different sizes were scaled using Equations 3.12, 3.13, 3.14. The scaling of the capital and fixed costs was exponential; however, the scaling of the variable cost was

proportional. The graphs followed an expected trend of decrease in COE with increase in plant size. However, the graphs reached a plateau at around 500 MW, further increase in plant size did not have significant impact on the COE. This is because further increase in size results in an increase in cost equal to the increase in power output, hence keeping the COE relatively constant.

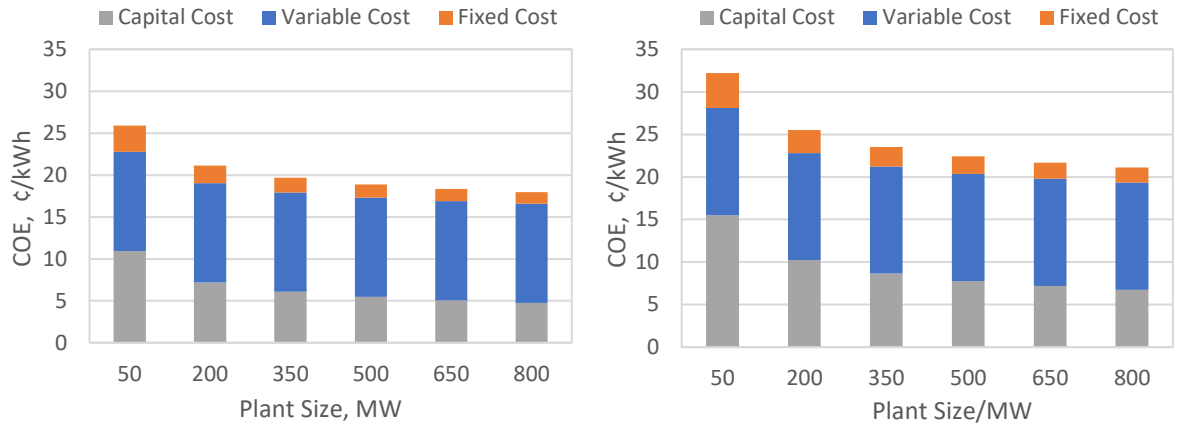

Figure 4.7. Effect of Non-CCS (A) and CCS (B) plant size on the COE

4.3.3 Sensitivity Analysis to COE

A sensitivity analysis was conducted to test the effect of different variables on the COE of both, CCS and Non-CCS plants. Figure 4.8A and B represent the effect of TPC, Biomass price, discount rate, plant life, labour cost, OC price and lifetime on both CCS and Non-CCS power plants, respectively. For CCS, it can be observed that if TPC is varied by +/- 30% the COE (21.7 ¢/kWh) will vary between 24.1 – 19.2 ¢/kWh (11.3% difference in COE), whereas for Non-CCS the COE (18.4 ¢/kWh) will vary between 20.1 – 16.6 ¢/kWh (9.5% change in COE). The bigger gap between both values shows that varying the TPC has a greater effect on the COE in a CCS compared to a Non-CCS power plant, which is due to the additional cost of the carbon capture unit. Moreover, since this type of power plant has not been constructed on large scale before, its project and process contingencies are quite higher, hence increasing its capital cost and COE. The price and lifetime of the OC seemed to have a very negligible effect on the COE for both CCS and Non-CCS due to the low price of hematite (95 $/ton). Labour cost had a slight effect on the COE, but a greater effect was observed when the plant life increases from 20 to 25 years (increased by 0.27 ¢/kWh and 0.19 ¢/kWh for both CCS and Non-CCS). Discount rate seems to be the third most effective variable on the COE after TPC and biomass price.

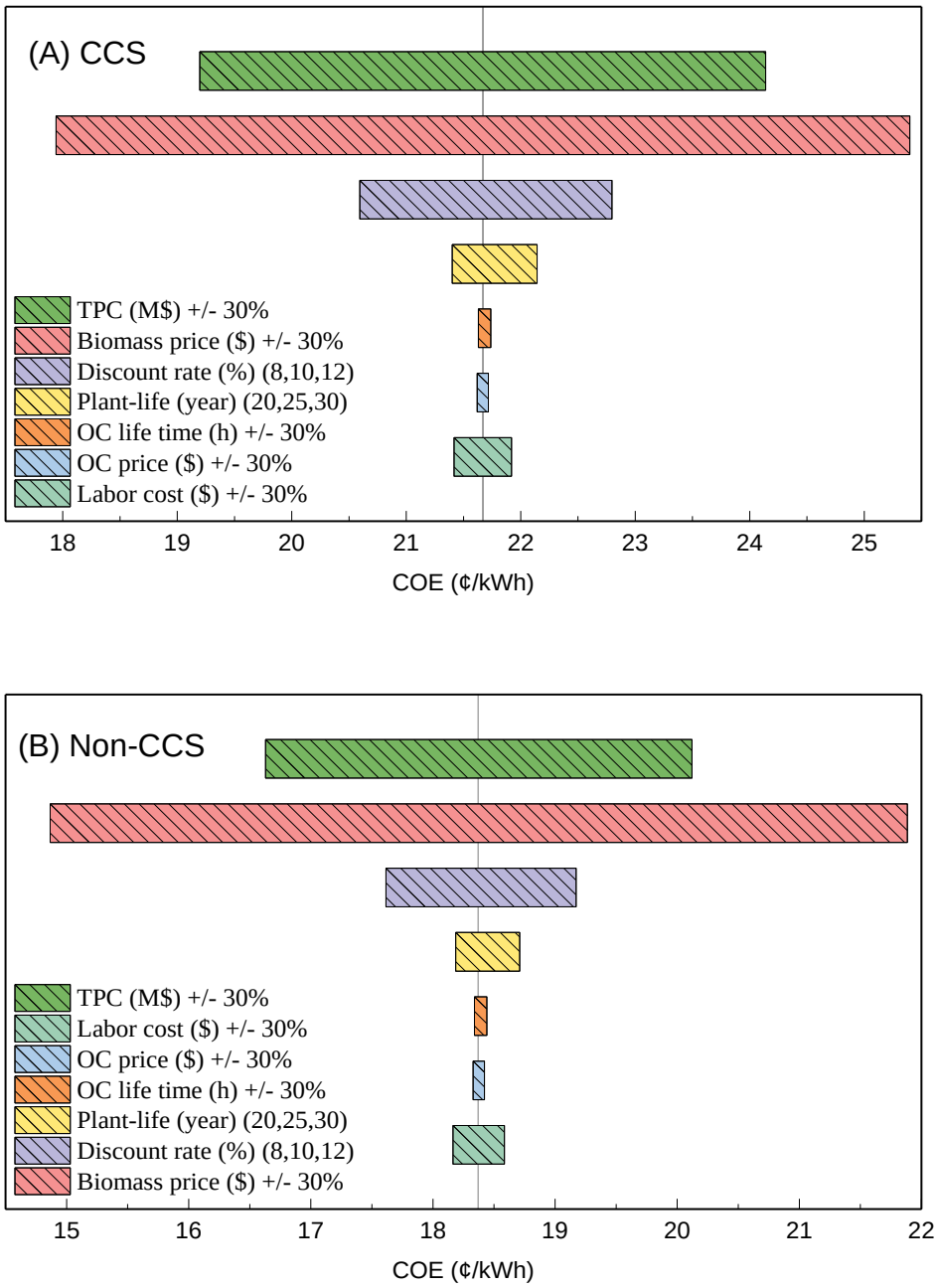

Figure 4.8. Sensitvity analysis of different variable for both CCS (A) & Non-CCS (B)

Regarding the effect of biomass price (12.4 $/GJ), if we vary its price by +/- 30%, COE will range from 17.9 – 25.4 ¢/kWh and 14.9 – 21.9 ¢/kWh for CCS and Non-CCS, respectively.

It can also be observed that the price of biomass had the highest effect on the COE for both CCS and Non-CCS plants followed by the TPC. This shows the key role biomass price plays in influencing the economic feasibility of the entire process. In the UK, biomass is generally imported from the US and Canada [284], therefore increasing its price due to shipping, however this process could be more feasible in geographic locations where biomass is

abundant and cheap. Nevertheless, the main current financial support scheme presented by the UK government for renewable electricity is the Renewable Obligation Certificate (ROC) [285]. The ROC's current value for generating electricity using 100% biomass is 4.84 p/kWh (5.8 ¢/kWh). This would therefore reduce the COE for both CCS and Non-CCS to 15.9 ¢/kWh and 12.8 ¢/kWh, respectively, which reduces the costs below the average cost of electricity in the UK (17.7 ¢/kWh (14.37 p/kWh) [286]). Figure 4.9 tests the effect in variation in ROC value as it could change throughout the years. It can be observed that a 30% change in ROC value varies the value of COE by 11% and 14% for CCS and Non-CCS plants, respectively. From a policies perspective, further incentives can be introduced for negative emissions which could drive the commercialization of BECCS technology. The graphs showing the effect of varying each of the aforementioned variables on the COE can be found in the **Appendix** (Figure A1).

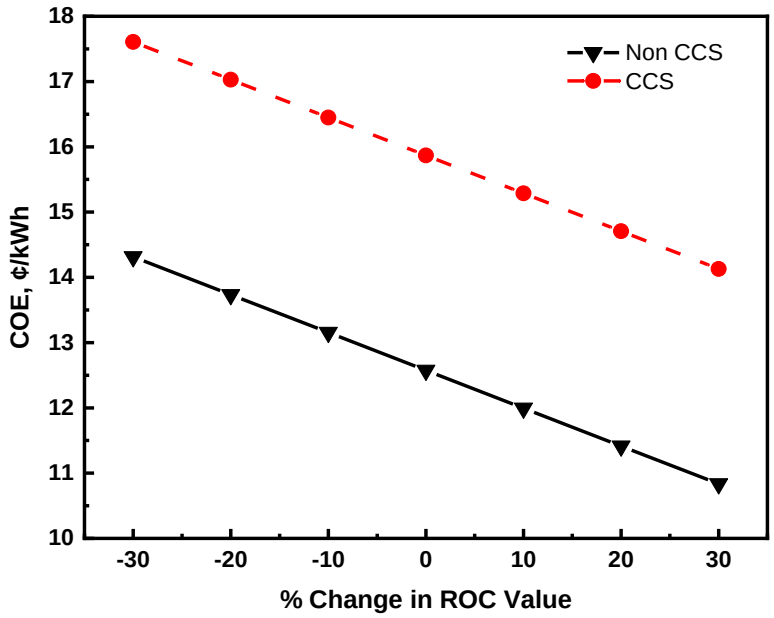

Figure 4.9. Effect of change in ROC value on COE

Figure 4.10A estimated the effect of increasing negative emissions incentive and its effect on the COE for both CCS and Non-CCS. It had no effect on the Non-CCS plant as expected, however it would have an effect on the CCS plant since capture of CO_2 will result in negative emissions. The COE including the ROC government subsidies for CCS (15.9 ¢/kWh) is already lower than the average COE in the UK (approximately 17.7 ¢/kWh). Introducing negative emissions incentive of no more than 39 \$/t-CO_2 in addition to renewable government subsidies can further reduce the COE to 12.8 ¢/kWh (which is the same as the Non-CCS plant).

Figure 4.10B shows the effect of the capacity factor on the COE. It can be observed that the CF has more effect on the CCS plant compared to the Non-CCS plant, with a difference of 7.16 ¢/kWh and 5.12 ¢/kWh between 0.5 and 1 capacity factor, respectively. Figure 4.10C illustrates that the COE increases as the WGS degree increases, converting more CO into CO_2. This is due to more energy being consumed for CO_2 capture, as a result reducing the plant's net power. The COE increases from 20.9 ¢/kWh to 21.7 ¢/kWh as the WGS degree increases from 0.4 to 0.99, however, the cost of CO_2 capture decreases from 64.6 $/t-$CO_2$ to 342.7 $/t-$CO_2$. Table 4.3 compares the cost and performance of the 3 main biomass-based technologies, including; biomass combustion, biomass integrated gasification combined cycle (BIGCC) and BCLGCC. Coal direct combustion and coal integrated gasification combined cycle technologies are also introduced and compared. From previous literature data regarding the capital cost, COE and efficiency of both capture and non-capture plants were collected and compared for an estimated gross 650 MW plant size. The values in Table 4.3 do not include any government subsidies or renewable energy incentive. The results showed that BCLGCC shows promising net electric efficiency and COE compared conventional power generation technology (biomass combustion and BIGCC).

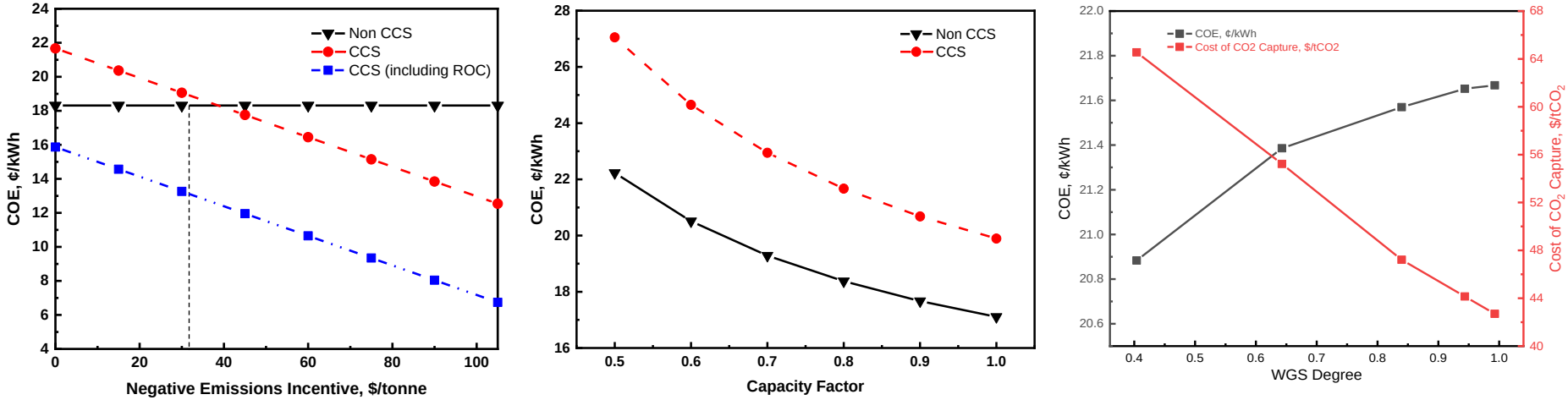

Figure 4.10. Effect of negative emissions incentive (A), capacity factor (B), WGS degree and cost of CO_2 capture (C) on COE

Table 4.3. Techno-economic comparison between 5 power generation technologies [43 – 48, 200, 204, 233, 239]

Items	Direct Combustion		Integrated Gasification Combined Cycle		Chemical Looping Gasification Combined Cycle		Direct Combustion		Integrated Gasification Combined Cycle	
Gross Plant Power	~650		~650		~650		~650		~650	
Fuel	Biomass		Biomass		Biomass		Coal		Coal	
Carbon Capture	No CCS	CCS	No CCS	CCS	No CCS	CCS	No CCS	CCS	No CCS	CCS
Percentage Capture, %	0	~90	0	~90	0	~90	0	~90	0	~90
CO_2 Purity, %	-	~99	-	~99	-	~99	-	~99	-	~99
Biomass LHV, MJ/kg	16.5 - 18.5						25 - 32			
Cost of Fuel, $/GJ	9 - 12						2 - 3			
Plant Capital Cost, M$/$MW_{(Net)}$	1.4 - 1.8	3.3 – 3.8	2.6 – 3.0	3.7 – 4.2	2.4 – 2.8	3.4 – 3.9	1.2 - 1.6	2.6 – 3.0	1.8 – 2.2	2.7 – 3.1
Cost of Electricity, ¢/kWh	12 - 16	18 - 22	15 - 19	19 - 25	16 - 20	19 - 23	6 - 8	11 - 14	7 - 9	10 - 13
Net Electric Efficiency, %	34 - 37	24 - 28	35 - 40	26 - 33	40 - 43	34 - 37	35 - 38	25 - 28	37 - 41	30 - 34

4.4 Sustainability Analysis

The previously mentioned (methodology chapter, section 3.1.4.3) indicators (economic, social, environmental and technical indicators) and sub-indicators for the sustainability assessment is presented in Table 4.4. The values for each indicator, including the reference point (worst and best case for each indicator) were either taken from literature [200, 233, 238, 237] or are calculated for the worst possible value based on the fuel feedstock properties. The results are presented in a graphical form in Figure 4.11, for the CCS and non-CCS plants.

4.4.1 Economic Sustainability

Comparing between the economic performance of the 5 different power generation technologies (with and without capture), it can be implied that gasification (BIGCC, BCLGCC and CIGCC) require a higher capital cost per unit power as well as higher COE due to the complexity of the system, except for BCLGCC which demonstrates a lower COE which is due to its higher efficiency compared to the other processes. Additionally, we can see that coal power plants have a slightly lower capital investment per unit energy compared to biomass power plants, however a significantly lower COE due to the lower cost and higher heating value of coal compared to biomass. Moreover, CCS technology increased the capital cost of the power plants on average by approximately 1.1 M$/MW, which then resulted in an increase in COE by approximately 4 - 5 ¢/kWh.

4.4.2 Environmental Sustainability

Biomass fuelled power plants showed lower efficiencies compared to coal fired power plants, except for BCLGCC which demonstrated similar efficiencies for CCS and non-CCS plants (36% and 41%, respectively) in comparison to coal fuelled IGCC. Biomass IGCC requires higher water consumption compared to BDC for tar scrubbing. BCLGCC requires less water due to the catalytic cracking of the tar by the oxygen carrier. In terms of renewability, the biomass-based power plants are 100% renewable since biomass is a renewable source of energy, whereas for coal-based power plants the renewability is zero. The CO_2 emissions from the biomass-based power plants is assumed to be equal to zero due to biomass being carbon neutral, whereas CFP and coal IGCC released 905 and 821 g/kWh, respectively, which is due to the higher efficiency of IGCC. The CCS process is assumed to capture approximately 90% of the

CO_2, hence resulting in 114 and 103 g/kWh being released, respectively. Biomass-based power plants technically should have negative emissions as they are removing CO_2 from the atmosphere, but in this analysis, it is assumed to be zero.

4.4.3 Social Sustainability

Developing biomass-based power plants can increase the number of jobs by 8 - 12/ MWe, since more agricultural residue will be required as fuel. Therefore, requiring the agricultural industry to restructure, hence creating more jobs. Whereas coal-based power plants provide much less jobs (0.5 - 1.5 jobs/MWe). However, sourcing the biomass from abroad would improve the job market for the location where the biomass is sourced. Take the UK as an example, however, most of the biomass in the UK is imported from the US and Canada, hence will not provide as many jobs within the UK. The shift towards biomass is to move towards renewable sources of energy while ensuring energy security. Currently the energy security from coal power plants is low (approx. 3%), while biomass power plants is relatively higher (6%), and zero energy security from CCS power plants. The UK parliament recently passing a bill to reach net-zero emissions by 2050, therefore biomass energy sources will see a greater push and an increase in its use in the following decades. Drax power plant will be the first biomass power plant in the UK to be integrated with CCS technology [287]. With BCLGCC technology utilizing biomass efficiently in power generation while providing a lower COE, even with CCS technology, we could see an increase in its energy security in the following decades.

4.4.4 Technical Sustainability

This indicator measures the maturity level of the technology for it to achieve a specified function and to demonstrate whether the technology is commercially feasible. The specified power generation technologies in Table 4.4 shows that combustion technologies are the most mature due to their simple process compared to gasification, especially with coal power generation technology being more mature compared to biomass fuelled technology. Biomass gasification process to power is slightly complicated compared to that of coal. BCLGCC has only been demonstrated as pilot plants, hence is still under research stage, therefore reducing its maturity and commercial reliability. CCS technology have been demonstrated; however, the technologies maturity is not as mature relative to Non-CCS processes.

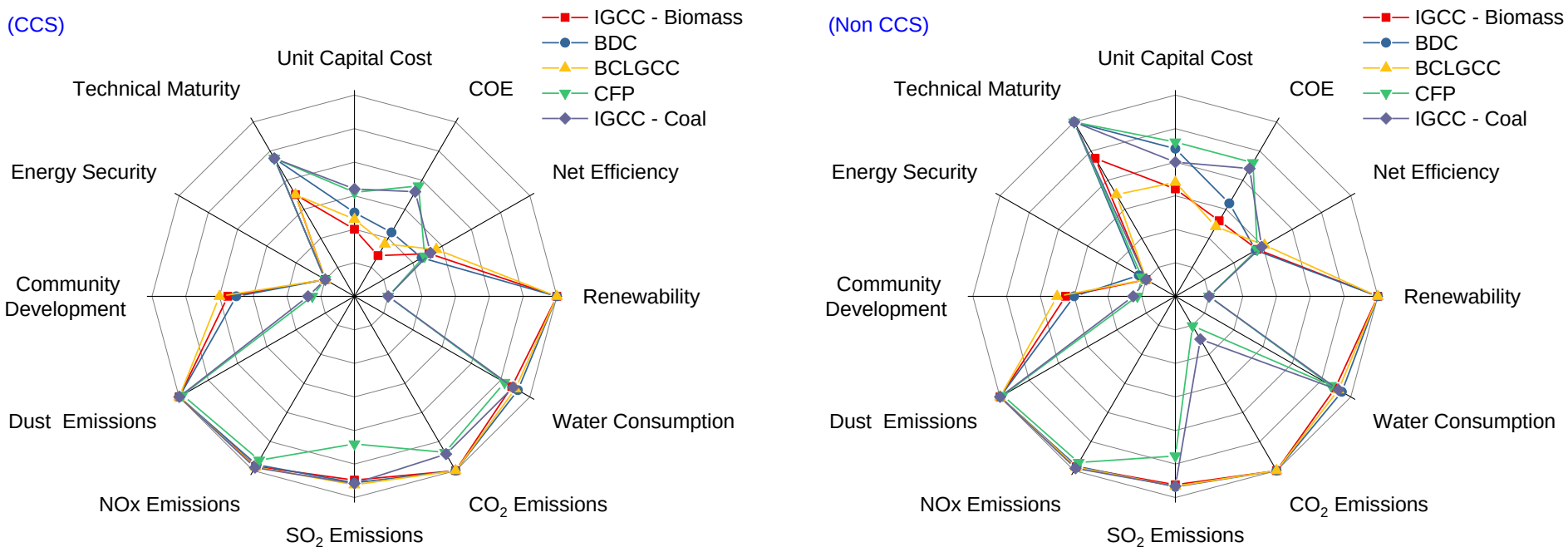

Figure 4.11. Sustainability evaluation of biomass and coal power generation processes

Table 4.4. Sustainability performance assessment between 5 power generation technologies

Indicator (sub-indicator)	IGCC -Biomass		BDC		BCLGCC		CFP		IGCC – Coal		Reference Value	
CCS/Non-CCS	CCS	Non-CCS	CCS	Non-CCS	CCS	Non-CCS	CCS	Non-CCS	CCS	Non-CCS	Best	Worst
Economic												
Unit capital cost, M$/MW	4.0	2.8	3.5	1.6	3.7	2.6	2.9	1.4	2.8	2.0	0	5
COE, ¢/kWh	23	16	19	14	21	18	13	7	12	8	0	25
Environmental												
Net Electric Efficiency, %	31	36	26	35	36	41	28	36	32	39	100	0
Renewability, %	100	100	100	100	100	100	0	0	0	0	100	0
Water consumption, kg/kWh	3.50	3.02	2.30	1.71	2.80	2.40	4.9	3.83	3.25	2.4	0	28.4
CO_2 emissions, g/kWh	0	0	0	0	0	0	114	905	103	821	0	908
SO_2 emissions, g/kWh	2.6	1.9	2.2	1.6	1.9	1.7	8.0	6.2	2.1	1.7	0	25
NO_X emissions, g/kWh	1.7	1.5	2.4	1.8	1.5	1.4	4.2	3.3	1.2	0.95	0	59
Dust emissions, g/kWh	0.034	0.030	0.081	0.060	0.030	0.026	2.2	1.7	0.10	0.08	0	93.6*
Social												
Community Development, staff/$MW_{(e)}$	11	9	10	8	12	10	1	0.5	1.5	1	20	0
Energy Security, %	0	0.05	0**	5	0	0	0	3	0	0	100	0
Technical												
Technical Maturity	0.5	0.75	0.75	1	0.5	0.5	0.75	1	0.75	1	1	0

*All ash in the fuel is assumed to be dust
** Will be operating in early 2020's[287]

4.5 Conclusion

This chapter uses Aspen Plus software to establish a reliable and validated biomass chemical looping gasification combined cycle with and w/o CCS simulation process using experimental data. The plant was scaled up to test its economic and technical feasibility in an industrial scale (650 MW gross power). The key technical parameters including temperature, OC/B ratio, pressure, S/B ratio and WGS degree were tested to optimize the system and obtain optimum operational conditions. It was concluded that the optimum conditions from the technical analysis are as the following: 875°C FR temperate, 1 atm FR pressure, OC/B ratio equal to 2, S/B ratio equal to 1.5 and 0.993 WGS degree. This resulted in giving a net efficiency of approximately 36% and 41% for non-CCS and CCS plants, respectively, showing higher and promising results compared to conventional power generation processes. Following the technical analysis, an economic feasibility study was conducted estimating the capital, fixed and variable costs and finally the cost of electricity. The high efficiencies of these processes are associated with the costs, hence a lower COE of 21.7 ¢/kWh and 18.4 ¢/kWh for CCS and Non-CCS processes, respectively. Moreover, government subsides can reduce costs to 15.9 ¢/kWh and 12.8 ¢/kWh, respectively, with negative emissions incentive further reducing the COE for the CCS plant. The techno - economic performance of BCLGCC is then compared with other power generation technologies, showing that BCLGCC demonstrates higher net efficiency and lower COE. Finally, a sustainability assessment is conducted comparing between 5 different power generation technologies (with and w/o CCS) demonstrates that BCLGCC presents promising economic and environmental results, with an increase in community development, but a low energy security due to the process not being commercially established, as a result it is still not as technically mature as the other power generation technologies. In conclusion, BCLGCC power plant seems to demonstrate positive results which makes it a technology that could play a big role in BECCS towards achieving a net-zero carbon emissions by 2050.

5 CHAPTER 5: LIFE CYCLE & ENVIRONMENTAL ANALYSIS

5.1 Introduction

This chapter deals with conducting a life cycle energy, cost, and CO_2 emission analysis of a BCLGCC power plant which is then compared to four other power generation technology. For clarity, the results have been presented in pseudo-Sankey form rather than in tabular form and summarized in bar chart for easier comparison. The tabular form of the results can be found in the **Appendix** (Tables A7 – A15). A sensitivity analysis is then conducted and presented in a graph form. This is followed by conducting a life cycle environmental impact assessment comparing between BCLGCC and BIGCC power plants. The work in this chapter is conducted according to the methodology outlined in chapter 3 section 3.2.

5.2 Life Cycle Assessment of Energy Distribution

The energy input distribution of both a BCLGCC with and without CCS power plants, generating a gross power of 650 MW is shown in Figure 5.1. BCLGCC (1429.2 MW) requires 26 MW more biomass than BCLGCC with CCS (1403.2 MW) implying that the WGS and carbon capture units increase the energy density of the syngas, hence increasing the gross power by 26 MW. However, this decreases the overall net power of the CCS plant by 42 MW (Energy for carbon capture: 45.5 MW). Both CCS and non-CCS plants requires a TLCEI of 2160.3 MJ/MWh and 1764.5 MJ/MWh, respectively. The most energy intensive stage is the drying and pelletization stage, which require 1596.2 MJ/MWh and 1500.7 MJ/MWh for CCS and non-CCS plant, respectively, accounting for 73.9% and 85.0% of the TLCEI. The second most energy intensive stage is the CCS process which requires an energy input of 259.9 MJ/MWh. The biomass transport supply chain process also accounts for a high energy input of 239.6 MJ/MWh and 227.6 MJ/MWh for CCS and non-CCS, respectively. The overall lifecycle net power of the CCS and non-CCS plant is equal to 242.7 MW and 279.9 MW, respectively. Figure 5.2 illustrates the life cycle energy input distribution of a BIGCC power plant with and without CCS, with both power plants having a gross power equal to 650MW. The TLCEI required for the CCS power plant is equal to 2482.6 MJ/MWh whereas for the non-CCS power plant it is equal to 1775.1 MJ/MWh. The CCS power plant biomass feedstock (1694.5 MW) requirement is 177.7 MW higher compared to the non-CCS (1516.8 MW) plant. The most energy intensive

process is the wood processing stage, accounting for 71.3% and 85.2% of the CCS and non-CCS power plants, respectively. The CO_2 capture, transport and storage added a 403.2 MJ/MWh to the CCS power plant. Figure 5.3 illustrates the life cycle energy input distribution of a CIGCC power plant with and without CCS. The gross power for both CCS and non-CCS power plants is equal to 650 MW. The percentage coal mining and washing energy input for both the CCS and non-CCS power plants is equal to 98.5% (628.1 MJ/MWh) and 65.7% (755.3 MJ/MWh), respectively. The total life cycle energy input required for the coal supply chain for the CCS power plant is equal to 1149.1 MJ/MWh whereas non-CCS power plant is 637.9 MJ/MWh. The CCS power plant consumes an additional 382.0 MJ/MWh (33.2%) for CO_2 compression, transport, and storage.

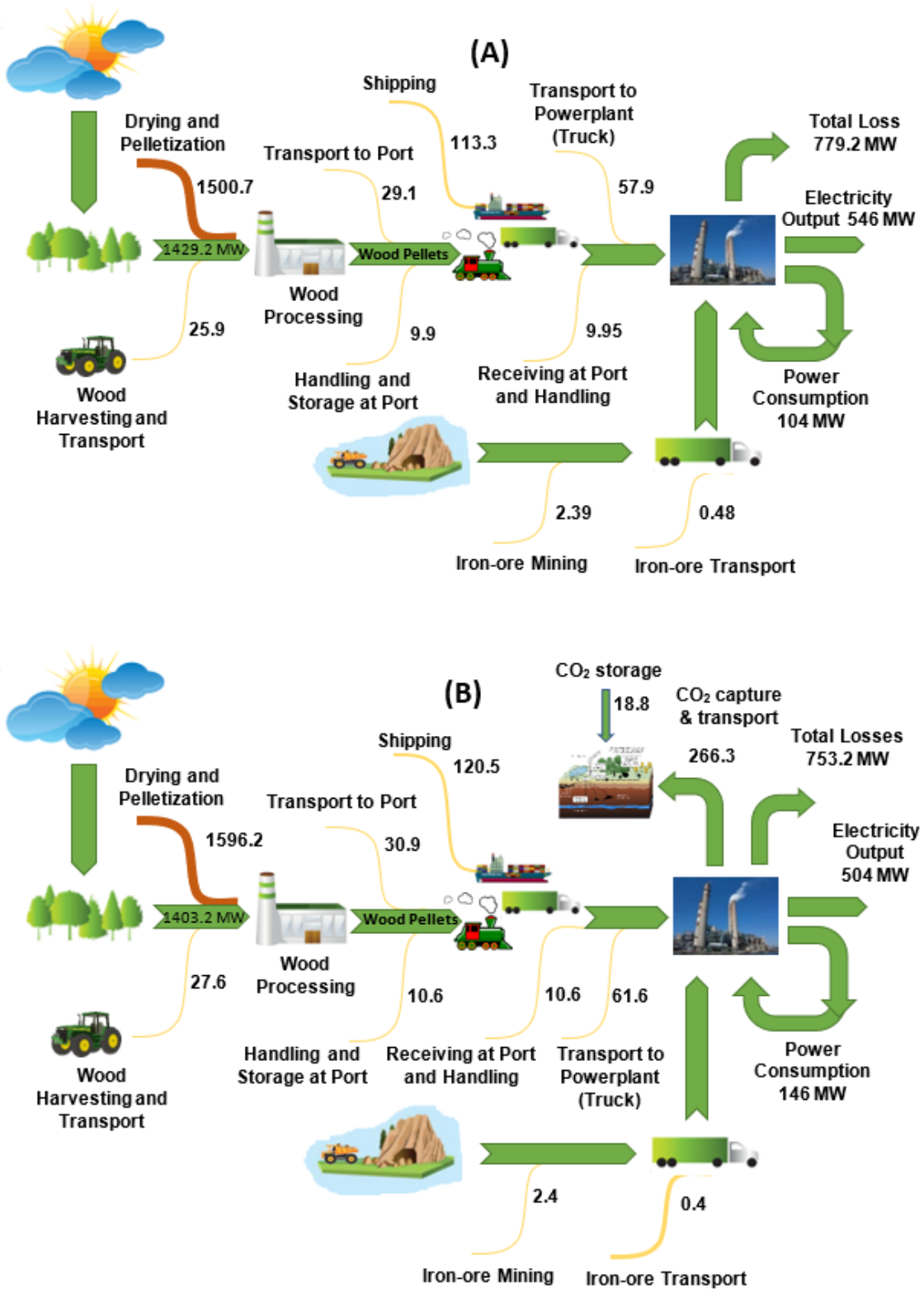

Figure 5.1. Life cycle energy input distribution for a BCLGCC power plant w/o (A) and with (B) CCS. Unit: MJ/MWh unless shown.

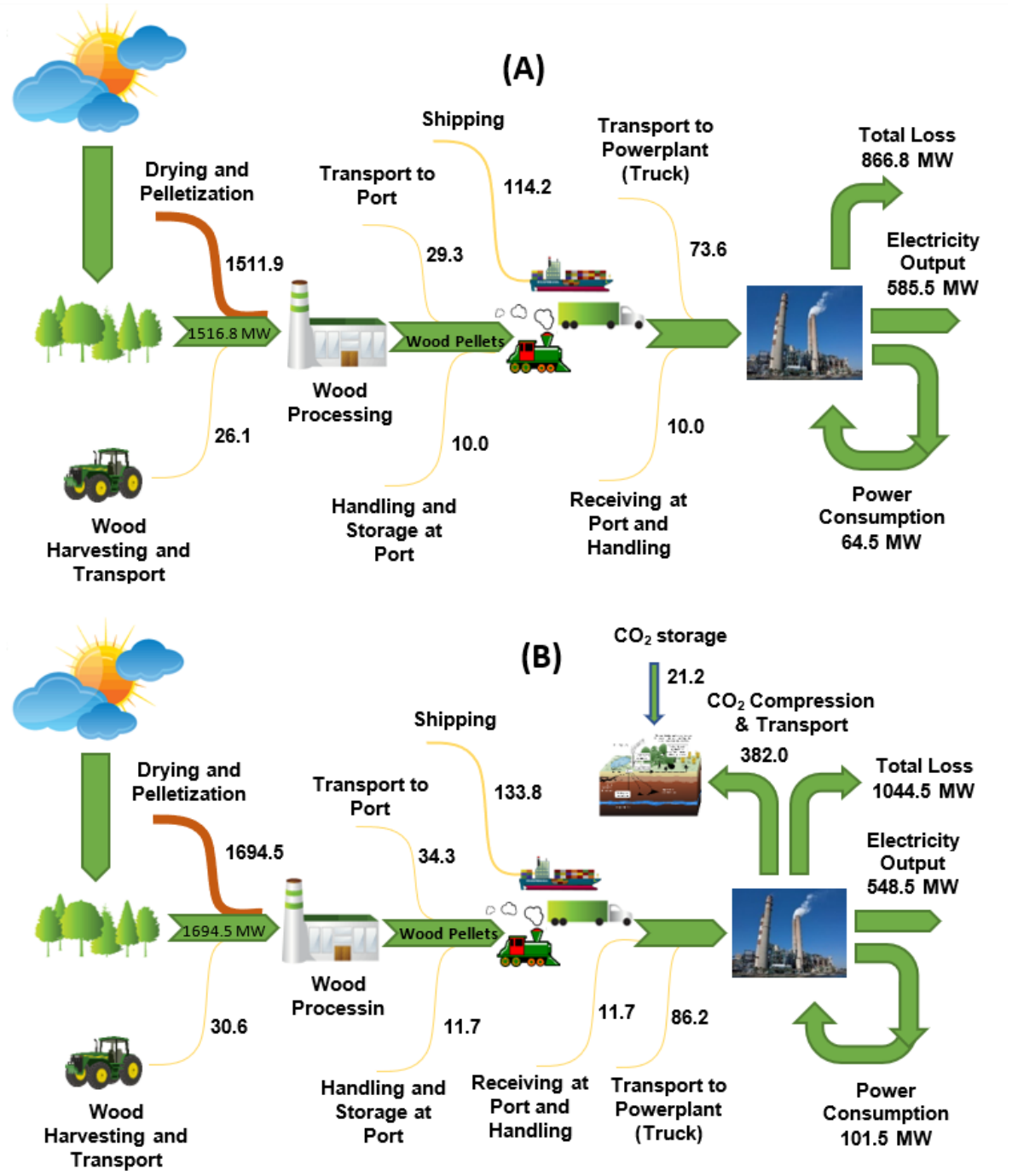

Figure 5.2. Life cycle energy input distribution for a biomass IGCC power plant w/o (A) and with (B) CCS

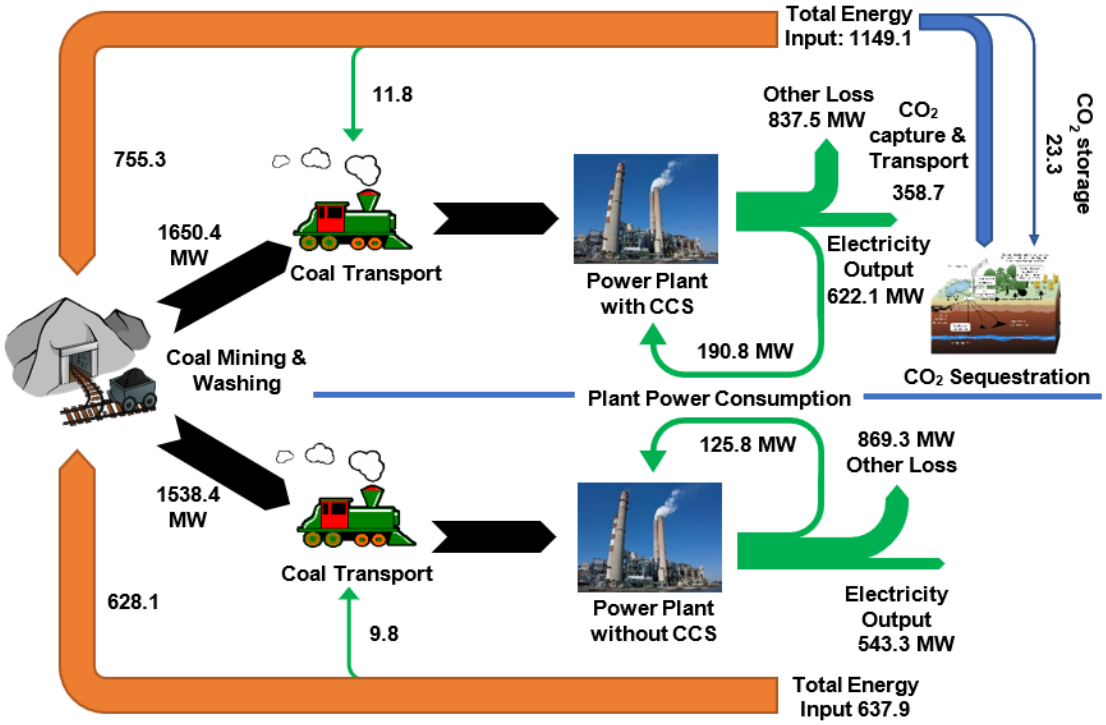

Figure 5.3. Life cycle energy input distribution for a CIGCC power plant with and w/o CCS. Unit: MJ/MWh unless shown.

5.3 Life Cycle Assessment of CO_2 Emissions Distribution

The total estimated life cycle CO_2 emission distribution for the BCLGCC power plant, with and without CCS is shown in Figure 5.4. The TLCCE is equal to 874.0 kg CO_2/MWh, of which 32.7 kg-CO_2/MWh (34.9 kg-CO_2/MWh for the CCS power plant) is released from wood harvesting, transport, and processing accounting for the highest emissions for both CCS and non-CCS plants, followed by 20.4 kg-CO_2/MWh (22.5 kg-CO_2/MWh for the CCS power plant) from the pellet's transportation and 0.2 kg-CO_2/MWh (0.22 kg-CO_2/MWh for the CCS power plant) from the iron-ore supply chain. The total emissions from fossil-based fuel during the feedstock supply chain process is 54.1 kg-CO_2/MWh. The other 820.0 kg-CO_2/MWh is released from the biomass power generation process which is released into the atmosphere and absorbed by plants during photosynthesis to regrow biomass. The BCLGCC-CCS power plant has a total life cycle CO_2 emission of 921.8 kg-CO_2/MWh (47.8 kg-CO_2/MWh more than the non-CCS process) of which 744.0 kg-CO_2/MWh is captured. The remaining 115.1 kg-CO_2/MWh is emissions from the power plant (from both fuel and air reactors) and 62.7 kg-CO_2/MWh is emitted from fossil-based fuel during the supply chain and CCS processes. This results in a net

CO_2 emission of 54.1 kg-CO_2/MWh and a negative emission of 680.1 kg-CO_2/MWh for the non-CCS and CCS plants, respectively. The total life cycle CO_2 emission for the BIGCC power plants with and without CCS is illustrated in Figure 5.5, respectively. The CCS power plant (1033.7 kg-CO_2/MWh) released 192.6 kg-CO_2/MWh more than the non-CCS plant (841.1 kg-CO_2/MWh). The non-CCS power plant emits into the atmosphere from the flue gas 93.5% (786.8 kg-CO_2/MWh) of its TLCCE, whereas the CCS plant emissions emits 11.9% (122.8 kg-CO_2/MWh) into the atmosphere while 81.2% (839.9 kg-CO_2/MWh) is stored. Nevertheless, indirect emissions from CO_2 compression, transport, and storage accounts to 7.5 kg-CO_2/MWh. Looking at the life cycle CO_2 emissions of a CIGCC power plant, the CCS power plant (867.0 kg-CO_2/MWh) released 254.3 kg-CO_2/MWh more than the non-CCS plant (1056.1 kg-CO_2/MWh). The non-CCS power plant emits into the atmosphere from the flue gas 97.7% (846.7 kg-CO_2/MWh) of its total cycle CO_2 emissions, whereas the CCS plant emits 9.3% (98.6 kg-CO_2/MWh) and 87.6% (925.1 kg-CO_2/MWh) stored. Nevertheless, indirect emissions from CO_2 compression, transport, and storage accounts to 6.5 kg-CO_2/MWh. The life cycle CO_2 emission distribution diagram of a CIGCC plant is summarized in Figure 5.7.

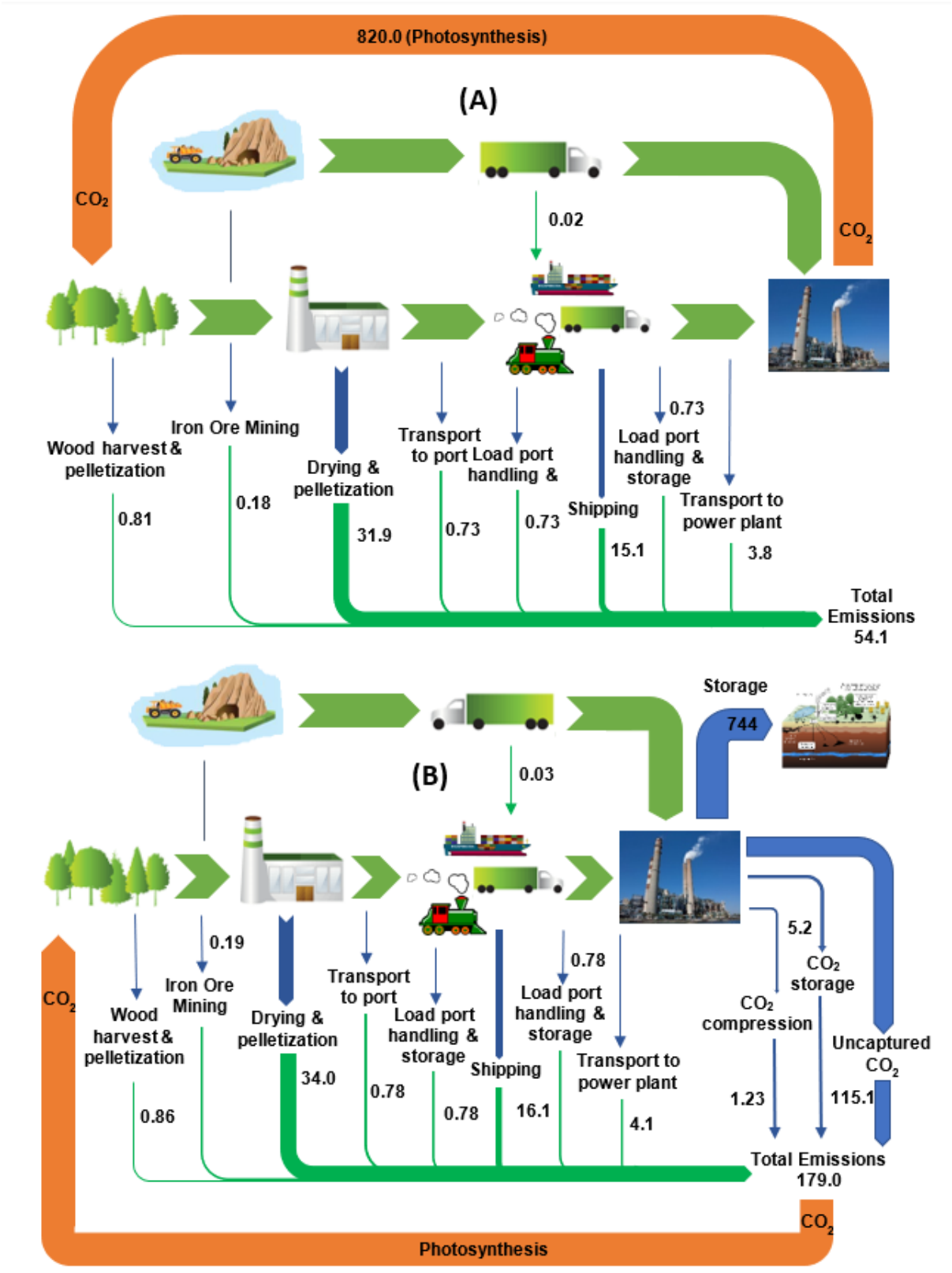

Figure 5.4. Life cycle CO_2 emission distribution for a BCLGCC power plant w/o (A) and with (B) CCS. Unit: kg-CO_2/MWh unless shown.

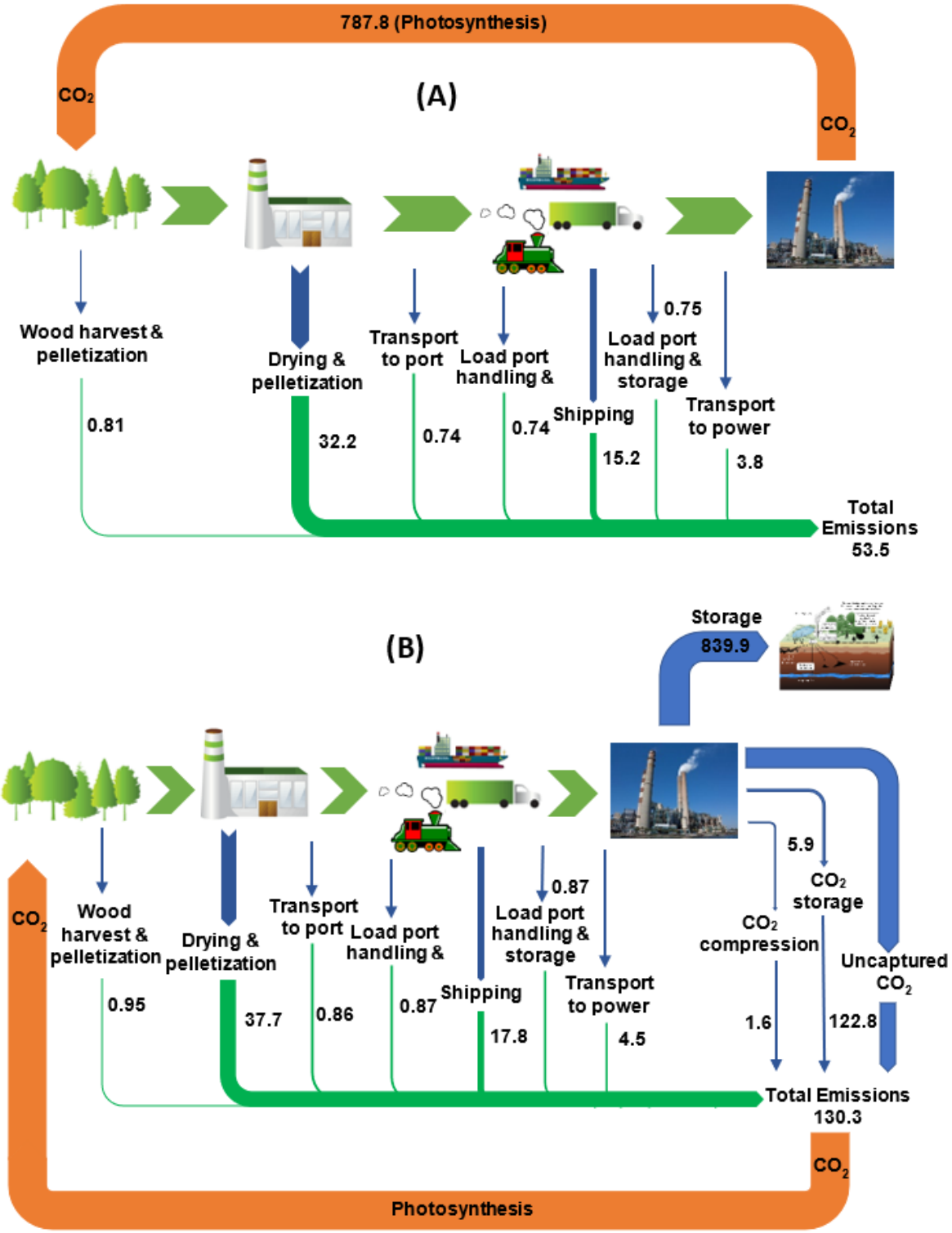

Figure 5.5. Life cycle CO_2 emission distribution diagram for a IGCC power plant w/o (A) and with (B) CCS. Unit: kg-CO_2/MWh unless shown.

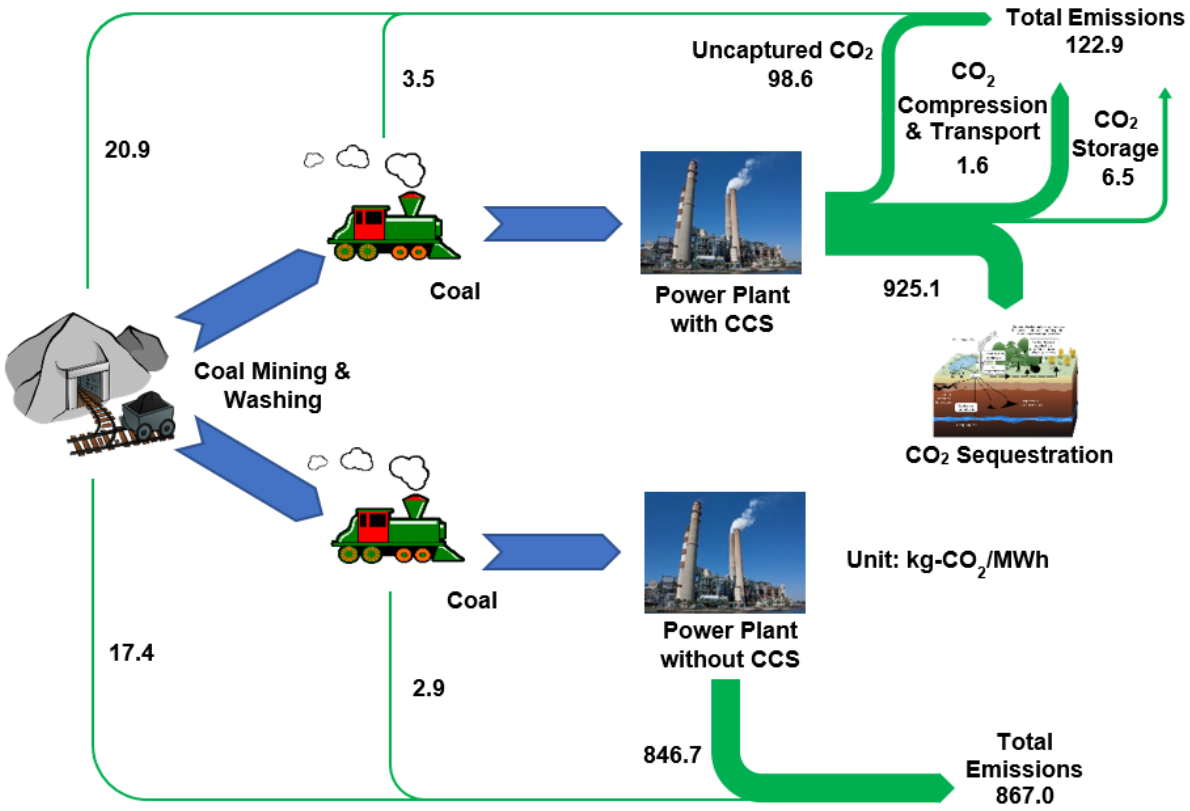

Figure 5.6. Life cycle CO_2 emission distribution diagram for a CIGCC power plant with and w/o CCS. Unit: kg-CO_2/MWh unless shown.

5.4 Life Cycle Assessment of Cost Input Distribution

The life cycle cost input of both BCLGCC with and without CCS are equal to 200.5 £/MWh and 150.1 £/MWh, respectively, as shown in Figure 5.7. The two most cost intensive stages in the whole process are within the biomass supply chain process; wood harvesting & processing (84.6 £/MWh and 79.5 £/MWh for CCS and non-CCS) and wood transport (41.4 £/MWh and 38.9 £/MWh for CCS and non-CCS), accounting for 62.8% and 78.9% of the cost of electricity for CCS and non-CCS, respectively. From the cost required during the biomass supply chain the cost of biomass can be estimated to be equal to 10 £/$GJ_{(Biomass)}$. The annual capital cost and O&M labour cost of the BCLGCC with CCS power plant is 17.1 £/MWh and 3.6 £/MWh higher than the non-CCS power plant, respectively. Furthermore, CO_2 transport and storage contributes approximately 18.8 £/MWh to the electric cost of the CCS power plant. Figure 5.8 illustrates the life cycle cost input of both BIGCC with and without CCS are equal to 212.2 £/MWh and 159.5 £/MWh, respectively. The complete biomass supply chain process contributed the most to the total cost with 111.8 £/MWh for CCS and 95.4 £/MWh to non-

CCS. The annual cost and O&M labour cost for CCS is equal to 57.0 £/MWh and 22.2 £/MWh respectively (47.9 £/MWh and 16.2 £/MWh higher than the non-CCS plant), with an additional cost of 21.2 £/MWh for the CO_2 transport and storage. The life cycle cost input of both CIGCC with and without CCS are equal to 119.9 £/MWh and 72.5 £/MWh, respectively, as shown in Figure 5.9. The annual cost contributed the highest to the TLCCI with 54.1 £/MWh and 38.1 £/MWh for CCS and non-CCS plants. The complete coal supply chain process (mining, washing and transport) contributed the second highest cost to the TLCCI with 27.3 £/MWh for CCS and 22.7 £/MWh for non-CCS. This resulted for the price of coal to be equal to 1.78 £/GJ. Finally, the CCS plant adds an additional cost of 23.4 £/MWh for the CO_2 transport and storage.

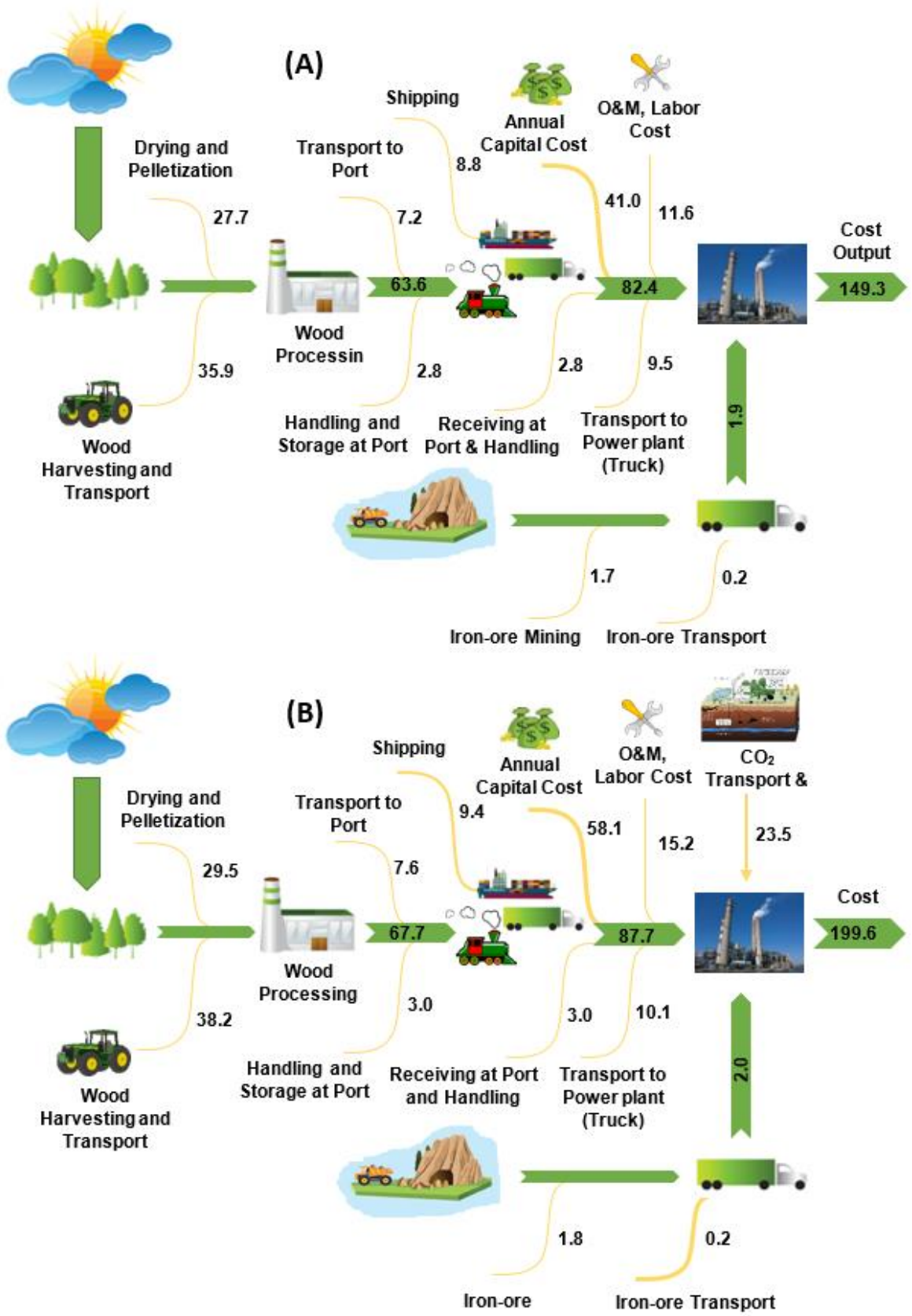

Figure 5.7. Life cycle cost input distribution diagram for a BCLGCC power plant w/o (A) and with (B) CCS. Unit: £/MWh unless shown.

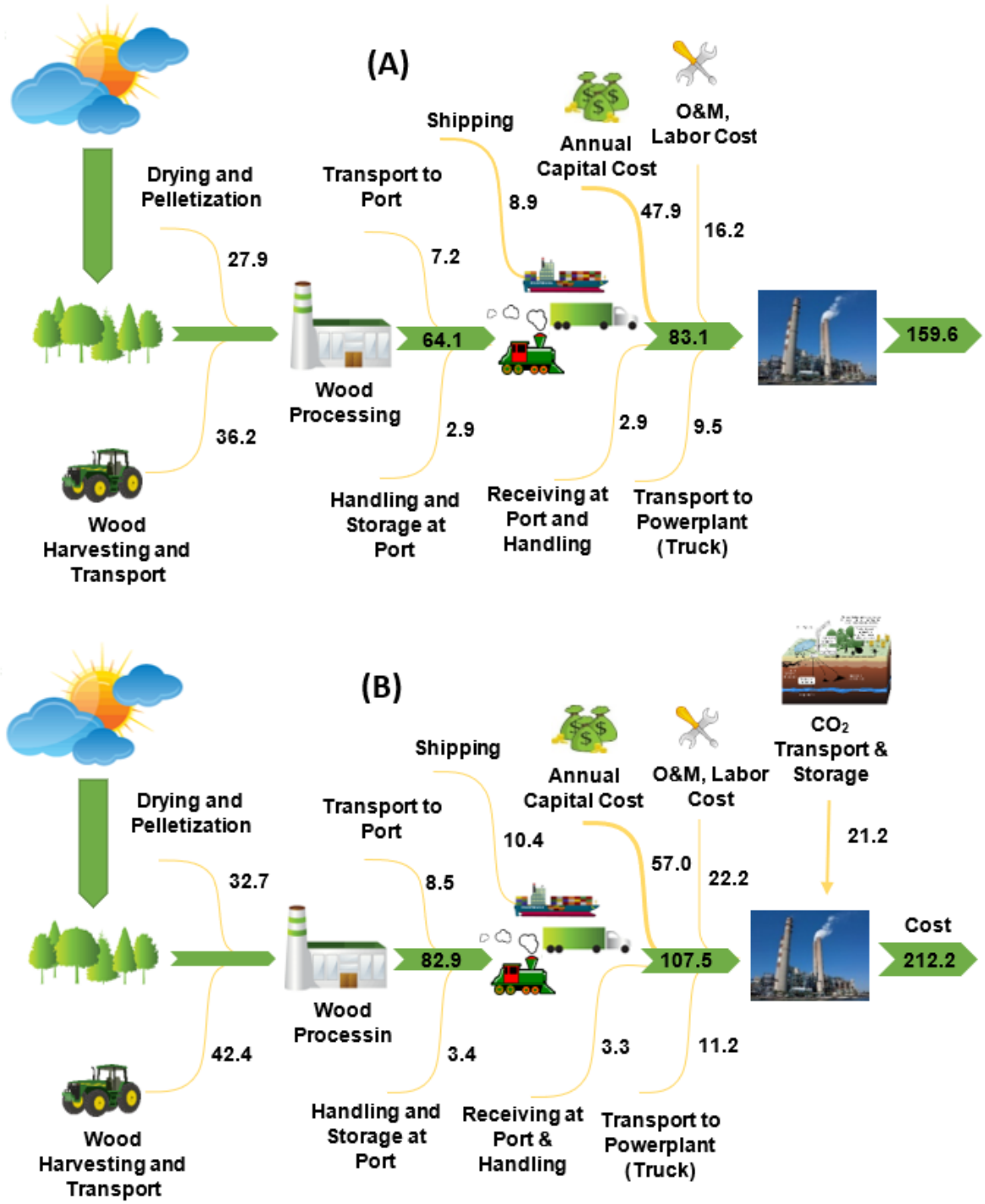

Figure 5.8. Life cycle cost input distribution diagram for a biomass IGCC power plant w/o (A) and with (B) CCS. Unit: £/MWh unless shown.

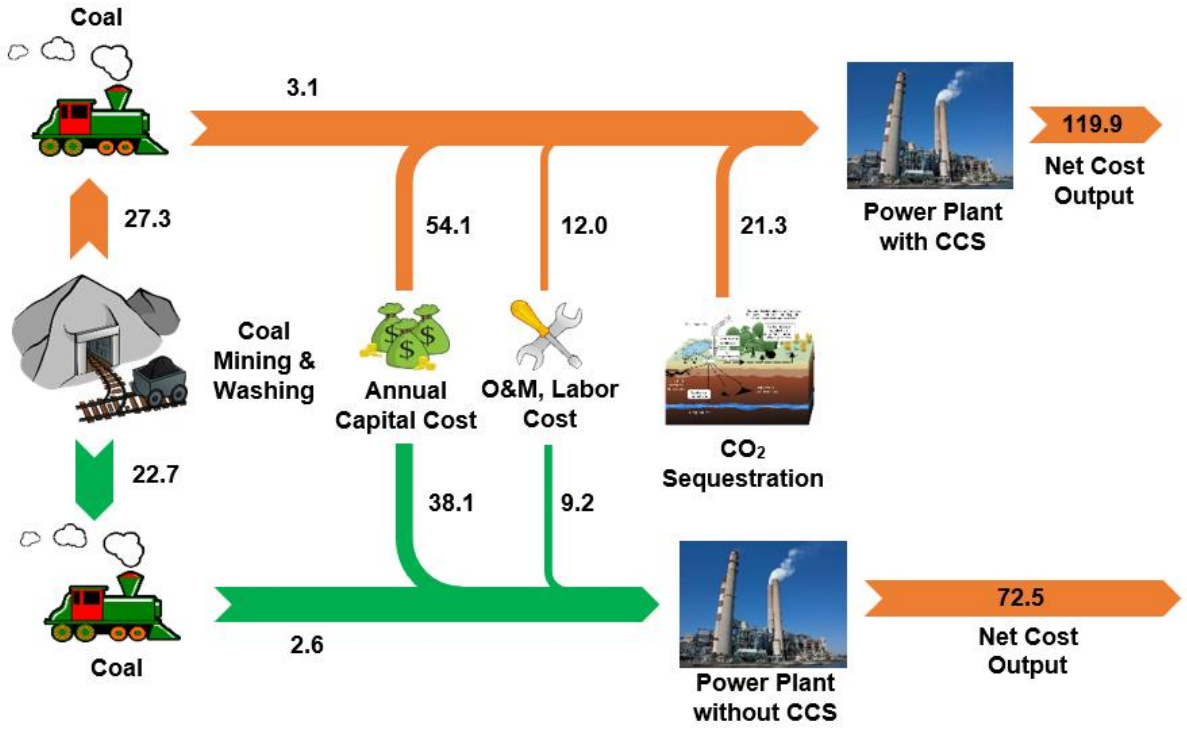

Figure 5.9. Life cycle cost input distribution diagram for a coal IGCC power plant with and w/o CCS. Unit: £/MWh unless shown.

5.5 Performance Comparison Among the Different Types of Power Generation Technologies

The BCLGCC, BIGCC and CIGCC power generation technology were analysed with respect to energy, economic, and CO_2 emission aspects (presented in Figure 5.1 – Figure 5.9). The results of these technologies are then compared with each other and with direct biomass/coal combustion technology based on the same gross power plant scale (650MW). Figure 5.10 presents a result summary of the life cycle energy input (a), CO_2 emissions (b) and cost distribution (c) in a stacked bar chart, which also included results of a BDC and a PCC power plants with and without CCS [245]. To sum up in terms of efficiency, combustion power generation is lower than gasification power generation technology, which is mainly due to the low efficiency of heat transfer in combustion process and the high efficiency of gasification-combined cycle. However, the low energy density of biomass, as well as the transportation and pre-treatment of biomass results in higher energy consumption, while at the same time results in an increase in production cost. Therefore, the advantage of biomass gasification power generation technology in energy efficiency and cost is not obvious compared with that of coal gasification power generation technology.

Comparing between gasification and combustion technologies we can see that the gasification technology has a higher thermal efficiency compared to direct combustion, however this is associated with high maintenance cost due to the complexity of the process. This is because the combustion process experiences a higher energy loss during the conversion of the solid fuel into heat, whereas gasification controls the dispersion of the thermal energy, hence reducing the overall loss when converting the biomass into syngas. Moreover, syngas can combust at higher temperatures compared to the combustion of solid fuels, hence increasing its thermodynamic upper limit as stated by Carnot's theorem. Furthermore, combustion technology is coupled with a steam turbine to generate electricity, whereas gasification technology is coupled with a combined gas and steam turbines which results in a higher efficiency due to better utilisation of waste heat. This results in less fuel being consumed for gasification processes compared to combustion due to better fuel utilization for the same power output. As a result, Figure 5.1 demonstrates that the CIGCC power plant requires a lower TLCEI per net power, 637.9 MJ/MWh and 1149.1 MJ/MWh, compared to the PCC power plant, 730.7 MJ/MWh and 1420.4 MJ/MWh, for non-CCS and CCS, respectively. However, when comparing between the non-CCS biomass power plants there doesn't seem to be much difference in terms of the TLCEI per net power. Even though gasification technology (BIGCC and BCLGCC) utilizes less biomass feedstock compared to BDC to produce the same gross power (650 MW), it consumes a lot more power within the power plant hence reducing its net power, which consequently increases its TLCEI per net power. However, when comparing between the gasification technologies (BCLGCC and BIGCC) with CCS to combustion technology (DBC) with CCS, they required 825.6 MJ/MWh and 488.9 MJ/MWh less TLCEI, respectively. This is due to the BCLGCC and BIGCC power plants emitting less CO_2 which is required to be captured for storage (744 kg-CO_2/MWh and 925.1 kg-CO_2/MWh, respectively) compared to DBC (1081.3 kg-CO_2/MWh) which is as a result of less biomass feedstock processed. Therefore, requiring less energy for CO_2 capture, transport, and storage compared to the DBC (459.3 MJ/MW) power plant. This increases the amount of energy consumed by the power plant by combustion, therefore significantly reducing its net power compared to gasification. This hence results in the TLCEI of the BIGCC and BCLGCC with CCS (285.1 MJ/MW and 403.2 MJ/MW, respectively) to be less than combustion (DBC) with CCS (459.3 MJ/MW) power plant, therefore increasing the cost requirements. Comparing between the TLCCI between gasification and combustion technologies, combustion with non-

CCS seems to require lower costs compared to gasification. PCC and BDC require 57.8 £/MWh and 116.7 £/MWh whereas CIGCC, BIGCC and BCLGCC require 72.5 £/MWh, 159.5 £/MWh and 149.3 £/MWh. One of the main reasons for the difference in the TLCCI is the initial capital cost which is the most cost depleting steps within gasification power generation processes. Combustion is an already proven and well-established commercial technology in large scales which reduces its capital cost. Moreover, compared to combustion technology, gasification is a more complex process, resulting in more capital investment and operational costs. As a result, gasification power plants require higher annual capital and operational costs, hence higher TLCCI. When comparing between gasification and combustion CCS power plants, combustion is still cheaper however the gap between both technologies narrows owing to less biomass pre-treatment for gasification and the higher cost required for CO_2 handling for combustion.

When comparing between BIGCC and BCLGCC, we observe that a lower energy input is required by the BCLGCC process which is due to less biomass feedstock required to generate the same power output which is attributed to the more efficient biomass utilization in BCLG technology. This is due to BCLGCC having a higher efficiency compared to conventional BIGCC. This is attributed to the flameless gasification process resulting in less exergy loss during the thermal conversion process. In addition, the tar catalytic cracking ability of the OC in BCLGCC process increases by converting more tar and char into syngas, hence biomass utilization ability increases compared to BIGCC. Therefore, reducing the amount of biomass feedstock for BCLGCC power plant to generate the same output (650 MW). Furthermore, BCLGCC can avoid the cost and energy depleting step of air separation to produce oxygen. Finally, looking at the TLCCI for both gasification technologies, BCLGCC requires less TLCCI due to its high energy efficiency, therefore requiring less biomass to be processed within the system, hence reducing the feedstock cost. Additionally, this decreases the physical size of the plant, therefore decreasing its annual capital cost. On the other hand, BCLG technology is more complex than conventional gasification which should slightly increase its cost, yet the TLCCI remains less than the BIGCC process.

Comparing between coal and biomass power plants, on average wood harvesting, processing, and transport (biomass supply chain) consumes approximately 3 and 2.5 times the energy required for coal mining, washing and transport (coal supply chain) per MWh for IGCC and

combustion power plants, respectively, with wood processing being the most energy demanding step. This is due to coal being more energy dense compared to biomass hence less coal feedstock processing is required. In addition, coal transport distance is less compared to biomass, which is sourced from North America, hence requiring more energy throughout its supply chain. It was calculated that the life cycle costs of biomass and coal is equal to 10.0 £/GJ and 1.78 £/GJ, respectively, which is in line with the prices in the UK. The TLCCI for coal power plants are much cheaper than biomass power plants due to less feedstock consumed as well as due to the higher cost of biomass transport. The second most cost intensive process is the wood harvesting and transport process. Even though coal powered plants produce cheaper electricity, but government renewable energy incentives and carbon tax schemes (discussed in section 3.6) will reduce the cost of biomass power plants making them suitable towards achieving a net-zero carbon emissions by 2050.

The energy (cost) required by CCS accounts for approximately 15.0% (11.7%) of the TLCEI (TLCCI) for biomass power plants and 32.0% (2.2%) for coal power plants. The higher percentage in the coal power plant is due to their lower TLCEI. The flue gas CO_2 emissions from the non-CCS plants ranges from 841 – 899 kg-CO_2/MWh, with DBC having the highest emissions (899 kg-CO_2/MWh), however since biomass is the fuel source, it can be assumed to be carbon neutral. Whereas the CIGCC plant releases the most CO_2 (867 kg-CO_2/MWh) from a non-renewable source. Even though biomass-based power plants can be assumed to be carbon neutral, fossil fuel-based CO_2 is released during the supply chain process, hence increasing the net CO_2 emissions by approximately 54 – 85 kg-CO_2/MWh. Regarding coal power plants, the coal supply chain emits between 20 - 36 kg-CO_2/MWh. The highest net total life cycle CO_2 emitter was the PCC with CCS (147.9 kg-CO_2/MWh) power plant, followed by CIGCC with CCS (131.0 kg-CO_2/MWh), then BIGCC with CCS (negative 854.1 kg-CO_2/MWh) and finally DBC with CCS power plant (negative 996.2 kg-CO_2/MWh).

5.6 Future Technological Development and Recommendations from this Study

After a thorough energy, cost, and CO_2 emission comparison between the thermal conversion technologies in the previous section. It was concluded that from an energy efficiency perspective, biomass/coal gasification power generation technology is more efficient than combustion power generation due to the step-by-step chemical energy utilized and high

thermal conversion efficiency (gas turbine combined cycle). From the perspective of clean and efficient utilization of energy, the future development of biomass/coal gasification power generation technology is the primary technology to be considered. However, high investment in biomass/coal gasification is required, while some key core technologies (such as tar cracking, high temperature desulfurization, air separation unit, etc.) need a breakthrough. BCLGCC with and w/o CCS demonstrates itself to be a potential alternative which is due to its efficient fuel utilization and carbon neutral and carbon negative emissions. Moreover, in line with the UK policies, BCLGCC shows better results than BDC and BIGCC coupled with a CCS process which can support the push towards establishing bioenergy with carbon capture and storage (BECCS) technology for a net zero 2050. However, there are a few drawbacks associated with the technology which can be researched into and improved to reduce the cost, energy input and CO_2 emission. These include researching into finding a suitable and effective oxygen carrier, developing and enhancing the design of a two-staged fluidized bed reactor and looking into integrating the system by energy matching and incorporating waste heat recovery technology.

Looking at the life cycle energy input and CO_2 emission aspects in details, wood processing and pelletization stage consumes the most amount of energy, hence should be researched into by developing low energy and low-cost biomass pre-treatment and biomass moulding technology, hence reducing the high CO_2 emissions. Moreover, the second most cost intensive process within the life cycle of the power plant is biomass harvesting and transport to the wood pellet plant. This could be reduced if biomass is sourced from a different country with cheaper costs and an abundant source of biomass. It could also have an effect on the supply chain process depending on how far the country the biomass is sourced from, which could also affect the energy input and CO_2 emission. This is one of the main reasons delaying biomass technology from fast commercialization. Moreover, BCLGCC consumes a large amount of the gross power produced within the plant hence reduces the net power. Most of the power is consumed in compressing the syngas before the combined cycle process, hence researching into reducing the energy consumption within the plant is essential to further improve overall efficiency of the technology. This effect can be minimized by developing high temperature and pressure syngas cleaning technology.

In terms of the TLCCI, the annual capital cost consumes the highest cost throughout the life cycle cost input. It is not expected for combustion technology to reduce in capital cost in the near future as it has significantly developed and commercialized, however BIGCC and BCLGCC are still commercializing hence are expected to reduce in costs with further research, especially with BCLGCC. Even though coal is much cheaper compared to biomass in the UK, the UK is planning on closing all coal power plants by 2025, hence the idea of building CIGCC and PCC power plants in the UK will not be applicable, however it could be suitable for other countries that carry on using coal or are interested in coal power plants with CCS. This would have an effect on the fuel supply chain, which will be considered in the following section. Moreover, biomass gasification not only can it generate syngas to power generation but can also be used as an alternative to simultaneously produce hydrogen for hydrogen powered cars since after the year 2035 when selling petrol and diesel cars ban come to effect. In addition syngas can be used in the MIDREX Direct Reduction Plant process instead of the conventional coking process for steel making (coking-steel making causing large amount of carbon emission and pollution) [288]. In conclusion, BCLGCC/BIGCC presents a promising alternative, however further research into this technology can be very much effective in presenting a pathway towards a carbon neutral 2050 from the perspective of life cycle energy input, economy, and CO_2 emissions.

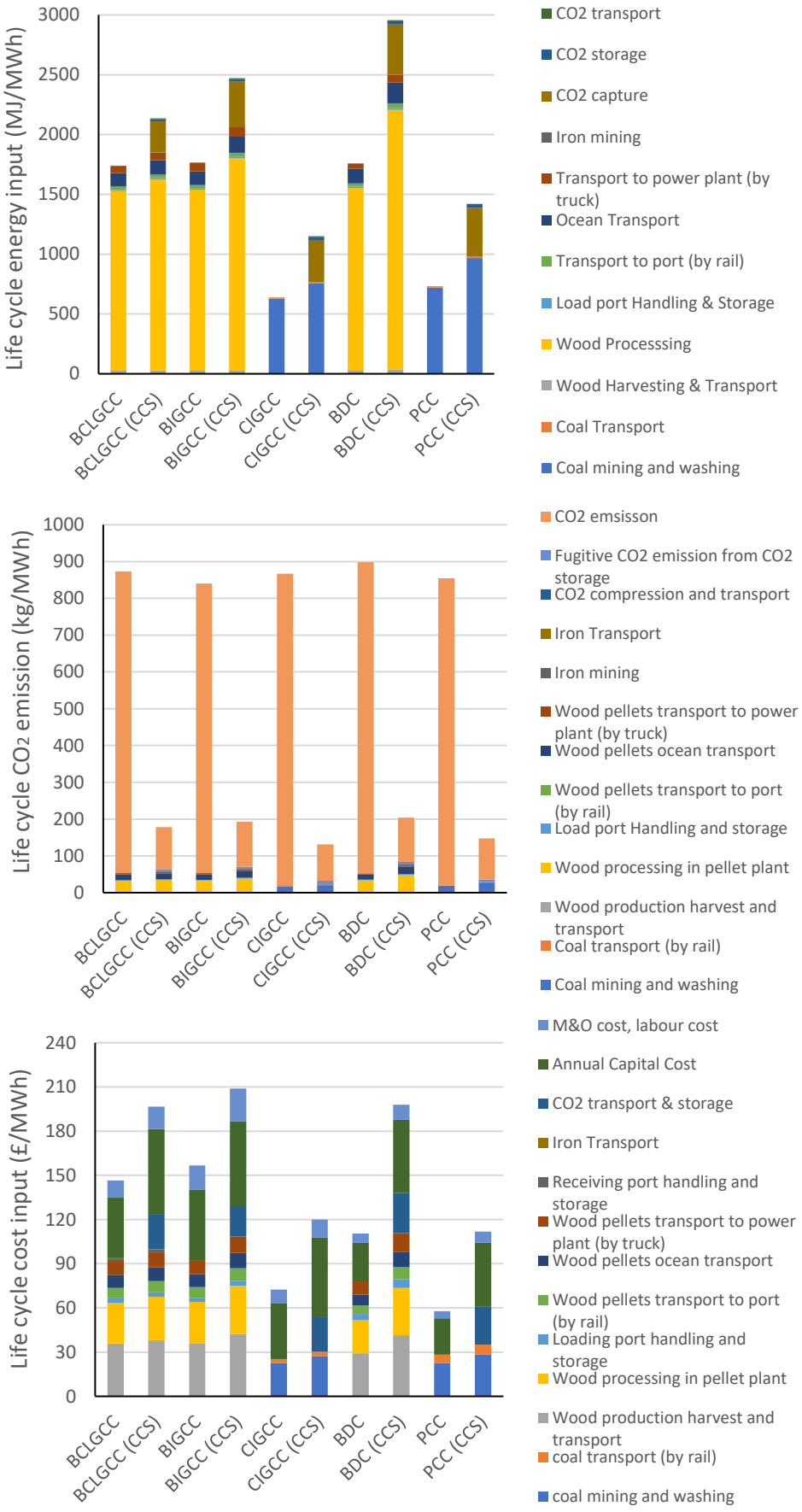

Figure 5.10. Comparing life cycle energy-CO2 emission-cost input of eight power plants

5.7 Sensitivity Analysis

Since the values used in this research could change with time, location, technological development or could have a percentage uncertainty, a sensitivity analysis has been performed to identify parameters that would have the most significant impact on the life cycle assessment (Figure 5.11 – Figure 5.13). The supply chain processes of all feedstock as well as the CO_2 capture, transport and storage have been used as the base parameters for the sensitivity analysis to measure their effect on the total life cycle energy input, CO_2 emissions and cost input. Additionally, to further measure the effect of the TLCCI, the variable cost, capital cost and plant life were tested. This has been performed on the BCLGCC, BIGCC and CIGCC plants with and w/o CCS. The parameters that had the highest impact on the TLCEI and consequently TLCCE are the wood processing, coal mining and washing, CO_2 capture, and biomass transport. However, out of the biomass transport process, ocean transport resulted in the highest impact on the life cycle values. The biomass transport process varies the TLCEI by approximately 8.0% and 6.8% for both CCS and non-CCS power generation systems, respectively, as the biomass transport energy input varies by 60%. This also results in the TLCCE to vary by around 1.4% and 7.6% for biomass non-CCS and CCS power plants, respectively. Since coal power plants are not expected to be invested into in the near future in the UK, the values can be applied in other countries (e.g. China, USA, India) that still heavily invest in coal power station. Changing the geographical location of the plant will have an effect on the coal transport for the CIGCC plant. Increasing the coal transport energy by 60% increases the TLCEI and TLCCE by 0.9% (0.6% for CCS) and 0.2% (1.7% for CCS), respectively. Establishing the power plant in other geographical locations could reduce the fuel supply chain energy input, CO_2 emission and cost input depending on the abundance of the fuel (biomass or coal). However coal would still be preferred due to its lower overall cost unless government subsidies and policies are put in place to encourage using biomass fuel. In the UK government subsidies are known as Renewable Obligation Certificate (ROC)'s requiring 100% of the electricity to be produced from a renewable source to be given £50.05 per each MWh produced [289]. Another factor from the fuel supply chain that heavily influences the TLCEI and TLCCE are wood processing for biomass and mining & washing for coal. As wood processing value varies by 60%, the overall TLCEI varies by approximately 51% for non-CCS (43% for CCS), while the overall TLCCE varies by approximately 2.1% for non-CCS (11.9% for

CCS). This shows that wood processing has a higher sensitivity impact on TLCEI compared to the TLCCE, with it having a greater impact on CCS plants compared to non-CCS for the TLCCE. Similarly, with the CIGCC power plant, a 60% increase in coal mining and washing increases the TLCEI by 59.1% for non-CCS (39.4% for CCS) and increases the TLCCE by 19.4% for non-CCS (13.9% for CCS). Regarding the CCS stage, it also has a higher sensitivity on the TLCEI compared to the TLCCE. In terms of cost, the annual cost, wood harvesting, wood processing and coal mining & washing cause the highest sensitivity to the TLCCI. A 60% change in annual capital cost will result in approximately 17.0% change in the TLCCI for the biomass power plants (CCS and non-CCS) and 30.5% for the CIGCC plant (24.4% for CIGCC with CCS). Looking at the supply chain of the fuel feedstock which depends on the location of the power plant, increasing the biomass supply chain by 60% increases the TLCCI by approximately 10 – 13%, and increasing the coal supply chain by 60% increases the TLCCI by 2 – 4%. Therefore, establishing a biomass-based power plant in a geographic location surrounded by an abundant source of biomass would significantly reduce the costs. Additionally, the cost of CO_2 capture and storage varies TLCCI by 7.1% for BCLGCC, 6.6% for BIGCC and 13.9% for CIGCC when its cost varies by 60%. Taking into consideration the 50.05 £/MWh ROC government subsidy in the TLECI values, this will reduce the TLCEI of the BCLGCC, BIGCC and BDC plants to 99.2 £/MWh (149.6 £/MWh with CCS), 109.5 £/MWh (162.2 £/MWh with CCS) and 66.7 £/MWh (156.6 MWh with CCS), respectively. A comparison between the TLCCI of all the 10 different power generation technologies with and without CCS including the ROC government subsidies is summarized in Figure 5.14.

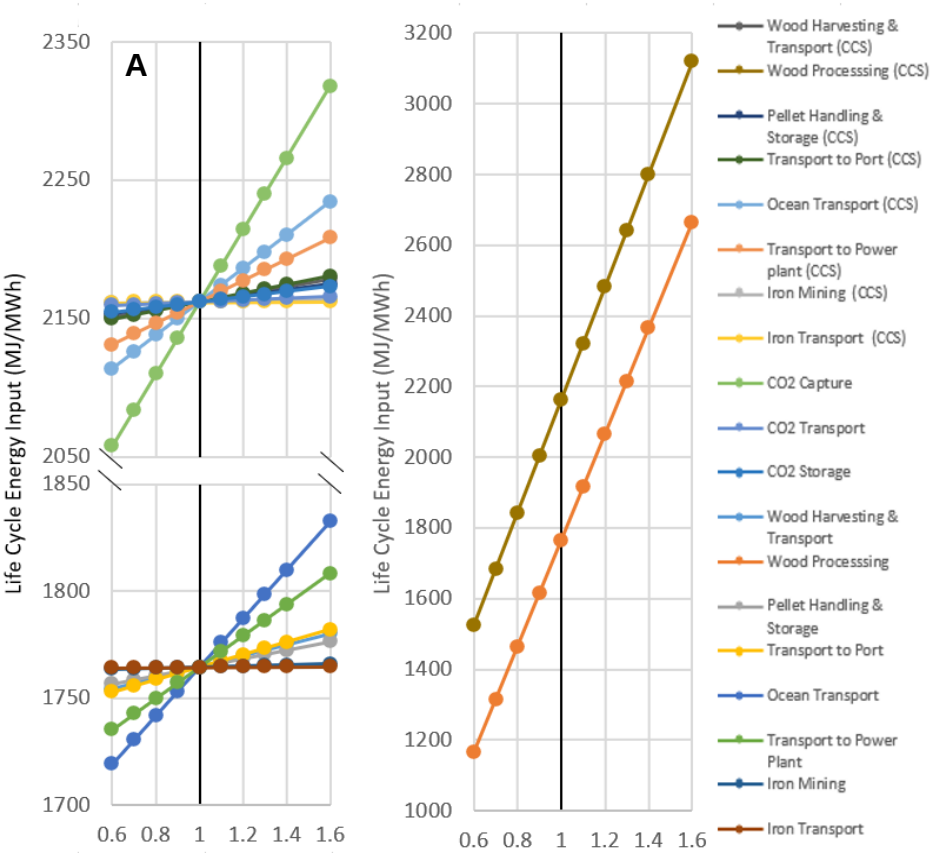
A
Life Cycle Energy Input (MJ/MWh)
2350
2250
2150
2050
1850
1800
1750
1700
0.6 0.8 1 1.2 1.4 1.6
3200
3000
2800
2600
2400
2200
2000
1800
1600
1400
1200
1000
Wood Harvesting & Transport (CCS)
Wood Processsing (CCS)
Pellet Handling & Storage (CCS)
Transport to Port (CCS)
Ocean Transport (CCS)
Transport to Power plant (CCS)
Iron Mining (CCS)
Iron Transport (CCS)
CO2 Capture
CO2 Transport
CO2 Storage
Wood Harvesting & Transport
Wood Processsing
Pellet Handling & Storage
Transport to Port
Ocean Transport
Transport to Power Plant
Iron Mining
Iron Transport

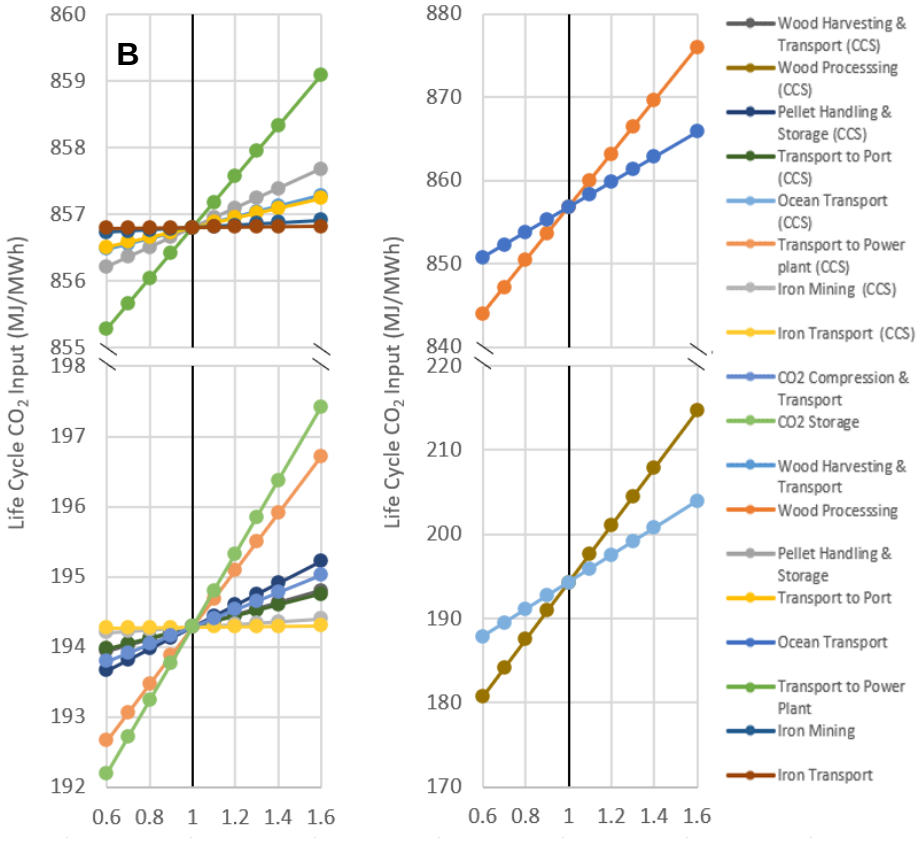
B
Life Cycle CO_2 Input (MJ/MWh)
860
859
858
857
856
855
198
197
196
195
194
193
192
0.6 0.8 1 1.2 1.4 1.6
880
870
860
850
840
220
210
200
190
180
170
Wood Harvesting & Transport (CCS)
Wood Processsing (CCS)
Pellet Handling & Storage (CCS)
Transport to Port (CCS)
Ocean Transport (CCS)
Transport to Power plant (CCS)
Iron Mining (CCS)
Iron Transport (CCS)
CO2 Compression & Transport
CO2 Storage
Wood Harvesting & Transport
Wood Processsing
Pellet Handling & Storage
Transport to Port
Ocean Transport
Transport to Power Plant
Iron Mining
Iron Transport

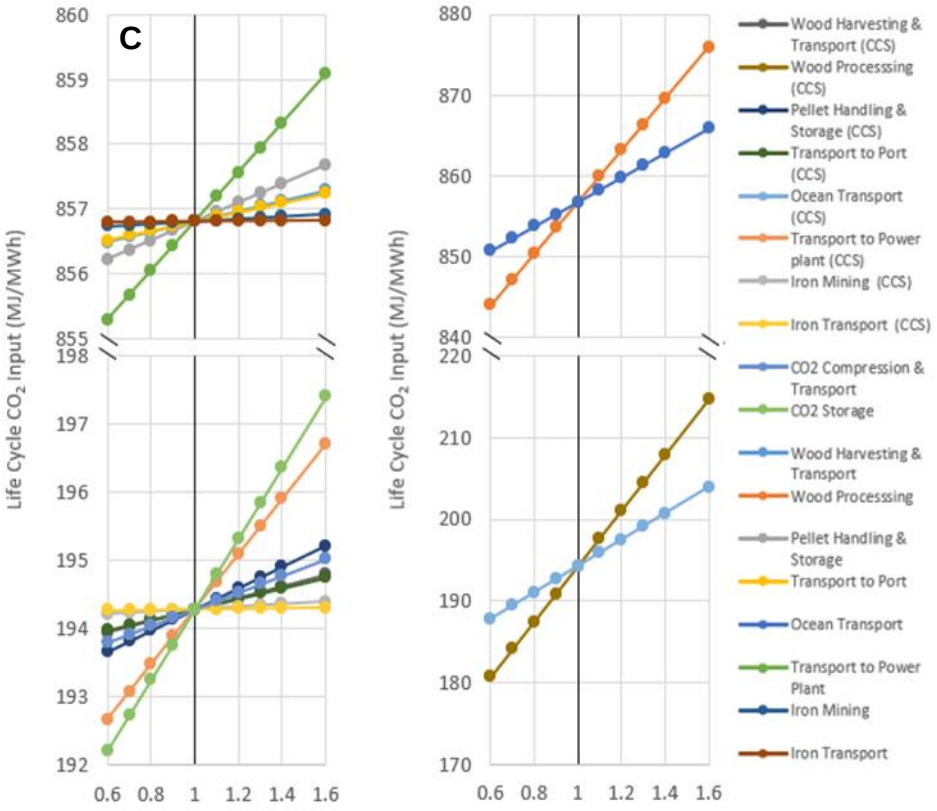

Figure 5.11. Sensitivity analysis of life cycle (A) energy input, (B) CO_2 emissions and (C) cost input of a BCLGCC power plant

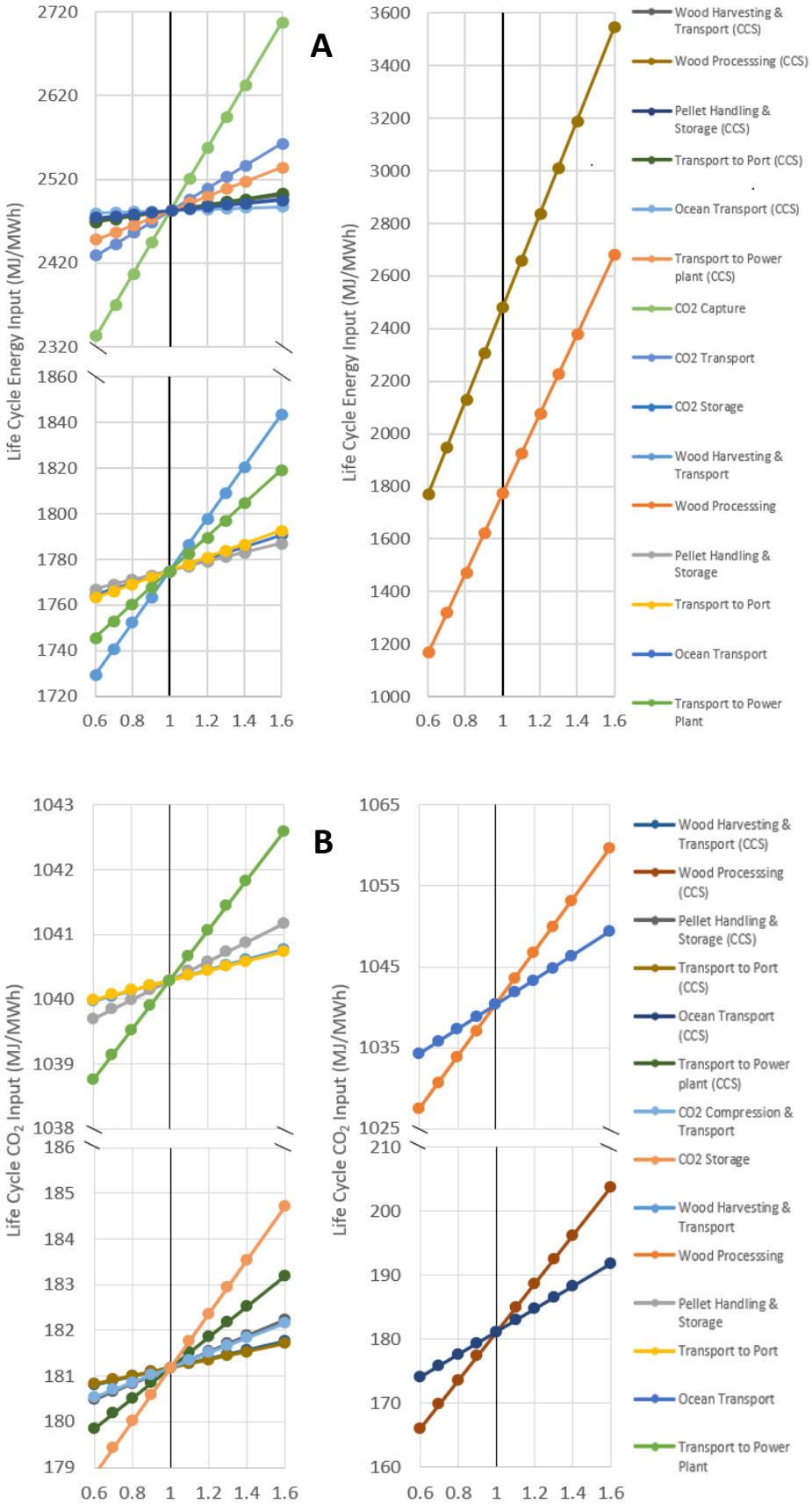
A
Life Cycle Energy Input (MJ/MWh)
2720
2620
2520
2420
2320
1860
1840
1820
1800
1780
1760
1740
1720
0.6 0.8 1 1.2 1.4 1.6
3600
3400
3200
3000
2800
2600
2400
2200
2000
1800
1600
1400
1200
1000
Wood Harvesting & Transport (CCS)
Wood Processsing (CCS)
Pellet Handling & Storage (CCS)
Transport to Port (CCS)
Ocean Transport (CCS)
Transport to Power plant (CCS)
CO2 Capture
CO2 Transport
CO2 Storage
Wood Harvesting & Transport
Wood Processsing
Pellet Handling & Storage
Transport to Port
Ocean Transport
Transport to Power Plant
B
Life Cycle CO2 Input (MJ/MWh)
1043
1042
1041
1040
1039
1038
186
185
184
183
182
181
180
179
0.6 0.8 1 1.2 1.4 1.6
1065
1055
1045
1035
1025
210
200
190
180
170
160
Wood Harvesting & Transport (CCS)
Wood Processsing (CCS)
Pellet Handling & Storage (CCS)
Transport to Port (CCS)
Ocean Transport (CCS)
Transport to Power plant (CCS)
CO2 Compression & Transport
CO2 Storage
Wood Harvesting & Transport
Wood Processsing
Pellet Handling & Storage
Transport to Port
Ocean Transport
Transport to Power Plant

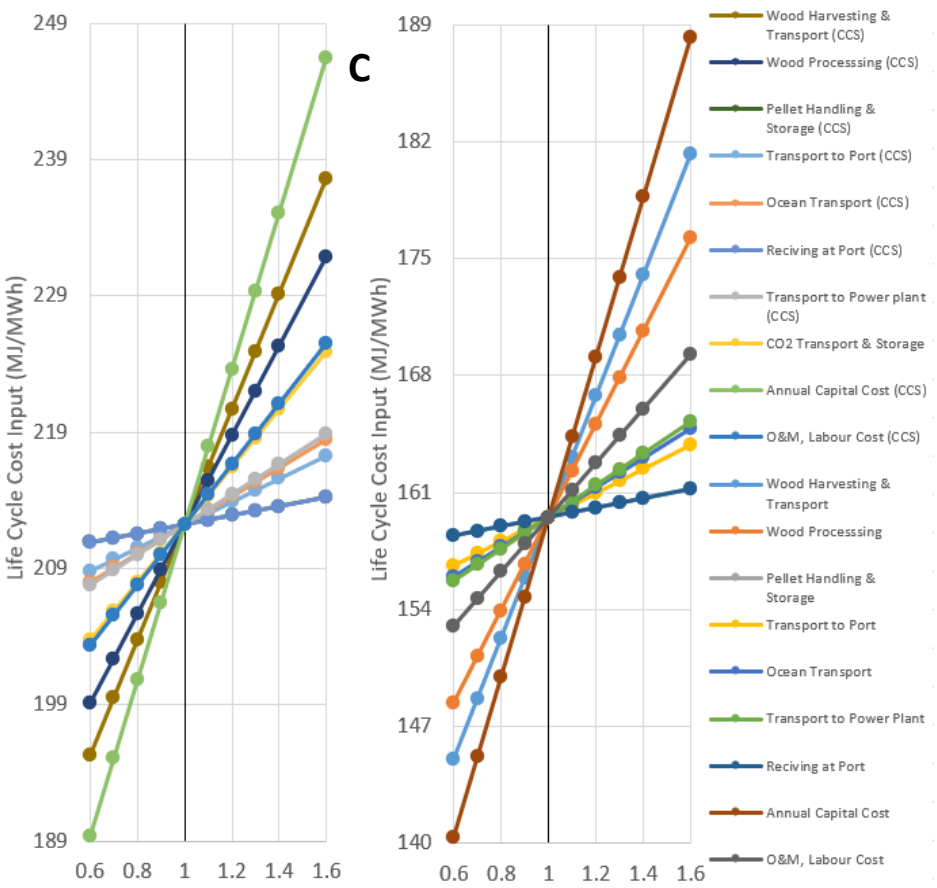

Figure 5.12. Sensitivity analysis of life cycle energy input (a), CO_2 emissions (b) and cost input (c) of a BIGCC power plant

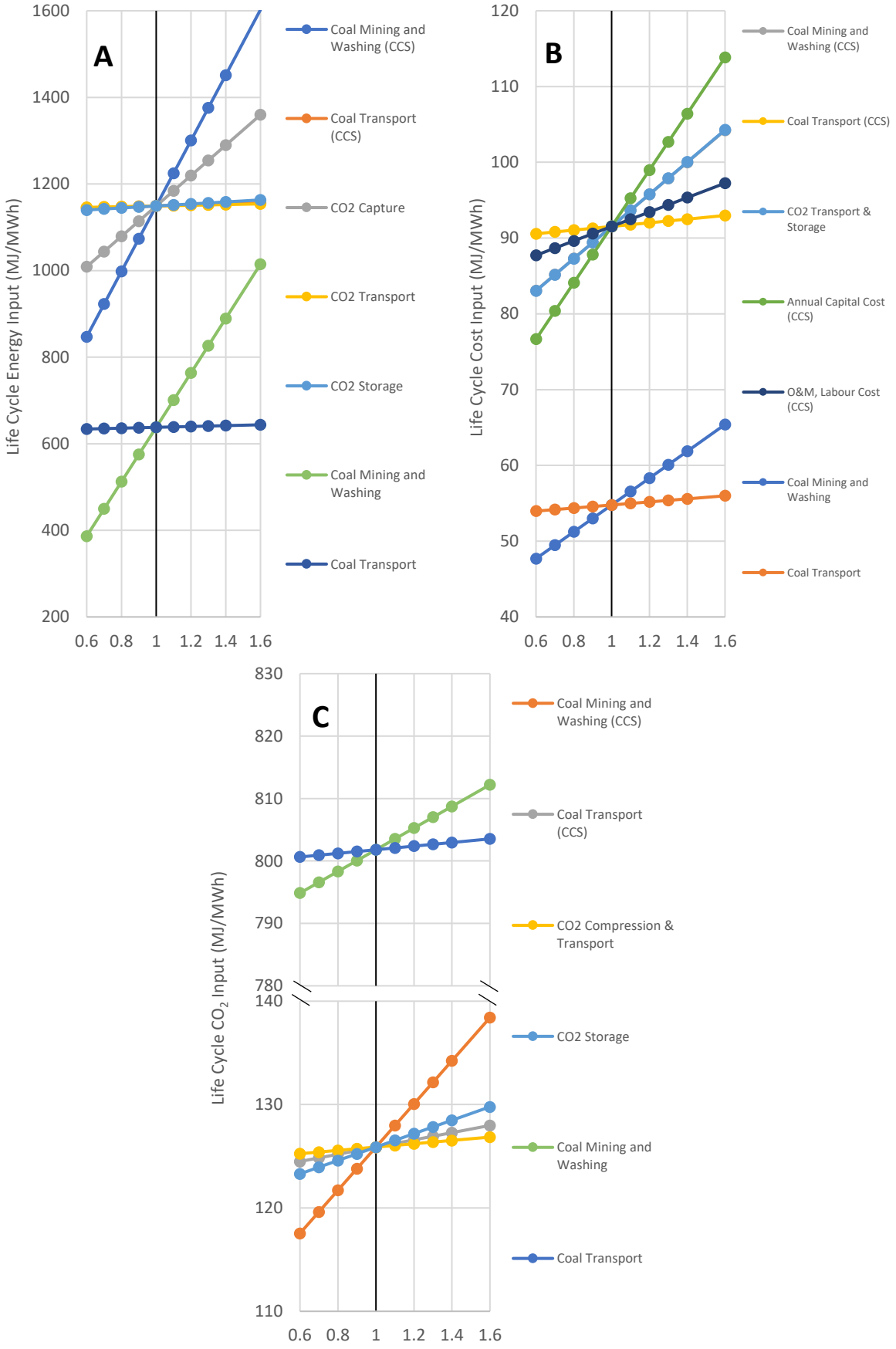

Figure 5.13. Sensitivity analysis of life cycle energy input (a), CO_2 emissions (b) and cost input (c) of a CIGCC power plant

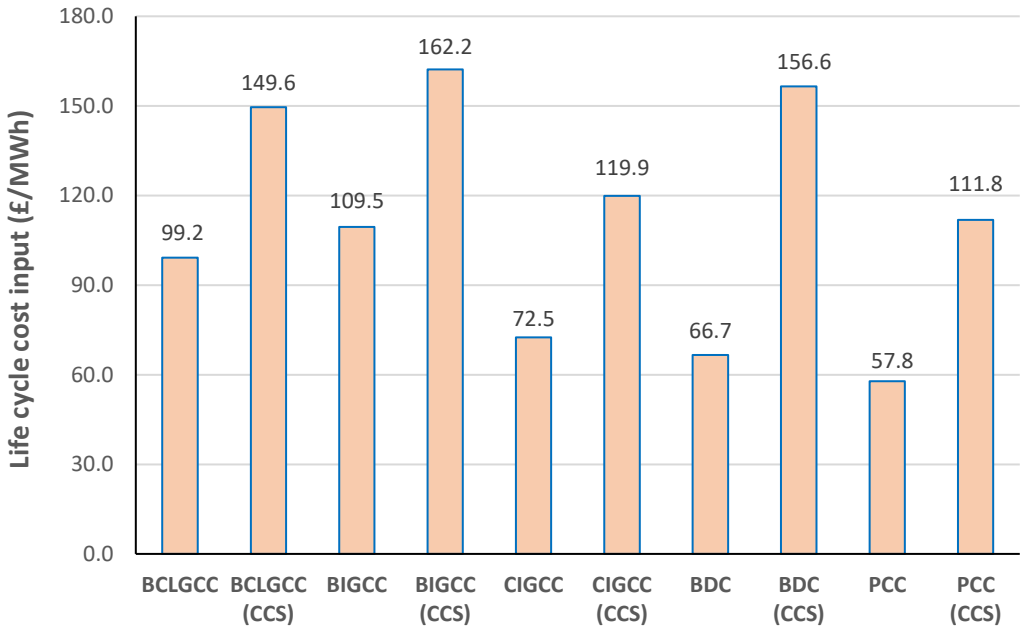

Figure 5.14. Comparison of TLCCI when taking into consideration the UK's ROC subsides

5.8 Environmental Impact Assessment

The results comparing between BCLGCC and BIGCC power plant life cycle with and w/o CCS for 5 environmental impact factors are illustrated in Figure 5.15 and elaborated on in the following sections.

5.8.1 Photochemical Ozone Creation Potential

Ozone formation in the troposphere or ground level can cause severe health, environmental and economic impacts. The formation of ozone can take place under the influence of sunlight, nitrogen oxides and volatile organic compounds VOCs. The presence of VOCs results in peroxy radical's formation, which as a result can result in the formation of ozone. This can be measured using the photochemical ozone creation potential (POCP) indicator. The POCP indicator is reported as a relative amount, in which the amount of ozone produced per mass of VOC is measured by the mass of ozone produce by ethene. Ethene was used as the reference VOC since it is the most potent ozone precursors out of the other VOCs. The unit used is kg ethene-e/MWh. It can be seen from Figure 5.15A that the stage that allows for the highest ozone creation is the biomass pre-treatment and pellets formation stage, accounting between 51 – 58% of the entire life cycle for the BCLGCC and BIGCC with and w/o CCS processes. This is due to the higher formation and release of VOC during that stage. The second highest stage is the biomass transportation stage since fossil fuel is used which release

more NO_X as well as VOCs accounting for 31- 36% of the total life cycle. When comparing between BCLGCC and BIGCC processes, it is demonstrated that BCLGCC with and w/o CCS releases less ozone into the atmosphere for each MWh-net produced. Moreover, the additional air separation unit used by the BIGCC process results in an extra 1.38 and 1.64 kg (10^{-3}) ethene-e/MWh produced. On the other side, iron ore mining process which produces the oxygen carrier int the BCLG process illustrates negative POCP values (0.65 and 0.69 for non-CCS and CCS respectively), which may be explained as a result of the mining process consuming VOC's and NO_X which hence reducing the overall ozone formation. It can be summarized that BCLGCC reduces the overall ozone formation potential when it comes to oxygen supply as well as releasing less ethene per MWh-net for each stage.

5.8.2 Ozone Depletion Potential

Ozone depletion potential (ODP) is the measure of relative stratospheric ozone depletion taking place with CFC-11 (R-11) fixed at an ODP of 1.0, since it has serious destructive effect on the ozone layer. Other chemicals that are involved in the breakdown of the ozone layer include bromine and chlorine compounds, nitrous oxide, water vapour and methane. Seeing from Figure 5.15B, the carbon capture process emitted the most chemicals that resulted in ozone depletion with the BCLGCC carbon capture stage emitting 8.69E-13 kg-R11-e/MWh (accounting for 68.5% of the total life cycle of the process) while BIGCC carbon capture stage emitting 10.3E-13 kg-R11-e/MWh (accounting for 53.2% of the total life cycle of the process). The second stage with the highest ODP is the ASU as part of the BIGCC process. This as a result further increases the BIGCC life cycle ODP compared to the BCLGCC life cycle process.

5.8.3 Abiotic Depletion Potential (fossil)

Abiotic depletion potential (ADP) refers to the depletion of nonliving resources. ADP can be measured via two different methods, either via elemental depletion potential ($ADP_{element}$) or fossil fuel depletion potential (ADP_{fossil}). Here we focus on the latter which is calculated in GJ/MWh as shown in Figure 5.15C. Since the supply chain processes and CO_2 capture and storage processes use of fossil fuel hence it will be depleted in those stages. Biomass pelleting accounted for the highest ADP_{fossil} with the biomass supply chain (biomass pelleting and transport) consumes the highest amount accounting to 99.0% of the total life cycle for BCLGCC w/o CCS and 62.9% with CCS, whereas for BIGCC w/o CCS is 81.6% and with CCS is 56.7%. It can also be seen that the ASU has a significant contribution due to the large amount

of energy it consumes contributing towards 18.4% and 12.9% for CCS and non-CCS plants respectively, whereas BCLGCC process consumed only 0.6 - 1% for the oxygen carrier production (iron mining). This is as a result increased the BIGCC life cycle ADP_{fossil} compared to the BCLGCC life cycle. In regard to carbon capture, since less CO_2 is produced in a BCLGCC process compared to BIGCC per MWh, less energy is required, hence the ADP_{fossil} for both processes was equal to 0.339 and 357 GJ/MWh, respectively.

5.8.4 Acidification Potential

The acidification potential (AP) is an indicator for the amount of acid gas being released in the life cycle. These gases include SO_2, NO_X, NH_3, HCL and HF. Acidification can be caused by the release of hydrogen ions into the aquatic and terrestrial ecosystems. Its effect tends to be regional. AP is calculated relative to SO_2, hence the unit was kg SO_2-e/MWh. As shown in Figure 5.15D in both BCLGCC and BIGCC life cycles, biomass harvesting resulted in the most acid gas being released, having an impact value ranging from 0.31 – 0.38 kg SO_2-e/MWh. The stage with the second most acid gas emission is the wood pelleting stage. Moreover, BCLGCC process releases less acid gas per MWh compared to BIGCC process life cycle, with the difference between both processes increases when comparing the CCS plants.

5.8.5 Eutrophication Potential

Eutrophication potential (EP) is the measure of the amount of phosphorus and nitrogen compounds being released. It is generally reported as kg-phosphate-/MWh. BCLGCC power plant life cycle releases less phosphate (0.073 and 0.081 kg-phosphate-e/MWh for non-CCS and CCS, respectively) compared to the BIGCC process (0.076 and 0.096 kg-phosphate-e/MWh for non-CCS and CCS, respectively) as shown in Figure 5.15E. The stage that released most phosphate was the biomass transport, accounting for approximately 52.0% for both BCLGCC and BIGCC with and w/o CCS, followed by 36% from the biomass pre-treatment and pelletization. Comparing between the oxygen supply for both processes, iron ore mining and transport for BCLGCC released approximately 0.00038 kg-phosphate-e/MWh (accounting for 0.5% of the whole life cycle), whereas the ASU for the BIGCC process released approximately 0.0021 kg-phosphate-e/MWh (accounting for 2.4% of the whole life cycle). The amount of NH_3 released in the flue gas is not very high in gasification power plants, hence the low values of EP in the combined cycle stage.

5.8.6 Discussion

BCLGCC power plant life cycle exhibited a lower environmental impact potential compared to BIGCC in several factors including POCP, ODP, ADP_{fossil}, AP and EP. The stages that resulted in the highest environmental impact was the wood pelleting and transport stages. Therefore, since BCLGCC process requires less biomass feedstock due to its higher biomass utilization efficiency compared to BIGCC, it would result in lower life cycle impact values for the biomass supply chain. Hence reducing the overall environmental impact. Moreover, comparing between the oxygen source of both processes, the ASU in the BIGCC process emitted more pollutants into the atmosphere compared to the iron mining and transport to supply the oxygen carrier for the BCLGCC process. When comparing the biomass gasification process to previous literature about biomass combustion [278], biomass gasification results in less environmental impact especially due to the higher efficiency, less biomass processing, hence less CO_2 captured and transported. In addition, biomass gasification employs pre-combustion capture which uses selexol compared to combustion which employs post-combustion capture technologies using monoethylene amine, hence increases environmental impact of the process due to it releasing ethylene oxide which has severe environmental impacts compared to selexol. Finally, a move towards BCLGCC would results in reduced negative impact on the atmosphere.

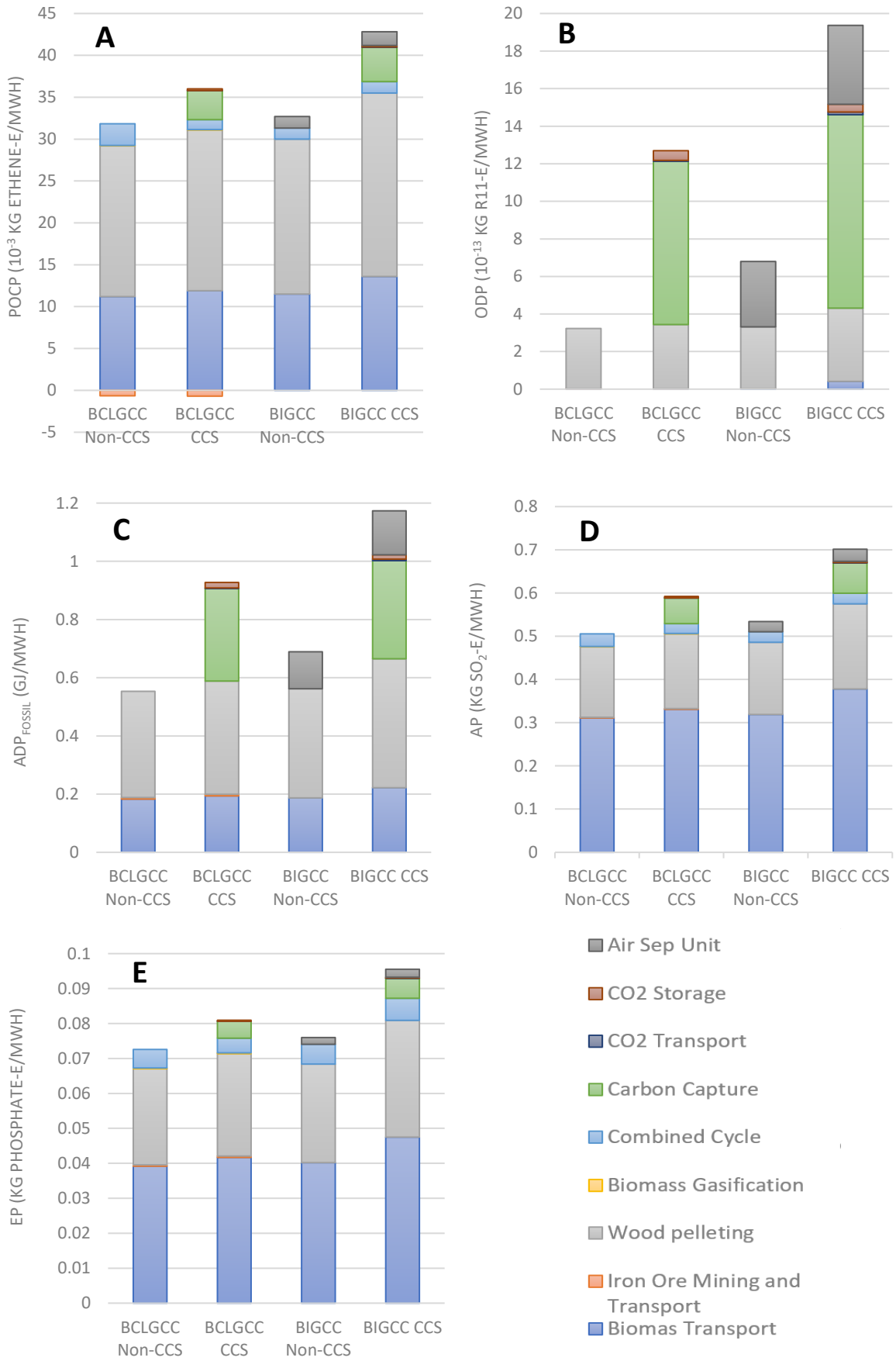

Figure 5.15. Environmental impact potential of BCLGCC power plants

5.8.7 Conclusion

This study conducted a life cycle energy – economy – CO_2 emissions analysis of the BCLGCC power plant and compared it to conventional coal/biomass gasification as well as biomass direct combustion. A sensitivity analysis was also conducted on the results. Furthermore, an environmental impact assessment was conducted used Gabi software with data supplied from IECM, Aspen Plus and previous literature comparing between BCLGCC with and w/o CCS and BIGCC with and w/o CCS. Major conclusions are as follows:

1) Coal power plants illustrated the least energy and cost input compared to biomass power plants, however resulted in higher net CO_2 emissions, since biomass power plants can be assumed to be near carbon neutral.
2) CIGCC without CCS plant requires the lowest amount of TLCEI (637.9 MJ/MWh) whereas BDC with CCS requires the most (2971.5 MJ/MWh). However, out of the biomass power plants BCLGCC requires the lowest energy requirement, were BCLGCC with CCS required 336.7 MJ/MWh and 827.3 MJ/MWh less energy input than BIGCC and BDC both with CCS technology.
3) In terms of TLCCI, PCC plant demonstrates the lowest value (57.8 £/MWh) and BIGCC showing the highest (159.5 £/MWh) out of the non-CCS processes, and similarly with the CCS power plants (212.2 £/MWh for BIGCC and 111.8 £/MWh for PCC), with BCLGCC having a higher TLCCI compared to BDC which is due to the higher capital cost of the plant as it is still in its development stage, hence higher process, and project contingencies.
4) The biomass supply chain process accounted for approximately 85% of energy input 31% of CO_2 emissions, 50% of cost input for CCS power plants. BCLGCC plant required 14.3% and 11.6% (23.0 & 25.8% with CCS) less biomass compared to BIGGCC and DBC power plants to generate the same amount of power, respectively. Wood processing & pelletization stage should be improved to reduce the high energy requirement and CO_2 emissions as suggested in section 5.5. This will result in a reduction in the cost of the process, hence reducing the overall cost of biomass.
5) The parameters that had the highest effects on the TLCEI and TLCCE are the wood processing, coal mining and washing, CO_2 capture, and biomass transport. Whereas in terms of cost, the annual cost, wood harvesting, wood processing and coal mining & washing caused the highest influence on the TLCCI. Regarding the CCS power plants, the

carbon capture and storage section had the highest impact of TLCCI followed by TLCCE and finally TLCEI.

6) BCLGCC power plant life cycle showed that it has a lower environmental impact potential compared to BIGCC in several factors including POCP, ODP, ADP_{fossil}, AP and EP. The stages that resulted in the highest environmental impact was the wood pelleting and transport stages. This significantly contributed to the reduction in the environmental impact values due to BCLGCC utilizing less feedstock compared to BIGCC.
7) Comparing between the oxygen source of both processes, the ASU in the BIGCC process emitted more pollutants into the atmosphere compared to the iron mining and transport to supply the oxygen carrier for the BCLGCC process.

6 CHAPTER 6: HEMATITE CHARECTARIZATION

6.1 Introduction

A suitable oxygen carrier is required for the BCLGCC system to be commercially technical, economically, and environmentally viable in large scales. A big factor preventing the deployment of this technology is the oxygen carrier. Therefore, this chapter will deal with conducting a set of experimental investigations to better determine the feasibility of using fresh hematite oxygen carrier as a source of oxygen. Hematite being an environmentally benign, cheap, and widely available mineral (as previously mentioned in chapter 2, section 2.1.5) presents itself as a suitable oxygen source from an economic and environmental perspectives. Therefore, several experiments are conducted under different conditions (temperature, OC/B ratio, reaction time and continuous cycles) in a fixed bed reactor to determine its technical capability. The gas yield was measured, carbon conversion, LHV and efficiency were calculated followed by conducting an XRD analysis coupled with a SEM-EDX oxygen carrier characterization test. The work in this chapter is conducted according to the methodology outlined in chapter 3 section 3.3.

6.2 Effect of Temperature

6.2.1 Hematite vs Blank Test

In this section, hematite is tested to find out if it can be used as a suitable oxygen carrier at a range of temperatures, followed by conducting an XRD and SEM-EDX material characterization of the oxygen carrier. This is done by reacting 1g of biomass in a fixed bed reactor in the presence of 1.7g inert silica sand bed material at different temperatures then comparing it with using 1.7g hematite oxygen carrier at five temperature points (50°C intervals) ranging from 700 – 900°C. The gas compositions were recorded and used to calculate the gas yield values, carbon conversion, combustible gas yield (CGY), cold gas efficiency (CGE) and lower heating value (LHV) presented in Figure 6.1 – Figure 6.4. Comparing the gas yield of the blank experiment and the hematite-based experiment, the latter showed higher CO_2 yields which proves that more O_2 is present allowing for more complete combustion to take place. The extra oxygen is supplied through the hematite, which increased the CO_2 yield. At the same time the blank experiment resulted in higher CO and H_2 yields, which can be explained as a result of less O_2 present, hence less CO and H_2 being converted

into CO_2 and H_2O, respectively. The same applies to CH_4, the presence of an oxygen carrier promotes its consumption to produce CO_2 and H_2O. Moreover, the hematite experiment demonstrates higher carbon conversion, yet a lower LHV, CGY and CGE. Therefore, we can conclude that hematite can act as an oxygen source.

Looking at the effect of temperature on biomass chemical looping gasification (BCLG) using hematite or inert silica sand (pyrolysis reaction) bed material, we can observe an increase in carbon conversion in both cases. However, using hematite bed material compared to silicon demonstrates a significant increase in carbon capture as temperature increases. This is due to the hematite oxygen carrier being more active at higher temperatures, resulting in more catalytic cracking of the tar and increased reaction rate with the pyrolysis gas, hence increasing the extent of the reaction. Figure 6.2 shows that as temperature increases CO_2 and CO yields increase due to the increase in carbon conversion, whereas H_2 initially increases up to 775°C, then decreases as temperature further increases. CGY and CGE experience an increasing trend, whereas LHV experiences a steady increase followed a decrease which coincides with the temperature where the H_2 yield started decreasing (775°C). However, as temperature further increases, CO yield increases significantly hence shifting the trend to an increasing syngas LHV.

Having said that, it can be seen that the carbon conversion is relatively lower compared to other papers that use iron-based oxygen carriers and a fixed bed reactor for the BCLG reaction with several different parameters to the one set up in this thesis. Hu et al., [152] uses pretreated Fe_2O_3 with 99% purity and chlorella vulgaris (with 53.32% carbon content) as the biomass achieving around 85% carbon conversion. Moreover, the author's experiment is set up differently using a crucible places in the reactor with the carrier gas passing horizontally. Huang et al., [92] assembles a similar set up to the one in this thesis but uses sewage sludge biomass with around 22% carbon content achieving up to 85% carbon conversion. Wei et al., [290] uses cooking oil with 99.94% volatile matter and 76% carbon content, achieving a carbon conversion of 48%. Finally, Huang et al., [151] uses biomass char with 86.3% carbon content, achieving 35.7% carbon conversion. The reason for the relatively low carbon conversion in this thesis could be due to the characteristics of pine sawdust (meaning the composition having lower carbon content and volatile matter, moisture content and a

different structure, etc.) as this biomass source has not been tested before in a fixed bed reactor.

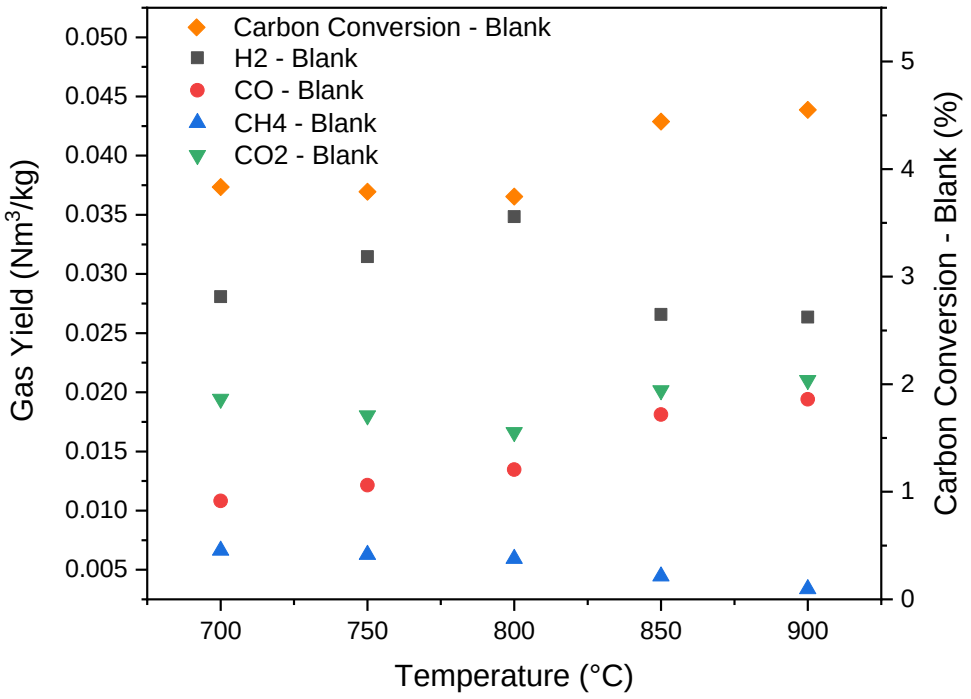

Figure 6.1. Effect of temperature of gas yield and carbon conversion using silica sand bed

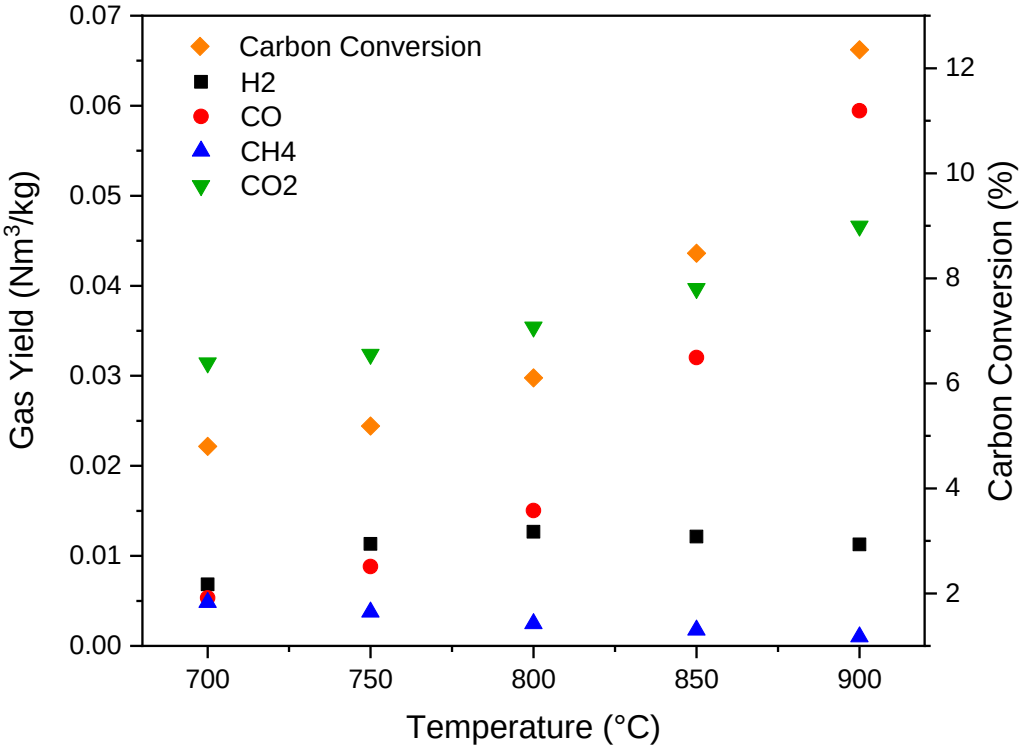

Figure 6.2. Effect of temperature of gas yield and carbon conversion using hematite bed

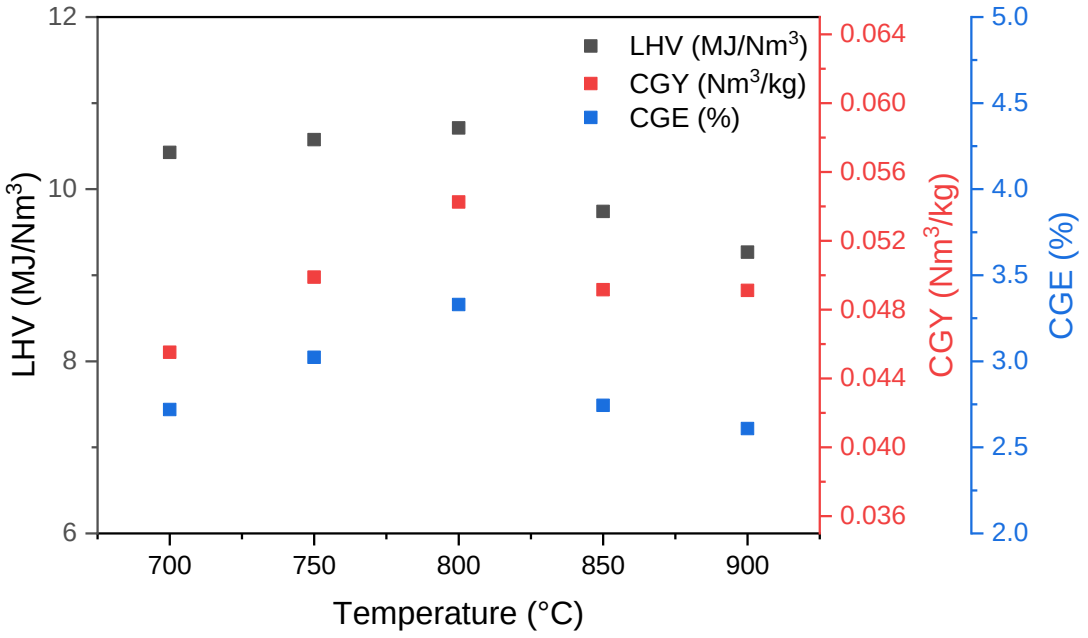

Figure 6.3. Effect of temperature of LHV, GCY and CGE using silica sand bed

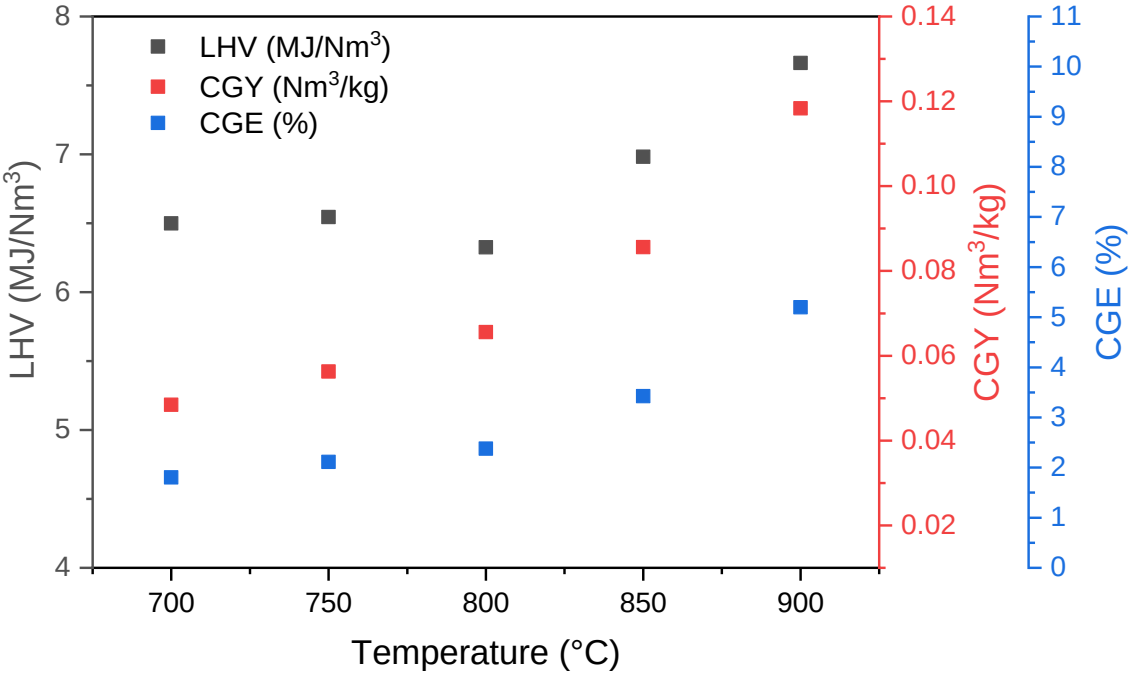

Figure 6.4. Effect of temperature on LHV, GCY and CGE using hematite bed

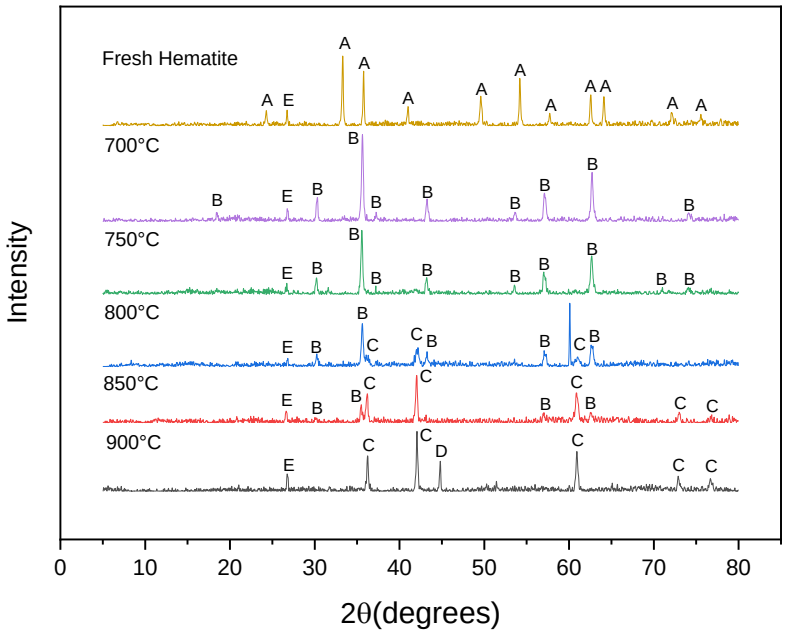

Figure 6.5. Effect of gasification temperature on the OC XRD results after gasification (A: Fe_2O_3, B: Fe3O4, C: Fe_XO, D: Fe E: carbon)

The XRD results of the OC samples after the gasification reaction with biomass in the fuel reactor at different temperatures are presented in Figure 6.5. We can observe that after the gasification reaction takes place all the Fe_2O_3 peaks disappear and Fe_3O_4, Fe_XO and Fe peaks are formed, which supports the claim that hematite is a source of oxygen during gasification. We can see that as the reaction temperature increases the oxidation state of the oxygen carrier shifts from Fe_2O_3 → Fe_3O_4 → Fe_XO → Fe. At 700°C the main iron oxide crystalline phase is Fe_3O_4 with a single peak representing carbon, meaning that the Fe_2O_3 has been reduced. As temperature increases the Fe_3O_4 peaks (around 35.6 degrees) start getting smaller while Fe_XO starts forming at 800°C and increasing in height around 850°C. As temperature further increases to 900°C all the Fe_3O_4 peaks disappear with Fe_XO peaks intensity increasing and Fe iron peaks forming. This whole process of iron oxide reduction shows that hematite can be used as an oxygen source during the gasification process and that an increase in temperature promotes chemical looping gasification to take place. Moreover, there is no detection of new solid solution compounds formed, showing the stability of the other present oxides (Al_2O_3 and SiO_2). When comparing these results to results from literature, Huang et al., [117] reacts hematite with pine sawdust in a fluidized bed reactor instead of a fixed bed and observed that there is uneven reaction on the surface of the oxygen carrier, due to presence of a Fe_2O_3 peak remaining after the gasification reaction at a range of temperature (740 – 940°C). Whereas

from the test results in this chapter (using a fixed bed reactor) an even reaction on the surface of the oxygen carrier took place since there is no Fe_2O_3 peak observed after the reaction. The explanation for that could be due to the aggregative fluidization during the reaction due to nonuniform gas-solid contact in the fluidized bed reactor. Moreover, further reduction to FeO and even Fe was observed in the fixed bed reactors compared to the fluidized bed reactor at 950°C. Moreover, Hu et al., [152] reacted hematite with Chlorella vulgaris at different temperatures ranging from 600°C - 1000°C in a fixed bed reactor and observed that increasing temperature resulted in Fe_2O_3 decreasing, yet still a peak remained even at 900°C, however further increase to 1000°C did not further increase reduction to produce more FeO and Fe_3O_4 due to thermal sintering and agglomeration taking place, whereas when using pine sawdust in a fixed bed as shown in this thesis, further reduction takes place to produce Fe at 900°C. This could be due to synthetically treated hematite (99% Fe_2O_3) being used by Hu et al., [152], therefore providing sufficient oxygen for biomass oxidation to take place, hence the hematite does not undergo completely reduction. Finally, Huang et al., [92] gasified sewage sludge using hematite and observed similar results and concluded that further reduction of the hematite past Fe_3O_4, results in further sintering. Therefore, Huang et al., [92] suggests a temperature around 800°C for sewage sludge which is similar to the optimum temperature when reacting with pine sawdust in this thesis.

6.2.2 Oxygen Carrier Regeneration

The regeneration of the depleted oxygen carriers after the gasification reactions taking place between 700 – 900°C was conducted. The fixed bed reactor was converted from a fuel reactor into an air reactor by passing air through it at 100 ml/min at 950°C for 60 minutes. Figure 6.6 presents the product gas yields. The increase in temperature in the fuel reactor results in less oxygen being consumed in the air reactor due to higher carbon conversion taking place in the fuel reactor therefore less carbon particles are transferred to the air reactor. This as a result decreases the amount of CO and CO_2 produced in the air reactor as fuel reactor temperature increases. Moreover, the amount of carbon in the air reactor is calculated by calculating the amount of CO and CO_2 produced, hence calculating the carbon conversion in the air reactor as a percentage of the input biomass into the fuel reactor, shown in Table 6.1. The amount of tar produced is calculated by subtraction.

Table 6.1. Summarizing the carbon conversion in both fuel and air reactors (FR & AR)

Temperature (°C)	%CC- Solid (AR)	%CC – Tar (FR)	%CC – Gas (FR)
700	48.62	43.69	7.70
750	37.89	54.94	7.17
800	35.57	55.66	8.78
850	28.28	60.31	11.41
900	20.41	64.78	14.81

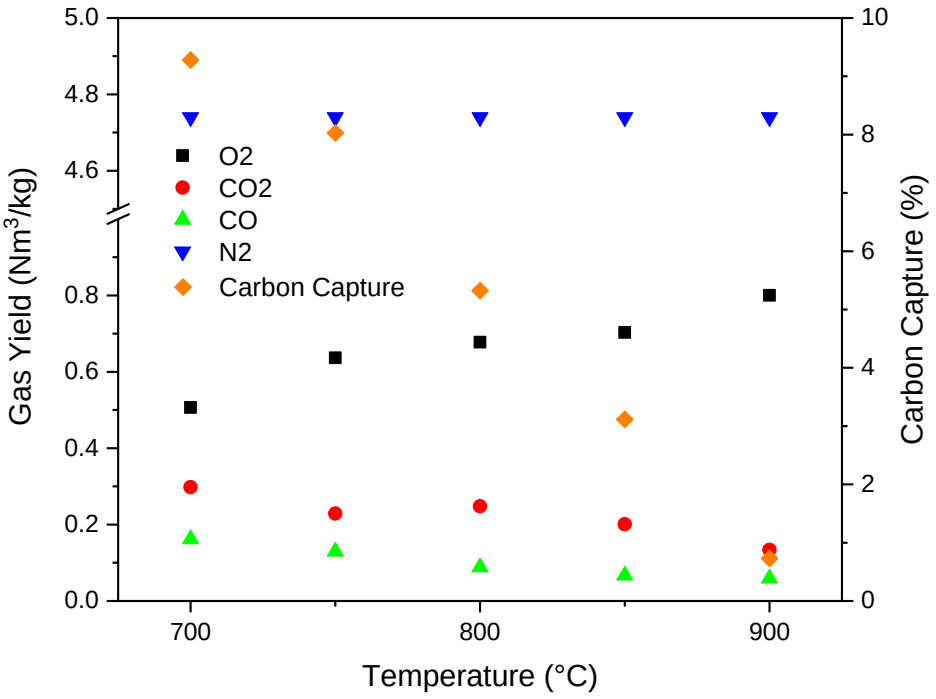

Figure 6.6. Effect of gasification temperature on the gas yield and carbon conversion in the air reactor

An XRD analysis was conducted on the regenerated samples as shown in Figure 6.7. It can be seen that all the reduced iron oxide crystalline phases are oxidized to regenerate the Fe_2O_3 which is similar to what has been observed by Huang et al., [117] when reacting pine sawdust with hematite in a fluidized bed reactor at 740°C and 940°C. In addition, a similar observation was made by Huang et al., [144] and Huang et al., [92] when using pine sawdust and sewage sludge, respectively. Moreover, all the samples regenerated between 700 – 850°C resulted in a Fe_2O_3 peaks with higher intensity than the fresh hematite sample. This could be due to the amount of carbon in the fresh hematite decreasing as shown in the XRD results with the carbon peak decreasing after being regenerated. Furthermore, when looking at the 900°C regenerated sample XRD result, the peaks seem to show a lower intensity compared to the other samples, which could mean that operating the gasification reaction at high temperatures could have affected the oxygen carrier's oxygen supply capacity after

regeneration. This can be supported by suggesting that sintering and agglomeration took place when Fe metal was formed at 900°C during the gasification reaction.

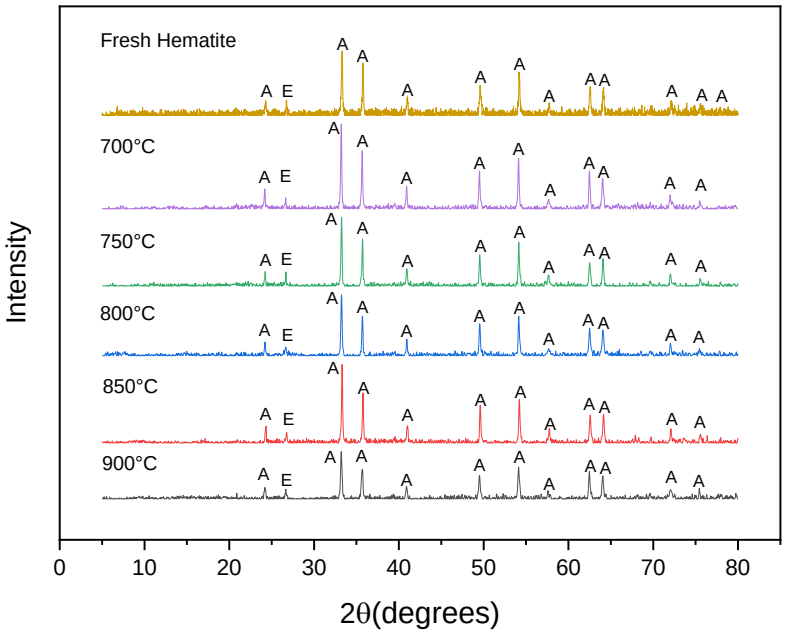

Figure 6.7. Effect of gasification temperature on the OC XRD results after regeneration (A: Fe_2O_3, B: Fe3O4, C: Fe_XO, D: Fe E: carbon)

As shown in Figure 6.8, the surface of the natural hematite is covered with granules as small as 2µm with a highly porous structure which allows for an increase in surface area, hence enhancing the reaction between the gas and the hematite (Additional SEM images in the **Appendix** Figure A2). It can be seen that reacting the oxygen carrier at different temperatures has an effect on its surface structure. The 700°C sample shows a surface structure with smooth and larger granule sizes, less porosity, but larger pore sizes. This could be a result of sintering and agglomeration of granules. A similar observation is seen in the 800°C SEM sample image. However more sintering and agglomeration takes place on the surface of the 900°C sample, with a greater decrease in the porosity while increase in granule sizes. This could be due to the formation of Fe metal as shown from the XRD results Figure 6.5, hence resulting in more agglomeration. Therefore, it would be recommended that the temperature remains around 800°C and avoiding higher temperatures that allow for Fe and FeO formation during the gasification reaction. Huang et al., [144] tests 1 cycle experiment gasifying pine sawdust with hematite at 840°C then regenerating at 800°C. The author observed that that the regenerated hematite has a smooth surface with no fines, with large interspaces occupied with small granules. In general, the microstructure of the hematite did not change, showing

no evidence to thermal sintering. The reason the results of the regenerated samples in this thesis observed sintering on the surface is because of the higher oxidation temperature (950°C). Moreover, Huang et al., [92] reacted sewage sludge with hematite in a fixed bed reactor (temperature was not mentioned in the paper) and did not observe much change with the porous structure maintaining itself, yet it found some ash deposits on the surface of the hematite, hence decreasing its specific surface area. The EDX results in Figure 6.9 shows that the amount of oxygen in the regenerated samples is more than that in the fresh oxygen carrier. Moreover, a small potassium and calcium peaks on the 700°C EDX result can be seen, but with the other two samples (800 and 900°C samples) the potassium peak disappears but calcium peak remains which could be due to potassium oxide being volatile and escapes at high temperatures. These elements are present due to the ash depositing on the surface of the oxygen carrier.

Fresh **700°C**

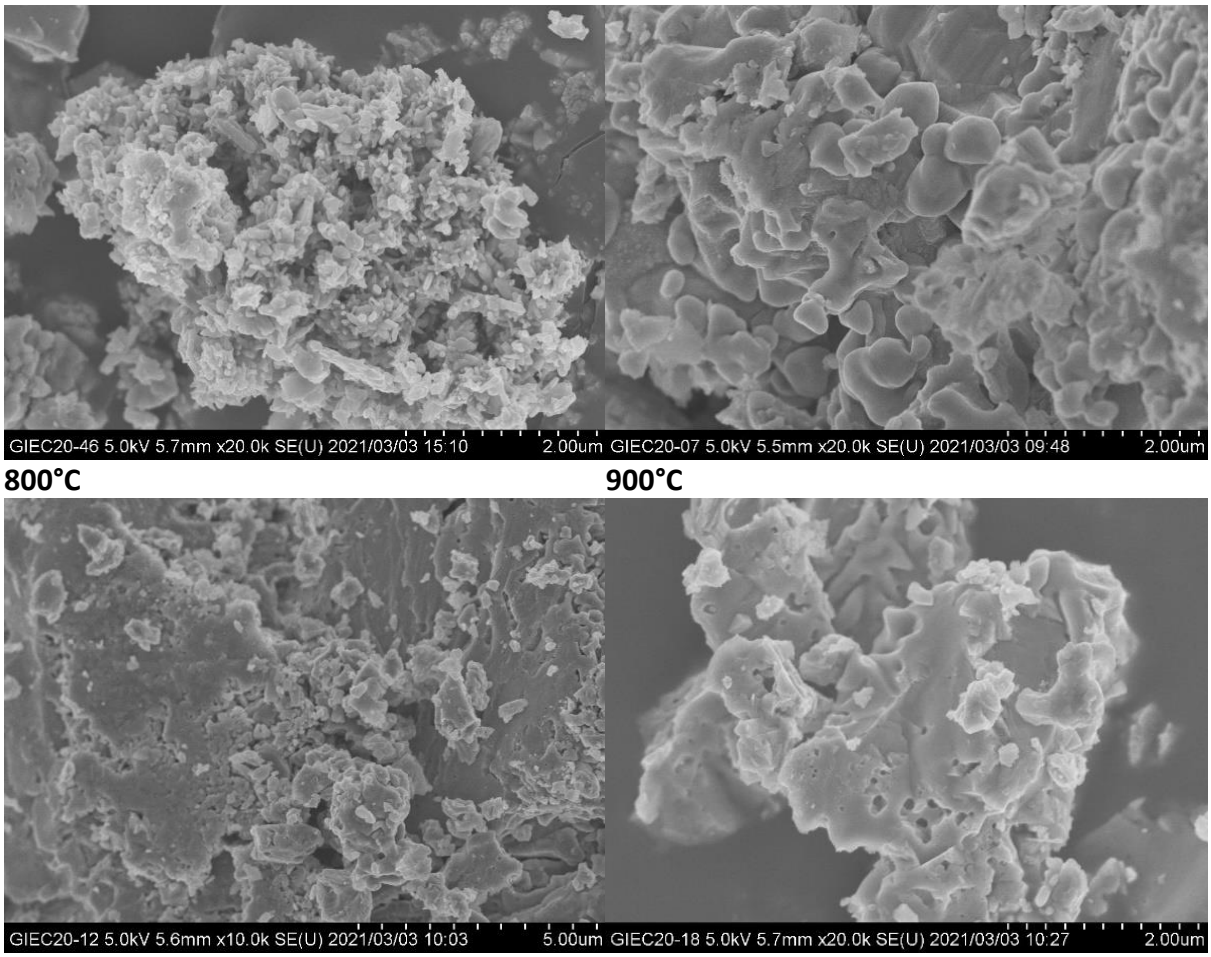

Figure 6.8. Effect of temperature on the SEM results after OC regeneration

Fresh Hematite **Fresh Hematite**

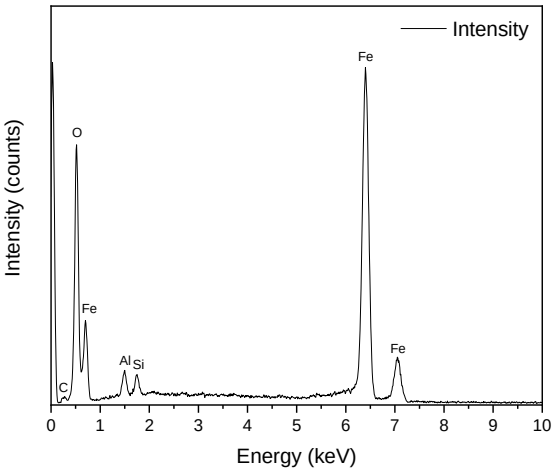

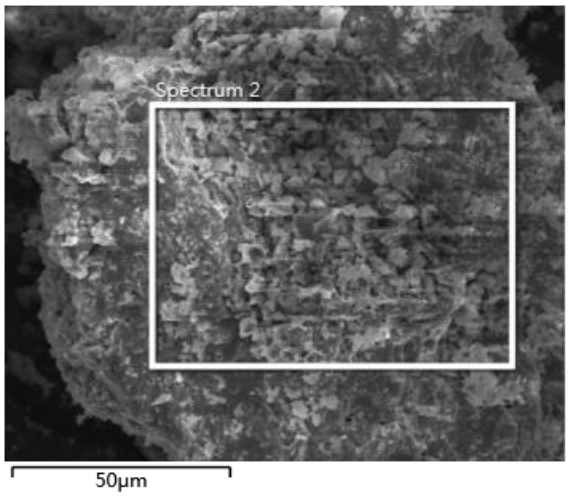

700

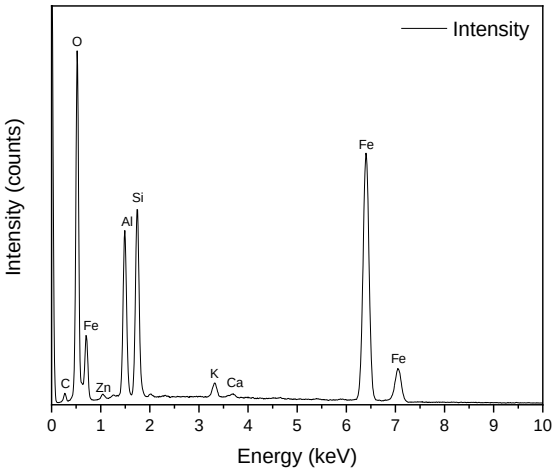

700

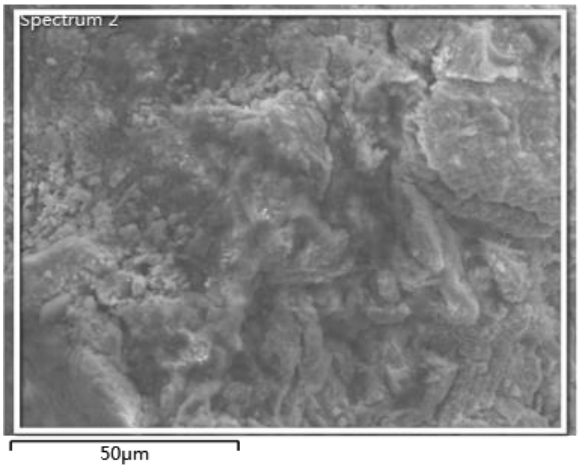

800

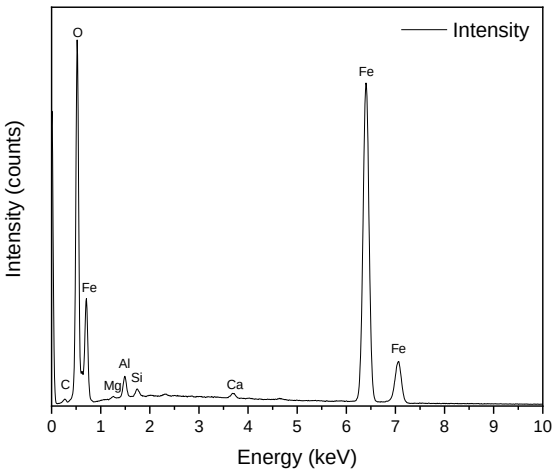

800

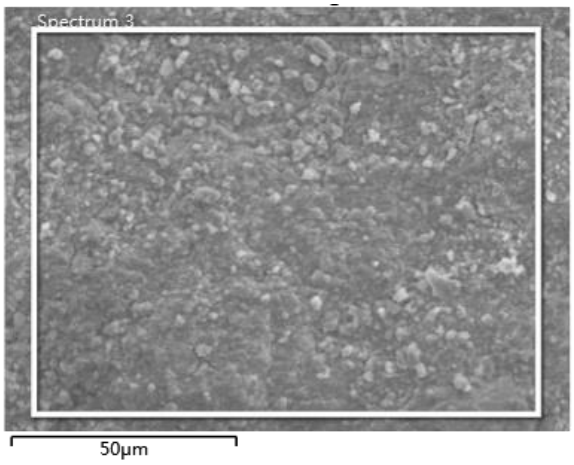

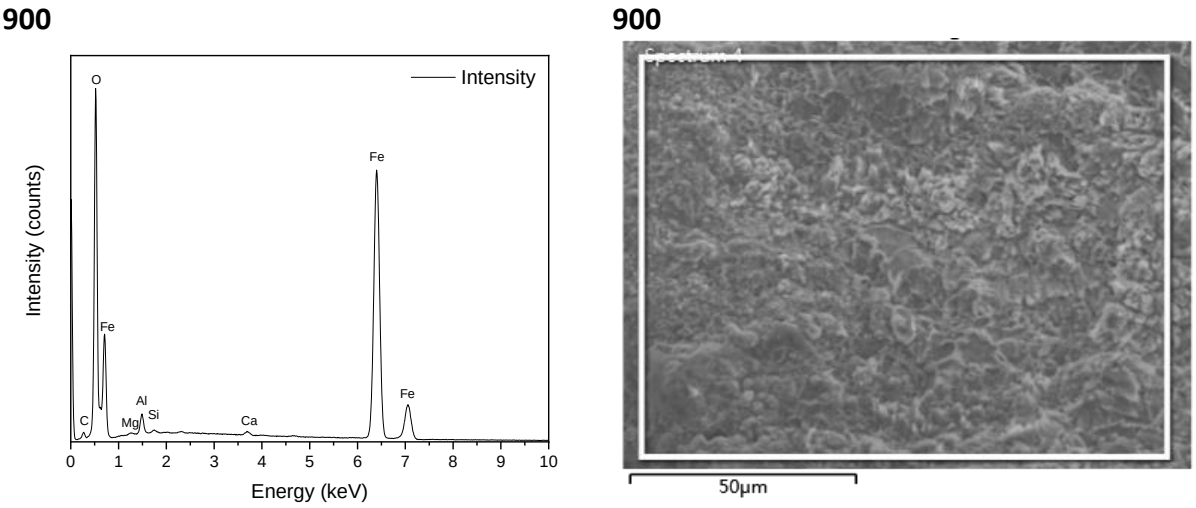

Figure 6.9. Effect of gasification temperature on the OC EDX results after regeneration

6.3 Effect of B/O Ratio

In this section the effect of B/OC (wt.) was tested ranging from 0.61 to 0.89. Figure 6.10 illustrates the gas yield of the syngas, showing that as B/OC increases the CO_2 yield decreases, while H_2, CO and CH_4 yields remains relatively constant. However, the amount of CO increases as you increase the B/OC ratio, while the amount of CO_2 gradually decreases. This is due to an increase in biomass which resulted in more carbon being present, hence the CO_2 is reduced by reacting with the excess carbon to produce CO in an oxygen starved atmosphere. Consequently, decreasing the percentage carbon conversion. The H_2 and CH_4 trends are relatively constant with H_2 very slightly increasing while CH_4 very slightly decreasing. Figure 6.11 shows that an increase in B/OC ratio increases the LHV and CGE, whereas the CGY gradually increases up to B/OC ratio equal to 0.73 followed by a steady decrease. This is because after the B/OC ratio exceeds 0.73, the increase in the amount of biomass supplied outweighs the increase in gas produced.

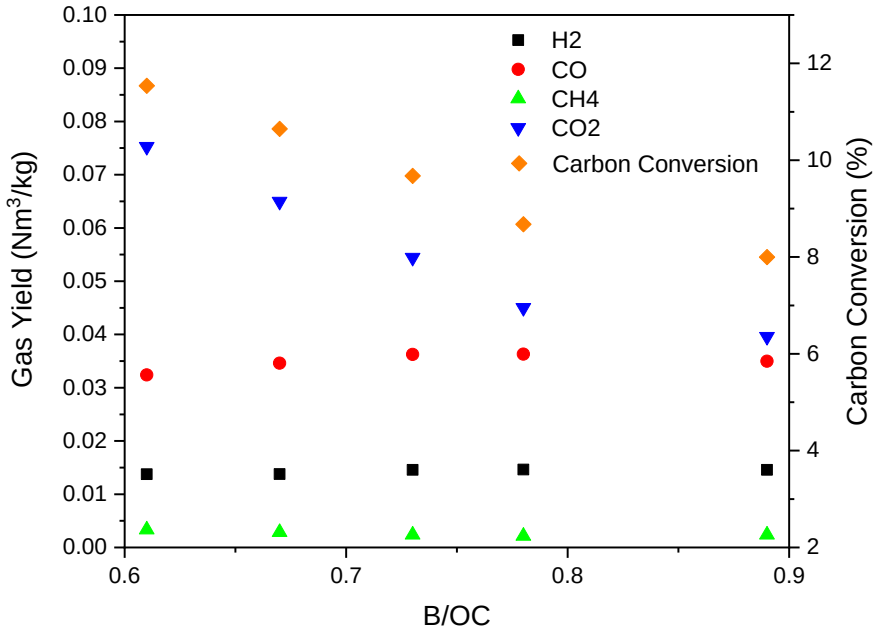

Figure 6.10. Effect of B/OC ratio on gas yield and carbon conversion

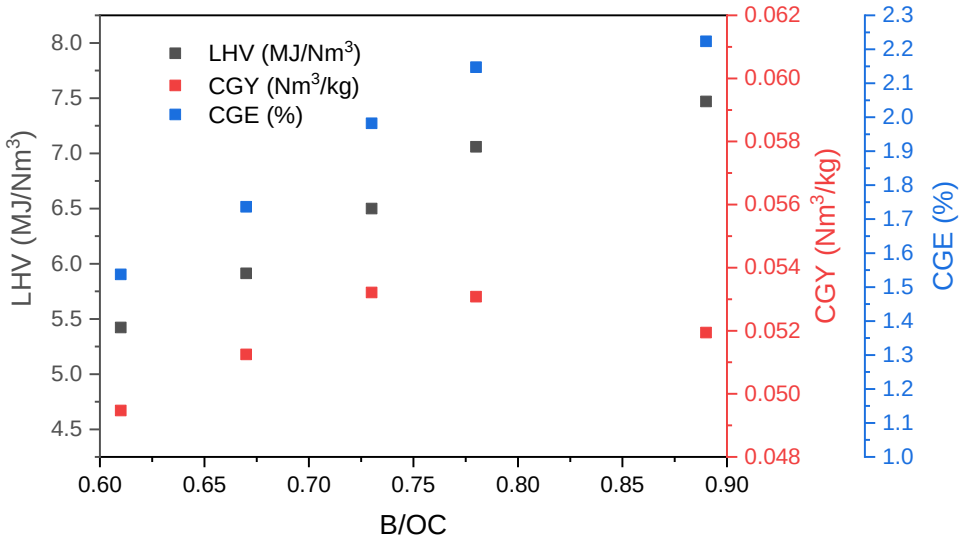

Figure 6.11. Effect of B/OC ratio on LHV, CGY and CGE

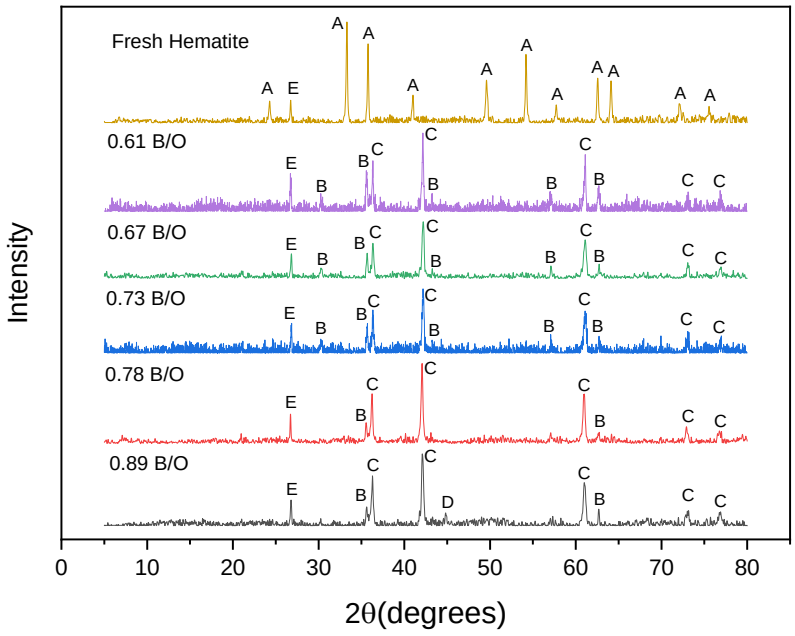

Figure 6.12. Effect of B/OC ratio on the OC XRD results after gasification (A: Fe_2O_3, B: Fe3O4, C: Fe_XO, D: Fe E: carbon)

An XRD analysis was conducted on the samples at different B/OC ratios after the gasification reaction. It can be seen that from the lowest biomass to oxygen carrier ratio (0.61) all the Fe_2O_3 crystal phases disappear while Fe_3O_4 and Fe_XO crystal phases appear. Further increase in B/OC ratio results in an increase in intensity of the Fe_XO crystal phase while a decrease in the Fe_3O_4 crystal phase peak intensity. At the B/O ratio 0.89 we can see a slight Fe peak forming. Possibly a lower B/OC ratio could have been more suitable as less Fe_XO would have formed. This is because even though a deeper reduction in the hematite would require less solid inventory, yet it could result in more sintering of the oxygen carrier and reduction in its specific surface area, hence effecting its reoxidation capacity. A very similar observation was made when testing hematite with sewage sludge [92] and Chlorella vulgaris [152], with the difference that when using pine sawdust, the hematite is further reduced at higher B/OC ratios.

Fresh **0.61 B/OC**

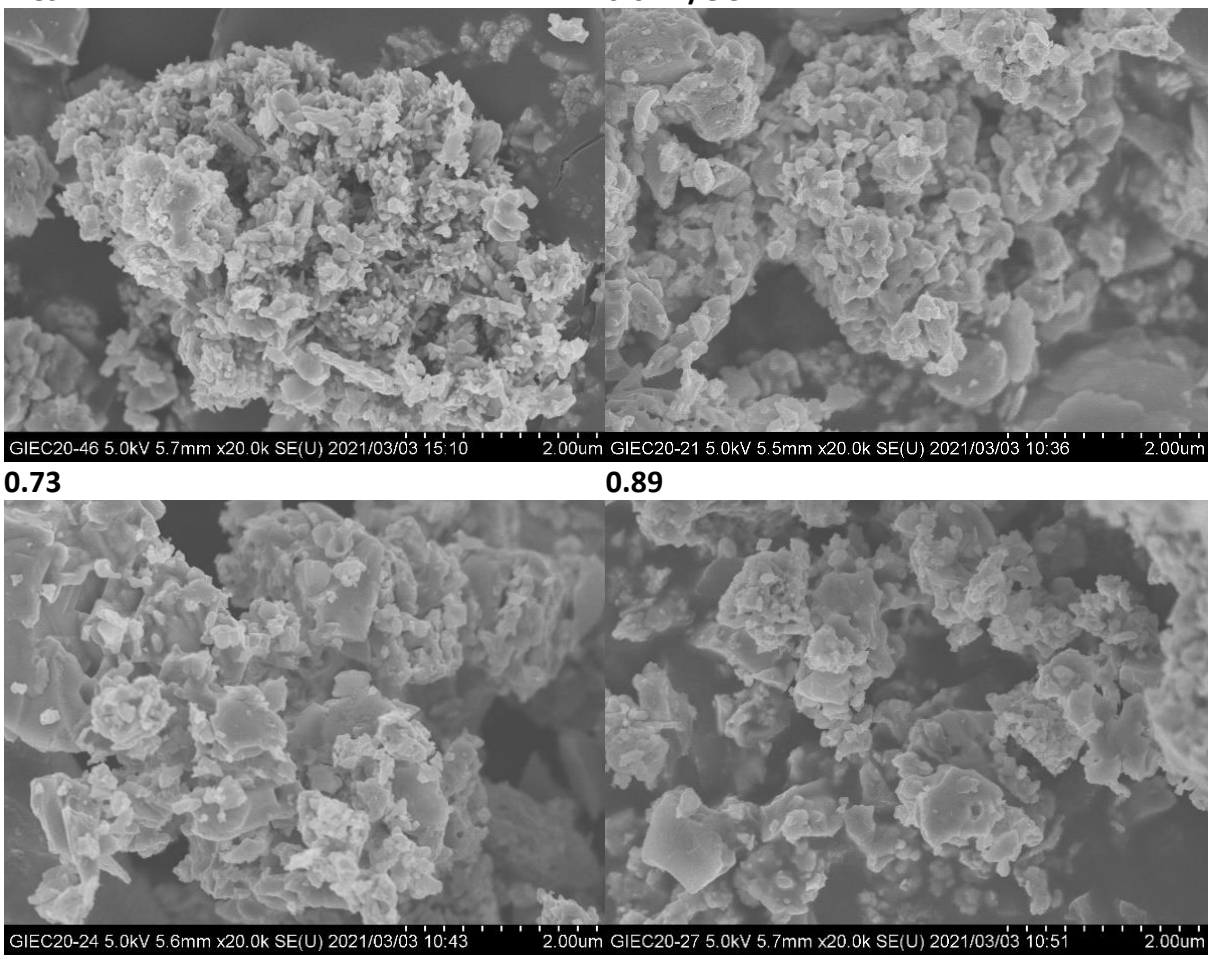

Figure 6.13. Effect of B/OC ratio on the SEM results after gasification

Fresh Hematite **Fresh Hematite**

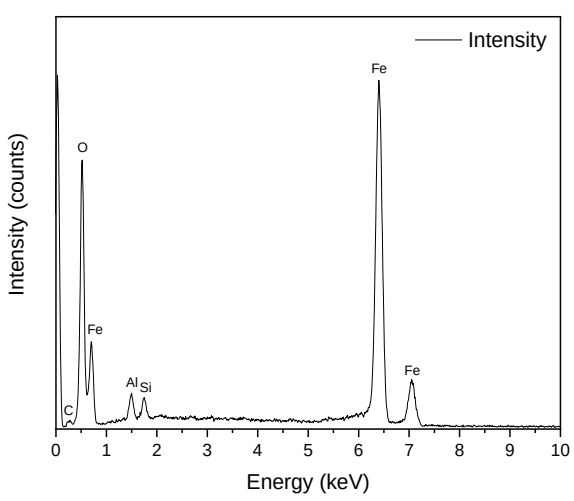

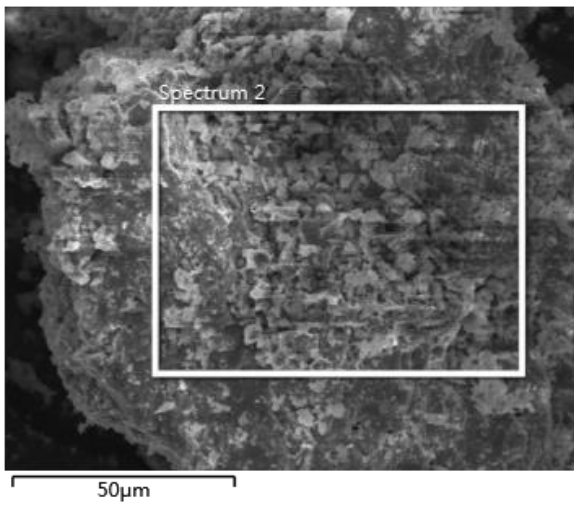

0.61 B/OC

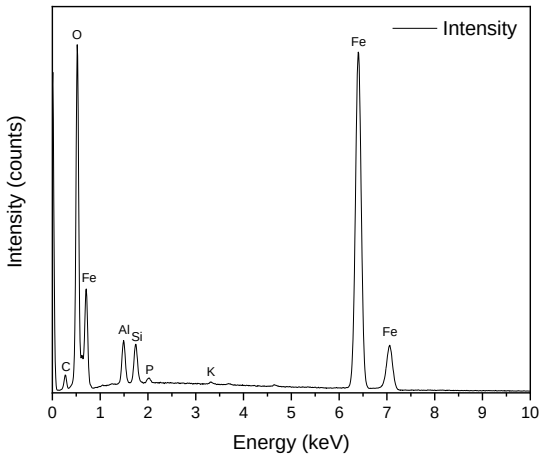

0.61 B/OC

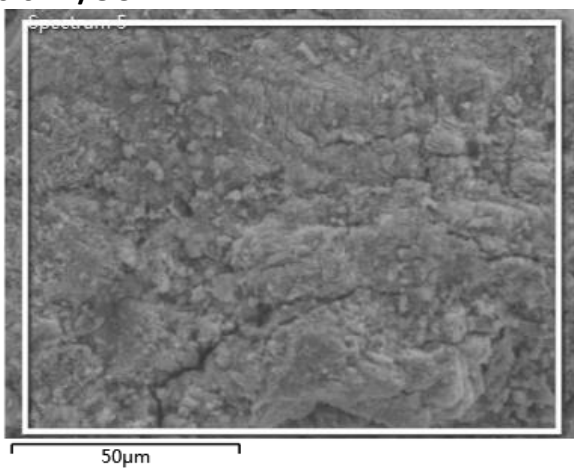

0.61 B/OC

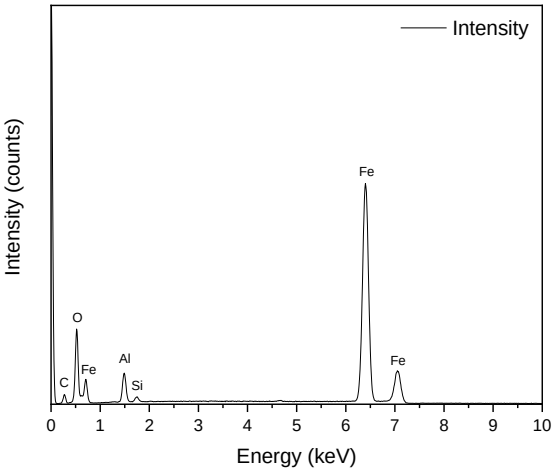

0.61 B/OC

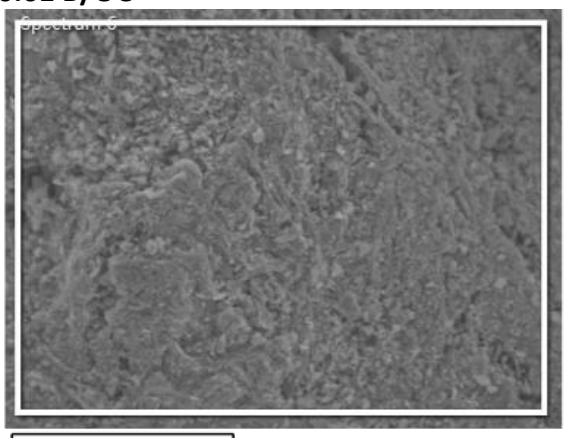

0.61 B/OC

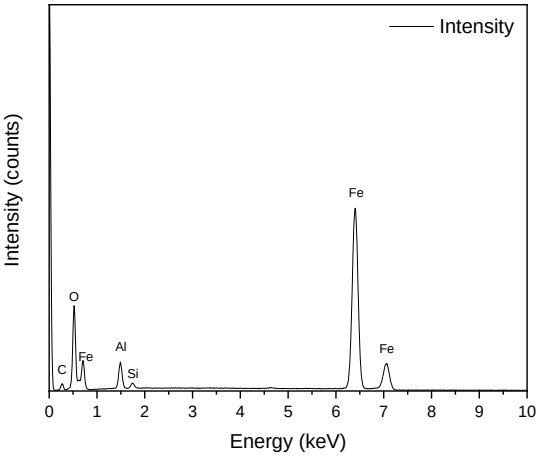

0.61 B/OC

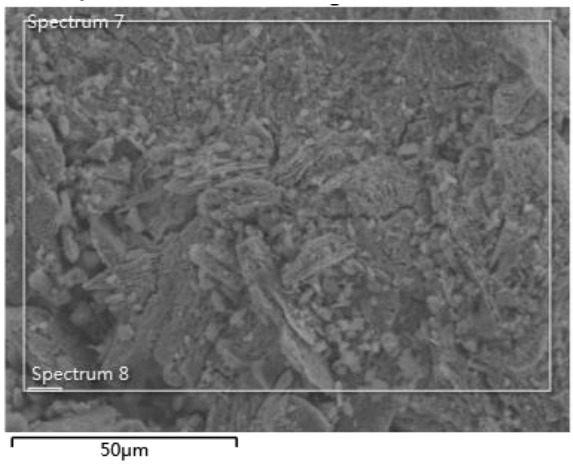

Figure 6.14. Effect of B/OC ratio on the OC EDX results after gasification

The effect of the B/OC ratio on the hematite surface can be seen in Figure 6.13 (Additional SEM images in the **Appendix** Figure A2). The 0.61 B/OC ratio sample shows a slight increase in granule size, hence a decrease in the porosity compared to the fresh oxygen carrier. An increase in B/OC ratio to 0.73 results in granule sizes up to 8µm with some small granules

around 2µm remain, however further increasing B/OC ratio to 0.89 forms larger granules and decreasing the number of smaller ones. This is expected as more Fe_2O_3/Fe_XO is being reduced and a small peak of Fe metal can be seen in the XRD results, hence resulting in more sintering and agglomeration. Therefore, it would be suggested to keep the B/OC ratio low to ensure less sintering taking place. Moreover, it can be seen from the EDX data in Figure 6.14 that the oxygen peak is decreasing with increase in B/OC ratio, however sample 0.61 shows a high intensity peak for O which should not be there. The reason could be due to the surface of the oxygen carrier that was analyzed did not come in contact with much biomass hence did not lose its oxygen. However, when looking at the other two EDX results (0.73 and 0.89 B/OC samples) we see a decrease in oxygen peak intensity as B/OC ratio increases. Moreover, a small carbon peak can be seen around 0.3 keV which can be seen on the 0.61 and 0.73 B/OC samples which could be due to carbon particles depositing on the oxygen carrier surface after the gasification.

6.4 Effect of Reaction Time

The effect of gas yield and carbon conversion as reaction time increases is illustrated in Figure 6.15. We can see that an increase in reaction time from 10 to 30 minutes results in an increase in CO and CO_2 produced hence increasing percentage carbon conversion, whereas H_2 and CH_4 increases up to around 20 minutes then starts decreasing which could be due to both gases reacting to produce H_2O and CO_2. As reaction time further increases carbon conversion is not affected, hence CO_2 and CO yields remain constant. The increase in reaction time up to 30min increases the CGY but decreases the LHV due to the increase in CO_2 concentration, this results in a general increase in CGE. The plateau in gas yields results in the CGY, LHV and CGE to plateau as shown in Figure 6.16. The reason for the slight increase in LHV for the 50 minutes test is due to the slight increase in H_2 and CH_4 values which could be a slight error in the experiment.

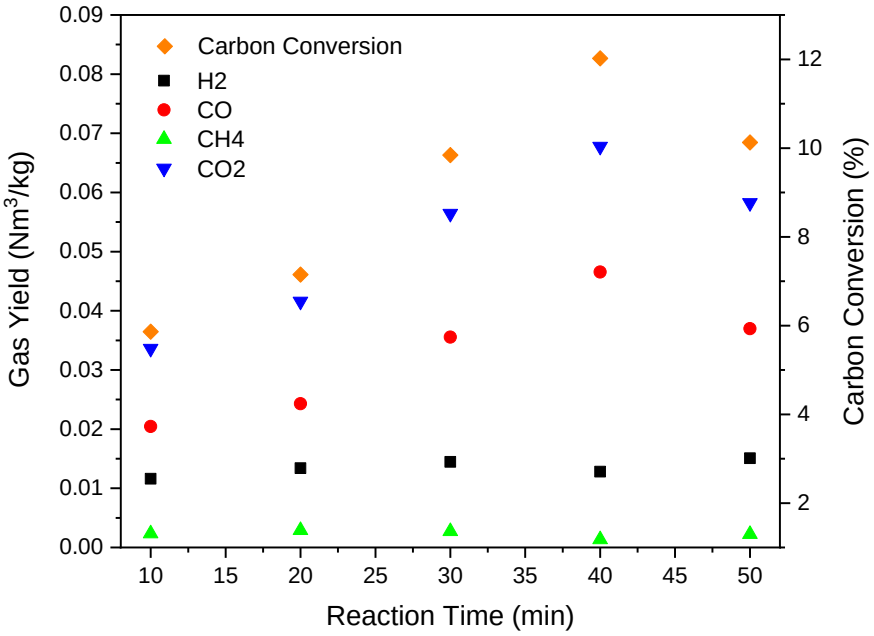

Figure 6.15. Effect of reaction time on gas yield and carbon conversion

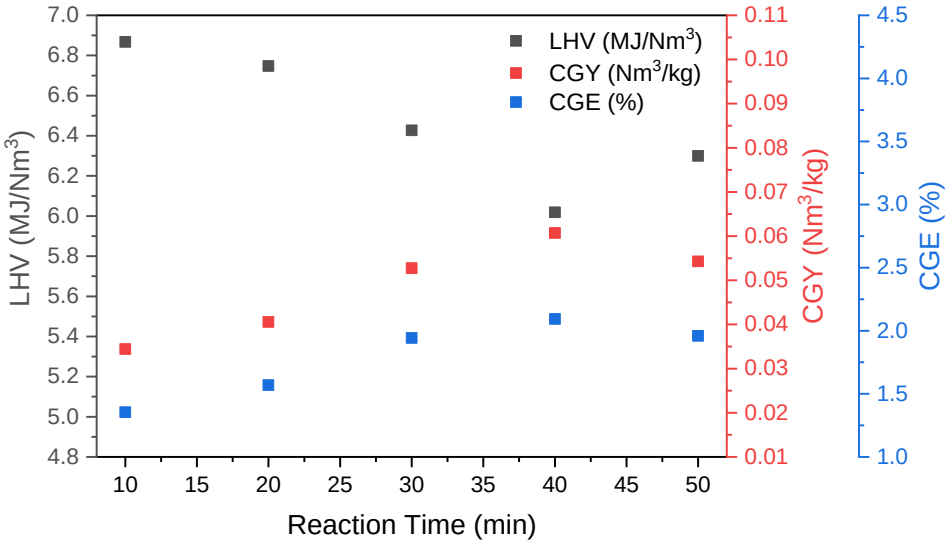

Figure 6.16. Effect of reaction time on LHV, CGY and CGE

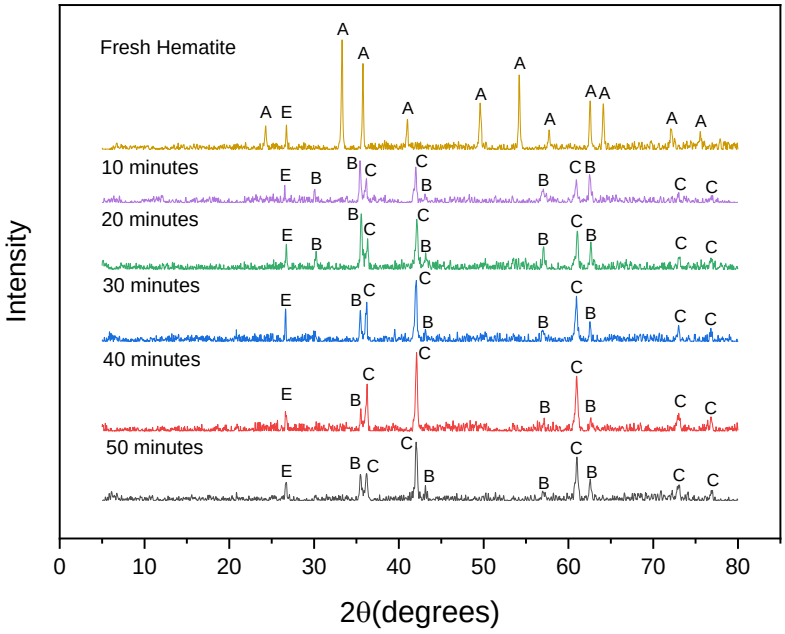

Figure 6.17. Effect of reaction time on the OC XRD results after gasification (A: Fe_2O_3, B: Fe3O4, C: Fe_XO, D: Fe E: carbon)

An XRD analysis was conducted on the gasified samples in the fuel reactor at various time intervals ranging from 10 – 50min as shown in Figure 6.17. It can be observed that all the Fe_2O_3 crystal phase peaks disappear within 10 minutes of the process with mainly Fe_3O_4 and some Fe_XO peaks appearing. The longer the reaction time, the more Fe_3O_4 is consumed hence peak intensity diminishes with an increase in the Fe_XO peak intensity. The XRD result for the 50 minutes reaction experiment seems to give faulty results since it is expected that the intensity of the Fe_XO peaks should increase while the Fe_3O_4 peaks should decrease. This is because an increase in reaction time should further the extent of the reaction, however as shown in Figure 6.15 the carbon conversion decreased.

Fresh **10 min**

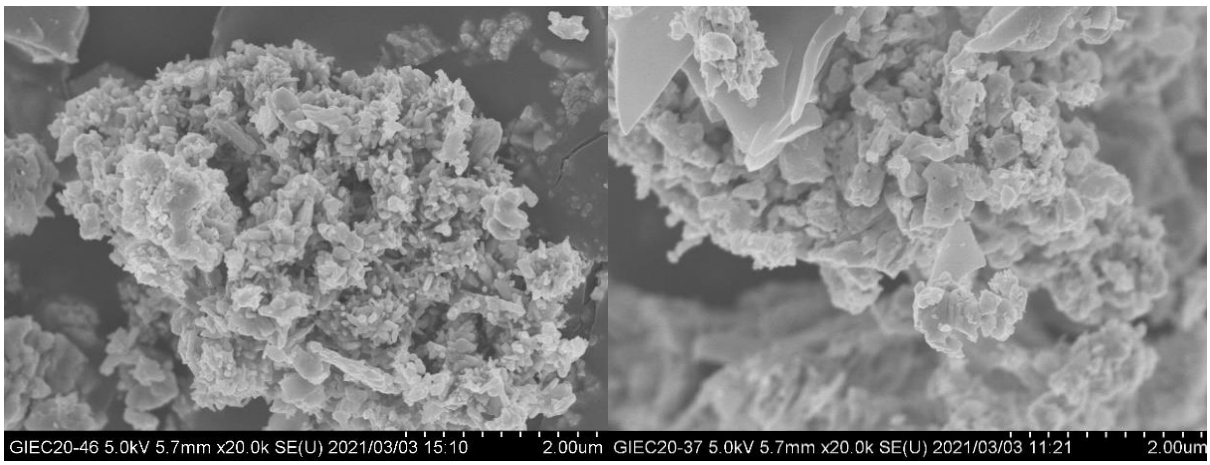

30 min **50 min**

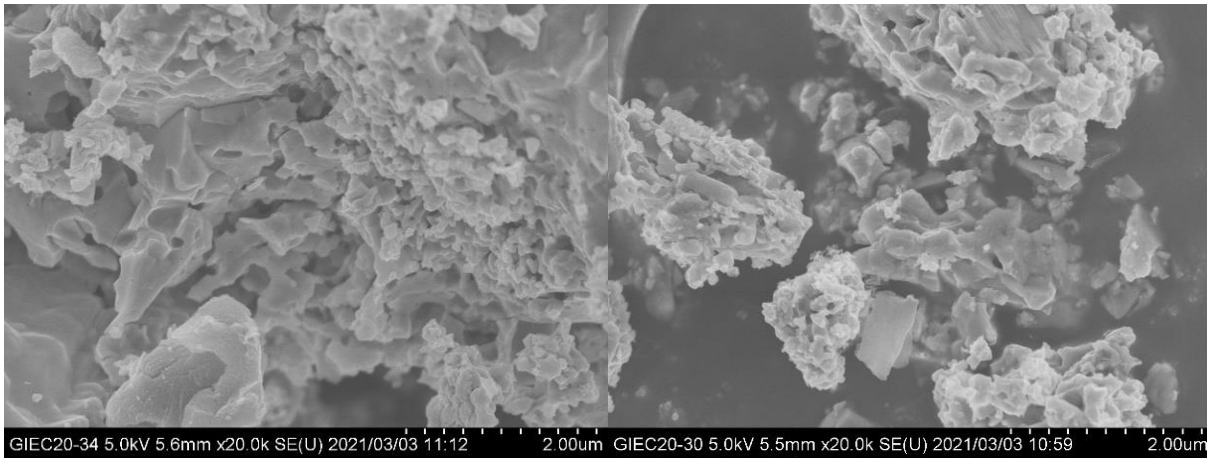

Figure 6.18. Effect of reaction time on the SEM results after OC gasification

Fresh Hematite

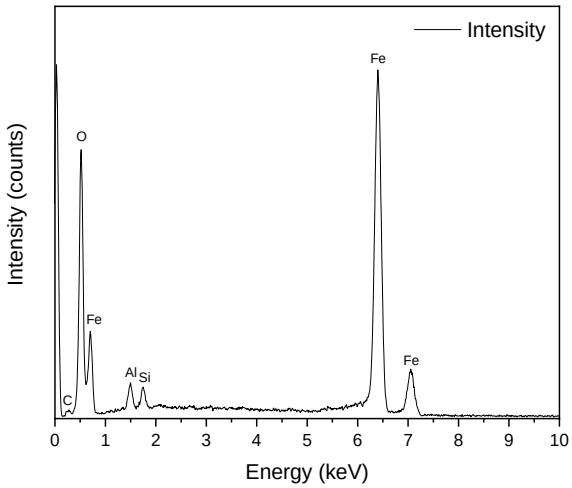

Fresh Hematite

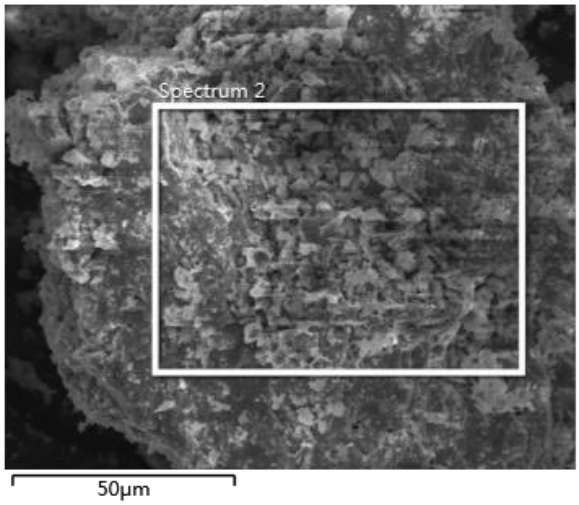

10 minutes

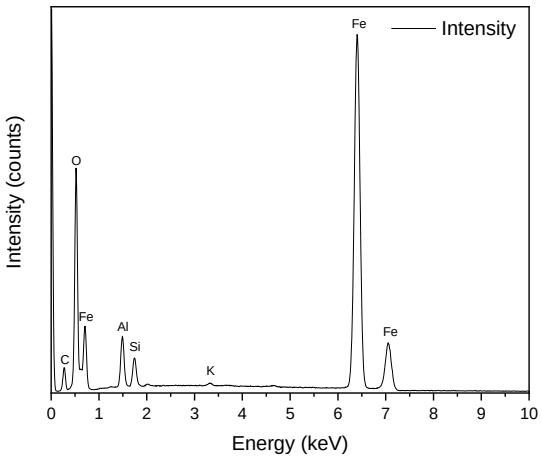

10 minutes

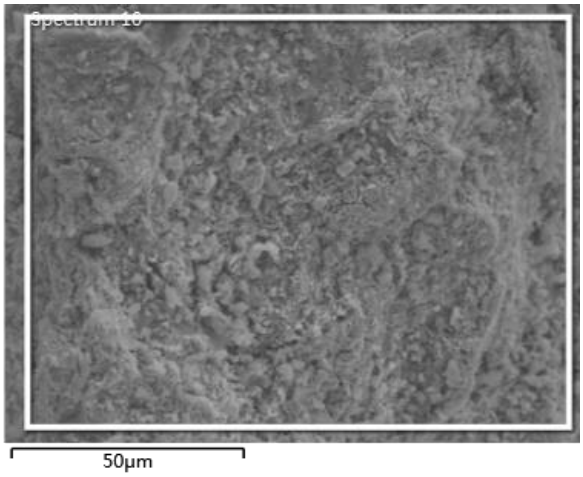

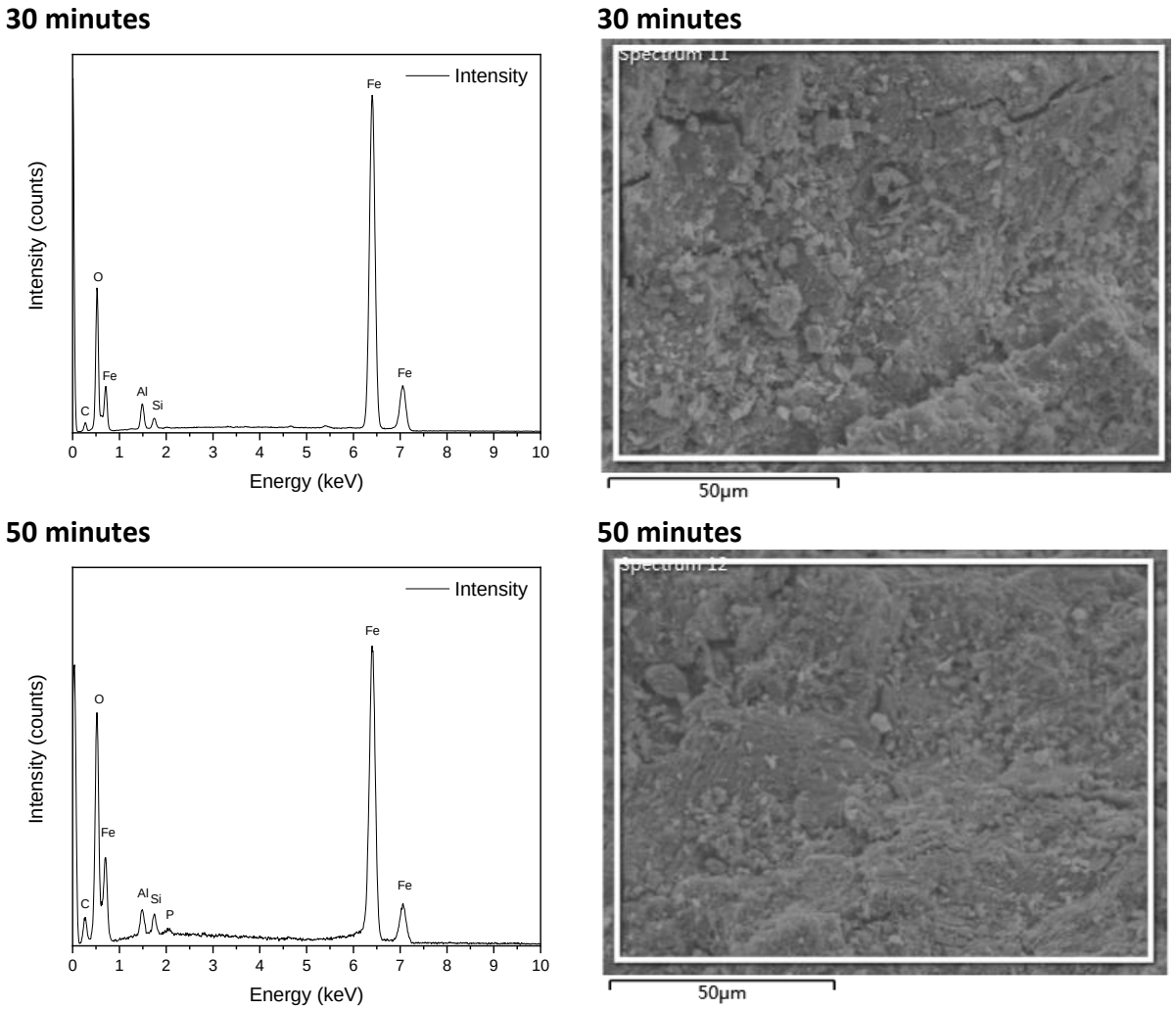

Figure 6.19. Effect of reaction time on the OC EDX results after gasification

The SEM images shown in Figure 6.18 (Additional SEM images in the **Appendix** Figure A2) show that there is a change in the average size of the particles after 10 minutes of the reaction compared to the fresh hematite. The granules average sizes appear to slightly increase as the reaction time increases due to sintering. This is because as reaction time increases more FeO is formed which has a lower melting point compared to Fe_2O_3 and Fe_3O_4, hence causes the agglomeration of small granules. It can be seen from the EDX tests in Figure 6.19 that the amount of oxygen decreases as reaction time increases. However, at reaction time equal to 50 minutes the oxygen peak increases. This is as previously mentioned that the 50-minute experiment could have been an anomaly as it does not follow the expected results in the gas yields, XRD and SEM results. There has been no previous literature testing the effect of time on the hematite characteristics to compare the results with.

6.5 Cycle Experiment

This experiment was conducted to test the regenerative ability of the oxygen carrier when reacted with pine sawdust to be used in multiple cycles. Therefore 1.7g of hematite was used to react with 1g of biomass in a fuel reactor at 840°C followed by regenerating the hematite OC by reacting with air at 950°C. This was repeated for 9 cycles and results of the gas yield and carbon conversion were recorded in Figure 6.20. We can observe that the gas yields and carbon conversion experience a slight decrease after the first 4 cycles but then goes on to plateau up till the 9th cycle. This could be due to the fresh hematite containing carbon on the surface as shown in the XRD results in Figure 6.23, hence increasing the amount of carbon emissions during the first four cycles or it could be due to the decrease in the reactive surface area on the surface of the hematite due to sintering as shown in the SEM results in Figure 6.21. After several cycles, the carbon on the regenerated oxygen carrier shows not carbon peak in the XRD results (Figure 6.23), which supports the aforementioned point. This decrease in carbon conversion results in a decrease in the LHV, CGY and consequently CGE. The gas yield from the air reactor appears to be relatively the constant after 9 cycles, similarly with the carbon conversion but with slight fluctuation as shown in Figure 6.22. From the XRD results in Figure 6.23, it can be seen that the oxygen carrier can still reattain its crystal phases as the fresh hematite after 9 cycles.

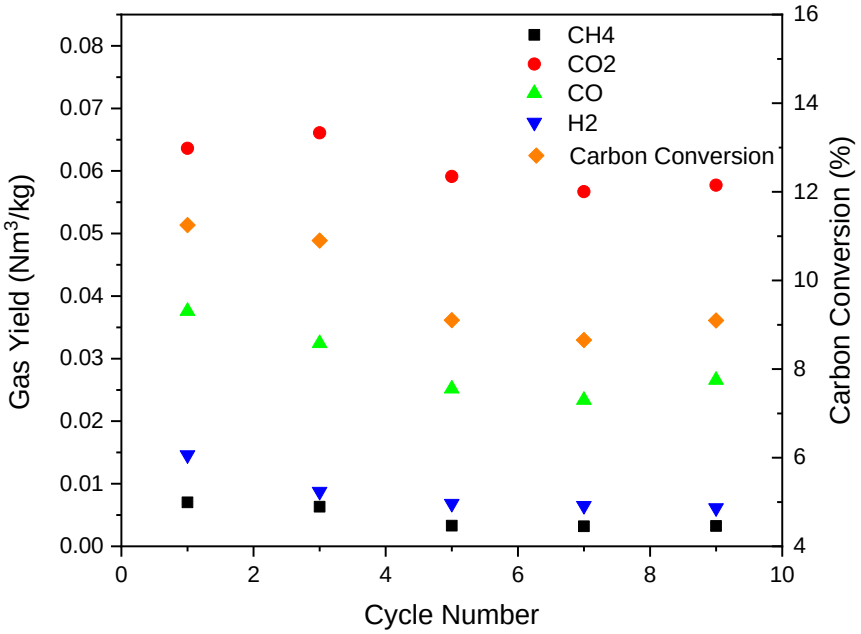

Figure 6.20. Effect of 9 cycles on gas yield and carbon conversion

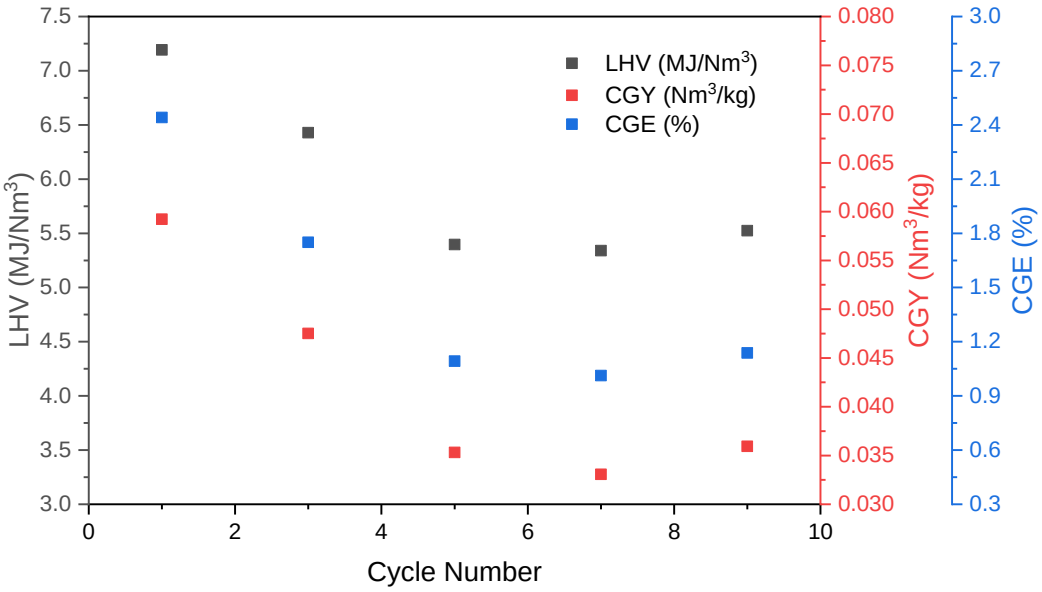

Figure 6.21. Effect of 9 cycles on LHV, CGY and CGE

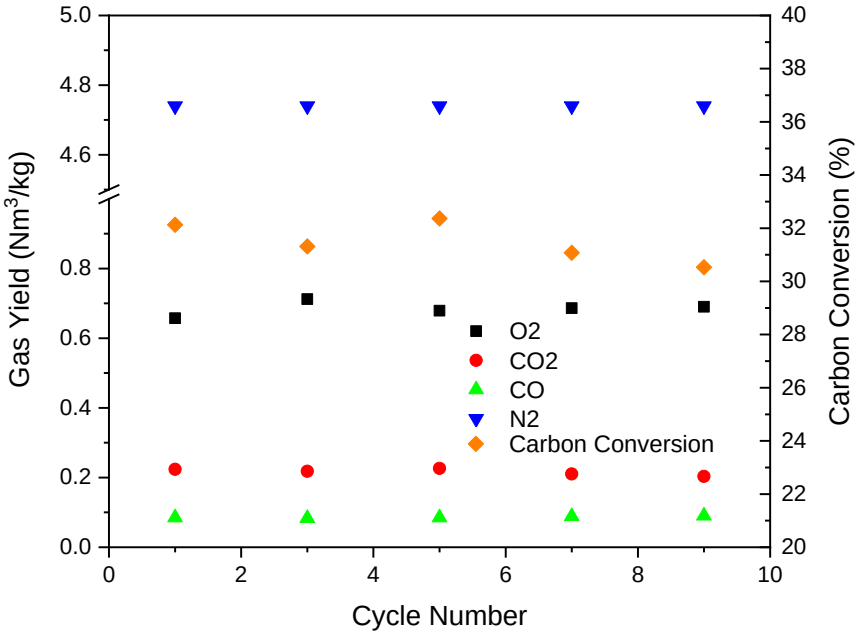

Figure 6.22. Effect of 9 cycles on gas yield and carbon conversion in the air reactor

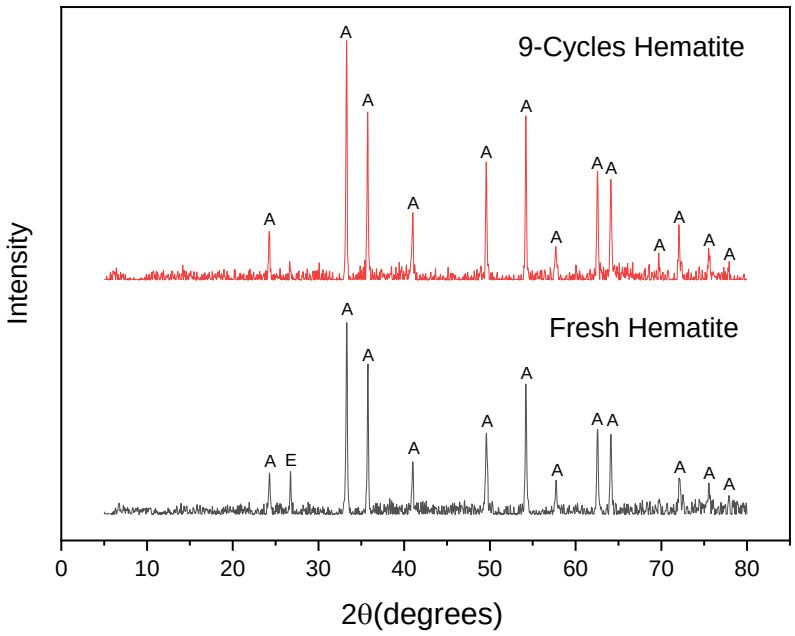

Figure 6.23. Effect of 9 cycles on the OC XRD results (A: Fe_2O_3, E: carbon)

After 9 cycles the sintering and agglomeration can be clearly seen in the SEM images in Figure 6.24 (Additional SEM images in the **Appendix** Figure A2) when compared to fresh hematite, which results in the slight decrease in porosity of the surface, hence reducing the total surface area for the reaction to take place. This is supported with the decrease in carbon conversion observed in Figure 6.25. Moreover, the carbon peak seems to have reduced which could be do the carbon on the surface of the hematite evaporating or reacting with O_2 in the air reactor to produce CO_2. A reduction/disappearance of the carbon peak was also experienced in the XRD results which complements this observation. In addition, the absence of silicon in the 9-cycle sample cannot be due to escaping the sample due to its silicon dioxide not being volatile, but more likely due to the absence of silicon with the local area where the EDX test was conducted. Finally, the amount of oxygen in the 9-cycle appears to be relatively more than the fresh hematite sample, which shows that not all of the iron oxide in the fresh hematite is at its maximum oxidation state. Huang et al., [151] shows that after 20 cycles reacting biomass char with hematite, the hematite fully recovered however with MgO deposits on the surface because of the ash. Regarding the SEM analysis, the surface of the hematite maintained its porous structure, however the porosity decreased, with slight sintering. Similarly, yet to a higher extent Huang et al., [92] reacts sewage sludge with hematite in a fixed bed and after 12 cycles observed 3 additional crystalline peaks on the regenerated hematite including, $CaAl_2Si_2O_8$, $CaH_2P_2O_7$ and $CaHPO_4$ which are because of sludge ash depositing on the surface.

The SEM image showed that the open pore structure nearly disappeared with the interconnected pores are filled by fragments. A large amount of sludge ash was deposited on the surface of the hematite, resulting in the blocking of the pore structure. However, when pine sawdust was used in this thesis, no additional peaks were observed in the regenerated hematite after 9 cycles, with the SEM image showing a very smooth surface of the hematite compared to the literature. The porous structure remained with the number of pores decreasing and pore size increasing.

Fresh **9-Cycles**

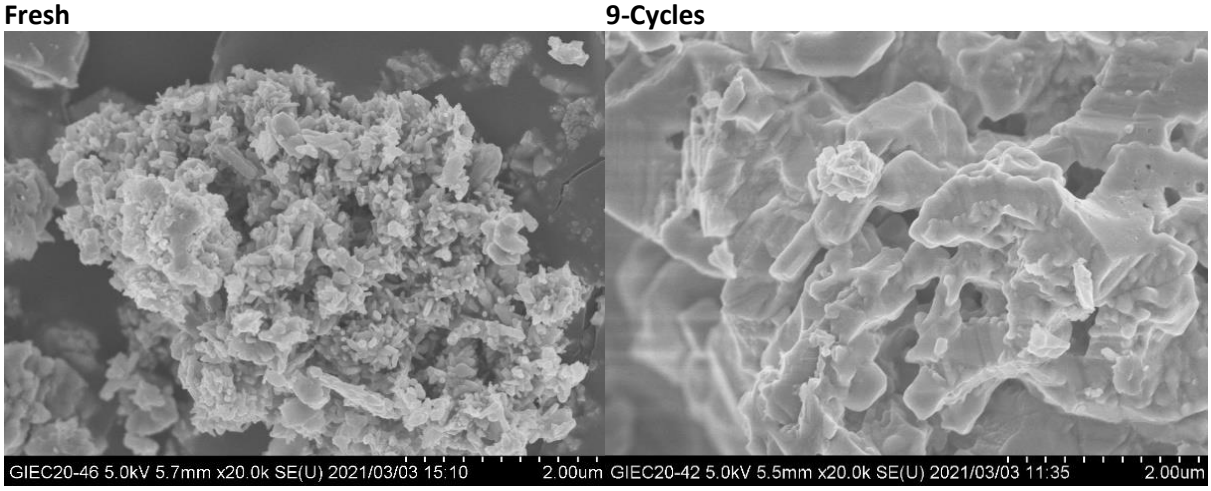

Figure 6.24. Effect of 9 cycles on the OC SEM results

Fresh Hematite **Fresh Hematite**

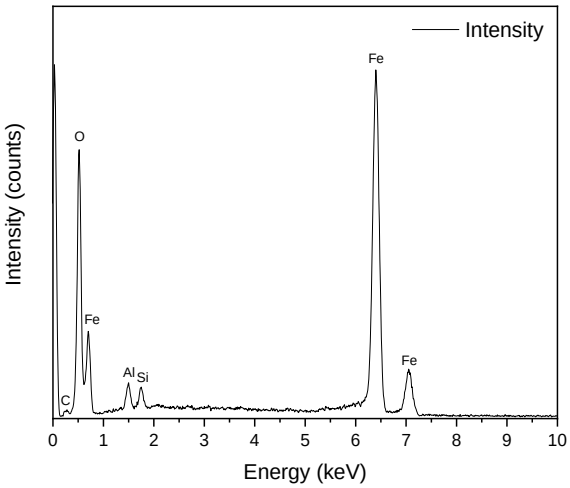

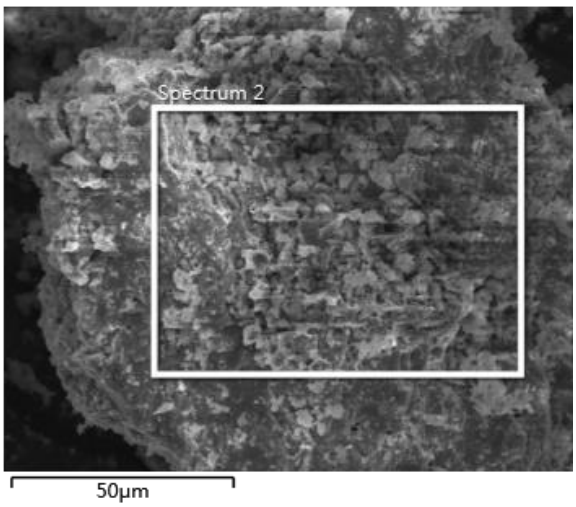

9-Cycles Test **9-Cycles Test**

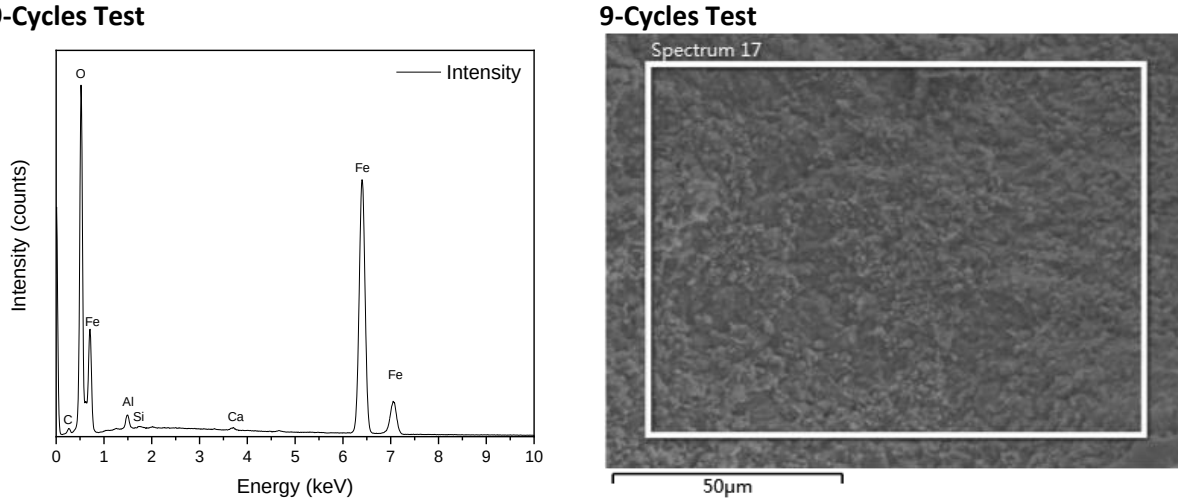

Figure 6.25. Effect of 9-cycles on the OC EDX results after gasification

6.6 Conclusion

An experimental investigation to better understand fresh hematite oxygen carrier as a source of oxygen in a BCLG process was conducted. Several experiments are conducted under different conditions (temperature, OC/B ratio, reaction time and 9 cycles) in a fixed bed reactor. The gas composition was measured followed by conducting an XRD analysis coupled with an SEM-EDX oxygen carrier characterization test. The results showed that fresh hematite can be used as an oxygen source during gasification with pine. However, it appeared that the carbon conversion was low compared to when using other sources of biomass, and consequently LHV, gas yield, cold gas efficiency. Moreover, it was observed that as temperature, reaction time and B/OC ratio increased the sintering and agglomeration on the surface of the oxygen carrier, with the oxygen being consumed reducing the main component of the hematite (Fe_2O_3) into three phases including Fe_3O_4, FeO and Fe. It was concluded that gasification temperature should be kept around 800°C, reaction time to take around 30 minutes, while B/OC ratio to be set around 0.61 or even less to prevent FeO formation. This is because excessive reduction of the OC can result in the formation of FeO and Fe metal, hence result in more sintering, which could decrease the oxygen capacity when regenerating. Finally, repetitive cycles result in a decrease in the porosity of the oxygen carrier, which also results in the decrease in reaction surface area between the OC and the biomass, hence decreasing the efficiency of the reaction to a point where there is no further decrease in surface area.

7 CONCLUSION AND FURTHER WORK

7.1 Conclusion

The push towards a greener economy as a result of the imminent and long-term threats of global warming is imperative. As a result, world governments agreed to maintain temperature rise below 2°C by the end of this century relative to pre-industrial levels according to the Paris agreement, with efforts to limit the increase to 1.5°C. As part of this global initiative, the UK house of commons passed a bill aiming to achieve a carbon neutral economy by the year 2050. This as a result will require radical change in the UK's economy to achieve that goal. BECCS technology can be seen as a possible pathway to help in decarbonising the economy. This thesis in particular focuses on BCLGCC to power generation technology and testing its technical and economic feasibility in large scales, followed by conducting a sustainability and life cycle analysis of the process. Finally, a material characterisation of the oxygen carrier (oxygen source) is tested and investigated.

7.1.1 Techno-Economic & Sustainability Analysis

BCLGCC proves to be a novel and effective power generation process. This thesis establishes a reliable simulation process of biomass chemical looping gasification combined cycle to power plant. The key technical parameters are optimized to obtain the maximum electricity output. Subsequently, a comprehensive study of the technical and economic feasibility of an industrial scale (**650 MW** gross power) BCLGCC power plant was conducted while taking into consideration the sustainability impact of the power plant relative to current power generation technologies. Both CCS and Non-CCS processes were modelled and evaluated, giving a **net efficiency of approximately 36% and 41%**, respectively. These values are higher compared to conventional coal/biomass combustion and IGCC processes. The high efficiencies of these processes are associated with the costs, hence a lower **COE of 21.7 ¢/kWh and 18.4 ¢/kWh for CCS and Non-CCS processes**, respectively. Taking into consideration the UK's **government renewable energy subsides, further decrease of the COE to 15.9 ¢/kWh and 12.8 ¢/kWh for CCS and Non-CCS power plants**, respectively, could be achieved. Additionally, if negative emissions incentives are also introduced, the economic feasibility of the power plant with CCS will be more obvious. When comparing the techno - economic performance of BCLGCC with other power generation technology, it can be seen

that BCLGCC demonstrates higher net efficiency with a lower COE. A sustainability assessment is conducted comparing between 5 different power generation technologies (with and w/o CCS) demonstrates that **BCLGCC presents promising economic and environmental results, with an increase in community development, but a low energy security due to the process not being commercially established, as a result it is still not as technically mature as the other power generation technologies**. However, its promising results, especially with the UK heading towards a net-zero emissions by 2050, BECCS technologies will become a vital option and will play a big role to achieve this target.

7.1.2 Life Cycle & Sustainability Analysis

As a push towards more efficient and renewable technology, research in gasification to power technology has become more prominent during the past decades. This study presented a life cycle energy – economy – CO_2 emissions analysis of the BCLGCC power plant and compared it to conventional coal/biomass gasification and combustion. Major conclusions are as follows:

1) Coal power plants demonstrate the least energy and cost input compared to biomass power plants, however resulted in higher net CO_2 emissions, since biomass power plants can be assumed to be near carbon neutral. Coal CCS plants can reduce CO_2 emissions to near zero, with BCLGCC and BIGCC plants with CCS can result in negative **680 kg-CO2/MWh** and **768.9 kg-CO_2/MWh**, respectively, yet BIGCC requires more TLCEI for the same power output since more energy is required for the CCS due to more CO_2 emission.

2) CIGCC without CCS plant requires the lowest amount of TLCEI (**637.9 MJ/MWh**) whereas BDC with CCS requires the most (**2971.5 MJ/MWh**). However, out of the biomass power plants BCLGCC requires the lowest energy requirement, were BCLGCC with CCS required **336.7 MJ/MWh** and 827.3 MJ/MWh less energy input compared to BIGCC and BDC with CCS technology.

3) In terms of TLCCI, PCC plant demonstrates the lowest value (**57.8 £/MWh**) while BIGCC showing the highest (**159.5 £/MWh**) out of the non-CCS processes, and similarly with the CCS power plants (**212.2 £/MWh** for BIGCC and **111.8 £/MWh** for PCC), with BCLGCC having a higher TLCCI compared to BDC which is due to the higher capital cost of the plant as it is still in its development stage, hence higher process and project contingencies.

4) The biomass supply chain process accounted for approximately 85% of the energy input 31% of CO_2 emissions, 50% of cost input for CCS power plants. BCLGCC plant required 14.3% and 11.6% (23.0 & 25.8% with CCS) less biomass compared to BIGGCC and DBC power plants to generate the same amount of power, respectively. **Wood processing & pelletization stage should be improved to reduce the high energy requirement and CO_2 emissions. This will result in a reduction in the cost of the process, hence reducing the overall cost of biomass.**

5) The parameters that had the highest effects on the TLCEI and TLCCE are the wood processing, coal mining and washing, CO_2 capture, and biomass transport. Whereas in terms of cost, the annual cost, wood harvesting, wood processing and coal mining & washing caused the highest influence on the TLCCI. Regarding the CCS power plants, the carbon capture and storage section had the highest impact on TLCCI followed by TLCCE and finally TLCEI.

Moreover, in line with the UK policies, BCLGCC shows better results than BDC and BIGCC coupled with CCS technology to help drive bioenergy with carbon capture and storage (BECCS) technology towards a net zero 2050. Government subsidies and negative emissions incentives are essential for project feasibility. These results can be a guide for a comprehensive comparison between BCLGCC and conventional thermochemical power generation technology with and w/o CCS in a move towards a carbon neural 2050 via BECCS technology.

Regarding the environmental impact assessment, Gabi software was used to develop a life cycle model to study and compare the environmental impact potential of BCLGCC and BIGCC power plants. The following conclusions were made:

1) **BCLGCC power plant life cycle exhibited lower environmental impact potential compared to BIGCC in several factors including POCP, ODP, ADP_{fossil}, AP and EP.**
2) The stages that resulted in the highest environmental impact was the wood pelleting and transport stages. This significantly contributed to the reduction in the environmental impact values due to BCLGCC utilizing less feedstock compared to BIGCC.
3) Comparing between the oxygen source of both processes, **the ASU in the BIGCC process emitted more pollutants into the atmosphere compared to the iron mining and transport to supply the oxygen carrier for the BCLGCC process.**

4) Biomass **gasification results in less environmental impact compared to biomass combustion** especially due to its higher efficiency, less biomass processing, hence less CO_2 captured and transported.

7.1.3 Hematite Characterization

An experimental investigation to better understand fresh hematite oxygen carrier as a source of oxygen in a BCLG process was conducted. Several experiments are conducted under different conditions (temperature, OC/B ratio, reaction time and 9 cycles) in a fixed bed reactor. The gas composition was measured followed by conducting an XRD analysis coupled with an SEM-EDX oxygen carrier characterization test. The results showed that fresh hematite can be used as an oxygen source during gasification with pine. However, it appeared that the carbon conversion was low compared to when using other sources of biomass, and consequently LHV, gas yield, cold gas efficiency. Moreover, it was observed that as temperature, reaction time and B/OC ratio increased the sintering and agglomeration on the surface of the oxygen carrier, with the oxygen being consumed reducing the main component of the hematite (Fe_2O_3) into three phases including Fe_3O_4, FeO and Fe. **It was concluded that gasification temperature should be kept around 800°C, reaction time to take around 30 minutes, while B/OC ratio to be set around 0.61 or even less to prevent FeO formation. This is because excessive reduction of the OC can result in the formation of FeO and Fe metal, hence result in more sintering, which could decrease the oxygen capacity when regenerating.** Finally, repetitive cycles result in a decrease in the porosity of the oxygen carrier, which also results in the decrease in reaction surface area between the OC and the biomass, hence decreasing the efficiency of the reaction to a point where there is no more decrease in surface area.

7.2 Further Work

Biomass chemical looping to power generation has not been researched into for scale up purposes as previously stated in literature (Chapter 2). Further research can focus on developing scale up models of other chemical looping to power generation including, biomass chemical looping combustion and chemical looping water splitting technologies and conducting a comprehensive assessment and comparison between the technologies. Moreover, other oxygen carriers can be used and compared to hematite which was used in

this thesis. Furthermore, there seems to be a gap in regard to developing a computational fluid dynamics model to better understand the heat and mass transfer within the fuel and air reactors. This can be further studied to allow for better understanding of the system when scaling up. In addition, it is also recognised that a major challenge is to decarbonise energy intensive industries like steel and glass production. The work presented in this thesis and the models developed could be adapted to integrate BCLG to reduce/eliminate fossil carbon in the supply of energy to these processes. Currently these industries are heavily fossil fuel dependent using natural gas, coking coal and pulverised coal. For example, in steel making BCLG could supply fuel gas (hydrogen/CO) from a renewable source for reduction processes and process heat. Direct hydrogen reduction is a fast-developing technology and process integration modelling could provide a tool for optimisation.

BIBLIOGRAPHY

[1] EIA (2017). *International Energy Outlook 2017*. U.S: U.S Energy Information Administration.

[2] Agbor, E., Oyedun, A., Zhang, X. and Kumar, A. (2016). Integrated techno-economic and environmental assessments of sixty scenarios for co-firing biomass with coal and natural gas. *Applied Energy*, 169, pp.433-449.

[3] World Energy Resources. (2017). 24th ed. [ebook] London: World Energy Council - Executive Summary, p.3. Available at: http://www.worldenergy.org/wp-content/uploads/2016/10/World-Energy-Resources_ExecutiveSummary_2016.pdf [Accessed 13 Aug. 2019].

[4] Paris Agreement, (2015), United Nations Framework Convention on Climate Change.

[5] UK Climate action following the Paris Agreement. In: Change CoC, 2016.

[6] Committee on Climate Change (2019). Net Zero: The UK's contribution to stopping global warming.

[7] De Gouw, J.A., Parrish, D.D., Frost, G.J. and Trainer, M., 2014. Reduced emissions of CO_2, NOx, and SO2 from US power plants owing to switch from coal to natural gas with combined cycle technology. *Earth's Future*, *2*(2), pp.75-82.

[8] Energy Live News. (2019). UK going net-zero 'impossible without bioenergy' - Energy Live News. [online] Available at: https://www.energylivenews.com/2019/06/04/uk-going-net-zero-impossible-without-bioenergy/ [Accessed 13 Aug. 2019].

[9] Drax. 2020. End of Coal Generation at Drax Power Station - Drax. [online] Available at: <https://www.drax.com/investors/end-of-coal-generation-at-drax-power-station/> [Accessed 26 June 2020].

[10] Nsenergybusiness.com. 2020. UK Coal: What Will Happen To Britain's Power Stations After 2025 Deadline?. [online] Available at: <https://www.nsenergybusiness.com/features/uk-coal-power-stations> [Accessed 26 June 2020].

[11] BBC News. 2020. Ban on Petrol And Diesel Car Sales Brought Forward. [online] Available at: <https://www.bbc.co.uk/news/science-environment-51366123> [Accessed 26 June 2020].

[12] Department for Business, Energy & Industrial Strategy, 2020. Section 2 – UK Solid Fuels and Derived Gases January To March 2020.

[13] Ukconstructionmedia.co.uk. 2020. World'S First Zero Carbon Cluster - UK Construction Online. [online] Available at: <https://www.ukconstructionmedia.co.uk/news/first-zero-carbon-cluster/> [Accessed 26 June 2020].

[14] The Independent. 2020. UK's Record Coal-Free Power Run Comes to An End. [online] Available at: <https://www.independent.co.uk/environment/coal-free-power-uk-record-time-2020-how-long-renewable-energy-a9570891.html> [Accessed 26 June 2020].

[15] Mandova, H., Gale, W.F., Williams, A., Heyes, A.L., Hodgson, P. and Miah, K.H., 2018. Global assessment of biomass suitability for ironmaking–opportunities for co-location of sustainable biomass, iron and steel production and supportive policies. Sustainable Energy Technologies and Assessments, 27, pp.23-39.

[16] Leung, D.Y., Caramanna, G. and Maroto-Valer, M.M., 2014. An overview of current status of carbon dioxide capture and storage technologies. Renewable and Sustainable Energy Reviews, 39, pp.426-443.

[17] Platform, E.B.T., 2012. Biomass with CO_2 capture and storage (Bio-CCS)-The way forward for Europe.

[18] Department for Business, Energy and Industrial Strategy, 2020. UK ENERGY IN BRIEF.

[19] Linderholm, C., Lyngfelt, A., Azar, C., Benson, S., Berndes, G., Berntsson, T., Canadell, J., Ciais, P., Cowie, A., Fuss, S. and Hansen, J., Highlights and Key Messages from the International Conference on Negative CO_2 Emissions.

[20] Stocker, T.F., Qin, D., Plattner, G.K., Tignor, M., Allen, S.K., Boschung, J., Nauels, A., Xia, Y., Bex, V., Midgley, P.M. and Alexander, L.V., 2013. Climate Change 2013. The Physical Science Basis. Working Group I Contribution to the Fifth Assessment Report of the Intergovernmental Panel on Climate Change-Abstract for decision-makers; Changements climatiques 2013.

[21] EASAC, 2018. Negative emission technologies: What role in meeting Paris Agreement targets?. *EASAC policy report 35*.

[22] Gasser, T., Guivarch, C., Tachiiri, K., Jones, C.D. and Ciais, P., 2015. Negative emissions physically needed to keep global warming below 2 C. *Nature communications*, *6*(1), pp.1-7.

[23] McCulloch, S., Keeling, S., Malischek, R. and Stanley, T., 2019. IEA. 20 Years of Carbon Capture and Storage. Accelerating Future Deployment.

[24] Creutzig, F., Ravindranath, N.H., Berndes, G., Bolwig, S., Bright, R., Cherubini, F., Chum, H., Corbera, E., Delucchi, M., Faaij, A. and Fargione, J., 2015. Bioenergy and climate change mitigation: an assessment. *Gcb Bioenergy*, *7*(5), pp.916-944.

[25] Newbold, T., Hudson, L.N., Hill, S.L., Contu, S., Lysenko, I., Senior, R.A., Börger, L., Bennett, D.J., Choimes, A., Collen, B. and Day, J., 2015. Global effects of land use on local terrestrial biodiversity. *Nature*, *520*(7545), pp.45-50.

[26] Vispute, T., Zhang, H., Sanna, A., Xiao, R. and Huber, G. (2010). Renewable chemical commodity feedstocks from integrated catalytic processing of pyrolysis oils. *Science*, 330(6008), pp.1222-1227.

[27] Grammelis, P., Karampinis, E. and Nikolopoulos, A., (2011). Fluidized bed combustion of solid biomass for electricity and/or heat generation. In Solid Biofuels for Energy (pp. 123-149)

[28] Cao, Y., Casenas, B. and Pan, W. (2006). Investigation of Chemical Looping Combustion by Solid Fuels. 2. Redox Reaction Kinetics and Product Characterization with Coal, Biomass, and Solid Waste as Solid Fuels and CuO as an Oxygen Carrier. *Energy & Fuels*, 20(5), pp.1845-1854.

[29] McKendry, P., 2002. Energy production from biomass (part 1): overview of biomass. *Bioresource technology*, *83*(1), pp.37-46.

[30] Prins, M., Ptasinski, K. and Janssen, F. (2007). From coal to biomass gasification: Comparison of thermodynamic efficiency. *Energy*, 32(7), pp.1248-1259

[31] Williams, G.H., 1992. Fuel from biomass. *Chemical & Engineering News*, *70*(47), pp.3-3.

[32] Jenkins, B., Baxter, L.L., Miles Jr, T.R. and Miles, T.R., 1998. Combustion properties of biomass. *Fuel processing technology*, *54*(1-3), pp.17-46.

[33] Khan, A., de Jong, W., Jansens, P. and Spliethoff, H. (2009). Biomass combustion in fluidized bed boilers: Potential problems and remedies. *Fuel Processing Technology*, 90(1), pp.21-50.

[34] DEMİRBAŞ, A., 2005. Fuel and combustion properties of bio-wastes. *Energy sources*, *27*(5), pp.451-462.

[35] Demirbas, A., 2004. Effect of initial moisture content on the yields of oily products from pyrolysis of biomass. *Journal of analytical and applied pyrolysis*, *71*(2), pp.803-815.

[36] Demirbas, A., 2004. Combustion characteristics of different biomass fuels. *Progress in energy and combustion science*, *30*(2), pp.219-230.

[37] Nielsen, H.P., Frandsen, F.J., Dam-Johansen, K. and Baxter, L.L., 2000. The implications of chlorine-associated corrosion on the operation of biomass-fired boilers. *Progress in energy and combustion science*, *26*(3), pp.283-298.

[38] Anukam, A., Mamphweli, S., Reddy, P., Meyer, E. and Okoh, O. (2016). Pre-processing of sugarcane bagasse for gasification in a downdraft biomass gasifier system: A comprehensive review. *Renewable and Sustainable Energy Reviews*, 66, pp.775-801.

[39] Kobayashi, N. and Fan, L. (2011). Biomass direct chemical looping process: A perspective. *Biomass and Bioenergy*, 35(3), pp.1252-1262

[40] Verma, M., Godbout, S., Brar, S., Solomatnikova, O., Lemay, S. and Larouche, J. (2012). Biofuels Production from Biomass by Thermochemical Conversion Technologies. International Journal of Chemical Engineering, 2012, pp.1-18.

[41] Han, J. and Kim, H., 2008. The reduction and control technology of tar during biomass gasification/pyrolysis: an overview. *Renewable and sustainable energy reviews*, *12*(2), pp.397-416.

[42] Lu, H. and Baxter, L.L., 2011. Biomass combustion characteristics and implications for renewable energy. In *Solid Biofuels for Energy* (pp. 95-121). Springer, London.

[43] Al-Qayim, K., Nimmo, W. and Pourkashanian, M., 2015. Comparative techno-economic assessment of biomass and coal with CCS technologies in a pulverized combustion power plant in the United Kingdom. International Journal of Greenhouse Gas Control, 43, pp.82-92.

[44] Oreggioni, G.D., Friedrich, D., Brandani, S. and Ahn, H., 2014. Techno-economic study of adsorption processes for pre-combustion carbon capture at a biomass CHP plant. *Energy Procedia*, *63*, pp.6738-6744.

[45] Zang, G., Jia, J., Tejasvi, S., Ratner, A. and Lora, E.S., 2018. Techno-economic comparative analysis of biomass integrated gasification combined cycles with and without CO_2 capture. *International Journal of Greenhouse Gas Control*, 78, pp.73-84.

[46] Domenichini, R., Gasparini, F., Cotone, P. and Santos, S., 2011. Techno-economic evaluation of biomass fired or co-fired power plants with post combustion CO2 capture. *Energy Procedia*, *4*, pp.1851-1860.

[47] Do, T.X., Lim, Y.I., Yeo, H., Choi, Y.T. and Song, J.H., 2014. Techno-economic analysis of power plant via circulating fluidized-bed gasification from woodchips. *Energy*, *70*, pp.547-560.

[48] McIlveen-Wright, D.R., Huang, Y., Rezvani, S., Redpath, D., Anderson, M., Dave, A. and Hewitt, N.J., 2013. A technical and economic analysis of three large scale biomass combustion plants in the UK. *Applied energy*, *112*, pp.396-404.

[49] Ernsting, A., 2015. *Biomass Gasification & Pyrolysis*. Biofuelwatch.

[50] Prins, M.J., Ptasinski, K.J. and Janssen, F.J., 2007. From coal to biomass gasification: Comparison of thermodynamic efficiency. *Energy*, *32*(7), pp.1248-1259.

[51] Shrestha, P., 2019. *UK'S 'Largest' Waste Wood Gasification Plant Fired Up in Cheshire - Energy Live News*. [online] Energy Live News. Available at: <https://www.energylivenews.com/2019/03/26/uks-largest-waste-wood-gasification-plant-fired-up-in-cheshire/> [Accessed 26 June 2020].

[52] Cooper, S., Blanco-Sanchez, P., Welfle, A. and McManus, M., 2019. *Bioenergy And Waste Gasification In The UK: Barriers And Research Needs*. Bath: Supergen Bioenergy Hub.

[53] Biofuelwatch.org.uk. 2020. *Map of UK Biomass Power Stations*. [online] Available at: <http://biofuelwatch.org.uk/wp-content/maps/uk-biomass.html> [Accessed 13 September 2020].

[54] CoGen. 2020. *Projects — Cogen*. [online] Available at: <https://www.cogenuk.com/projects> [Accessed 13 September 2020].

[55] Udomsirichakorn, J. and Salam, P. (2014). Review of hydrogen-enriched gas production from steam gasification of biomass: The prospect of CaO-based chemical looping gasification. Renewable and Sustainable Energy Reviews, 30, pp.565-579.

[56] Sansaniwal, S.K., Pal, K., Rosen, M.A. and Tyagi, S.K., 2017. Recent advances in the development of biomass gasification technology: A comprehensive review. *Renewable and sustainable energy reviews*, *72*, pp.363-384.

[57] Sikarwar, V., Zhao, M., Clough, P., Yao, J., Zhong, X., Memon, M., Shah, N., Anthony, E. and Fennell, P. (2016). An overview of advances in biomass gasification. *Energy & Environmental Science*, 9(10), pp.2939-2977.

[58] Maniatis, K., 2008. Progress in biomass gasification: an overview. Progress in thermochemical biomass conversion.

[59] National Energy Technology Laboratory. (2018). Fluidized bed gasifiers. https://www.netl.doe.gov/research/Coal/energy-systems/gasification/gasifipedia/ugas [Accessed 10 Jun. 2018].

[60] Tavoulareas, E. (1991). Fluidized-Bed Combustion Technology. *Annual Review of Energy and the Environment*, 16(1), pp.25-57.

[61] Arnold, M., Gale, J. and Laughlin, M. (1992). The british coal spouted fluidised bed gasification process. *The Canadian Journal of Chemical Engineering*, 70(5), pp.991-997.

[62] Netl.doe.gov. (2017). *Fluidized bed | netl.doe.gov*. [online] Available at: http://www.netl.doe.gov/research/coal/energy-systems/gasification/gasifipedia/fluidizedbed [Accessed 21 Dec. 2017].

[63] Zhao, X., Zhou, H., Sikarwar, V., Zhao, M., Park, A., Fennell, P., Shen, L. and Fan, L. (2017). Biomass-based chemical looping technologies: the good, the bad and the future. *Energy & environmental Science*, 10(9), pp.1885-1910

[64] Mendiara, T., García-Labiano, F., Abad, A., Gayán, P., de Diego, L.F., Izquierdo, M.T. and Adánez, J., 2018. Negative CO2 emissions through the use of biofuels in chemical looping technology: a review. Applied Energy, 232, pp.657-684.

[65] Zhao, X., Zhou, H., Sikarwar, V.S., Zhao, M., Park, A.H.A., Fennell, P.S., Shen, L. and Fan, L.S., 2017. Biomass-based chemical looping technologies: the good, the bad and the future. Energy & Environmental Science, 10(9), pp.1885-1910.

[66] Adanez, J., Abad, A., Garcia-Labiano, F., Gayan, P. and Luis, F., 2012. Progress in chemical-looping combustion and reforming technologies. Progress in energy and combustion science, 38(2), pp.215-282.

[67] Mattisson, T., Lyngfelt, A. and Leion, H., 2009. Chemical-looping with oxygen uncoupling for combustion of solid fuels. International journal of greenhouse gas control, 3(1), pp.11-19.

[68] Wen, C.Y., 1968. Noncatalytic heterogeneous solid-fluid reaction models. Industrial & Engineering Chemistry, 60(9), pp.34-54.

[69] Yan, X., Hu, J., Zhang, Q., Zhao, S., Dang, J. and Wang, W., 2020. Chemical-looping gasification of corn straw with Fe-based oxygen carrier: Thermogravimetric analysis. Bioresource technology, 303, p.122904.

[70] Keller, M., Leion, H. and Mattisson, T., 2016. Chemical looping tar reforming using La/Sr/Fe-containing mixed oxides supported on ZrO2. Applied Catalysis B: Environmental, 183, pp.298-307.

[71] Hu, Q., Mao, Q., Ren, X., Yang, H. and Chen, H., 2019. Inert chemical looping conversion of biochar with iron ore as oxygen carrier: Products conversion kinetics and structural evolution. Bioresource technology, 275, pp.53-60.

[72] Huang, Z., Deng, Z., Chen, D., He, F., Liu, S., Zhao, K., Wei, G., Zheng, A., Zhao, Z. and Li, H., 2017. Thermodynamic analysis and kinetic investigations on biomass char chemical looping gasification using Fe-Ni bimetallic oxygen carrier. Energy, 141, pp.1836-1844.

[73] Liu, C. and Wang, W., 2018. Chemical looping gasification of pyrolyzed biomass and coal char with copper ferrite as an oxygen carrier. Journal of Renewable and Sustainable Energy, 10(6), p.063101.

[74] Qi, B., Xia, Z., yuan Huang, G. and Wang, W., 2019. Study of chemical looping co-gasification (CLCG) of coal and rice husk with an iron-based oxygen carrier via solid–solid reactions. Journal of the Energy Institute, 92(2), pp.382-390.

[75] Virginie, M., Adánez, J., Courson, C., de Diego, L., García-Labiano, F., Niznansky, D., Kiennemann, A., Gayán, P. and Abad, A. (2012). Effect of Fe-olivine on the tar content during biomass gasification in a dual fluidized bed. Applied Catalysis B: Environmental, 121, pp.214-222.

[76] Jin, H., Hong, H. and Han, T. (2009). Progress of energy system with chemical-looping combustion. Science Bulletin, 54(6), pp.906-919.

[77] Yin, S., Shen, L., Dosta, M., Hartge, E.U., Heinrich, S., Lu, P., Werther, J. and Song, T., 2018. Chemical looping gasification of a biomass pellet with a manganese ore as an oxygen carrier in the fluidized bed. Energy & fuels, 32(11), pp.11674-11682.

[78] Ge, H., Guo, W., Shen, L., Song, T. and Xiao, J., 2016. Experimental investigation on biomass gasification using chemical looping in a batch reactor and a continuous dual reactor. Chemical Engineering Journal, 286, pp.689-700.

[79] Huang, X., Wu, J., Wang, M., Ma, X., Jiang, E. and Hu, Z., 2020. Syngas production by chemical looping gasification of rice husk using Fe-based oxygen carrier. Journal of the Energy Institute, 93(4), pp.1261-1270.

[80] Shen, T., Ge, H. and Shen, L., 2018. Characterization of combined Fe-Cu oxides as oxygen carrier in chemical looping gasification of biomass. International Journal of Greenhouse Gas Control, 75, pp.63-73.

[81] Huijun, G., Laihong, S., Fei, F. and Shouxi, J., 2015. Experiments on biomass gasification using chemical looping with nickel-based oxygen carrier in a 25 kWth reactor. Applied Thermal Engineering, 85, pp.52-60.

[82] Hu, J., Li, C., Zhang, Q., Guo, Q., Zhao, S., Wang, W., Lee, D.J. and Yang, Y., 2019. Using chemical looping gasification with Fe2O3/Al2O3 oxygen carrier to produce syngas (H2+ CO) from rice straw. International Journal of Hydrogen Energy, 44(6), pp.3382-3386.

[83] Hu, J., Li, C., Guo, Q., Dang, J., Zhang, Q., Lee, D.J. and Yang, Y., 2018. Syngas production by chemical-looping gasification of wheat straw with Fe-based oxygen carrier. Bioresource technology, 263, pp.273-279.

[84] Wei, G., He, F., Zhao, W., Huang, Z., Zhao, K., Zhao, Z., Zheng, A., Wu, X. and Li, H., 2017. Experimental investigation of Fe–Ni–Al oxygen carrier derived from hydrotalcite-like

precursors for the chemical looping gasification of biomass char. Energy & Fuels, 31(5), pp.5174-5182.

[85] Xue, N., Wang, Z., Wu, J., He, T., Zhang, J., Li, J. and Wu, J., 2019. Effect of equivalence ratio on the CO selectivity of Fe/Ca-based oxygen carriers in biomass char chemical looping gasification. Fuel, 252, pp.220-227.

[86] Niu, P., Ma, Y., Tian, X., Ma, J. and Zhao, H., 2018. Chemical looping gasification of biomass: Part I. screening Cu-Fe metal oxides as oxygen carrier and optimizing experimental conditions. Biomass and Bioenergy, 108, pp.146-156.

[87] Hu, J., Li, C., Lee, D.J., Guo, Q., Zhao, S., Zhang, Q. and Li, D., 2019. Syngas production from biomass using Fe-based oxygen carrier: Optimization. Bioresource technology, 280, pp.183-187.

[88] Fan, Y., Tippayawong, N., Wei, G., Huang, Z., Zhao, K., Jiang, L., Zheng, A., Zhao, Z. and Li, H., 2020. Minimizing tar formation whilst enhancing syngas production by integrating biomass torrefaction pretreatment with chemical looping gasification. Applied Energy, 260, p.114315.

[89] Wei, G.Q., Zhao, W.N., Meng, J.G., Feng, J., Li, W.Y., He, F., Huang, Z., Yi, Q., Du, Z.Y., Zhao, K. and Zhao, Z.L., 2018. Hydrogen production from vegetable oil via a chemical looping process with hematite oxygen carriers. Journal of Cleaner Production, 200, pp.588-597.

[90] Liu, G., Liao, Y., Wu, Y., Ma, X. and Chen, L., 2017. Characteristics of microalgae gasification through chemical looping in the presence of steam. International Journal of Hydrogen Energy, 42(36), pp.22730-22742.

[91] Liu, G., Liao, Y., Wu, Y. and Ma, X., 2018. Synthesis gas production from microalgae gasification in the presence of Fe2O3 oxygen carrier and CaO additive. Applied energy, 212, pp.955-965.

[92] Huang, Z., Xu, G., Deng, Z., Zhao, K., He, F., Chen, D., Wei, G., Zheng, A., Zhao, Z. and Li, H., 2017. Investigation on gasification performance of sewage sludge using chemical looping gasification with iron ore oxygen carrier. International Journal of Hydrogen Energy, 42(40), pp.25474-25491.

[93] Liu, Q., Hu, C., Peng, B., Liu, C., Li, Z., Wu, K., Zhang, H. and Xiao, R., 2019. High H2/CO ratio syngas production from chemical looping co-gasification of biomass and polyethylene with CaO/Fe2O3 oxygen carrier. Energy Conversion and Management, 199, p.111951.

[94] Gu, H., Lang, S., Song, G., Zhang, S., Niu, M., Liu, W. and Shen, L., 2019. Enhanced chemical looping hydrogen production based on biomass ash-promoted iron ore oxygen carrier. Chemical Engineering Journal, 360, pp.260-270.

[95] Zhang, S., Gu, H., Zhao, J., Shen, L. and Wang, L., 2019. Development of iron ore oxygen carrier modified with biomass ash for chemical looping combustion. Energy, 186, p.115893.

[96] Yan, J., Shen, L., Ou, Z., Wu, J., Jiang, S. and Gu, H., 2019. Enhancing the performance of iron ore by introducing K and Na ions from biomass ashes in a CLC process. Energy, 167, pp.168-180.

[97] Luo, S., Zeng, L. and Fan, L.S., 2015. Chemical looping technology: oxygen carrier characteristics. Annual review of chemical and biomolecular engineering, 6, pp.53-75.

[98] Lin, Y., Wang, H., Wang, Y., Huo, R., Huang, Z., Liu, M., Wei, G., Zhao, Z., Li, H. and Fang, Y., 2020. Review of biomass chemical looping gasification in China. Energy & Fuels, 34(7), pp.7847-7862.

[99] Bao, J., Li, Z. and Cai, N., 2013. Promoting the reduction reactivity of ilmenite by introducing foreign ions in chemical looping combustion. Industrial & Engineering Chemistry Research, 52(18), pp.6119-6128.

[100] LIAO, Y., ZHANG, H., WU, Y., LIU, G. and MA, X., 2018. Investigation of the Influence of Potassium on Biomass Chemical Looping Gasification. Journal of South China University of Technology (Natural Science Edition), (4), p.11.

[101] Hu, Q., Shen, Y., Chew, J.W., Ge, T. and Wang, C.H., 2020. Chemical looping gasification of biomass with Fe2O3/CaO as the oxygen carrier for hydrogen-enriched syngas production. Chemical Engineering Journal, 379, p.122346.

[102] Wu, Y., Liao, Y., Liu, G., Ma, X. and Zhang, H., 2019. Reactivity investigation on biomass chemical looping conversion for syngas production. Journal of the Energy Institute, 92(4), pp.1137-1148.

[103] Huang, Z., He, F., Feng, Y., Zhao, K., Zheng, A., Chang, S., Wei, G., Zhao, Z. and Li, H., 2014. Biomass char direct chemical looping gasification using NiO-modified iron ore as an oxygen carrier. Energy & fuels, 28(1), pp.183-191.

[104] Berguerand, N., Lind, F., Israelsson, M., Seemann, M., Biollaz, S. and Thunman, H., 2012. Use of nickel oxide as a catalyst for tar elimination in a chemical-looping reforming reactor operated with biomass producer gas. Industrial & engineering chemistry research, 51(51), pp.16610-16616.

[105] Skulimowska, A., Di Felice, L., Kamińska-Pietrzak, N., Celińska, A., Pławecka, M., Hercog, J., Krauz, M. and Aranda, A., 2017. Chemical looping with oxygen uncoupling (CLOU) and chemical looping combustion (CLC) using copper-enriched oxygen carriers supported on fly ash. Fuel Processing Technology, 168, pp.123-130.

[106] He, F., Huang, Z., Wei, G., Zhao, K., Wang, G., Kong, X., Feng, Y., Tan, H., Hou, S., Lv, Y. and Jiang, G., 2019. Biomass chemical-looping gasification coupled with water/CO2-splitting using NiFe2O4 as an oxygen carrier. Energy Conversion and Management, 201, p.112157.

[107] Lin, Y., Wang, H., Huang, Z., Liu, M., Wei, G., Zhao, Z., Li, H. and Fang, Y., 2020. Chemical looping gasification coupled with steam reforming of biomass using NiFe2O4: Kinetic analysis of DAEM-TI, thermodynamic simulation of OC redox, and a loop test. Chemical Engineering Journal, p.125046.

[108] Yan, J., Sun, R., Shen, L., Bai, H., Jiang, S., Xiao, Y. and Song, T., 2020. Hydrogen-rich syngas production with tar elimination via biomass chemical looping gasification (BCLG) using BaFe2O4/Al2O3 as oxygen carrier. Chemical Engineering Journal, 387, p.124107

[109] Liu, G., Liao, Y., Wu, Y. and Ma, X., 2018. Application of calcium ferrites as oxygen carriers for microalgae chemical looping gasification. Energy conversion and management, 160, pp.262-272.

[110] Chen, J., Zhao, K., Zhao, Z., He, F., Huang, Z. and Wei, G., 2019. Identifying the roles of MFe2O4 (M= Cu, Ba, Ni, and Co) in the chemical looping reforming of char, pyrolysis gas and tar resulting from biomass pyrolysis. International Journal of Hydrogen Energy, 44(10), pp.4674-4687.

[111] Wang, S., Song, T., Yin, S., Hartge, E.U., Dymala, T., Shen, L., Heinrich, S. and Werther, J., 2020. Syngas, tar and char behavior in chemical looping gasification of sawdust pellet in fluidized bed. Fuel, 270, p.117464.

[112] Condori, O., García-Labiano, F., Luis, F., Izquierdo, M.T., Abad, A. and Adánez, J., 2020. Biomass chemical looping gasification for syngas production using ilmenite as oxygen carrier in a 1.5 kWth unit. Chemical Engineering Journal, 405, p.126679.

[113] Guo, L., Zhao, H. and Zheng, C., 2015. Synthesis gas generation by chemical-looping reforming of biomass with natural copper ore as oxygen carrier. Waste and Biomass Valorization, 6(1), pp.81-89.

[114] Zhao, H., Guo, L. and Zou, X., 2015. Chemical-looping auto-thermal reforming of biomass using Cu-based oxygen carrier. Applied Energy, 157, pp.408-415.

[115] Zeng, J., Xiao, R., Zhang, S., Zhang, H., Zeng, D., Qiu, Y. and Ma, Z., 2018. Identifying iron-based oxygen carrier reduction during biomass chemical looping gasification on a thermogravimetric fixed-bed reactor. Applied Energy, 229, pp.404-412.

[116] Deng, Z., Huang, Z., He, F., Zheng, A., Wei, G., Meng, J., Zhao, Z. and Li, H., 2019. Evaluation of calcined copper slag as an oxygen carrier for chemical looping gasification of sewage sludge. International Journal of Hydrogen Energy, 44(33), pp.17823-17834.

[117] Huang, Z., He, F., Zhao, K., Feng, Y., Zheng, A., Chang, S., Zhao, Z. and Li, H. (2014b). Natural iron ore as an oxygen carrier for biomass chemical looping gasification in a fluidized bed reactor. Journal of Thermal Analysis and Calorimetry, 116(3), pp.1315-1324.

[118] Cho, P., Mattisson, T. and Lyngfelt, A. (2004). Comparison of iron-, nickel-, copper- and manganese-based oxygen carriers for chemical-looping combustion. Fuel, 83(9), pp.1215-1225.

[119] Yates, J. (1983). Fundamentals of fluidized-bed chemical processes. London: Butterworths, pp.1, 4 - 62.

[120] Leckner, B. (1998). Fluidized bed combustion: Mixing and pollutant limitation. Progress in Energy and Combustion Science, 24(1), pp.31-61.

[121] Koornneef, J., Junginger, M. and Faaij, A. (2007). Development of fluidized bed combustion—An overview of trends, performance and cost. Progress in Energy and Combustion Science, 33(1), pp.19-55.

[122] Halvorsen, B.M. and Arvoh, B., 2009. Minimum fluidization velocity, bubble behaviour and pressure drop in fluidized beds with a range of particle sizes. WIT Transactions on Engineering Sciences, 63, pp.227-238.

[123] Siriwardane, R., Riley, J., Bayham, S., Straub, D., Tian, H., Weber, J. and Richards, G., 2018. 50-kWth methane/air chemical looping combustion tests with commercially prepared CuO-Fe2O3-alumina oxygen carrier with two different techniques. Applied energy, 213, pp.92-99.

[124] Son, S.R. and Kim, S.D., 2006. Chemical-looping combustion with NiO and Fe2O3 in a thermobalance and circulating fluidized bed reactor with double loops. Industrial & Engineering Chemistry Research, 45(8), pp.2689-2696.

[125] Shen, L., Wu, J., Xiao, J., Song, Q. and Xiao, R., 2009. Chemical-looping combustion of biomass in a 10 kWth reactor with iron oxide as an oxygen carrier. Energy & Fuels, 23(5), pp.2498-2505.

[126] Rifflart, S., Hoteit, A., Yazdanpanah, M.M., Pelletant, W. and Surla, K., 2011. Construction and operation of a 10 kW CLC unit with circulation configuration enabling independent solid flow control. Energy Procedia, 4, pp.333-340.

[127] Thon, A., Kramp, M., Hartge, E.U., Heinrich, S. and Werther, J., 2014. Operational experience with a system of coupled fluidized beds for chemical looping combustion of solid fuels using ilmenite as oxygen carrier. Applied Energy, 118, pp.309-317.

[128] Kolbitsch, P., Pröll, T., Bolhar-Nordenkampf, J. and Hofbauer, H., 2009. Design of a chemical looping combustor using a dual circulating fluidized bed (DCFB) reactor system. Chemical Engineering & Technology: Industrial Chemistry-Plant Equipment-Process Engineering-Biotechnology, 32(3), pp.398-403.

[129] Ströhle, J., Orth, M. and Epple, B., 2014. Design and operation of a 1 MWth chemical looping plant. Applied Energy, 113, pp.1490-1495.

[130] Abdulally, I., Beal, C., Andrus, H., Epple, B., Lyngfelt, A. and Lani, B., 2012, June. Alstom's chemical looping prototypes, program update. In 37th International Technical Conference on Clean Coal & Fuel Systems, Clearwater, FL, USA.

[131] Abad, A., Adánez, J., Gayán, P., Luis, F., García-Labiano, F. and Sprachmann, G., 2015. Conceptual design of a 100 MWth CLC unit for solid fuel combustion. Applied Energy, 157, pp.462-474.

[132] Lyngfelt, A. and Leckner, B., 2015. A 1000 MWth boiler for chemical-looping combustion of solid fuels–Discussion of design and costs. Applied Energy, 157, pp.475-487.

[133] Bayham, S., McGiveron, O., Tong, A., Chung, E., Kathe, M., Wang, D., Zeng, L. and Fan, L.S., 2015. Parametric and dynamic studies of an iron-based 25-kWth coal direct chemical looping unit using sub-bituminous coal. Applied Energy, 145, pp.354-363.

[134] Fan, L.S., 2011. Chemical looping systems for fossil energy conversions. John Wiley & Sons.

[135] Noorman, S., van Sint Annaland, M. and Kuipers, H., 2007. Packed bed reactor technology for chemical-looping combustion. Industrial & Engineering Chemistry Research, 46(12), pp.4212-4220.

[136] Noorman, S., van Sint Annaland, M. and Kuipers, J.A.M., 2010. Experimental validation of packed bed chemical-looping combustion. Chemical Engineering Science, 65(1), pp.92-97.

[137] Matsuoka, K., Shimbori, T., Kuramoto, K., Hatano, H. and Suzuki, Y., 2006. Steam reforming of woody biomass in a fluidized bed of iron oxide-impregnated porous alumina. Energy & fuels, 20(6), pp.2727-2731.

[138] HUSEYIN, S., WEI, G.Q., LI, H.B., Fang, H.E. and HUANG, Z., 2014. Chemical-looping gasification of biomass in a 10 kWth interconnected fluidized bed reactor using Fe2O3/Al2O3 oxygen carrier. Journal of Fuel Chemistry and Technology, 42(8), pp.922-931.

[139] Zeng, J., Xiao, R., Zhang, H., Wang, Y., Zeng, D. and Ma, Z., 2017. Chemical looping pyrolysis-gasification of biomass for high H_2/CO syngas production. Fuel Processing Technology, 168, pp.116-122.

[140] Wei, G., He, F., Zhao, Z., Huang, Z., Zheng, A., Zhao, K. and Li, H., 2015. Performance of Fe–Ni bimetallic oxygen carriers for chemical looping gasification of biomass in a 10 kWth

interconnected circulating fluidized bed reactor. International Journal of Hydrogen Energy, 40(46), pp.16021-16032.

[141] Wei, G., He, F., Huang, Z., Zheng, A., Zhao, K. and Li, H., 2014. Continuous operation of a 10 kWth chemical looping integrated fluidized bed reactor for gasifying biomass using an iron-based oxygen carrier. Energy & Fuels, 29(1), pp.233-241.

[142] Huang, Z., He, F., Feng, Y., Zhao, K., Zheng, A., Chang, S. and Li, H. (2013a). Synthesis gas production through biomass direct chemical looping conversion with natural hematite as an oxygen carrier. Bioresource Technology, 140, pp.138-145.

[143] He, F., Huang, Z., Li, H. and Zhao, Z., 2011, March. Biomass direct chemical looping conversion in a fluidized bed reactor with natural hematite as an oxygen carrier. In Power and Energy Engineering Conference (APPEEC), 2011 Asia-Pacific (pp. 1-7). IEEE.

[144] Huang, Z., He, F., Feng, Y., Liu, R., Zhao, K., Zheng, A., Chang, S., Zhao, Z. and Li, H., (2013c). Characteristics of biomass gasification using chemical looping with iron ore as an oxygen carrier. International journal of hydrogen energy, 38(34), pp.14568-14575.

[145] Huang, Z., He, F., Zheng, A., Zhao, K., Chang, S., Zhao, Z. and Li, H. (2013b). Synthesis gas production from biomass gasification using steam coupling with natural hematite as oxygen carrier. Energy, 53, pp.244-251.

[146] Sarvaramini, A. and Larachi, F., 2012. Catalytic oxygenless steam cracking of syngas-containing benzene model tar compound over natural Fe-bearing silicate minerals. Fuel, 97, pp.741-750.

[147] Zeng, J., Xiao, R., Zhang, H., Wang, Y., Zeng, D. and Ma, Z. (2017a). Chemical looping pyrolysis-gasification of biomass for high H_2 /CO syngas production. Fuel Processing Technology, 168, pp.116-122.

[148] Hu, J., Li, C., Guo, Q., Dang, J., Zhang, Q., Lee, D. and Yang, Y. (2018). Syngas production by chemical-looping gasification of wheat straw with Fe-based oxygen carrier. Bioresource Technology, 263, pp.273-279.

[149] Zeng, J., Xiao, R., Zeng, D., Zhao, Y., Zhang, H. and Shen, D. (2016). High H2/CO Ratio Syngas Production from Chemical Looping Gasification of Sawdust in a Dual Fluidized Bed Gasifier. Energy & Fuels, 30(3), pp.1764-1770.

[150] Zeng, J., Xiao, R., Zhang, H., Chen, X., Zeng, D. and Ma, Z., 2017. Syngas production via biomass self-moisture chemical looping gasification. Biomass and Bioenergy, 104, pp.1-7.

[151] Huang, Z., Zhang, Y., Fu, J., Yu, L., Chen, M., Liu, S., He, F., Chen, D., Wei, G., Zhao, K. and Zheng, A., 2016. Chemical looping gasification of biomass char using iron ore as an oxygen carrier. International Journal of Hydrogen Energy, 41(40), pp.17871-17883.

[152] Hu, Z., Jiang, E. and Ma, X., 2019. The effect of oxygen carrier content and temperature on chemical looping gasification of microalgae for syngas production. Journal of the Energy Institute, 92(3), pp.474-487.

[153] Kolbitsch, P., Bolhar-Nordenkampf, J., Pröll, T. and Hofbauer, H., 2009. Comparison of two Ni-based oxygen carriers for chemical looping combustion of natural gas in 140 kW continuous looping operation. Industrial & engineering chemistry research, 48(11), pp.5542-5547.

[154] Kolbitsch, P., Bolhàr-Nordenkampf, J., Pröll, T. and Hofbauer, H., 2010. Operating experience with chemical looping combustion in a 120 kW dual circulating fluidized bed (DCFB) unit. International Journal of Greenhouse Gas Control, 4(2), pp.180-185.

[155] Mayer, K., Penthor, S., Pröll, T. and Hofbauer, H., 2015. The different demands of oxygen carriers on the reactor system of a CLC plant–Results of oxygen carrier testing in a 120 kWth pilot plant. Applied Energy, 157, pp.323-329.

[156] Ohlemüller, P., Busch, J.P., Reitz, M., Ströhle, J. and Epple, B., 2016. Chemical-looping combustion of hard coal: autothermal operation of a 1 MWth pilot plant. Journal of Energy Resources Technology, 138(4).

[157] Kremer, J., Galloy, A., Stroehle, J. and Epple, B., 2013. Continuous CO2 capture in a 1-MWth carbonate looping pilot plant. *Chemical Engineering & Technology*, *36*(9), pp.1518-1524.

[158] Kluger, F., Abdulally, I., Andrus, H., Levasseur, A., Beal, C. and Marion, J., 2015, October. Overview of Alstom's chemical looping programs. In 5th Meeting of the IEAGHG International Oxyfuel Combustion Research Network, Wuhan, China.

[159] Vilches, T.B., Lind, F., Rydén, M. and Thunman, H., 2017. Experience of more than 1000 h of operation with oxygen carriers and solid biomass at large scale. *Applied Energy*, *190*, pp.1174-1183.

[160] Lyngfelt, A. and Thunman, H., 2005. Construction and 100 h of operational experience of a 10-kW chemical-looping combustor. Carbon dioxide capture for storage in deep geologic formations-results from the CO_2 capture project, 1, pp.625-645.

[161] Baek, J.I., Kim, U., Jo, H., Eom, T.H., Lee, J.B. and Ryu, H.J., 2016. Chemical looping combustion development in Korea. In *4th International Conference on Chemical Looping*.

[162] Langorgen, O., Saanum, I. and Haugen, N.E., 2016. Performance of a 150 kW chemical looping combustion reactor system for gaseous fuels using a copper-based oxygen carrier. In 4th International Conference on Chemical Looping (pp. 26-28).

[163] Hsieh, T.L., Xu, D., Zhang, Y., Nadgouda, S., Wang, D., Chung, C., Pottimurthy, Y., Guo, M., Chen, Y.Y., Xu, M. and He, P., 2018. 250 kWth high pressure pilot demonstration of the syngas chemical looping system for high purity H2 production with CO2 capture. Applied Energy, 230, pp.1660-1672.

[164] Bayham, S.C., Kim, H.R., Wang, D., Tong, A., Zeng, L., McGiveron, O., Kathe, M.V., Chung, E., Wang, W., Wang, A. and Majumder, A., 2013. Iron-based coal direct chemical looping combustion process: 200-h continuous operation of a 25-kWth subpilot unit. Energy & fuels, 27(3), pp.1347-1356.

[165] Flynn, T.J., Velazquez-Vargas, L.G., Bao, J., Zhang, Y., Tong, A. and Fan, L.S., 2019. *" 250 kWt Pilot Testing in Support of a 10 MWe Coal-Direct Chemical Looping Demonstration Feasibility Study*. The Babcock & Wilcox Company.

[166] Gogolev, I., Linderholm, C., Gall, D., Schmitz, M., Mattisson, T., Pettersson, J.B. and Lyngfelt, A., 2019. Chemical-looping combustion in a 100 kW unit using a mixture of synthetic and natural oxygen carriers–Operational results and fate of biomass fuel alkali. International Journal of Greenhouse Gas Control, 88, pp.371-382.

[167] Linderholm, C. and Schmitz, M., 2016. Chemical-looping combustion of solid fuels in a 100 kW dual circulating fluidized bed system using iron ore as oxygen carrier. *Journal of environmental chemical engineering*, *4*(1), pp.1029-1039.

[168] Schmitz, M. and Linderholm, C., 2018. Chemical looping combustion of biomass in 10- and 100-kW pilots–analysis of conversion and lifetime using a sintered manganese ore. *Fuel*, *231*, pp.73-84.

[169] Saito, T., Lin, S., Sharma, A., Matsumura, A. and Hatanaka, T., 2018, October. Chemical Looping Combustion by Using 100kW Three-Tower CFB Facility. In *14th Greenhouse Gas Control Technologies Conference Melbourne* (pp. 21-26).

[170] Shen, T., Wang, S., Yan, J., Shen, L. and Tian, H., 2020. Performance improvement of chemical looping combustion with coal by optimizing operational strategies in a 3 kWth interconnected fluidized bed. International Journal of Greenhouse Gas Control, 98, p.103060.

[171] Shen, L., Wu, J. and Xiao, J., 2009. Experiments on chemical looping combustion of coal with a NiO based oxygen carrier. Combustion and Flame, 156(3), pp.721-728.

[172] Xiao, R., Chen, L., Saha, C., Zhang, S. and Bhattacharya, S., 2012. Pressurized chemical-looping combustion of coal using an iron ore as oxygen carrier in a pilot-scale unit. International Journal of Greenhouse Gas Control, 10, pp.363-373.

[173] Ma, J., Zhao, H., Tian, X., Wei, Y., Rajendran, S., Zhang, Y., Bhattacharya, S. and Zheng, C., 2015. Chemical looping combustion of coal in a 5 kWth interconnected fluidized bed reactor using hematite as oxygen carrier. Applied Energy, 157, pp.304-313.

[174] Abad, A., Pérez-Vega, R., Luis, F., García-Labiano, F., Gayán, P. and Adánez, J., 2015. Design and operation of a 50 kWth Chemical Looping Combustion (CLC) unit for solid fuels. Applied Energy, 157, pp.295-303.

[175] Ma, J., Tian, X., Wang, C., Chen, X. and Zhao, H., 2018. Performance of a 50 kWth coal-fuelled chemical looping combustor. International Journal of Greenhouse Gas Control, 75, pp.98-106.

[176] Sozinho, T., Pelletant, W., Gauthier, T. and Stainton, H., 2012, September. Main results of the 10 kW coal pilot plant operation. In 2nd Int. Conf. on Chemical Looping.

[177] Tilland, A., Lambert, A., Pelletant, W., Chiche, D., Bounie, C. and Bertholin, S., 2017. Comparison of two oxygen carriers performances for chemical looping combustion application. In Proceedings of the 9th Trondheim Conference on CO_2 Capture, Transport and Storage (pp. 12-14).

[178] Lambert, A., Tilland, A., Pelletant, W. and Bertholin, S., 2018. Ageing and characterization of CaMn0, 775Ti0, 1Mg0, 1O3-δ particles in a 10 kWth CLC pilot plant. In 5th International Conference on Chemical Looping.

[179] Mayer, F., Bidwe, A.R., Schopf, A., Taheri, K., Zieba, M. and Scheffknecht, G., 2012. Comparison of a new micaceous iron oxide and ilmenite with respect to syngas conversion in a BFB reactor and adaptation of a 10 kWth DFB system for CLC to solid fuels. In Proceedings of the 2nd International Conference on Chemical Looping.

[180] Cao, Y., Sit, S.P. and Pan, W.P., 2012, September. The development of 10 kW chemical looping combustion technology in ICSET, WKU. In 2nd International Conference on Chemical Looping (pp. 26-28).

[181] Haus, J., Feng, Y., Hartge, E.U., Heinrich, S. and Werther, J., 2018. High volatiles conversion in a dual stage fuel reactor system for Chemical Looping Combustion of wood biomass. In International Conference on Negative CO_2 Emissions.

[182] Abad, A., Pérez-Vega, R., Pérez-Astray, A., Mendiara, T., De Diego, L. and García-Labiano, F., 2018. Biomass combustion with CO2 capture by chemical looping: experimental results in a 50 kWth pilot plant. In International conference on negative CO_2 emissions, Gothemburg (Sweden).

[183] Pikkarainen, T. and Hiltunen, I., 2017, June. Chemical looping combustion of solid biomass–performance of ilmenite and braunite as oxygen carrier materials. In 25th European Biomass Conference and Exhibition. Stockholm, Sweden.

[184] Xu, D., Zhang, Y., Hsieh, T., Guo, M., Qin, L., Chung, C., Fan, L. and Tong, A. (2018). A novel chemical looping partial oxidation process for thermochemical conversion of biomass to syngas. *Applied Energy*, 222, pp.119-131.

[185] Kong, F., Swift, J., Zhang, Q., Fan, L.S. and Tong, A., 2020. Biogas to H2 conversion with CO2 capture using chemical looping technology: Process simulation and comparison to conventional reforming processes. *Fuel*, *279*, p.118479.

[186] Zeng, L., He, F., Li, F. and Fan, L.S., 2012. Coal-direct chemical looping gasification for hydrogen production: reactor modeling and process simulation. *Energy & fuels*, *26*(6), pp.3680-3690.

[187] Yan, L., He, B., Pei, X., Wang, C., Duan, Z., Song, J. and Li, X., 2014. Design and comparisons of three biomass-based hydrogen generation systems with chemical looping process. *International journal of hydrogen energy*, *39*(31), pp.17540-17553.

[188] Gopaul, S., Dutta, A. and Clemmer, R. (2014). Chemical looping gasification for hydrogen production: A comparison of two unique processes simulated using ASPEN Plus. *International Journal of Hydrogen Energy*, 39(11), pp.5804-5817.

[189] Li, G., Chang, Y., Chen, L., Liu, F., Ma, S., Wang, F. and Zhang, Y., 2020. Process design and economic assessment of butanol production from lignocellulosic biomass via chemical looping gasification. *Bioresource Technology*, *316*, p.123906.

[190] Cormos, C.C., 2015. Biomass direct chemical looping for hydrogen and power co-production: Process configuration, simulation, thermal integration and techno-economic assessment. *Fuel processing technology*, *137*, pp.16-23.

[191] Kuo, P.C., Chen, J.R., Wu, W. and Chang, J.S., 2018. Hydrogen production from biomass using iron-based chemical looping technology: Validation, optimization, and efficiency. *Chemical Engineering Journal*, *337*, pp.405-415.

[192] Li, F., Zeng, L. and Fan, L.S., 2010. Biomass direct chemical looping process: process simulation. *Fuel*, *89*(12), pp.3773-3784.

[193] Zaini, I.N., Nurdiawati, A. and Aziz, M., 2017. Cogeneration of power and H2 by steam gasification and syngas chemical looping of macroalgae. *Applied Energy*, *207*, pp.134-145.

[194] Sorgenfrei, M. and Tsatsaronis, G., 2014. Design and evaluation of an IGCC power plant using iron-based syngas chemical-looping (SCL) combustion. Applied energy, 113, pp.1958-1964.

[195] Yan, L., Yue, G. and He, B., 2016. Thermodynamic analyses of a biomass–coal co-gasification power generation system. *Bioresource technology*, *205*, pp.133-141.

[196] Zhou, L., Deshpande, K., Zhang, X. and Agarwal, R.K., 2020. Process simulation of Chemical Looping Combustion using ASPEN plus for a mixture of biomass and coal with various oxygen carriers. *Energy*, *195*, p.116955.

[197] Ge, H., Zhang, H., Guo, W., Song, T. and Shen, L., 2019. System simulation and experimental verification: Biomass-based integrated gasification combined cycle (BIGCC)

coupling with chemical looping gasification (CLG) for power generation. *Fuel*, *241*, pp.118-128.

[198] Aghabararnejad, M., Patience, G.S. and Chaouki, J., 2015. Techno-Economic Comparison of a 7-MWth Biomass chemical looping gasification unit with conventional Systems. *Chemical Engineering & Technology*, 38(5), pp.867-878.

[199] Shabani, S., Delavar, M.A. and Azmi, M., 2013. Investigation of biomass gasification hydrogen and electricity co-production with carbon dioxide capture and storage. *International journal of hydrogen energy*, *38*(9), pp.3630-3639.

[200] National Energy Technology Laboratory (2010). Cost and Performance Baseline for Fossil Energy Plants Volume 1: Bituminous Coal and Natural Gas to Electricity.

[201] Hoffmann, B.S. and Szklo, A., 2011. Integrated gasification combined cycle and carbon capture: a risky option to mitigate CO2 emissions of coal-fired power plants. *Applied Energy*, *88*(11), pp.3917-3929.

[202] Mohamed, U., Zhao, Y., Huang, Y., Cui, Y., Shi, L., Li, C., Mohamed, P., Wei, G., Yi, Q. and Nimmo, W., 2020. Sustainability evaluation of biomass direct gasification using chemical looping technology for power generation with and w/o CO_2 capture. Energy, p.117904.

[203] Hammond, G.P. and Spargo, J., 2014. The prospects for coal-fired power plants with carbon capture and storage: A UK perspective. *Energy Conversion and Management*, *86*, pp.476-489.

[204] Catalanotti, E., Hughes, K.J., Porter, R.T., Price, J. and Pourkashanian, M., 2014. Evaluation of performance and cost of combustion-based power plants with CO2 capture in the United Kingdom. *Environmental Progress & Sustainable Energy*, *33*(4), pp.1425-1431.

[205] Liang, X., Wang, Z., Zhou, Z., Huang, Z., Zhou, J. and Cen, K., 2013. Up-to-date life cycle assessment and comparison study of clean coal power generation technologies in China. *Journal of cleaner production*, *39*, pp.24-31.

[206] Yang, K., Zhu, N. and Yuan, T., 2017. Analysis of optimum scale of biomass gasification combined cooling heating and power (CCHP) system based on life cycle assessment (LCA). *Procedia Engineering*, *205*, pp.145-152.

[207] Mann, M.K. and Spath, P.L., 1997. *Life cycle assessment of a biomass gasification combined-cycle power system* (No. NREL/TP-430-23076; ON: DE98002709). National Renewable Energy Lab., Golden, CO (US).

[208] Zang, G., Zhang, J., Jia, J., Lora, E.S. and Ratner, A., 2020. Life cycle assessment of power-generation systems based on biomass integrated gasification combined cycles. *Renewable Energy*, *149*, pp.336-346.

[209] Carpentieri, M., Corti, A. and Lombardi, L., 2005. Life cycle assessment (LCA) of an integrated biomass gasification combined cycle (IBGCC) with CO_2 removal. *Energy Conversion and Management*, *46*(11-12), pp.1790-1808.

[210] Odeh, N.A. and Cockerill, T.T., 2008. Life cycle GHG assessment of fossil fuel power plants with carbon capture and storage. *Energy Policy*, *36*(1), pp.367-380.

[211] Stamford, L. and Azapagic, A., 2014. Life cycle sustainability assessment of UK electricity scenarios to 2070. *Energy for Sustainable Development*, *23*, pp.194-211.

[212] Wang, Z., Li, L. and Zhang, G., 2018. Life cycle greenhouse gas assessment of hydrogen production via chemical looping combustion thermally coupled steam reforming. *Journal of Cleaner Production*, *179*, pp.335-346.

[213] Li, G., Liu, F., Liu, T., Yu, Z., Liu, Z. and Fang, Y., 2019. Life cycle assessment of coal direct chemical looping hydrogen generation with Fe_2O_3 oxygen carrier. *Journal of Cleaner Production*, *239*, p.118118.

[214] Heng, L., Xiao, R. and Zhang, H., 2018. Life cycle assessment of hydrogen production via iron-based chemical-looping process using non-aqueous phase bio-oil as fuel. *International Journal of Greenhouse Gas Control*, *76*, pp.78-84.

[215] Petrescu, L., Müller, C.R. and Cormos, C.C., 2014. Life cycle assessment of natural gas-based chemical looping for hydrogen production. *Energy Procedia*, *63*, pp.7408-7420.

[216] Salkuyeh, Y.K., Saville, B.A. and MacLean, H.L., 2017. Techno-economic analysis and life cycle assessment of hydrogen production from natural gas using current and emerging technologies. *International Journal of hydrogen energy*, *42*(30), pp.18894-18909.

[217] Bareschino, P., Mancusi, E., Urciuolo, M., Paulillo, A., Chirone, R. and Pepe, F., 2020. Life cycle assessment and feasibility analysis of a combined chemical looping combustion and

power-to-methane system for CO2 capture and utilization. *Renewable and Sustainable Energy Reviews*, *130*, p.109962.

[218] Navajas, A., Mendiara, T., Goñi, V., Jiménez, A., Gandía, L.M., Abad, A., García-Labiano, F. and Luis, F., 2019. Life cycle assessment of natural gas fuelled power plants based on chemical looping combustion technology. *Energy Conversion and Management*, *198*, p.111856.

[219] He, Y., Zhu, L., Li, L. and Rao, D., 2019. Life-cycle assessment of SNG and power generation: The role of implement of chemical looping combustion for carbon capture. *Energy*, *172*, pp.777-786.

[220] Fan, J., Hong, H. and Jin, H., 2018. Power generation based on chemical looping combustion: will it qualify to reduce greenhouse gas emissions from life-cycle assessment?. *ACS Sustainable Chemistry & Engineering*, *6*(5), pp.6730-6737.

[221] Petrescu, L. and Cormos, C.C., 2017. Environmental assessment of IGCC power plants with pre-combustion CO2 capture by chemical & calcium looping methods. *Journal of Cleaner Production*, *158*, pp.233-244.

[222] Fan, J., Hong, H. and Jin, H., 2019. Life cycle global warming impact of CO_2 capture by in-situ gasification chemical looping combustion using ilmenite oxygen carriers. *Journal of Cleaner Production*, *234*, pp.568-578.

[223] Tagliaferri, C., Görke, R., Scott, S., Dennis, J. and Lettieri, P., 2018. Life cycle assessment of optimised chemical looping air separation systems for electricity production. *Chemical Engineering Research and Design*, *131*, pp.686-698.

[224] Yi, Q., Feng, J. and Li, W. (2012). Optimization and efficiency analysis of polygeneration system with coke-oven gas and coal gasified gas by Aspen Plus. *Fuel*, 96, pp.131-140.

[225] Adnan, M.A. and Hossain, M.M., 2018. Gasification performance of various microalgae biomass–A thermodynamic study by considering tar formation using Aspen plus. *Energy conversion and management*, *165*, pp.783-793.

[226] Dhanavath, K.N., Shah, K., Bhargava, S.K., Bankupalli, S. and Parthasarathy, R., 2018. Oxygen–steam gasification of karanja press seed cake: Fixed bed experiments, ASPEN Plus

process model development and benchmarking with saw dust, rice husk and sunflower husk. *Journal of Environmental Chemical Engineering*, *6*(2), pp.3061-3069.

[227] Barrera, R., Salazar, C. and Pérez, J.F., 2014. Thermochemical equilibrium model of synthetic natural gas production from coal gasification using Aspen Plus. *International Journal of Chemical Engineering*, *2014*, pp.1-18.

[228] Zhu, Y. 2004. Evaluation of gas turbine and gasifier-based power generation system. PhD thesis, North Carolina State University.

[229] Huang, Z., He, F., Feng, Y., Zhao, K., Zheng, A., Chang, S. and Li, H. (2013). Synthesis gas production through biomass direct chemical looping conversion with natural hematite as an oxygen carrier. *Bioresource technology*, 140, pp.138-145.

[230] Yi, Q., Fan, Y., Li, W. and Feng, J., 2013. CO_2 capture and use in a novel coal-based polygeneration system. *Industrial & Engineering Chemistry Research*, *52*(39), pp.14231-14240.

[231] Porrazzo, R., White, G. and Ocone, R., 2016. Techno-economic investigation of a chemical looping combustion-based power plant. *Faraday discussions*, 192, pp.437-457.

[232] GmbH, f., 2020. *Iron Ore PRICE Today | Iron Ore Spot Price Chart | Live Price Of Iron Ore Per Ounce | Markets Insider*. [online] markets.businessinsider.com. Available at: <https://markets.businessinsider.com/commodities/iron-ore-price> [Accessed 2 June 2020].

[233] ya Nsakala, N. and Liljedahl, G.N., 2003. Greenhouse gas emissions control by oxygen firing in circulating fluidized bed boilers. Alstom Power Inc.(US).

[234] Meerman, J.C., Knoope, M.M.J., Ramírez, A., Turkenburg, W.C. and Faaij, A.P.C., 2013. Technical and economic prospects of coal-and biomass-fired integrated gasification facilities equipped with CCS over time. *International Journal of Greenhouse Gas Control,* 16, pp.311-323.

[235] Rubin, E.S., Rao, A.B. and Berkenpas, M.B., 2007. *Development and application of optimal design capability for coal gasification systems*. Carnegie-Mellon University.

[236] Zhu, L., He, Y., Li, L. and Wu, P., 2018. Tech-economic assessment of second-generation CCS: Chemical looping combustion. *Energy*, 144, pp.915-927.

[237] Bellotti, D., Sorce, A., Rivarolo, M. and Magistri, L., 2019. Techno-economic analysis for the integration of a power to fuel system with a CCS coal power plant. *Journal of CO_2 Utilization*, 33, pp.262-272.

[238] Huang, Y., Zhao, Y.J., Hao, Y.H., Wei, G.Q., Feng, J., Li, W.Y., Yi, Q., Mohamed, U., Pourkashanian, M. and Nimmo, W., 2019. A feasibility analysis of distributed power plants from agricultural residues resources gasification in rural China. *Biomass and bioenergy*, *121*, pp.1-12.

[239] Long III, H.A. and Wang, T., 2016. Parametric techno-economic studies of coal/biomass co-gasification for IGCC plants with carbon capture using various coal ranks, fuel-feeding schemes, and syngas cooling methods. *International Journal of Energy Research*, *40*(4), pp.473-496.

[240] International Organisation for Standardisation (ISO), 2006. Environmental Management–Life Cycle Assessment–Requirements and Guidelines (ISO 14044).

[241] International Organization for Standardization, 2006. *Environmental Management: Life Cycle Assessment; Principles and Framework* (No. 2006). ISO.

[242] Cmu.edu. 2020. *Integrated Environmental Control Model - About*. [online] Available at: <https://www.cmu.edu/epp/iecm/about.html> [Accessed 27 June 2020].

[243] Rubin, E.S., Berkenpas, M.B., Kietzke, K., Diwekar, U., Frey, H.C., Kalagnanam, J. and Fry, J.J., 1999. *IECM. Integrated Environmental Control Model* (No. ESTSC--001311IBMPC00). Carnegie-Mellon Inst. of Research, Pittsburgh, PA (United States).

[244] Barisano, D., Canneto, G., Nanna, F., Alvino, E., Pinto, G., Villone, A., Carnevale, M., Valerio, V., Battafarano, A. and Braccio, G. (2016). Steam/oxygen biomass gasification at pilot scale in an internally circulating bubbling fluidized bed reactor. *Fuel Processing Technology*, 141, pp.74-81.

[245] Yi, Q., Zhao, Y., Huang, Y., Wei, G., Hao, Y., Feng, J., Mohamed, U., Pourkashanian, M., Nimmo, W. and Li, W., 2018. Life cycle energy-economic-CO2 emissions evaluation of biomass/coal, with and without CO_2 capture and storage, in a pulverized fuel combustion power plant in the United Kingdom. Applied energy, 225, pp.258-272.

[246] Gabi-software.com. 2020. *CML 2001*. [online] Available at: <http://www.gabi-software.com/support/gabi/gabi-lcia-documentation/cml-2001/> [Accessed 20 December 2020].

[247] Encyclopedia Britannica. 2020. *Coal Utilization - Coal Combustion*. [online] Available at: <https://www.britannica.com/topic/coal-utilization-122944/Coal-combustion> [Accessed 26 October 2020].

[248] Lu, G. and Yan, Y., 2006. Temperature profiling of pulverized coal flames using multicolor pyrometric and digital imaging techniques. *IEEE transactions on instrumentation and measurement*, *55*(4), pp.1303-1308.

[249] Williams, A., Pourkashanian, M. and Jones, J.M., 2001. Combustion of pulverised coal and biomass. *Progress in energy and combustion science*, *27*(6), pp.587-610.

[250] Ma, L., Jones, J.M., Pourkashanian, M. and Williams, A., 2007. Modelling the combustion of pulverized biomass in an industrial combustion test furnace. *Fuel*, *86*(12-13), pp.1959-1965.

[251] Nussbaumer, T., 2003. Combustion and co-combustion of biomass: fundamentals, technologies, and primary measures for emission reduction. *Energy & fuels*, *17*(6), pp.1510-1521.

[252] Salzmann, R. and Nussbaumer, T., 2001. Fuel staging for NO x reduction in biomass combustion: experiments and modeling. *Energy & Fuels*, *15*(3), pp.575-582.

[253] Allam, R.J., 2009. Improved oxygen production technologies. *Energy Procedia*, *1*(1), pp.461-470.

[254] Ratafia-Brown, J., Manfredo, L., Hoffmann, J. and Ramezan, M., 2002. Major environmental aspects of gasification-based power generation technologies-final report. *US Department of Energy (DOE), the National Energy Technology Laboratory (NETL), Gasification Technologies Program*.

[255] Cargill, P., DeJonghe, G., Howsley, T., Lawson, B., Leighton, L. and Woodward, M., 2001. Piñon Pine IGCC Project; Final Technical Report to the Department of Energy. *DOE Award Number: DE-FC21-92MC29309, Sparks, Nevada*.

[256] Phillips, J., 2006. Different types of gasifiers and their integration with gas turbines. *The gas turbine handbook*, *1*.

[257] Wang, M., Lawal, A., Stephenson, P., Sidders, J. and Ramshaw, C., 2011. Post-combustion CO_2 capture with chemical absorption: a state-of-the-art review. *Chemical engineering research and design*, *89*(9), pp.1609-1624.

[258] GHG, I., 2007. Post combustion carbon capture from coal fired plants–solvent scrubbing. *International Energy Agency Greenhouse Gas R&D Programme*.

[259] Freguia, S. and Rochelle, G.T., 2003. Modeling of CO2 capture by aqueous monoethanolamine. *AIChE Journal*, *49*(7), pp.1676-1686.

[260] Metz, B., Davidson, O. and De Coninck, H. eds., 2005. *Carbon dioxide capture and storage: special report of the intergovernmental panel on climate change*. Cambridge University Press.

[261] Katzer, J., Moniz, E.J., Deutch, J., Ansolabehere, S. and Beer, J., 2007. *The future of coal: an interdisciplinary MIT study*. Technical report, Massachusetts Institute of Technology, Cambridge, MA.

[262] Sahraei, M.H., McCalden, D., Hughes, R. and Ricardez-Sandoval, L.A., 2014. A survey on current advanced IGCC power plant technologies, sensors and control systems. *Fuel*, *137*, pp.245-259.

[263] Hoffman, Z., 2005. Simulation and economic evaluation of coal gasification with sets reforming process for power production.

[264] Carolyn Beeler, J., 2020. *The UK'S Move Away from Coal Means They're Burning Wood From The US*. [online] Keranews.org. Available at: <https://www.keranews.org/post/uk-s-move-away-coal-means-they-re-burning-wood-us> [Accessed 12 May 2020].

[265] Ricardo Energy & Environment, 2018. *Global Biomass Markets*. Department for Business, Energy and Industrial Strategy.

[266] Beets, M.D.A., 2017. *A Torrefied Wood Pellet Supply Chain. A detailed cost analysis of the comptetitiveness of torrefied wood pellets compared to white wood pellets* (Master's thesis).

[267] Ssethermal.com. 2020. *SSE Thermal Opens Consultation for Proposed Keadby 3 Low-Carbon Power Station | SSE Thermal*. [online] Available at: <https://www.ssethermal.com/news-and-views/2020/06/sse-thermal-opens-consultation-for-proposed-keadby-3-low-carbon-power-station/> [Accessed 29 June 2020].

[268] Gårdbro, G., 2014. Techno-economic modeling of the supply chain for torrefied biomass (Master's thesis).

[269] Sea-distances.org. 2020. *SEA-DISTANCES*. [online] Available at: <https://sea-distances.org/> [Accessed 18 October 2020].

[270] Google Maps. 2020. *Google Maps*. [online] Available at: <https://www.google.co.uk/maps/> [Accessed 18 October 2020].

[271] Aditnow.co.uk. 2020. *Lists And Maps Of UK And International Mines And Quarries*. [online] Available at: <https://www.aditnow.co.uk/Database/> [Accessed 27 June 2020].

[272] Holloway, S., Karimjee, A., Akai, M., Pipatti, R. and Rypdal, K., 2006. Carbon dioxide transport, injection and geological storage. *In: IPCC guidelines for national greenhouse gas inventories/edited by Intergovernmental Panel on Climate Change [IPCC]. Paris, France: OECD. p.*, *5*, pp.5-1.

[273] Energy Technologies Institute, 2020. *A Picture Of CO2 Storage In The UK - Learnings From The ETI'S UKSAP And Derived Projects*.

[274] Li, S., Gao, L. and Jin, H., 2016. Life cycle energy use and GHG emission assessment of coal-based SNG and power cogeneration technology in China. Energy Conversion and Management, 112, pp.91-100

[275] IEA-ETSAP. 2014. Coal mining and logistics.

[276] Norgate, T. and Haque, N., 2010. Energy and greenhouse gas impacts of mining and mineral processing operations. Journal of Cleaner Production, 18(3), pp.266-274.

[277] Koornneef, J., van Keulen, T., Faaij, A. and Turkenburg, W., 2008. Life cycle assessment of a pulverized coal power plant with post-combustion capture, transport and storage of CO2. International journal of greenhouse gas control, 2(4), pp.448-467.

[278] Yang, B., Wei, Y.M., Hou, Y., Li, H. and Wang, P., 2019. Life cycle environmental impact assessment of fuel mix-based biomass co-firing plants with CO2 capture and storage. Applied Energy, 252, p.113483.

[279] Yujia, W., Zhaofeng, X. and Zheng, L., 2014. Lifecycle analysis of coal-fired power plants with CCS in China. Energy Procedia, 63, pp.7444-7451.

[280] MDS TRANSMODAL LIMITED, 2012. *Analysis of road and rail costs between coal mines and power stations*. Estimating road and rail costs between coal mines and power stations.

[281] Government Office for Science, 2019. *Understanding The UK Freight Transport System*. Future of Mobility: Evidence Review.

[282] Singh, B., Strømman, A.H. and Hertwich, E.G., 2011. Comparative impact assessment of CCS portfolio: Life cycle perspective. *Energy Procedia*, *4*, pp.2486-2493.

[283] Alsultannty, Y.A. and Al-Shammari, N.N., 2014. Oxygen specific power consumption comparison for air separation units. *Engineering Journal*, *18*(2), pp.67-80.

[284] Drax. (2019). *Environment - Drax*. [online] Available at: https://www.drax.com/sustainability/environment/#sourcing-sustainable-biomass [Accessed 14 Aug. 2019].

[285] Department of Business, Energy & Industrial Strategy (2019). THE RENEWABLES OBLIGATION FOR 2019/20 - Calculating the Level of the Renewables Obligation for 2019/20.

[286] Ukpower.co.uk. 2020. *Compare Gas and Electricity Prices Per Kwh | Ukpower*. [online] Available at: <https://www.ukpower.co.uk> [Accessed 10 June 2020].

[287] Drax. (2019). Drax to pilot Europe's first carbon capture storage project - Drax. [online] Available at: https://www.drax.com/press_release/drax-to-pilot-europes-first-carbon-capture-storage-project-beccs/ [Accessed 16 Oct. 2019].

[288] Rectisol, L., 2010. Coal gasification for DRI production–An Indian solution. *Steel Times International*.

[289] Ofgem, 2020. *Renewables Obligation: Guidance For Suppliers*.

[290] Wei, G., Wu, X., Meng, J., Huang, Z., He, F., Zhao, W., Zhao, K., Zheng, A., Zhao, Z. and Li, H., 2018. Performance evaluation of hematite oxygen carriers in high purity hydrogen

generation from cooking oil by chemical looping reaction. *International Journal of Hydrogen Energy*, *43*(45), pp.20500-20512.

APPENDIX

Figure A1. Photos of the experimental rig used to extract data to validate the model

FORTRAN statement calculation for biomass pyrolysis to decomposed into its constituent components.

The RYield is used to simulate the biomass pyrolysis which is only temporary placeholder. Fortran expression is defined to calculate the actual yield distribution of pyrolysis. The following Fortran code shows the process in detail:

```
FACT IS THE FACTOR TO CONVERT THE ULTIMATE ANALYSIS TO A WET BASIS.
            FACT = (100 - WATER) / 100
            H2O = WATER / 100
            ASH = ULT(1) / 100 * FACT
            CARB = ULT(2) / 100 * FACT
            H2 = ULT(3) / 100 * FACT
            N2 = ULT(4) / 100 * FACT
            SULF = ULT(6) / 100 * FACT
            O2 = ULT(7) / 100 * FACT
```

These calculations assume that the inlet stream consists entirely of biomass. ULT is defined as the biomass ultimate analysis on a dry basis. The variable WATER, defined as the percent H_2O in the PROXANAL of biomass, is used to convert the ultimate analysis to a wet basis. The remaining seven variables (H_2O through O_2) are defined as the individual component yields in the RYield block.

Table A1. Gabi input data for BCLGCC w/o CCS

Input	kg/MWh
Fuel Reactor	
Biomass	402.93
OC	14.71
Steam	604.40
Air Reactor	
N_2	163.907
O_2	49.769
Gas Turbine	
N_2	1790.02
O_2	543.77
Output	kg/MWh
CC Emissions	
CO	0.04
N_2	1790.24
O_2	128.99
CO_2	629.20
H_2O	440.37
H_3N	7.85E-06
SO_2	0.01
NO_X	0.04
Dust	0.02
Air Reactor	
N_2	163.90
O_2	4.80
CO_2	26.72
Hematite Waste (Non-Hazardous Waste)	14.71
SLAG	1.55
NO_X	0.00162

Table A2. Gabi input data for BCLGCC with CCS

Input	kg/MWh
Fuel Reactor	
Biomass	428.57
OC	15.64
Steam	642.86
Air Reactor	
N_2	172.492
O_2	52.376
Gas Turbine	
N_2	1868.97
O_2	567.76
Output	kg/MWh
CC Emissions	
CO	3.45E-04
N_2	1869.19
O_2	126.60
CO_2	65.44
H_2O	525.22
H_3N	6.76E-06
SO_2	7.79E-03
NO	4.49E-02
Dust	1.80E-02
Air Reactor	
N_2	172.43
O_2	4.48
CO_2	26.41
Hematite Waste (Non-Hazardous Waste)	15.64
SLAG	1.65
NO_X	0.00171
WGS and Carbon Capture	kg/MWh
Syngas (In)	664.24
Syngas (Out)	357.61
Steam (In)	289.53
Carbon Dioxide (Out)	690.40
Selexol	4.17E-03
Energy for CO_2 Capture (MJ/MWh)	259.94

Table A3. Gabi input data for BIGCC w/o CCS

Parameters	Value (kg/MWh)
Air Separation Unit (In)	
Air	587.09
Air Out (N2)	354.05
Energy for O2 Separation (MJ/MWh)	104.00
Gasifier (In)	
O2	115.56
Biomass	413.13
Combined Cycle (In)	
Air	5144.29
Syngas	486.06
Combined Cycle (Out)	
Nitrogen (N2)	3155.92
Oxygen (O2)	612.40
Water Vapor (H2O)	195.05
Carbon Dioxide (CO2)	637.24
Sulfur Dioxide (SO2)	2.18E-03
Nitrogen Oxides (NOX)	4.36E-02
Slag	1.74
Particulate Emissions to Air	3.32E-03

Table A4. Gabi input data for BIGCC with CCS

Parameters	Value (kg/MWh)
Air Separation Unit (In)	
Air	695.94
Air Out (N_2)	419.70
Energy for O_2 Separation (MJ/MWh)	123.34
Gasifier (In)	
O_2	115.56
Biomass	413.13
WGS and Carbon Capture	
Syngas (In)	612.63
Steam (In)	188.17
Carbon Dioxide (Out)	690.40
Selexol	4.83E-03
Energy for CO_2 Capture (MJ/MWh)	308.07
Combined Cycle (In)	
Air	5859.82
Syngas	110.40
Combined Cycle (Out)	
Nitrogen (N_2)	3596.11
Oxygen (O_2)	682.24
Water Vapor (H_2O)	419.16
Carbon Dioxide (CO_2)	100.92
Sulfur Dioxide (SO_2)	2.54E-04
Nitrogen Oxides (NO_X)	4.86E-02
Slag	2.58
Particulate Emissions to Air	4.91E-03

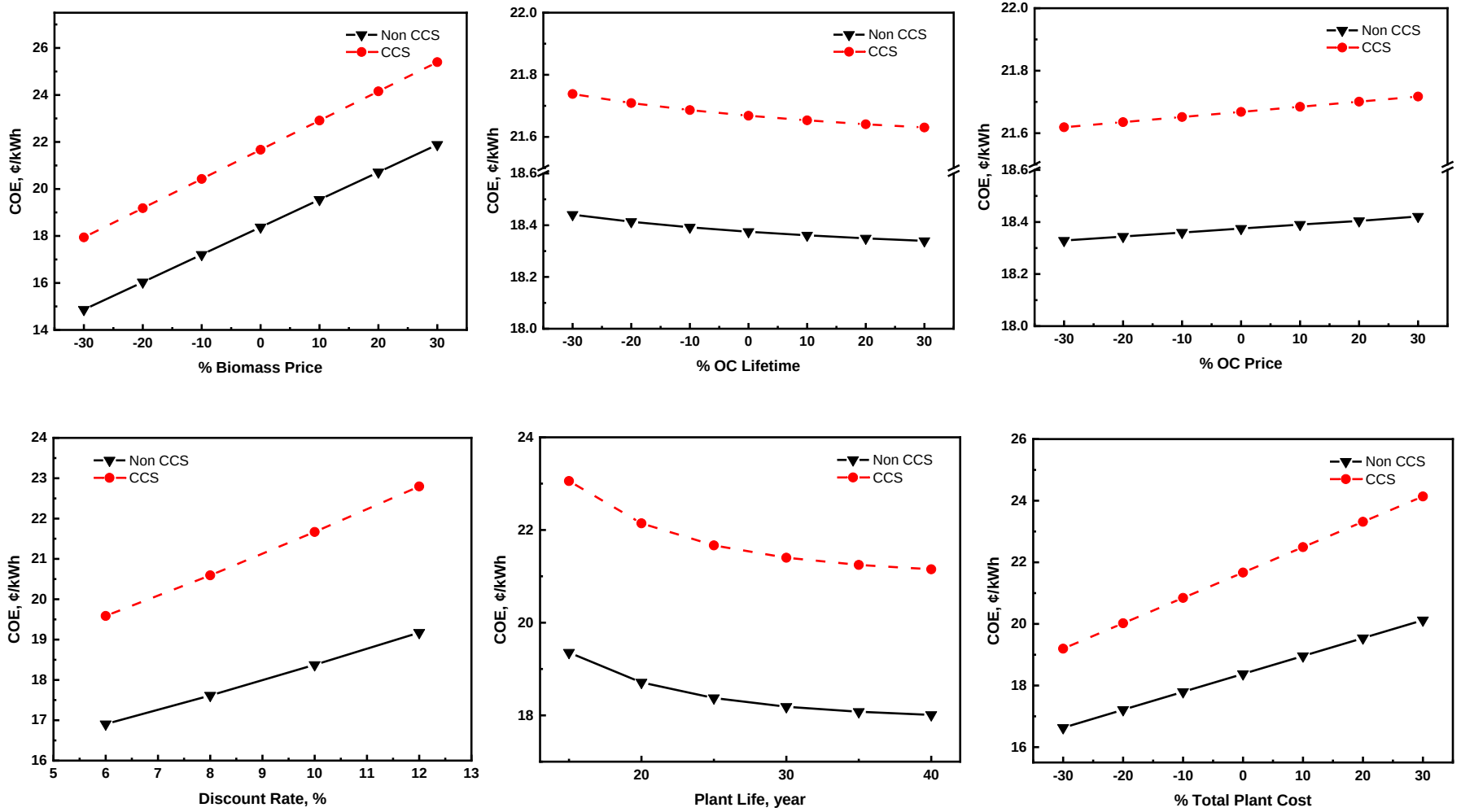

Figure A2. Effects of some key economic variables on COE

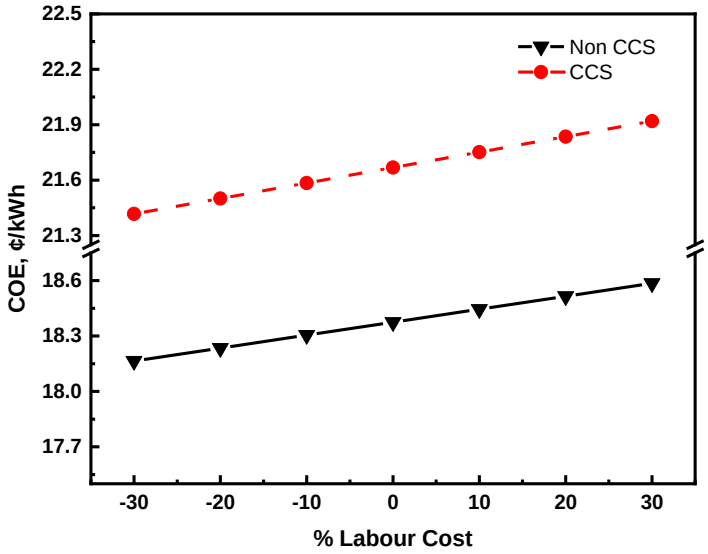

Figure A2. ***(continued)***

Table A5. Composition of streams in Figure 3.9(A-D)

Power plants	Stream No.	Mole Percentage (Gas, %)											Mass Percentage (solid, %)				
		CO	N_2	CH_4	CO_2	H_2	O_2	NH_3	H_2S	COS	NO_X	SO_2	C	B	UR-C	OC	Slag
BCLGCC with CCS (A)	1	0	0	0	0	0	0	0	0	0	0	0	0	100	0	0	0
	2	0	0	0	0	0	0	0	0	0	0	0	0	0	0	0	100
	3	33.89	0.02	0.97	12.49	52.62	0	1.61E-05	0	3.99E-03	0	0	0	0	0	0	0
	4	0	0	0	0	0	0	0	0	0	0	0	0	0	0.21	99.79	0
	5	0	0	0	0	0	0	0	0	0	0	0	0	0	0	100	0
	6	0	87.51	0	7.25	0	5.18	0	0	0	6.13E-02	0	0	0	0	0	0
	7	0	79	0	0	0	21	0	0	0	0	0	0	0	0	0	0
	8	0.29	0.02	1.06	5.01	93.62	0	1.41E-05	4.33E-04	2.41E-07	0	0	0	0	0	0	0
	9	0	80.81	0	1.16	0	18.03	9.97E-08	0	0	6.62E-03	1.15-04	0	0	0	0	0
BCLGCC w/o CCS (B)	1	0	0	0	0	0	0	0	0	0	0	0	0	100	0	0	0
	2	0	0	0	0	0	0	0	0	0	0	0	0	0	0	0	100
	3	33.89	0.02	0.97	12.49	52.62	0	1.61E-05	0	3.99E-03	0	0	0	0	0	0	0
	4	0	0	0	0	0	0	0	0	0	0	0	0	0	0.21	99.79	0
	5	0	0	0	0	0	0	0	0	0	0	0	0	0	0	100	0
	6	0	83.10	0	14.03	0	2.81	0	0	0	5.82E-02	0	0	0	0	0	0
	7	0	79	0	0	0	21	0	0	0	0	0	0	0	0	0	0
	8	0.20	0.02	0.73	34.51	64.54	0	9.75E-06	2.99E-03	1.66E-06	0	0	0	0	0	0	0
	9	0	74.6	0	8.95	8.95	15.44	1.18E-07	0	0	6.12E-03	1.10E-3	0	0	0	0	0
Biomass IGCC w/o CCS (C)	1	0	79.0	0	0	0	21.0	0	0	0	0	0	0	0	0	0	0
	2	0	100	0	0	0	0	0	0	0	0	0	0	0	0	0	0
	3	0	99.2	0	0	0	0.80	0	0	0	0	0	0	0	0	0	0
	4	0	0	0	0	0	0	0	0	0	0	0	0	0	100	0	0
	5	40.83	0.04	7.00	21.76	30.36	0	3.42E-04	6.83E-03	6.39E-04	0	0	0	0	0	0	0
	6	40.83	0.04	7.00	21.76	30.36	0	3.42E-04	6.83E-03	6.39E-04	0	0	0	0	0	0	0
	7	0	79.0	0	0	0	21.0	0	0	0	0	0	0	0	0	0	0
	8	0	76.27	0	10.78	0	12.95	0	0	0	9.57E-04	2.30E-05	0	0	0	0	0
Biomass IGCC with CCS (D)	1	0	79.0	0	0	0	21.0	0	0	0	0	0	0	0	0	0	0
	2	0	100	0	0	0	0	0	0	0	0	0	0	0	0	0	0
	3	0	99.2	0	0	0	0.80	0	0	0	0	0	0	0	0	0	0

	4	0	0	0	0	0	0	0	0	0	0	0	0	0	100	0	0
	5	40.83	0.04	7.00	21.76	30.36	0	3.42E-04	6.83E-03	6.39E-04	0	0	0	0	0	0	0
	6	0	0.04	8.68	2.56	88.72	0	4.23E-04	1.11E-05	7.95E-06	0	0	0	0	0	0	0
	7	0	79.0	0	0	0	21.0	0	0	0	0	0	0	0	0	0	0
	8	0	84.34	0	1.66	0	14.0	0	0	0	1.04E-03	2.61E-04	0	0	0	0	0
Coal IGCC w/o CCS (C)	1	0	79.0	0	0	0	21.0	0	0	0	0	0	0	0	0	0	0
	2	0	100	0	0	0	0	0	0	0	0	0	0	0	0	0	0
	3	0	99.2	0	0	0	0.80	0	0	0	0	0	0	0	0	0	0
	4	0	0	0	0	0	0	0	0	0	0	0	100	0	0	0	0
	5	59.29	6.16	0.18	2.15	31.30	0	0	0.85	7.21E-02	0	0	0	0	0	0	0
	6	59.29	6.16	0.18	2.15	31.30	0	0	0.85	7.21E-02	0	0	0	0	0	0	0
	7	0	79.0	0	0	0	21.0	0	0	0	0	0	0	0	0	0	0
	8	0	76.63	0	9.95	0	13.42	0	0	0	9.40E-04	2.82E-03	0	0	0	0	0
Coal IGCC with CCS (D)	1	0	79.0	0	0	0	21.0	0	0	0	0	0	0	0	0	0	0
	2	0	100	0	0	0	0	0	0	0	0	0	0	0	0	0	0
	3	0	99.2	0	0	0	0.80	0	0	0	0	0	0	0	0	0	0
	4	0	0	0	0	0	0	0	0	0	0	0	100	0	0	0	0
	5	59.29	6.16	0.18	2.15	31.30	0	0	0.85	7.21E-02	0	0	0	0	0	0	0
	6	3.18	0.04	0.03	2.14	94.61	0	0.01	1.18E-03	7.77E-03	0	0	0	0	0	0	0
	7	0	79.0	0	0	0	21.0	0	0	0	0	0	0	0	0	0	0
	8	0	84.66	0	1.15	0	14.19	0	0	0	1.05E-03	3.24E-04	0	0	0	0	0

Table A6. Composition of streams in Figure 3.9(E-F)

Power plants	Stream No.	Mole Percentage (Gas, %)										Mass Percentage (solid, %)	
		CO	**N_2**	**CO_2**	**O_2**	**NH_3**	**NO_X**	**SO_2**	**N2O**	**HCN**	**HCL**	**C**	**B**
Biomass combustion w/o CCS (E)	1	0	79.0	0	21.0	0	0	0	0	0	0	0	0
	2	0	0	0	0	0	0	0			0	0	100
	3	0.14	79.24	14.77	5.80	9.49E-04	0.048	2.11E-04	1.10E-03	4.22E-04	1.37E-03	0	0
Biomass/ combustion with CCS (F)	1	0	79.0	0	21.0	0	0	0	0	0	0	0	0
	2	0	0	0	0	0	0	0	0	0	0	0	100
	3	0.14	79.24	14.77	5.80	9.49E-04	0.048	2.11E-04	1.10E-03	4.22E-04	1.37E-03	0	0
	4	0.16	91.39	1.70	6.69	1.1E-03	0.055	2.40E-04	1.22E-03	4.87E-04	1.58E-03	0	0
Coal combustion w/o CCS (E)	1	0	79.0	0	21.0	0	0	0	0	0	0	0	0
	2	0	0	0	0	0	0	0			0	100	0
	3	0.24	90.95	13.22	5.33	1.07E-04	0.22	3.12E-02	7.46E-03	4.58E-03	3.20E-04	0	0
Coal combustion with CCS (F)	1	0	79.0	0	21.0	0	0	0	0	0	0	0	0
	2	0	0	0	0	0	0	0	0	0	0	100	0
	3	0.24	90.95	13.22	5.33	1.07E-04	0.22	3.12E-02	7.46E-03	4.58E-03	3.20E-04	0	0
	4	0.28	91.88	1.50	6.05	1.21E-04	0.25	3.55E-02	8.47E-04	5.20E-03	3.63E-04	0	0

Table A7. BCLGCC energy consumption values (Figure 5.1)

Parameter		BCLGCC with CCS	BCLGCC w/o CCS
Energy input/output	Unit	Value	Value
Total Energy input	MW	2145.9	1775.1
Biomass	MW	1403.2	1429.2
Wood Harvesting & Transport	MJ/MWh	27.6	25.9
Wood Processing	MJ/MWh	1596.2	1500.7
Pellet Handling & Storage	MJ/MWh	10.6	9.9
Transport to port (by rail)	MJ/MWh	30.9	29.1
Ocean Transport	MJ/MWh	120.5	113.3
Transport to power plant (by truck)	MJ/MWh	77.6	73.0
Iron mining	MJ/MWh	2.4	2.3
Iron Transport	MJ/MWh	0.4	0.4
CO_2 capture	MJ/MWh	259.9	N/A
CO_2 storage	MJ/MWh	18.8	N/A
CO_2 transport	MJ/MWh	6.4	N/A
Total Energy output	MW	650	650

Table A8. BIGCC energy consumption values (Figure 5.2)

Parameter		BIGCC with CCS	BIGCC w/o CCS
Energy Consumption	Unit	Value	Value
Total Energy input	MW	2482.6	1775.1
Biomass	MW	1694.5	1511.9
Wood Harvesting & Transport	MJ/MWh	30.58	26.11
Wood Processing	MJ/MWh	1771.08	1511.87
Pellet Handling & Storage	MJ/MWh	11.74	10.02
Transport to port (by rail)	MJ/MWh	34.29	29.27
Ocean Transport	MJ/MWh	133.81	114.23
Transport to power plant (by truck)	MJ/MWh	86.18	73.56
CO_2 capture	MJ/MWh	374.77	N/A
CO_2 storage	MJ/MWh	7.26	N/A
CO_2 transport	MJ/MWh	21.16	N/A
Total Energy output	MW	650	650

Table A9. CIGCC energy consumption values (Figure 5.3)

Parameter		CIGCC with CCS	CIGCC w/o CCS
Energy Consumption	Unit	Value	Value
Total Energy input	MW	1149.1	637.9
Coal	MW	1650.4	1538.4
Coal mining and washing	MJ/MWh	755.32	628.08
Coal Transport	MJ/MWh	11.79	9.81
CO_2 storage	MJ/MWh	23.31	N/A
CO_2 capture	MJ/MWh	350.73	N/A
CO_2 transport	MJ/MWh	7.99	N/A
Total Energy output	MW	650	650

Table A10. BCLGCC CO_2 emission values (Figure 5.4)

Parameter CO_2 Emission	Unit	BCLGCC with CCS Value	BCLGCC w/o CCS Value
Wood production harvest and transport	kg-CO_2/MWh	0.86	0.81
Wood processing in pellet plant	kg-CO_2/MWh	33.97	31.94
Handling and storage	kg-CO_2/MWh	0.78	0.73
Wood pellets transport to port (by rail)	kg-CO_2/MWh	0.78	0.73
Wood pellets ocean transport	kg-CO_2/MWh	16.07	15.11
Wood pellets transport to power plant (by truck)	kg-CO_2/MWh	4.05	3.81
Iron mining	kg-CO_2/MWh	0.19	0.18
Iron transport	kg-CO_2/MWh	0.03	0.02
CO_2 compression (fugitive CO_2 emission compressor) + CO_2 transport (fugitive CO_2 emissions pipeline)	kg-CO_2/MWh	1.23	N/A
Fugitive CO_2 emission from CO_2 storage	kg-CO_2/MWh	5.22	N/A
CO_2 emission	kg-CO_2/MWh	115.08	820.00
CO_2 storage	kg-CO_2/MWh	744.05	N/A
Total CO_2 emission	kg-CO_2/MWh	923.1	874.0

Table A11. BIGCC CO_2 emission values (Figure 5.5)

Parameter CO_2 Emission	Unit	BIGCC with CCS Value	BIGCC w/o CCS Value
Wood production harvest and transport	kg-CO_2/MWh	0.95	0.81
Wood processing in pellet plant	kg-CO_2/MWh	37.69	32.17
Handling and storage	kg-CO_2/MWh	0.86	0.74
Wood pellets transport to port (by rail)	kg-CO_2/MWh	0.86	0.74
Wood pellets ocean transport	kg-CO_2/MWh	17.84	15.23
Wood pellets transport to power plant (by truck)	kg-CO_2/MWh	4.50	3.84
CO_2 compression (fugitive CO_2 emission compressor) + CO_2 transport (fugitive CO_2 emissions pipeline)	kg-CO_2/MWh	1.62	N/A
Fugitive CO_2 emission from CO_2 storage	kg-CO_2/MWh	5.89	N/A
CO_2 emission	kg-CO_2/MWh	122.77	787.80
CO_2 storage	kg-CO_2/MWh	839.87	N/A
Total CO_2 emission	kg-CO_2/MWh	1033.7	841.1

Table A12. BIGCC CO_2 emission values (Figure 5.6)

Parameter CO_2 Emission	Unit	BCLGCC with CCS Value	BCLGCC w/o CCS Value
Coal mining and washing	kg-CO_2/MWh	20.87	17.36
Coal transport (by rail)	kg-CO_2/MWh	3.48	2.90
CO_2 compression (fugitive CO_2 emission compressor) + CO_2 transport (fugitive CO_2 emissions pipeline)	kg-CO_2/MWh	1.61	N/A
Fugitive CO_2 emission from CO_2 storage	kg-CO_2/MWh	6.48	N/A
CO_2 emissions	kg-CO_2/MWh	98.58	846.75
CO_2 storage	kg-CO_2/MWh	925.06	N/A
Total CO_2 emission	kg-CO_2/MWh	1149.1	637.9

Table A13. BCLGCC cost requirement values (Figure 5.7)

Parameter Cost Required	Unit	BCLGCC with CCS Value	BCLGCC w/o CCS Value
Wood Harvesting & Transport	£/MWh	38.18	35.89
Wood Processing	£/MWh	29.48	27.71
Pellet Handling & Storage	£/MWh	3.01	2.83
Transport to port (by rail)	£/MWh	7.62	7.17
Ocean Transport	£/MWh	9.40	8.83
Transport to power plant (by truck)	£/MWh	10.06	9.46
Receiving port handling and storage	£/MWh	3.01	2.83
Iron mining	£/MWh	1.83	1.72
Iron Transport	£/MWh	0.24	0.23
CO2 transport & storage	£/MWh	23.51	N/A
Annual Capital Cost	£/MWh	58.11	41.02
M&O cost, labour cost	£/MWh	15.18	11.58
Total cost input	£/MWh	199.6	149.3

Table A14. BIGCC cost requirement values (Figure 5.8)

Parameter Cost Required	Unit	BCLGCC with CCS Value	BCLGCC w/o CCS Value
Wood Harvesting & Transport	£/MWh	42.36	36.16
Wood Processing	£/MWh	32.71	27.92
Pellet Handling & Storage	£/MWh	3.35	2.86
Transport to port (by rail)	£/MWh	8.46	7.22
Ocean Transport	£/MWh	10.43	8.90
Transport to power plant (by truck)	£/MWh	11.16	9.53
Receiving port handling and storage	£/MWh	3.35	2.86
CO2 transport & storage	£/MWh	21.23	N/A
Annual Capital Cost	£/MWh	57.03	47.86
M&O cost, labour cost	£/MWh	22.16	16.22
Total cost input	£/MWh	212.2	159.5

Table A15. CIGCC cost requirement values (Figure 5.9)

Parameter Cost Required	Unit	BCLGCC with CCS Value	BCLGCC w/o CCS Value
Coal mining and washing	£/MWh	27.28	22.68
Coal transport (by rail)	£/MWh	3.11	2.59
CO_2 transport & storage	£/MWh	23.38	N/A
Annual capital cost	£/MWh	54.14	38.09
M&O cost, labour cost	£/MWh	12.00	9.15
Total cost input	£/MWh	119.9	72.5

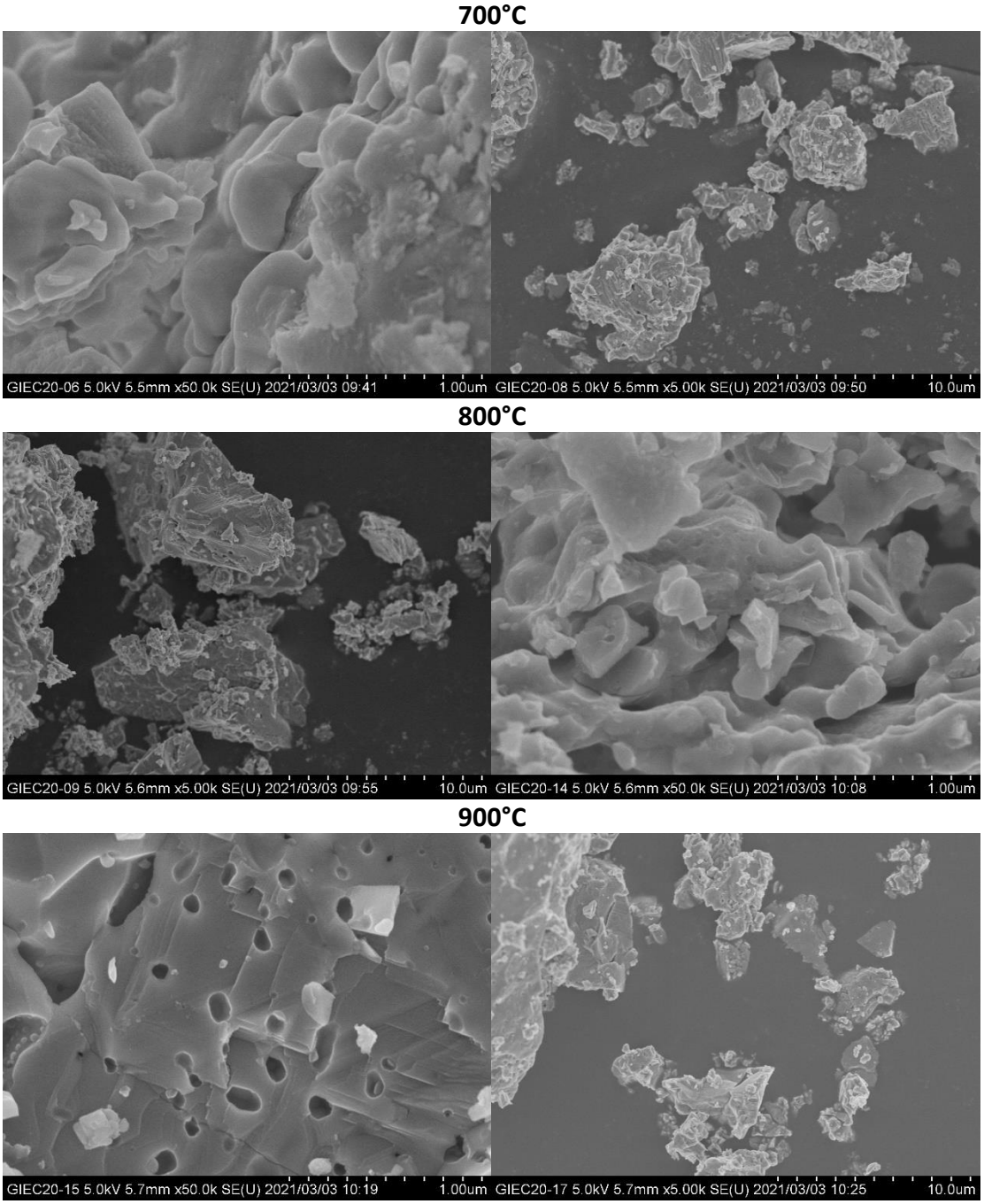

Figure A3. Additional SEM images complementing the results in chapter 6

0.61 B/OC

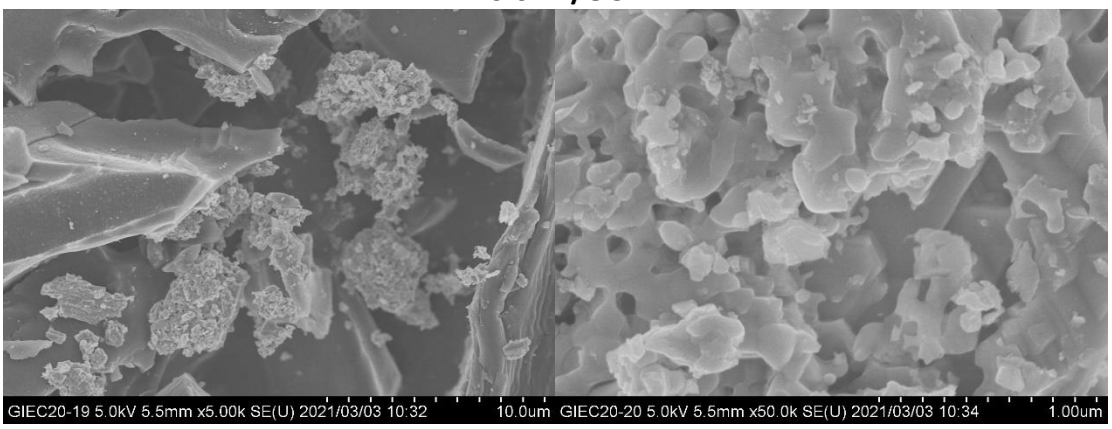

0.73 B/OC

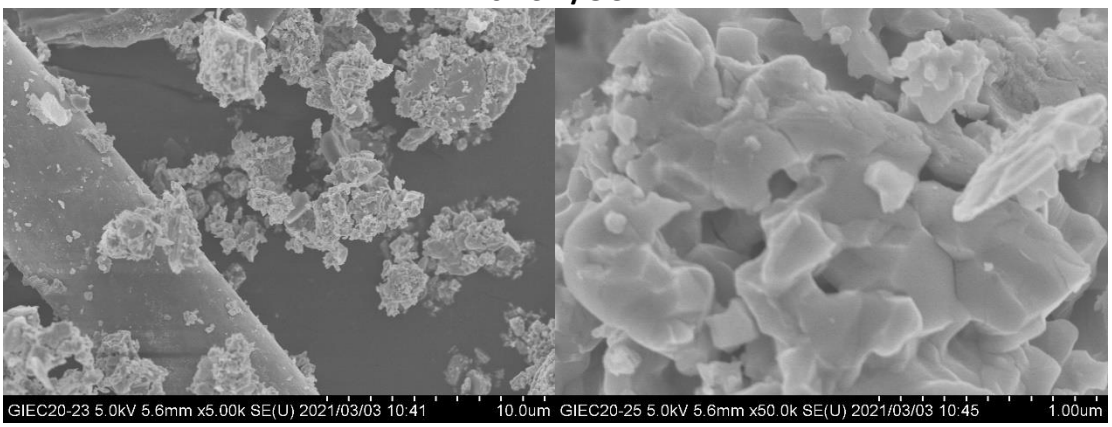

0.89 B/OC

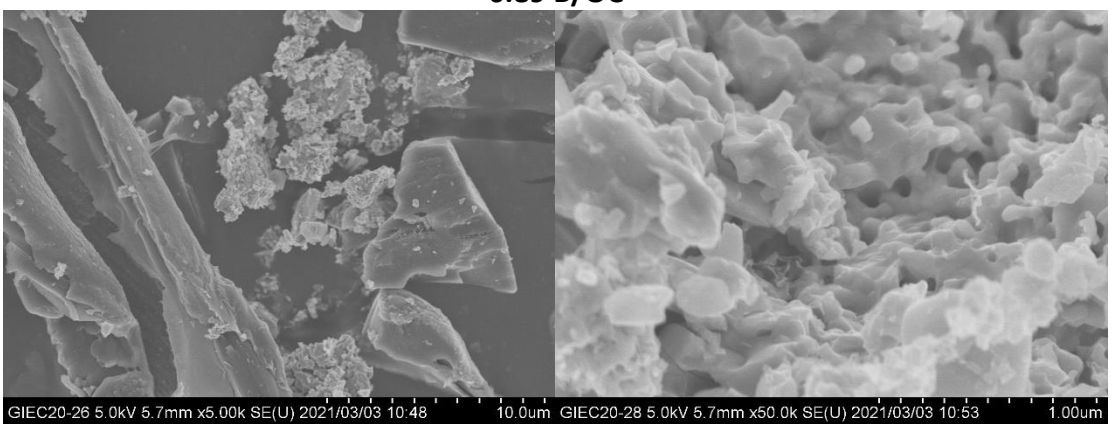

10 minutes

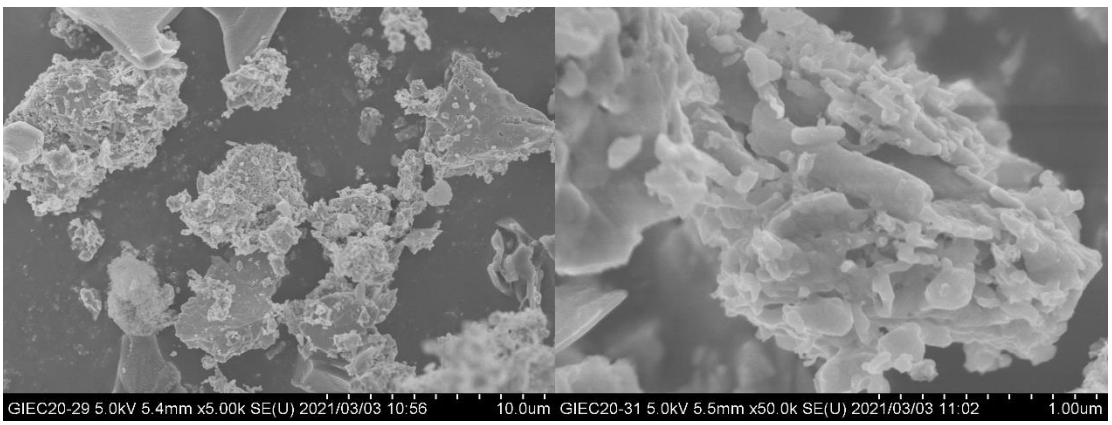

Figure A3. ***(continued)***

30 minutes

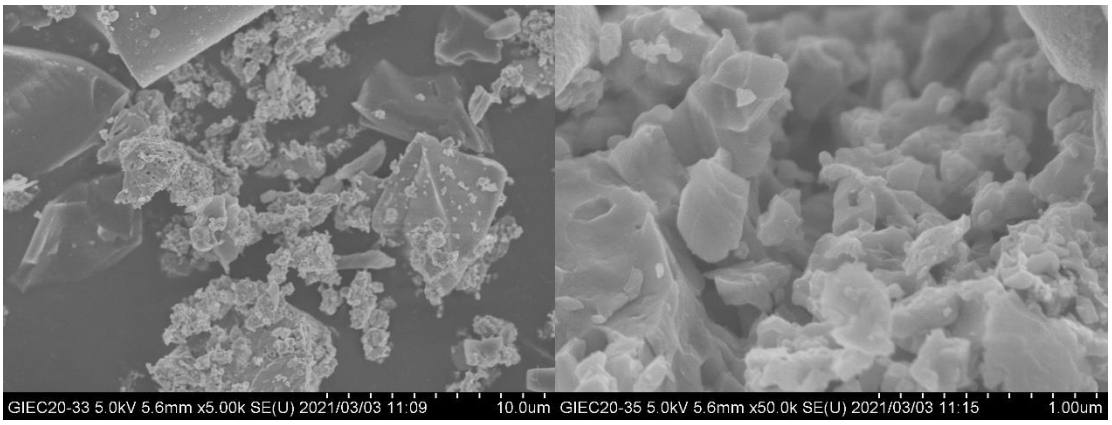

10 minutes

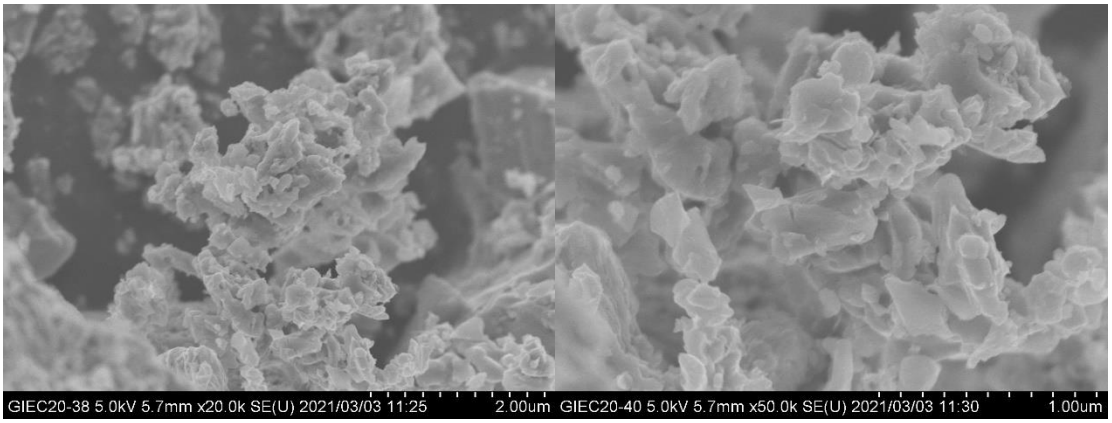

9-Cycles

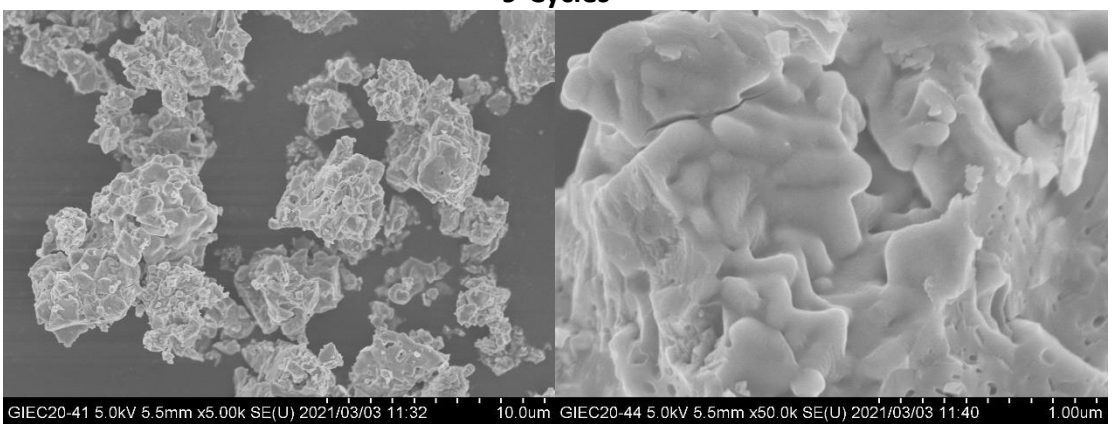

Fresh Hematite

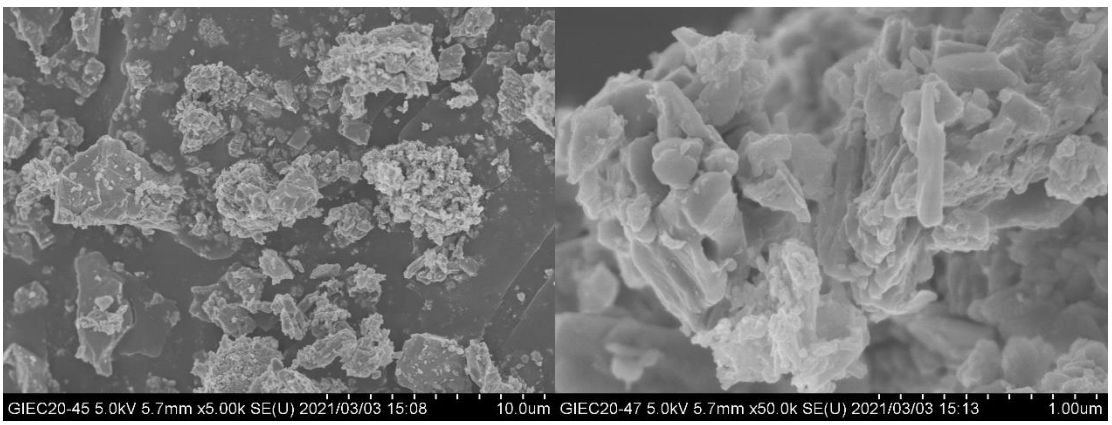

Figure A3. ***(continued)***

This page intentionally left blank